Roles for GLI Transcription Factors in Pancreas Development and Disease

by

Michael K. Scales

A dissertation submitted in partial fulfillment
of the requirements for the degree of
Doctor of Philosophy
(Cell and Developmental Biology)
in the University of Michigan
2022

Doctoral Committee:

Professor Andrzej A. Dlugosz, Chair
Associate Professor Benjamin L. Allen
Professor Howard C. Crawford, Henry Ford Health System
Professor Marina Pasca di Magliano
Professor Deneen M. Wellik, University of Wisconsin - Madison

Michael K. Scales

mkscales@umich.edu

ORCID iD: 0000-0002-3645-5643

© Michael K. Scales, 2022

Dedication

To Michelle

To my children, Scott and Eleanor

To my family

Acknowledgements

The work presented in this thesis is the end result of a highly collaborative effort, both scientifically and personally. The extent of my gratitude cannot be sufficiently expressed in this section, but I will strive to acknowledge the contribution of several key individuals and groups.

I would first like to thank my co-advisors, Drs. Ben Allen and Marina Pasca di Magliano. My Ph.D. is the direct product of a long and productive collaboration between Ben and Marina, and as a result that theme of collaboration has become a core tenet of my thesis work. Whether it has involved presenting in front of multiple group meetings, identifying additional sources of technical assistance, or simply meeting together each week to discuss my project, you have consistently supported and sought out new opportunities for collaboration and cooperation, which has played an instrumental role in advancing my research and professional. It is a lesson that I consider foundational to who I am as a scientist, and a lesson that I will carry with me as I advance to the next step of my career. I am also extremely grateful for your honesty, patience, integrity, humor, and support, as these attributes have truly made my graduate school experience extremely positive. I am the scientist I am today because of you. Thank you.

I would also like to acknowledge all former and current members of the Allen and Pasca di Magliano lab, including (but not limited to): Martha, Nicole, Bridget, Anna, Tyler, Hannah, Haeyoung, Ashley, Justine, Brandon, Alex, Ariel, Nina, Yaqing, Rosa, Katelyn, Wei, Zeribe, Joyce, and Carlos. Thank you for being a continual source of support and joy throughout my time in graduate school. I have appreciated for your scientific input, your desire to work together as a team, and your patience to put up with me for all of these years! I can honestly say that my

graduate experience would not have been nearly as productive or as fun without you, and for that I am immensely grateful. I would also like to acknowledge the work of three talented scientists: Anna Stabnick, Nayanna Mercado Soto, and Rajko Vucicevic, who made significant contributions to this work as undergraduate researchers. Being able to mentor you has truly been a privilege, and seeing you move on and succeed as you start your own careers has brought me an immense amount of pride. I am extremely excited to see where each of your careers takes you, and I am grateful to have been a small part of it.

I would also like to thank the members of my thesis committee: Drs. Deneen Wellik, Howard Crawford, and Andrzej Dlugosz. Your feedback and willingness to support my project and career has been an instrumental part of my development as a scientist. Thank you for your continued input, and for serving as exceptional role models at the onset of my career as an independent scientist.

I would like to acknowledge the staff of the Cell and Developmental Biology Department, including: Kristen, Brittney, Karen, Lori, Jackie, Brooke, Deontae, Annette, and Mohi. Thank you for your constant willingness to be helpful and kind, and for always going above and beyond for the students of CDB. I would also like to thank Craig Johnson, for providing bioinformatic support and insight into my project, which has become an instrumental component of my thesis work.

I would like to thank Henry Ho, who first hired me as a technician when I graduated from my undergraduate degree. You took a chance on an undergraduate with a limited amount of lab experience and gave me the opportunity to pursue science as a career. Your positivity, hard work, kindness, and continual support have shaped me as a scientist, and I cannot thank you enough for helping me start on this path.

I would like to acknowledge the support of all of the collaborators who have contributed to this work, including Howard Crawford, Carlo Maurer, Ken Olive, and Filip Bednar. I would also like to thank the Developmental Genetics and PANTERA groups, for providing opportunities to present and get feedback on my work. I would also like to acknowledge my funding sources throughout my graduate education, including the Bradley Merrill Patten Memorial Scholarship, the Organogenesis T32 Training Program, and the National Institutes of Health. I would also like to acknowledge the University of Michigan core facilities for providing equipment and access to resources for this work.

I would like to thank my extended family, including the Scales', the Browns, the Hoglunds, and the Fearons. Thank you for providing love and support, and for always being excited about my work! I would also like to thank my close friends: Casey, Ashley, and Jackie, for always making me laugh.

I would like to thank my brother Jonathan, for always being someone that I have looked up to. I would also like to thank my sister-in-law Ann and my niece Elisabeth, for joining our family and bringing joy to our lives!

I would like to thank my father, Douglas Scales, for imparting a sense of curiosity, joy, and wonder in me that I carry in all aspects of my life.

I would like to thank my mother, Dr. Wendy Scales, for inspiring me to pursue my dreams.

I would like to thank my children, Scott and Eleanor, for being a constant source of joy and love in my life.

Finally, I would like to thank my wife, Dr. Michelle Fearon Scales. For your dedication, your support, and for being the love of my life. Thank you.

Table of Contents

List of Tables

List of Figures

/

Abstract

The Hedgehog (HH) signaling pathway plays a fundamental role in patterning numerous developing tissues, and dysregulated HH signaling has been linked to malignant human diseases. HH signaling is regulated on a transcriptional level by the GLI family of transcription factors (GLI1, GLI2, GLI3). While GLI1 functions exclusively as a transcriptional activator, GLI2 and GLI3 have dual roles as both activators and repressors. Importantly, the functions of GLI proteins are highly dynamic, and can vary dramatically based on context.

The development and healthy function of the pancreas relies on tightly regulated HH signaling. HH signaling must be actively suppressed during pancreas specification, as ectopic activation leads to impaired organ formation and disrupted endocrine development. In addition, aberrant HH signaling is frequently detected in pancreatic ductal adenocarcinoma (PDA), one of the deadliest forms of cancer. While this pathway has been studied extensively at the level of ligands and receptors, the roles of GLI1-3 in pancreas development and disease remain largely unknown. In this dissertation, I investigate: 1) The role of GLI1-3 in PDA progression and 2) the contribution of GLI1-3 to pancreas development.

In the context of PDA, the role of HH signaling in PDA has been controversial, with both tumor-promoting and tumor-restricting roles reported. The controversy stems, in part from an incomplete understanding of the mechanisms of HH signal transduction in PDA. To determine the role of GLI1-3 in PDA, I utilized a combination of mouse genetics*, ex vivo* assays, and bioinformatic analysis. Expression analysis of both human and mouse tissue revealed that all

three *Gli* genes are expressed by pancreatic fibroblasts in the healthy pancreas, and that the expression of *Gli1-3* expands in PDA. Deleting *Gli2/Gli3* in pancreatic fibroblasts reduces immunosuppressive macrophage infiltration, promotes the recruitment of T cells, and restrains tumor growth. In contrast, combined deletion of *Gli1/Gli2/Gli3 in vivo* promotes macrophage infiltration and supports tumor growth. RNA sequencing analysis revealed that the loss of *Gli* alters the expression of cytokines in pancreatic fibroblasts. Further, fibroblasts directly regulate the migration of macrophages and T cells in a *Gli*-dependent manner. These data indicate that *Gli* expression in fibroblasts directly regulates the tumor microenvironment of pancreatic cancer, and that *Gli*-mediated changes in fibroblast function regulates tumor growth.

In this dissertation, I also investigated the role of GLI1-3 in pancreas development. My data reveal that *Gli2* and *Gli3* are expressed broadly throughout the mesenchyme during pancreas development, while *Gli1* is excluded from this tissue. Conditional deletion of *Gli2* has no significant impacts on pancreas development. In contrast, deleting mesenchymal *Gli3* leads to increased proliferation of pancreatic epithelial cells, abnormal organ morphogenesis, and reduced β-cells. Interestingly, the phenotypes observed depend on the timing of *Gli3* deletion, suggesting that GLI3 plays distinct roles at different stages of pancreas development. Together, the data presented in this thesis reveal that GLI proteins regulate pancreas development and disease progression by modifying the pancreatic microenvironment. These data also reveal new insights into the role of fibroblasts in PDA, and open new opportunities for the development of novel therapies.

Chapter 1 Hedgehog Signaling and Pancreatic Cancer[1]

1.1 Abstract

Pancreatic cancer relies on disrupted intercellular signaling in order to grow, evade treatment, and spread to metastatic sites. While alterations in numerous cell signaling pathways have been linked to pancreatic cancer, the exact roles of these different signaling pathways are complex. The Hedgehog (HH) signaling pathway is aberrantly activated during pancreatic cancer progression. However, the mechanisms of HH signal transduction in pancreatic cancer remain poorly understood. In development and other HH-driven diseases, the GLI family of HH transcription factors (GLI1, GLI2, GLI3) direct transcriptional responses to HH signaling. However, the roles of GLI1-3 in pancreatic cancer are largely unknown.

In this chapter, I will discuss our current understanding of HH signaling and pancreatic cancer. Specifically, I will review the factors driving pancreatic cancer progression and lethality, with a focus on the role of the tumor microenvironment. I will also provide an overview on HH signaling, with a particular focus on the role of GLIs in HH signal transduction, embryonic development, and human disease. Finally, I will discuss our understanding of HH signaling in pancreatic cancer, and highlight the open questions to be addressed in this thesis.

[1] Sections of this chapter have been published: Garcia PE*, Scales MK*, Allen BL, and Pasca di Magiano M. 2020. Pancreatic Fibroblast Heterogeneity: From Development to Cancer. *Cells* **9**: 1 – 25.

1.2 The Tumor Microenvironment of Pancreatic Cancer

Pancreatic ductal adenocarcinoma (PDA) is currently one of the deadliest forms of cancer, with a five-year survival rate of only 11% (Siegel et al. 2022). While the lethality of other cancers has significantly declined over the past 20 years, the death rate for pancreatic cancer is rising (Siegel et al. 2022). Although the reasons behind these striking statistics are complex, two major barriers continue to impede clinical progress: 1) the late stage of detection, and 2) the inefficacy of current treatments. These barriers persist, in part, due to an incomplete understanding of the mechanisms driving PDA progression. In the following sections, I will discuss the current challenges in treating PDA and the factors that contribute to tumor growth. In doing so, I will highlight the importance of the cellular microenvironment in PDA.

1.2.1 Factors Driving Pancreatic Cancer Lethality

One of the factors driving pancreatic cancer lethality is the late stage of detection. Symptoms associated with pancreatic cancer are often non-specific, and can include abdominal pain, nausea, and weight loss (Kleeff et al. 2016). As a result, a majority of PDA patients are diagnosed after the disease has already spread beyond the pancreas (Siegel et al. 2022). A PDA diagnosis requires cross-sectional imaging, in order to determine the location of tumor, the involvement of local vasculature, the presence of metastases in other organs, and the potential for resection (Chu et al. 2017; Zhang et al. 2018). While surgical resection can be curative, less than 20% of PDA cases are resectable (Kleeff et al. 2016; Chu et al. 2017). For patients who present with distant metastases, the five-year survival rate is only 3% (Siegel et al. 2022).

Given the limited options for late-stage PDA patients, there is an ongoing effort to detect PDA at earlier stages of disease. The antigen CA19-9 has been used as a biomarker to evaluate tumor stage and track responses to treatment in PDA patients (Poruk et al. 2013). However,

measuring CA19-9 has limited utility as an early detection method for PDA, as elevated CA19-9 levels are not specific to PDA. As a result, attempts to screen asymptomatic populations have had extremely high false positive rates, as the vast majority of patients with elevated CA19-9 levels did not have PDA (Homma and Tsuchiya 1991; Kim et al. 2004). As an alternative to CA19-9, some studies have proposed that analyzing circulating tumor-derived exosomes can be an effective method of identifying both pre-cancerous disease as well as advanced PDA (Melo et al. 2015; Yang et al. 2017). However, the proposed efficacy of this method remains controversial, and could not be replicated in an independent study (Lai et al. 2017). Until new techniques are developed to more reliably detect early stages of PDA, advanced disease at diagnosis will remain a barrier to patient survival.

Beyond late detection, PDA lethality is also driven by ineffective treatments. Currently, the only potentially curative strategy is tumor resection followed by adjuvant chemotherapy (Neoptolemos et al. 2017; Conroy et al. 2018). However, this strategy is only available to the minority of patients who present with resectable tumors. Further, even in this best-case scenario, the 5-year survival rate is still below 50% (Neoptolemos et al. 2017; Conroy et al. 2018), and the majority of patients will eventually die from disease recurrence (Kleeff et al. 2016; Neoptolemos et al. 2018). Patients with borderline resectable PDA may still qualify for surgery following neoadjuvant therapy, but the median overall survival for these patients remains less than 3 years (Oba et al. 2020). For patients with metastatic PDA, the current standard of care is single or multiagent chemotherapy (Burris et al. 1997; Conroy et al. 2011; Von Hoff et al. 2013), with a dismal 5-year survival rate of only 3% (Siegel et al. 2022). While novel treatments such as immunotherapy have shown promise in lung cancer (Horn et al. 2017; West et al. 2019) and melanoma (Callahan et al. 2018; Robert et al. 2019), these therapies have been largely

unsuccessful in PDA (Royal et al. 2010; O'Reilly et al. 2019; Wainberg et al. 2020). This is due, in part, to interactions between pancreatic tumor cells and the surrounding tumor microenvironment (TME). Pancreatic tumors are highly adept at manipulating the TME in order to support tumor growth, suppress the immune system, and resist therapy. While the TME is a severely disturbed cellular environment, its complexity has its origins in the healthy tissue.

1.2.2 The Physiology of the Healthy Pancreas

A striking feature of PDA is the diversity of cells that make up a pancreatic tumor. However, even in the absence of disease, the pancreas is home to numerous cell types which coordinate to fulfill the endocrine and exocrine roles of the organ. The endocrine function of the pancreas is carried out within the islets of Langerhans, clusters of hormone-producing cells including α cells (glucagon), β cells (insulin), δ cells (somatostatin), and pancreatic polypeptide cells (pancreatic polypeptide) (Bakhti et al. 2019). Beyond this cellular diversity within the islets themselves, the cells of the endocrine pancreas are surrounded by a network of nerves (Faber et al. 2020) and blood vessels (Brissova et al. 2006). This allows sympathetic and parasympathetic signals to activate endocrine secretion by islet cells, which then flow through the vasculature to regulate metabolism throughout the body (Faber et al. 2020). The maintenance of these cell types is critical to organismal health, as a loss of endocrine cells can lead to systemic diseases, such as Type 1 diabetes (Katsarou et al. 2017). Although endocrine cells are crucial to pancreas function, the majority of cells in the pancreas are dedicated to the exocrine function of the organ (Murtaugh and Keefe 2015). Clusters of pancreatic acinar cells receive stimulatory signals from the gut, and in turn secrete digestive enzymes into the lumen of the pancreatic ducts (Williams 2019). Digestive enzymes then flow through this network of ducts into the duodenum in order to aid in digestion.

Although the primary functions of the healthy pancreas are executed by epithelial cell types, the pancreas is also home to a heterogeneous population of fibroblasts. One group of fibroblasts with a relatively well-defined function are pancreatic pericytes. These cells are found adjacent to endothelial cells throughout the adult pancreas (Henderson and Moss 1985), but have primarily been studied in association with pancreatic islets. Pericytes respond to neural and islet-derived signals to regulate blood flow to the islets (Almaca et al. 2018), and are necessary for maintaining proper β-cell function (Sasson et al. 2016).

In contrast to the endothelial association of pericytes, mesenchymal stem cells (MSCs) have been found in close association with pancreatic exocrine tissue (Seeberger et al. 2006; Baertschiger et al. 2008). MSCs are defined based on their ability to differentiate *in vitro* into adipocytes, chondrocytes, and osteoblasts (Seeberger et al. 2006; Baertschiger et al. 2008; Mathew et al. 2016; Waghray et al. 2016). While cancer-associated MSCs have been shown to regulate myeloid infiltration and promote pancreatic tumor growth (Mathew et al. 2016; Waghray et al. 2016), their role in the healthy tissue remains unknown.

In addition to MSCs, the exocrine portion of the pancreas is also the reported niche for pancreatic stellate cells (PSCs). PSCs have received substantial attention for their suggested contribution to fibrosis in the context of pancreatic disease (Apte et al. 1999; Shek et al. 2002; Apte et al. 2004; Omary et al. 2007; Apte and Wilson 2012). PSCs have been defined by the presence of lipid droplets and their ability to "activate" α-Smooth Muscle Actin (αSMA) expression and deposit extracellular matrix (ECM) when isolated in 2D culture (Apte et al. 1998; Bachem et al. 1998). Additional PSC markers have been suggested that can be identified through staining, including desmin and glial fibrillary acidic protein (GFAP) (Apte et al. 1998). It is worth noting, however, that some of the markers frequently used to identify PSCs historically have either

been non-specific (such as the neuron-detecting GFAP) or overlap with general fibroblast markers (e.g., desmin) (Nielsen et al. 2017). Further, no direct lineage tracing of this specific population *in vivo* has been done, making their developmental origin as well as their direct contribution to pancreatic fibrosis unclear. It is therefore worth considering whether the cells we refer to as "PSCs" are not a single cell type, but rather a heterogeneous group of different fibroblast cell types that are independently capable of contributing to pancreatic fibrosis. Consistent with this notion, single cell RNA sequencing analysis of both mouse and human pancreata has identified two distinct clusters of PSCs in the healthy pancreas: "activated" (enriched for ECM-associated genes, including COL1A1 and FN1) and "quiescent" (enriched for adipogenic genes, including ADIRF and FABP4) PSCs (Baron et al. 2016). Within the human samples, the researchers also found a subgroup within the "activated" PSCs that was enriched for cytokines, suggesting a subpopulation capable of modulating the immune cells in the healthy organ. Although these data identify groups of PSCs with unique transcriptional profiles, it still remains unclear whether these groups have independent functions in the healthy pancreas.

1.2.3 The Role of Oncogenic Kras in Pancreatic Cancer Initiation

The diverse cell composition of the pancreas is dramatically disrupted as a result of oncogenic mutations. Specifically, a glycine to aspartic acid (G12D) mutation in the *Kras* gene makes the pancreas susceptible to neoplasia. KRAS is a small GTPase that regulates cell proliferation and survival through a wide variety of downstream effectors, including PI3K-AKT and MAPK-ERK signaling (Buscail et al. 2020). In the presence of a G12D mutation, KRAS becomes locked in a GTP-bound state, leading to constitutive activation of downstream targets (Jonckheere et al. 2017). This *Kras*-driven increase in cell growth is fueled by a rewiring of cellular metabolism. Specifically, oncogenic *Kras* activity drives glucose uptake, hexosamine

biosynthesis, ribose biogenesis, and reprograms glutamine metabolism (Ying et al. 2012; Son et al. 2013). Further, cells expressing oncogenic *Kras* exhibit enhanced nutrient scavenging via macropinocytosis (Commisso et al. 2013; Kamphorst et al. 2015). Together, these changes in cell physiology support tumor cell proliferation and growth.

Evidence from mouse models indicates that expressing $Kras^{G12D}$ in pancreatic epithelial cells (KC model: *Ptf1a-Cre* or *Pdx1-Cre*;$Kras^{LSL\text{-}G12D/+}$) leads to the formation of pancreatic intraepithelial neoplasia (PanIN) (Hingorani et al. 2003). An additional mutation of a tumor suppressor gene (e.g. KPC model = KC + $p53^{R172H}$, KIC model = KC + *p16-Ink4a/p19-*$Arf^{fl/fl}$) reliably produces metastatic pancreatic tumors that closely resemble human PDA (Aguirre et al. 2003; Hingorani et al. 2005). In mice, acinar cells are the more common cell of origin for pancreatic cancer (Kopp et al. 2012), although, under specific circumstances, ductal cells can be transformed as well (Bailey et al. 2016; Ferreira et al. 2017; Kopp et al. 2018).

Beyond these direct effects on tumor cells, oncogenic *Kras* can also drive non-autonomous effects within the local microenvironment. In mouse models, inducing oncogenic *Kras* expression in combination with acute pancreatitis led to an accumulation of fibrotic stroma within 3 weeks (Collins et al. 2012). However, when oncogenic *Kras* was then inactivated, this fibrotic stroma underwent significant remodeling, and within 2 weeks tissue histology was largely normal (Collins et al. 2012). Subsequent studies have shown that induction of oncogenic *Kras* in epithelial cells leads to the secretion of a vast array of signaling molecules to surrounding cells within the TME, including fibroblasts (Tape et al. 2016). In turn, fibroblasts secrete numerous factors back to tumor cells, and these reciprocal signals support mitochondrial function and proliferation in tumor cells (Tape et al. 2016). Understanding the relationships

between neoplastic cells and the diverse cell types of the TME is crucial to our understanding of PDA progression.

1.2.4 Cellular Composition of the Tumor Microenvironment

A somewhat unique feature of PDA is that tumor cells only account for a small minority of the total tumor volume (Maitra and Hruban 2008). The majority of a pancreatic tumor is made up of stroma, a dense tissue composed of myriad cell types (Figure 1.1), including fibroblasts, immune cells, nerves, and endothelial cells. Each of these populations have unique impacts on PDA progression, and their function can affect multiple compartments within the TME.

Among these different cell types, arguably the most understudied population is the nerves. Neurons of the parasympathetic and sympathetic nervous system are abundant in the healthy pancreas, and regulate both the endocrine and exocrine compartments (Faber et al. 2020). However, relatively little is known about the role of neural populations within the TME. Interestingly, ablating sensory neurons of the thoracic dorsal root ganglion reduced PanIN progression and increased survival in a mouse model of pancreatic cancer (Saloman et al. 2016). Further, co-culturing dorsal root ganglia with $Kras^{G12D}$-expressing cells promotes sphere formation, while disrupting β-adrenergic signaling between sympathetic neurons prolongs survival in KPC mice (Renz et al. 2018). Together, these data indicate that neurons support tumor growth in PDA.

Similar to neurons, the healthy pancreas also contains an expansive network of vasculature. However, pancreatic tumors in both humans and KPC mice are hypovascularized, and this poor perfusion limits the ability of chemotherapeutic agents to effectively penetrate tumor tissue (Olive et al. 2009). One suspected cause of this poor perfusion is the abundance of dense ECM in pancreatic tumors (Jacobetz et al. 2013; Provenzano and Hingorani 2013). The

pressure exerted by this ECM has been measured at over 100 mm Hg in mouse KPC tumors, approximately 10-fold higher than healthy tissue (Provenzano et al. 2012). As a result, blood vessels collapse and the TME becomes hypoxic. This hypoxic environment alters tumor cell metabolism to promote glycolysis and glutamine metabolism, and thereby promotes tumor cell growth and proliferation (Tao et al. 2021). Clinical trials have been launched to target the ECM in order to increase vascular perfusion and more effectively deliver chemotherapy. However, a recent late phase clinical trial targeting the ECM was unsuccessful (Van Cutsem et al. 2020).

One of the most critical populations in the pancreatic TME are the immune cells. PDA has been described as an immunologically "cold" disease, whereby T cells typically do not mount an effective immune response (Vonderheide 2018). However, that is not to say that the TME lacks immune cells. In fact, pancreatic tumor cells are highly adept at recruiting and manipulating immune cells in order to create an immunosuppressive TME (Carpenter et al. 2021). As a result, tumor cells are able to avoid the cytotoxic activity of our immune system. While an increasing number of immune cell types have been described, two major immune cell lineages at the center of immunosuppression in PDA are myeloid cells and T cells.

Myeloid cells are a highly diverse group of bone-marrow derived cells, which include monocytes, macrophages, dendritic cells, granulocytes, and mast cells (Zhang et al. 2019). In the context of an infection or injury, these cells accumulate at the affected site and respond to local cues to perform a diverse array of functions to combat pathogens and remodel the tissue (Rivera et al. 2016; Del Fresno and Sancho 2021). However, these processes can become severely disrupted in the context of PDA. Within the pancreatic TME, secreted cytokines from both neoplastic cells and stromal cells "educate" myeloid cells, with the net effect of promoting an immunosuppressive phenotype (Kemp et al. 2021). Although many myeloid cell types are

involved throughout this process, two of the best-studied populations are macrophages and myeloid-derived suppressor cells (MDSCs).

Macrophages accumulate in the pancreas in pre-cancerous stages of disease (Clark et al. 2007; Velez-Delgado et al. 2022), and actively drive ADM and $Kras^{G12D}$-driven lesion formation (Liou et al. 2013; Liou et al. 2015). Macrophages expand further in the context of invasive PDA (Clark et al. 2007), where they can directly promote tumor growth, chemoresistance, immune suppression, and metastasis (Mitchem et al. 2013; Griesmann et al. 2017; Zhang et al. 2017a). Neoplastic cells in PDA are able to recruit and reprogram macrophages by secreting an array of cytokines, including CSF1 and CCL2 (Monti et al. 2003; Sanford et al. 2013; Zhu et al. 2014). Originally, macrophage polarization was described as either M1 (classically activated) or M2 (alternatively activated), with the latter being associated with immunosuppressive function and decreased survival in PDA (Biswas and Mantovani 2010; Kurahara et al. 2011). However, macrophages *in vivo* display a broad spectrum of phenotypes along this M1/M2 axis (Qian and Pollard 2010). Interestingly, macrophage polarization is directly affected by oncogenic *Kras*. Conditioned media from $Kras^{G12D}$-expressing epithelial cells causes macrophages to upregulate *Arg1*, a marker of tumor-associated macrophages (TAMs) (Zhang et al. 2017b). Further, inactivating oncogenic *Kras* expression in an inducible $Kras^{G12D}$ (iKras*) mouse model (Collins et al. 2012) reduces the relative proportion of TAM-like macrophages *in vivo* (Zhang et al. 2017b; Velez-Delgado et al. 2022). Interestingly, fibroblasts express macrophage-polarizing cytokines in an oncogenic *Kras*-dependent manner (Velez-Delgado et al. 2022), indicating that macrophage polarization is regulated by complex signaling networks among diverse cell types within the TME.

Much like macrophages, MDSCs (also known as immature myeloid cells) play an essential role in establishing the immunosuppressive environment of PDA. Neoplastic cells recruit MDSCs to the pancreatic TME by expressing GM-CSF (Bayne et al. 2012; Pylayeva-Gupta et al. 2012). MDSCs are able to directly suppress the proliferation of T cells *in vitro*, and the presence of MDSCs inversely correlates with the presence of CD8+ T cells *in vivo* (Clark et al. 2007; Bayne et al. 2012; Pylayeva-Gupta et al. 2012). Further, shRNA-mediated suppression of GM-CSF reduces MDSC infiltration, promotes CD8+ T cell accumulation, and suppresses lesion/tumor growth in mice (Pylayeva-Gupta et al. 2012), demonstrating that MDSCs play a central role in T cell suppression in PDA. MDSCs are typically divided into two subpopulations, monocytic MDSCs (Mo-MDSCs) and polymorphonuclear MDSCs (PMN-MDSC, formerly granulocytic MDSCs) (Bronte et al. 2016). In a mouse model of PDA, specifically depleting PMN-MDSCs enhances CD8+ T cell infiltration into tumors and promotes tumor cell death (Stromnes et al. 2014). In human PDA, immunosuppressive Mo-MDSCs antagonize CD3+ T cell proliferation in a STAT3-dependent manner (Trovato et al. 2019). While both populations can suppress T cells, the two populations utilize unique molecular mechanisms to drive immunosuppression (Movahedi et al. 2008; Youn et al. 2008; Raber et al. 2012).

Although these different myeloid populations have unique characteristics, it is important to note that these different cell types work in concert to promote an immunosuppressive microenvironment throughout PDA progression. To determine the collective role of myeloid cells at different stages of PDA progression, transgenic mice expressing a diphtheria toxin receptor downstream of the CD11b promoter (CD11b-DTR) (Duffield et al. 2005) have been crossed into the iKras* mouse model. Depleting myeloid cells via diptheria toxin administration prior to lesion initiation prevents the formation of PanIN lesions (Zhang et al. 2017a), and

ablating myeloid cells in established PanIN lesions leads to lesion regression (Zhang et al. 2017b). Thus, myeloid cells are required for the formation and maintenance of PanIN lesions. Depleting myeloid cells also slows the growth of established tumors and impairs the formation of implanted tumors (Zhang et al. 2017a), indicating that myeloid cells are also necessary for tumor initiation and growth. However, myeloid cells do not solely function to promote disease progression, as myeloid cells are required for tissue recovery following inactivation of oncogenic *Kras* (Zhang et al. 2017b). Thus, myeloid cells play a multitude of roles in both carcinogenesis and recovery.

T cells are a heterogeneous lineage of immune cells that perform diverse functions within the TME. The interactions between these T cell lineages and the TME have a major influence over disease progression in PDA, and are of central importance in the pursuit of effective immune therapies. The CD8+ T cell lineage in particular has been the focus of considerable research effort in the cancer field, owing to their cytotoxic capabilities. In an effective T cell response, CD8+ T cells receive target cell peptides from antigen-presenting cells (APCs) via major histocompatibility complex class-I molecules (Raskov et al. 2021). Interactions with APCs stimulate the T cell receptor and CD28 receptor on CD8+ T cells, leading to the activation of CD8+ T cells. These activated CD8+ T cells then migrate and bind to the target cell, and initiate target cell death by delivering granzymes, perforin, cathepsin C, granulysin, and Fas ligands to the target cell (Raskov et al. 2021). Activated CD8+ T cells also secrete pro-inflammatory cytokines such as IFNγ and TNFα (Farhood et al. 2019). Pharmacological agents that stimulate the cytotoxic functions of CD8+ T cells has been shown to be effective in combination therapies for melanoma, renal cell carcinoma, colorectal cancer, and lung cancer (Raskov et al. 2021). However, eliciting an effective cytotoxic T cell response has proven challenging in PDA. Very

few CD8+ T cells infiltrate pancreatic tumors (Clark et al. 2007), and a large proportion of the CD8+ T cells that infiltrate tumors express markers of T cell exhaustion (Steele et al. 2020). While the reasons behind this effect are complex, the immunosuppressive activities of multiple cell types within the TME directly and indirectly inhibit the cytotoxic capabilities of CD8+ T cells. Investigating these processes has provided new insight into the mechanisms of immunosuppression in PDA and opened up new opportunities for potential future T cell driven therapies.

One of the primary ways that cells in the TME inhibit cytotoxic T cell activity is through immune checkpoint regulators, including PD-1 and CTLA-4. PD-1 is expressed by CD8+ T cells, and binding by one of its ligands (PD-L1, PD-L2) inhibits the cytotoxic activity of CD8+ T cells and eventually drives CD8+ T cell death (Raskov et al. 2021). In PDA, PD-1 ligands are expressed by multiple cell types within the TME, including tumor cells, fibroblasts, and subsets of myeloid cells (Winograd et al. 2015; Zhang et al. 2017a; Steele et al. 2020). In parallel, CTLA-4 is expressed by CD4+ T cell populations in PDA, including regulatory T cells (Tregs), and regulates the infiltration of additional CD4+ T cells into the pancreatic TME (Bengsch et al. 2017; Steele et al. 2020). Expression of CTLA-4 can disrupt the presentation of antigens by APCs to T cells, undermining an effective T cell response (Brunner-Weinzierl and Rudd 2018). Through these immune checkpoint regulators, cells within the TME inhibit cytotoxic T cell activity.

Beyond these direct effects, immunosuppressive cells within the TME can also indirectly limit T cell function through the depletion of L-arginine. CD8+ T cells uptake extracellular L-arginine in order to support survival and antagonize tumor growth (Bronte and Zanovello 2005; Geiger et al. 2016). Myeloid cells can deplete extracellular L-arginine by expressing Arginase 1

(ARG1), thereby restricting the cytotoxic function of T cells (Rodriguez et al. 2004). Interestingly, multiple cell types can upregulate *Arg1* expression in response to changes in the pancreatic TME. Depleting Tregs via Foxp3-DTR in KC mice leads to an increase in *Arg1* expression in macrophages, fibroblasts, and epithelial cells, which coincides with an increase in PanIN lesions (Zhang et al. 2020). Thus, upregulation *Arg1* may serve as a compensatory mechanism to maintain an immunosuppressive TME during PDA progression.

Given the success of immune checkpoint inhibitors in other forms of cancer (Raskov et al. 2021), inhibitors for PD-1 and CTLA-4 have been tested in clinical trials for PDA patients. However, single agent immune checkpoint inhibitors are not effective in PDA (Royal et al. 2010; Brahmer et al. 2012) One possible explanation could be a compensatory effect by other immunosuppressive cell types within the TME. In this scenario, targeting multiple axes of immunosuppression could enable an effective cytotoxic T cell response. Consistent with this notion, evidence from mouse models indicates that targeting the immunosuppressive activity of myeloid cells in parallel makes checkpoint inhibitors more effective. Disrupting CSF1-CSF1R signaling in tumor-bearing mice reduces the infiltration of TAMs and Mo-MDSCs and limits the ability of TAMs to activate CD8+ T cells (Zhu et al. 2014). Further, CSF1-CSF1R blockade in combination with checkpoint inhibitors and gemcitabine leads to 85% tumor regression, indicative of an effective anti-tumor immune response. In addition to their direct immunosuppressive effects, myeloid cells also induce PD-L1 expression in tumor cells via EGFR-MAPK signaling (Zhang et al. 2017a). Inhibition of EGFR-MAPK signaling in combination with checkpoint inhibitors reduces implanted tumor growth in mouse models (Zhang et al. 2017a; Li et al. 2021). Thus, combination therapies targeting multiple axes of immune suppression are promising options for generating an effective T cell response in PDA.

At the center of the interactions between tumor cells and the TME are pancreatic fibroblasts. These cells are instrumental in shaping the TME of pancreatic cancer, through both direct and indirect interactions with other cell types. However, their role in PDA is complex, and includes both tumor promoting (Hwang et al. 2008; Olive et al. 2009; Kraman et al. 2010; Provenzano et al. 2012; Feig et al. 2013; Jacobetz et al. 2013; Halbrook and Lyssiotis 2017) and tumor restricting roles (Lee et al. 2014; Mathew et al. 2014b; Ozdemir et al. 2014; Rhim et al. 2014). This duality is driven, in part, by significant heterogeneity among cancer-associated fibroblasts (CAFs) in PDA (Garcia et al. 2020b; Helms et al. 2020; Biffi and Tuveson 2021). Investigating this heterogeneity has revealed novel mechanisms through which fibroblasts impact PDA progression, and has opened potential avenues for future therapies.

1.2.5 The Diverse Functions of Fibroblast Populations in PDA

The TME of PDA is densely populated by cancer-associated fibroblasts (CAFs). Originally viewed as a uniform population, a growing body of research supports the idea that CAFs are heterogenous (Biffi and Tuveson 2021), both transcriptionally and functionally within the TME. In addition to their direct effects on tumor cells, CAFs also communicate with numerous cell types within the TME, and these interactions fundamentally influence PDA progression. Both the direct and indirect functions of CAFs have been targeted clinically in PDA. However, the diverse and adaptable nature of CAFs has limited the success of these clinical trials. In this section, I will discuss the identity and function of the diverse populations of CAFs within the TME. I will also discuss the clinical efforts to target the tumor-promoting functions of CAFs.

Evidence of cancer-associated fibroblast heterogeneity in PDA began to accumulate with descriptive reports of nonuniform staining of fibroblast markers. In human and mouse PDA,

researchers found that common fibroblast markers such as αSMA, podoplanin, PDGFRα/β, fibroblast specific protein 1 (FSP1), fibroblast activating protein (FAP), and desmin varied in their staining intensity, distribution, and overlap throughout the tumor tissue (Sugimoto et al. 2006; Yuzawa et al. 2012; Feig et al. 2013; Ohlund et al. 2017; Chen et al. 2018; Djurec et al. 2018; Haeberle et al. 2018; Hirayama et al. 2018). In particular, fibroblasts immediately adjacent to tumor cells appeared distinct from their counterparts at distal locations.

Recent studies have sought to characterize these spatially distinct populations. In both KPC mice and human PDA, tumor-adjacent fibroblasts express higher levels of αSMA, while more distant fibroblasts express IL6 (Ohlund et al. 2017; Biffi et al. 2019). These populations have been named "myCAF", for myofibroblasts, given the high level of αSMA expression, and "iCAF", characterized by higher expression of inflammatory cytokines. Further, different signals appeared to drive the differentiation of each type of fibroblasts, with TGF-β promoting myCAFs and IL1/Jak-Stat driving iCAFs (Ohlund et al. 2017; Biffi et al. 2019). myCAFs are believed to be tumor restricting, consistent with earlier studies that depleted αSMA-expressing fibroblasts and observed promotion of PDA progression (Ozdemir et al. 2014). myCAFs rely on TGF-β to maintain their tumor-restraining function (Biffi et al. 2019), and removing a key source of TGF-β (via regulatory T cell depletion) leads to myCAF reprogramming, increased immunosuppression, and accelerated neoplastic progression (Zhang et al. 2020). In contrast, iCAFs have been shown to have pro-tumor activity via IL1/JAK/STAT signaling (Biffi et al. 2019). Inhibition of JAK-STAT signaling reduced the expression of inflammatory cytokines in PSCs and reduced tumor growth in KPC mice (Biffi et al. 2019).

Both myCAFs and iCAFs are conserved across PDA models, as single cell RNA sequencing analyses from the KIC model also identified an IL1-driven iCAF-like population and

a TGFβ -driven myCAF-like population (Dominguez et al. 2020). Another recent single cell RNAseq study analyzed the fibroblasts throughout PDA progression, and determined that myCAFs and iCAFs may originate from distinct populations in the healthy and early lesion stages (Hosein et al. 2019) A third antigen-presenting "apCAF" population has recently been described in both *KPC* mice as well as humans (Elyada et al. 2019). However, this latter antigen-presenting population might represent the mesothelium in pancreatic cancer (Dominguez et al. 2020). Although these different studies all identified similar subtypes of fibroblasts, the exact profile of the fibroblast groups varied depending on the specific genetic mouse model used. Notably, these CAF subsets also appear to be interconvertible *in vitro* and share a common base fibroblast program (Biffi et al. 2019; Dominguez et al. 2020). For example, inflammatory CAFs can also contribute to ECM deposition by expressing hyaluronan and collagens (Elyada et al. 2019; Dominguez et al. 2020). Thus, the boundaries between CAF different subtypes are likely fluid and context-dependent.

Pancreatic CAFs were originally thought to derive from a resident population of PSCs. However, growing data supports the possibility that multiple fibroblast populations in the healthy pancreas may contribute to the heterogeneity of CAFs (Hosein et al. 2019). For example, MSCs have been identified in healthy tissue and are expanded in neoplastic tissue, raising the possibility that MSCs can contribute to neoplastic stroma (Mathew et al. 2016; Waghray et al. 2016). It has also been suggested that some CAFs may arise in part from bone marrow derived cells (Scarlett et al. 2011), pericytes, or endothelial cells (LeBleu and Kalluri 2018). Single-cell sequencing data has also suggested that some stromal cells may arise in part from cancer cells that have transformed through epithelial-to-mesenchymal transition (EMT), though they account for a relatively small portion of the stroma (Dominguez et al. 2020). Although these populations

have been suggested to give rise to CAFs, researchers have been largely limited by a lack of effective lineage-tracing tools for these populations *in vivo*. It is therefore difficult to conclusively determine the relative contributions of these different populations to the PDA stroma.

Our group has investigated the origin of stromal fibroblasts by lineage tracing two largely distinct populations of fibroblasts present in the normal pancreas, characterized by expression of *Gli1* (a downstream effector of Hedgehog signaling) and *Hoxb6* (a homeobox gene with a known role in the embryonic pancreatic mesenchyme (Larsen et al. 2015)). We found that *Gli1*-expressing fibroblasts, localized in the perivascular region of the healthy pancreas, expand during carcinogenesis, giving rise to about half of the total stromal fibroblasts. In contrast, *Hoxb6*-expressing cells do not expand during carcinogenesis, and are sparse in neoplastic lesions (Garcia et al. 2020a). While *Gli1*+ fibroblasts seem to largely give rise to myCAFs, it does not appear that they exclusively contribute to this population. Further, the functional role of *Gli1* in this process and the role of Hedgehog signaling in the formation of myCAFs both remain unclear. Future work is required to determine the origin of the remaining stromal fibroblasts.

While our understanding of CAFs in PDA is still evolving, interactions between CAFs and the TME have already been leveraged for potential therapies. CAFs have many reported tumor-promoting functions, including metabolic support, recruitment of immunosuppressive cells, and creating a physical barrier to drugs through ECM (Halbrook and Lyssiotis 2017; Farran and Nagaraju 2019; Zhang et al. 2019). Many clinical trials have sought to improve patient survival by targeting these CAF-associated elements of the TME. However, recent data demonstrates that CAFs also have tumor-restricting roles (Lee et al. 2014; Mathew et al. 2014b; Ozdemir et al. 2014; Rhim et al. 2014), making the clinical targeting of the stroma all the more complex.

The concept of targeting pro-tumor intercellular signaling pathways has been explored therapeutically with largely negative results. A notable attempt to target CAF signaling therapeutically involved inhibiting the HH signaling pathway. Although HH inhibitor IPI-926 with chemotherapeutic gemcitabine was reported to improve survival in mouse models of PDA (Olive et al. 2009), neither IPI-926 nor GDC-0449 (Vismodegib) significantly improved survival in human patients (Kim et al. 2014; Catenacci et al. 2015; Ko et al. 2016) In addition to HH, vascular endothelial growth factor (VEGF) signaling has been targeted as a potential anti-stromal therapy. VEGF is produced by both tumor cells as well as stromal cells (Buchler et al. 2002; Masamune et al. 2008), and VEGF expression has been correlated with decreased survival in human patients (Seo et al. 2000). Clinical trials tested anti-VEGFa monoclonal antibodies (bevacizumab) and small-molecule inhibitors of VEGF receptors (Axitinib) in combination with chemotherapy, but neither strategy improved survival in human patients (Kindler et al. 2010; Kindler et al. 2011). Although it is difficult to pinpoint the exact reasons these trials failed, one underappreciated factor could be the heterogeneity of the stroma, in which distinct populations respond differently to treatment.

Researchers have also tried to target the contribution of CAFs to chemoresistance. Numerous studies have shown that CAFs can directly protect tumor cells from common therapies, including radiation and chemotherapy (Hwang et al. 2008; Mantoni et al. 2011; Chan et al. 2016; Ireland et al. 2016; Hessmann et al. 2018). Beyond these direct effects, CAF-derived ECM has been shown to support PDA through multiple mechanisms. A potential role of CAFs is to create a physical barrier, through accumulation of dense ECM which in turn drives high interstitial pressure (Heldin et al. 2004; Stylianopoulos et al. 2012). This increase in interstitial pressure has been shown to restrict blood flow and impair drug delivery to the site of the tumor (Olive et al. 2009;

Provenzano et al. 2012; Jacobetz et al. 2013). As a result, the pancreatic cancer TME is nutrient poor and hypoxic, creating an environment that is immunosuppressive and drives metabolic reprogramming and chemoresistance in cancer cells (McCarroll et al. 2014; Lyssiotis and Kimmelman 2017). Beyond these physical effects, the stroma-derived ECM can also act as a nutrient source for tumor cells (Muranen et al. 2017). A recent study demonstrated that this process relies (in part) on *NetG1* expression in CAFs, as loss of stromal *NetG1* led to reduced tumor cell survival in response to nutrient deprivation (Francescone et al. 2021). The array of tumor-supporting roles has made the ECM an attractive target for new therapies.

One particular component of the ECM, hyaluronic acid (HA), is frequently overexpressed in PDA patients (Provenzano et al. 2012; Jacobetz et al. 2013), and can promote tumor growth and facilitate drug resistance (Toole and Slomiany 2008). Depleting HA with a stabilized version of hyaluronidase (PEGPH20) in KPC mice decreased interstitial pressure, increased drug delivery to the site of the tumor, and improved survival in combination with gemcitabine (Provenzano et al. 2012; Jacobetz et al. 2013). A phase II clinical trial found a minor improvement (1 month) in progression-free survival for all patients receiving PEGPH20 alongside dual chemotherapy (Nab-paclitaxel and Gemcitabine), and a moderate benefit (4 months) for patients with high HA expression (Hingorani et al. 2018). This suggested that this might be a viable strategy specifically for HA-high patients. However, a phase III clinical trial that specifically enrolled HA-high PDA patients failed to significantly improve overall survival (Doherty et al. 2018). An alternative strategy has utilized angiotensin receptor blockers (losartan) to target HA in combination with other ECM components, specifically collagen I (Chauhan et al. 2013). Losartan reduced *Col1* and *Has1-3* expression in CAFs, leading to a decrease in collagen and HA deposition in orthotopic tumor models. This reduction in ECM led to improved tumor perfusion, and improved survival

when combined with chemotherapy (Chauhan et al. 2013). Although these pre-clinical data are encouraging, further long-term studies in spontaneous tumor models will be needed to determine if this is a potential viable strategy in the clinic.

While many of the strategies described above antagonize the pro-tumorigenic products of CAFs, some researchers have sought to reprogram CAFs into a less pro-tumorigenic, quiescent state. Both all-trans retinoic acid and a vitamin D analog (calcipotriol) have been used to reverse the "activated" state of CAFs, leading to broad transcriptional changes consistent with a shift towards a quiescent cell identity (Froeling et al. 2011; Sherman et al. 2014). KPC mice treated with these components display a decrease in αSMA, a reduction in tumor cell growth, and an increase in cell death. Further, combination therapy of calcipotriol with gemcitabine improved survival in KPC mice (Sherman et al. 2014). However, a recent study reported that calcipotriol can have an immunosuppressive effect on CD8+ T cells (Gorchs et al. 2020), which may limit the long-term efficacy of vitamin D analogs in PDA patients and might explain the generally disappointing clinical trials.

Another potential therapeutic avenue is to target the immunosuppressive activities of CAFs. Immunotherapies that utilize checkpoint inhibitors have shown minimal efficacy against pancreatic cancer, and one proposed explanation is that CAFs interfere with an effective anti-tumor immune response (Hilmi et al. 2018). Therefore, targeting the immunosuppressive functions of CAFs or depleting immunosuppressive CAF populations might make immunotherapies more effective. The *Fap*-expressing population of fibroblasts has been identified as a potential population to target, as depleting *Fap*-expressing cells via a transgenic DTR expression or transferring FAP-targeted chimeric antigen receptor T cells slowed tumor growth in both subcutaneous and KPC models (Kraman et al. 2010; Feig et al. 2013; Lo et al. 2015). Depleting

FAP+ fibroblasts in immunodeficient mice did not impact tumor growth, suggesting that the tumor-promoting role of the FAP+ CAFs is not due to direct impacts on tumor cells, but rather through manipulations of the immune response (Kraman et al. 2010; Feig et al. 2013). However, depletion of FAP+ fibroblasts systemically via DT led to a loss in muscle mass and hematopoietic cells, indicating that FAP+ depletion is not a tenable therapeutic option (Roberts et al. 2013). Fortunately, FAP+ cells secrete CXCL12, a cytokine capable of restricting CD8+ T cell infiltration via the targetable receptor CXCR4. Pharmacologic CXCR4 inhibition effectively reduced tumor growth and was especially effective when paired with an immune checkpoint inhibitor α-PD-L1 (Feig et al. 2013). Although these results are promising, the efficacy of these treatment strategies at prolonging survival in PDA is still unknown. A clinical trial investigating the combined efficacy of CXCR4 and PD-1 inhibitors in pancreatic cancer is ongoing and expected to conclude in 2023 (NCT04177810).

1.3 The Role of Hedgehog Signaling in Development and Disease

Hedgehog (HH) signaling was first described in developing larvae of *Drosophila melanogaster*. A genetic screen identified *Drosophila* larvae with disrupted body segment development (Nusslein-Volhard and Wieschaus 1980). One of the mutants displayed abnormal denticle patterning on the abdominal body segments and had a shorter and stouter body shape. As a result of these features, the locus responsible for this mutation was given the name Hedgehog (*Hh*) (Nusslein-Volhard and Wieschaus 1980). Genetic and molecular analysis of the *Hh* gene revealed that it encodes a secreted protein predicted to be the ligand in a novel signal transduction pathway (Ingham et al. 1991; Lee et al. 1992; Ingham and Hidalgo 1993; Taylor et al. 1993).

In the 40 years since its discovery, we have learned that HH signaling is an essential developmental pathway across disparate metazoan species (Matus et al. 2008; Wilson and Chuang 2010). The genes and regulatory sequences of the HH signaling pathway have evolved throughout animal speciation, contributing to some of the most striking features of animal physiology – from loss of legs in snakes to the growth of beaks in birds (Marcucio et al. 2005; Leal and Cohn 2016). Mammals are unsurprisingly no exception, and the mechanics of HH signal transduction are intimately linked to mammalian development and disease. In the following sections, I will provide an overview of HH signal transduction in mammals, with a focus on the GLI family of HH transcription factors. I will summarize how GLIs are regulated in the HH signaling pathway and discuss the roles of GLIs in mammalian development and disease.

1.3.1 Mechanisms of Hedgehog Signal Transduction in Mammals

Mammals express three HH ligands: Sonic hedgehog (*Shh*), Indian hedgehog (*Ihh*), and Desert hedgehog (*Dhh*) (Echelard et al. 1993; Krauss et al. 1993; Riddle et al. 1993). HH ligands undergo post-translational modification prior to being secreted (Briscoe and Therond 2013). This consists of a cleavage of the C-terminal domain (Bumcrot et al. 1995), followed by the addition of a cholesterol (Porter et al. 1996) and palmitic acid (Pepinsky et al. 1998) to the N-terminal peptide. Following these modifications, HH ligands are released from HH-producing cells via the activity of Dispatched (DISP) and SCUBE2 proteins (Creanga et al. 2012; Tukachinsky et al. 2012). Evidence from tissues like the developing neural tube indicate that HH ligands are secreted into the extracellular space, forming a gradient (Dessaud et al. 2008). However, HH ligand delivery through specialized filipodia has also been reported (Sanders et al. 2013; Hall et al. 2021).

In canonical HH signal transduction, HH ligands bind to the receptor Patched 1 (PTCH1). PTCH1 is a twelve-pass transmembrane protein, and in the absence of HH ligand PTCH1 inhibits downstream signal transduction (Nakano et al. 1989; Ingham et al. 1991; Chen and Struhl 1996; Marigo et al. 1996; Stone et al. 1996). Once HH-ligand binds to PTCH1, however, its inhibitory activity is repressed (Chen and Struhl 1996; Taipale et al. 2002). As a result, the G protein-coupled receptor Smoothened (SMO) becomes de-repressed, leading to the activation of downstream HH pathway components (Alcedo et al. 1996; Chen and Struhl 1996; van den Heuvel and Ingham 1996). This process of ligand binding to HH-responsive cells can be regulated by HH co-receptors, including Patched 2 (PTCH2) (Carpenter et al. 1998; Holtz et al. 2013), Hedgehog interacting protein (HHIP) (Chuang and McMahon 1999), Growth arrest-specific gene 1 (GAS1) (Lee et al. 2001; Allen et al. 2007; Martinelli and Fan 2007), Cell adhesion molecule – related/down-regulated by oncogenes (CDON) (Tenzen et al. 2006), and Brother of CDON (BOC) (Tenzen et al. 2006). Importantly, the role of these co-receptors in HH signal transduction depends largely on context. For example, the co-receptor BOC positively regulates HH signal transduction in the developing neural tube, as overexpression of *Boc* leads to an expansion of ventral neural markers into the dorsal neural tube, indicative of enhanced HH signaling (Tenzen et al. 2006; Allen et al. 2011). Further, loss of *Boc* in $Cdon^{-/-}$ or $Gas1^{-/-}$ mice exacerbates HH loss-of-function phenotypes in the developing neural tube, further supporting a positive role for BOC in regulating HH signaling (Allen et al. 2011). However, $Boc^{-/-}$ embryos display an increase in internasal separation and an upregulation of HH target gene *Gli1* in nasal processes (Echevarria-Andino and Allen 2020). These data indicate that BOC negatively regulates HH signaling in craniofacial tissue, in contrast to its role in the neural tube.

Following de-repression from PTCH1, SMO translocates to the primary cilium (Corbit et al. 2005; Rohatgi et al. 2007). The primary cilium functions as a signaling node in mammalian cells, and is of particular importance in the trafficking and regulation of HH pathway components (Goetz and Anderson 2010). In the absence of HH, SMO cycles through the cilia at a low baseline level (Ocbina and Anderson 2008), but accumulates within cilia following HH stimulation (Corbit et al. 2005; Rohatgi et al. 2007). While ciliary accumulation of SMO is necessary for HH transduction, it is not by itself sufficient, as genetically and pharmacologically inactivated forms of SMO can still accumulate in the cilium (Kim et al. 2009; Wang et al. 2009). Ultimately, accumulation of SMO at the tips of cilia leads to the activation of the GLI transcription factors.

1.3.2 Regulation and Function of GLI Transcription Factors in Hedgehog Signal Transduction

The GLI family of proteins are the transcriptional effectors of the HH signaling pathway. These proteins are conserved throughout animal evolution, as GLI family members can be found in *Drophila,* zebrafish, and mammals (Wilson and Chuang 2010). Mammals possess three GLI proteins: GLI1, GLI2, and GLI3 (Figure 1.2). Structurally, all three GLIs contain a highly conserved DNA binding domain, and recognize a shared high-affinity consensus sequence GGGTGGTC (Kinzler and Vogelstein 1990; Vortkamp et al. 1995; Hallikas et al. 2006; Vokes et al. 2007; Vokes et al. 2008; Peterson et al. 2012). All three GLIs share a C-terminal activator domain, which is required to activate HH target gene transcription (Hui and Angers 2011). While GLI1 functions solely as an activator, GLI2 and GLI3 also contain an N-terminal repressor domain, giving them dual roles as transcriptional activators (GLI-A) or repressors (GLI-R) (Dai et al. 1999; Sasaki et al. 1999). GLI2 functions primarily as an activator while GLI3 primarily

functions as a repressor (Sasaki et al. 1997; Ding et al. 1998; Sasaki et al. 1999), but the exact function of each of these proteins depends on their context. These proteins are highly regulated in both the presence and absence of active HH signaling, and this regulation directly determines the outcome of HH pathway activity in mammalian tissues.

In the absence of HH stimulation, modification of GLI proteins maintains a "HH Off" state. *Gli1* is not expressed, and therefore cannot activate HH target genes (Bai et al. 2002). In contrast, GLI2 and GLI3 are expressed, but undergo post-translational modification. SUFU binds to GLI2/GLI3 and facilitates the processing of full-length GLI into GLI-R (Humke et al. 2010). Specifically, GLI2 and GLI3 are phosphorylated by PKA, GSK3, and CK1 at a cluster of phosphorylation sites C-terminal of the zinc finger domains (Wang et al. 2000; Pan et al. 2006; Wang and Li 2006). This phosphorylation primarily leads to the degradation of GLI2, although a small fraction of GLI2 protein is cleaved into a truncated transcriptional repressor (Pan et al. 2006). Phosphorylation of GLI3 leads to the cleavage of the C-terminal activator domain, and the truncated form of GLI3 functions as a potent transcriptional repressor (Dai et al. 1999; Wang et al. 2000). Mutating this cluster of PKA phosphorylation sites prevents this phosphorylation of both GLI2 and GLI3 and prevents the formation of the truncated GLI3-R protein, indicating that PKA-mediated phosphorylation is necessary to generate the GLI3-R product (Wang et al. 2000; Niewiadomski et al. 2014). Once cleaved, GLI3-R translocates to the nucleus and suppresses HH target genes (Haycraft et al. 2005; Humke et al. 2010). GLI-R suppresses target genes though epigenetic modifications, including compaction of chromatin and removal of activating markers such as K3K27 acetylation at target gene enhancer sequences (Lex et al. 2020). In order to make these epigenetic changes, GLI-R partners with co-repressors, including histone de-acetylases (HDACs) (Lex et al. 2020), the SWI/SNF complex (Jeon and Seong 2016), and SKI (Dai et al.

2002). However, the exact mechanisms appear to be tissue-dependent, and are still not fully understood.

In the presence of HH-stimulation, this process of proteolytic cleavage/degradation is restrained, and GLI2/GLI3 are maintained as full-length proteins (Wang et al. 2000; Pan et al. 2006). Full-length GLI2 and GLI3 are trafficked to the tips of the primary cilia and released by SUFU (Endoh-Yamagami et al. 2009; Humke et al. 2010; Tukachinsky et al. 2010; Wen et al. 2010). GLI2 and GLI3 then become phosphorylated at a distinct cluster of activating sites (Humke et al. 2010; Niewiadomski et al. 2014). As a result, activated full length GLI2 and GLI3 translocate to the nucleus as full-length transcriptional activators (GLI-A) and activate the transcription of HH target genes (Humke et al. 2010; Niewiadomski et al. 2014).

Importantly, the phosphorylation and post-translational processing of GLIs relies on the primary cilium. Mice with defective cilia or impaired ciliary trafficking by intraflagellar transport (IFT) have disrupted GLI-A function and an impaired ability to form GLI-R (Haycraft et al. 2005; Huangfu and Anderson 2005; Liu et al. 2005; May et al. 2005). The processing of GLIs in cilia relies on interactions with kinesins, including the KIF7 protein and the kinesin 2 motor complex. KIF7 binds to GLI1-3 and co-localizes with GLI3 at the tips of cilia in response to HH signaling, and loss of *Kif7* impairs GLI2 and GLI3 localization at the ciliary tips (Endoh-Yamagami et al. 2009). However, loss of *Kif7* also impairs GLI processing, leading to an increase in full-length GLI2/3 and a decrease in GLI3-R (Endoh-Yamagami et al. 2009; Liem et al. 2009), suggesting that KIF7 facilitates both GLI-A as well as GLI-R processing. Similar to KIF7, components of the kinesin 2 motor complex co-localize with GLI2 and GLI3 in the cilia and bind to all three GLIs (Carpenter et al. 2015). Disrupting the interactions between GLI2 and the KAP3 subunit of the kinesin 2 complex enhances the transcriptional activity of GLI2-A *in*

vitro and *in vivo*, indicating that kinesin-2 motors regulate GLI activity by restricting GLI-A (Carpenter et al. 2015). Together, these data indicate that kinesins play an essential role in facilitating GLI processing, both in the presence and absence of HH signaling. This fine-tuned control of GLI activity is essential, as disrupted GLI function can lead to disrupted morphogenesis and disease.

1.3.3 Roles for GLI Transcription Factors in Embryogenesis and Disease

As the primary transducers of HH signaling in vertebrates, the GLI transcription factors are essential to the formation and function of HH-dependent tissues. Unsurprisingly, disruption of GLI function can have severe consequences in embryonic, pediatric, and adult tissue. In this section, I will highlight the roles of GLI1-3 in several mammalian tissues, and how abnormal GLI function has been implicated in human disease.

One of the best-studied HH-dependent tissues is the neural tube. In mice, SHH produced by the notochord induces *Shh* expression in the ventral floor plate (Echelard et al. 1993; Riddle et al. 1993). This floorplate secretion of HH ligand/SHH creates a ventral-to-dorsal gradient of HH signal, and the different levels of HH signaling drive distinct neuronal fates (Dessaud et al. 2008). Unsurprisingly, GLIs play a crucial role in transducing the graded levels of HH signaling in the neural tube. Transfecting GLI-A constructs in chick neural tubes revealed that the levels of GLI activity dictate neuronal cell fate (Stamataki et al. 2005). Constructs with high GLI-A activity expand the expression of ventral markers (FOXA2, NKX2.2) throughout the neural tube (Stamataki et al. 2005). Constructs with medium GLI-A activity and low GLI-A activity do not affect the domains of these ventral populations, but do expand the domains of motor/V2 neurons and V1/V0 neurons, respectively, into the dorsal neural tube (Stamataki et al. 2005). Interestingly, the GLI-A-driven expansion of these ventral and intermediate markers reduces the

domains of dorsal neurons (Stamataki et al. 2005), indicating that GLI-A activity promotes ventral neural identity at the expense of dorsal fates in a dose-dependent manner.

While these *Gli* overexpression experiments demonstrated the effect of ectopic levels of GLI-A, neural tube development *in vivo* involves complex and opposing activities of endogenous GLI. *Gli1* is expressed in the ventral neural tube where the levels of HH response is highest, but is dispensable for neural tube patterning (Hui et al. 1994; Sasaki et al. 1997; Park et al. 2000; Bai et al. 2002). *Gli2* is excluded from the floor plate but otherwise expressed throughout the neural tube at E9.5 (Sasaki et al. 1997; Ding et al. 1998; Bai et al. 2002), and $Gli2^{-/-}$ mice fail to form *Shh*-expressing cells in the floor plate, and the domains of NKX2.2, ISL-1/2, and SIM1 shift ventrally (Ding et al. 1998; Matise et al. 1998). In contrast, *Gli3* expression is predominantly expressed in the dorsal neural tube at E9.5 (Sasaki et al. 1997), and opposes the HH signal originating in the ventral neural tube. The *Gli3 extra-toes* (*Xt*) mouse allele eliminates endogenous *Gli3* expression (Schimmang et al. 1992; Hui and Joyner 1993), and the expression domains of intermediate neural progenitors (p1, p0, dI6: expressing NKX6.2, *Dbx2*, and DBX1) expand dorsally at the expense of dI5 (expressing *Gsh1*) dorsal progenitors in $Gli3^{Xt/Xt}$ mice (Persson et al. 2002). However, *Gli1* reporter activity is reduced in the neural tubes of E10.5 *Gli3* null mice (Bai et al. 2004), indicating an additional role for GLI3-A in the neural tube. *Gli3* cDNA knocked into the *Gli2* locus can also partially rescue neural patterning defects caused by the loss of *Gli2*, further confirming that GLI3 can fulfill an activator role *in vivo* (Bai et al. 2004). $Gli3^{Xt/Xt}$ mice also display exencephaly (Hui and Joyner 1993), a failure to close the neural tube, indicating that GLI3 regulates the patterning as well as the morphogenesis of the developing neural tube.

Beyond embryogenesis, GLI function has also been implicated in pediatric and adult cancers of neural tissue. One of the best examples of this is medulloblastoma (MB), a cancer of the cerebellum. MB most often affects children under the age of 9, and accounts for 63% of embryonal brain tumors in children and adolescents (Ostrom et al. 2018). The SHH subgroup of MB features activating mutations in the HH signaling pathway and is the most common form of MB in infants and adults (Kool et al. 2012). Amplifications of *GLI1* or *GLI2* are detected in 9% of cases (Northcott et al. 2019). Interestingly, loss of function mutations in *SUFU* account for 10% of cases (Northcott et al. 2019), indicating that aberrant activation of GLI-A is a common consequence of SHH MB cases. Unsurprisingly, the growth of patient tumor cells featuring a mutation in *SUFU* is unaffected by SMO inhibition (Kool et al. 2014). In contrast, targeting GLI through administration of arsenic trioxide reduces tumor proliferation even in cells resistant to SMO inhibitors (Kool et al. 2014). However, this effect was only seen at high concentrations of arsenic trioxide, making the specificity and clinical utility for the use of this treatment in SHH MB patients questionable.

GLI1-3 also play essential roles during limb development. *Shh* is expressed in the developing limb bud starting around E9.5 in mice (Platt et al. 1997). SHH is secreted by cells in the zone of polarizing activity (ZPA) in the posterior limb bud and forms a gradient of HH signaling along a posterior-to-anterior axis. Along this gradient, GLIs are required for proper digit specification. At E10.5 *Gli1* is expressed in the posterior limb bud immediately adjacent to the ZPA where HH signaling levels are highest (Mo et al. 1997; Platt et al. 1997) . However, *Gli1*$^{-/-}$ mice do not display any obvious limb phenotypes (Park et al. 2000). *Gli2* is expressed more broadly throughout the mesenchyme of the developing limb bud, but the loss of *Gli2* alone also does not impact digit number (Mo et al. 1997). However, *Gli1*$^{-/-}$*;Gli2*$^{-/-}$ embryos feature a

postaxial nubbin at both E15.5 and E18.5 (Park et al. 2000). Additionally, genetic loss of *Gli2* in $Gli3^{Xt/+}$ in mice enhances the digit phenotypes of $Gli3^{Xt/+}$ in mice (Mo et al. 1997), suggesting that the function of GLI2 and GLI3 may partially overlap in the developing limb. *Gli3* mRNA is expressed broadly beyond the zone of polarizing activity at E10.5 (Mo et al. 1997). However, GLI3-R protein is enriched in the anterior limb bud and comparatively lower in the posterior limb bud (Wang et al. 2000). $Gli3^{Xt/Xt}$ mice display polydactyly (Hui and Joyner 1993), but the digits that form lack clear digit identity . Interestingly, losing a single copy of *Gli3* can partially rescue the severe limb phenotypes of $Shh^{-/-}$ mice (Litingtung et al. 2002). While $Shh^{-/-}$ mice lack all digits except an occasional digit 1, $Shh^{-/-};Gli3^{Xt/+}$ mice have several digits, all resembling digit 1 (Litingtung et al. 2002; te Welscher et al. 2002). Further, $Shh^{-/-};Gli3^{Xt/Xt}$ mice phenocopy $Gli3^{Xt/Xt}$ mice, including unspecified 6-11 digits (Litingtung et al. 2002; te Welscher et al. 2002). Thus, while the formation of digits can occur in the absence of SHH, proper digit specification requires a balance between opposing SHH and GLI3 activity. Additionally, digit 1 forms fully independent of SHH, but does require the presence of GLI3 to be properly specified.

In addition to specifying the digits, GLIs also regulate long bone development in the embryonic limbs. $Gli2^{-/-}$ mutant mice feature a shortening of the long bones of the limbs and a bowing of the radius (Mo et al. 1997). In contrast, the overall lengths of $Gli3^{Xt/Xt}$ limbs are relatively normal, but the tibia is significantly reduced (Mo et al. 1997). However, losing 1 copy of *Gli3* in $Gli2^{-/-}$ mice reduces the length of all long bones, exacerbating the shortened limb phenotype of $Gli2^{-/-}$ mice (Mo et al. 1997). Taken together, GLIs appear to have a combination of individual and overlapping roles within different tissues in the developing limb.

This “extra toes” phenotype described in *Gli3* mutant mice closely resembles the limbs of humans suffering from Greig cephalopolysyndactyly syndrome (GCPS) (Hui and Joyner 1993).

GCPS has been associated with translocation/deletion of the 7p13 chromosomal region in human beings, and GCPS patients can present with an excess number of digits and fusion of the skin between digits (Williams et al. 1997). Interestingly, GCPS patients also feature craniofacial defects (Williams et al. 1997), consistent with a role for GLI3 in this tissue as well.

Within endoderm tissues, GLIs are necessary for proper regulation of HH signaling. In the primitive gut tube, SHH and IHH are expressed in the gut epithelium starting at E8.5 (Echelard et al. 1993; Bitgood and McMahon 1995). In the developing intestine, these ligands signal in a paracrine manner to the underlying mesenchyme (Ramalho-Santos et al. 2000; Kolterud et al. 2009). HH signaling regulates multiple facets of intestinal development, including left-right patterning of gut organs, intestinal growth, and specification of neural crest cells (Walton and Gumucio 2021). This paracrine HH signaling causes mesenchymal clusters to form starting at E14.5 (Walton et al. 2012). These mesenchymal clusters serve as the locations for intestinal villi to form, and inhibition of HH signaling in intestinal cultures prevents villus formation (Walton et al. 2012). Interestingly, driving excessive HH signaling increases the width of both mesenchymal clusters and villi (Walton et al. 2012), indicating that proper villus morphogenesis requires carefully regulated levels of HH signaling.

Gli1 and *Gli2* are expressed broadly in the intestinal mesenchyme throughout gut development and are maintained in the adult intestine (Ramalho-Santos et al. 2000; Kolterud et al. 2009). In contrast, *Gli3* is only strongly expressed in the mesenchyme during a brief window around E12.5, and is expressed minimally at other stages of intestinal development (Kolterud et al. 2009). Consistent with its minimal expression, conditionally deleting *Gli3* in the intestinal mesenchyme does not impact intestinal development (Huang et al. 2013). In contrast, ectopic expression of *Gli2* is able to fully rescue villus formation in the absence of canonical HH

signaling (Huang et al. 2013). Thus, a GLI2-mediated transcriptional program drives villus formation, potentially by activating *Foxf1* and *Foxl1* genes (Madison et al. 2009). Recent data supports this hypothesis, as mice with impaired GLI processing and impaired GLI degradation (*Sufu;Spop* conditional knock-out) express higher levels of GLI2 and display a thickened intestinal mesenchyme (Coquenlorge et al. 2019). Analysis of GLI binding sites in this study supports GLI2-mediated expression of *Foxf1* and *Foxl1*, and further indicates that GLI2 may regulate the expression of *Wnt* ligands to supporting villus growth (Coquenlorge et al. 2019).

Abnormal GLI function has been associated with multiple diseases in the intestine. A germline variation in *GLI1* with impaired transcriptional activity has been associated with inflammatory bowel disease in human patients (Lees et al. 2008). Similarly, $Gli1^{lacZ/+}$ mice display enhanced inflammation and epithelial damage in response to chemically-induced colitis (Lees et al. 2008). Further, genetically or pharmacologically activating HH signaling in mice reduces colitis severity and prolongs survival (Lee et al. 2016). Together, these data indicate that impaired GLI function increases the susceptibility of intestinal tissue to inflammatory disorders.

Disrupted *GLI* function has also been linked to an enteric neuron disorder in humans known as Hirschsprung Disease. A subset of Hirschsprung patients have missense mutations in *GLI1, GLI2*, or *GLI3*, and these mutations enhance GLI-A activity *in vitro* (Liu et al. 2015). Excessive GLI-A (through *Sufu* deletion) in mice causes excessive differentiation and disorganized migration of neural crest cells, suggesting that the disrupted enteric neurons of Hirschsprung patients could be due in part to excessive GLI activity (Liu et al. 2015).

Dysregulation of GLI function can lead to developmental disorders and cancer in organ systems throughout the body, highlighting the importance of these proteins in regulating HH signaling. However, the roles of GLI1-3 in some tissues, like the pancreas, still remain poorly

understood. This is particularly true for PDA, a disease which features aberrant activation of HH signaling. In the next section, we will discuss our understanding of HH signaling in pancreatic cancer.

1.4 The Roles of Hedgehog Signaling in Pancreatic Cancer

The first evidence that HH signaling might be involved in pancreatic cancer came from human patients. Human PDA cell lines express *SHH* and *IHH* ligands, and SHH protein is present in both pre-invasive lesions as well as invasive tumor cells *in vivo* (Berman et al. 2003; Thayer et al. 2003) This expression of HH ligands is dependent on oncogenic *Kras,* as inactivation of $Kras^{G12D}$ in iKras* mice reduces *Shh* expression (Collins et al. 2012). While tumor cells express some HH pathway components, they are unable to respond canonically to HH stimulation (Yauch et al. 2008; Nolan-Stevaux et al. 2009; Tian et al. 2009). Instead, these HH ligands signal exclusively to fibroblasts in the surrounding stroma (Figure 1.3), which upregulate classic HH target genes (Yauch et al. 2008; Nolan-Stevaux et al. 2009; Tian et al. 2009). In addition to these HH targets, preoteomic analysis has revealed that $Kras^{G12D}$-driven SHH expression initiates a vast network of reciprocal signaling, wherein fibroblasts receiving HH ligand from tumors secrete an array of factors back to tumor cells (Tape et al. 2016). These reciprocal signals from fibroblasts drive additional AKT activity in tumor cells, which supports processes including protein translation, mitochondrial function, and DNA replication (Tape et al. 2016). While this paracrine model is well-established, the exact role of HH signaling in PDA has remained controversial.

Initially, HH signaling was believed to promote pancreatic tumor growth. Reports indicated that epithelial cells over-expressing *Shh* promote tumor growth, while inhibition of HH signaling (via cyclopamine or anti-SHH 5E1 antibody) reduces tumor cell growth (Berman et al.

2003; Thayer et al. 2003; Morton et al. 2007; Bailey et al. 2008; Bailey et al. 2009). Further, the combined treatment with a HH-inhibitor (IPI-926) and gemcitabine was reported to increase tumor perfusion, improve chemotherapy delivery to the tumor, and improve survival (Olive 2009). These promising results suggested that the use of HH-inhibitors clinically might be a promising avenue for PDA treatment. Multiple clinical trials were launched to test the role of HH-inhibitors in combination with chemotherapy in PDA patients. Unfortunately, HH-inhibitors failed to significantly improve patient survival (Kim et al. 2014; Catenacci et al. 2015). In fact, in one trial it was noted that the patients who received HH inhibitors experienced higher lethality than the control group, leading to the cancellation of the clinical trial.

The failure of HH inhibitors in the clinic called in to question what role HH signaling plays in PDA. In the following years, new evidence indicated that disruption of HH signaling can accelerate disease progression. One study demonstrated that conditional deletion of *Shh* in KPC mice leads to poorly differentiated tumors, featuring reduced αSMA+ fibroblasts and increased tumor cell proliferation (Rhim et al. 2014). Further, this study also showed that both *Shh* deletion and gemcitabine/IPI-926 treatment shortens survival in KPC (Rhim et al. 2014), in direct conflict with prior data (Olive et al. 2009). An independent study came to similar conclusions in a different model. KIC mice treated with the HH-inhibitor vismodegib display increased tumor growth and shortened survival compared to vehicle-treated mice (Lee et al. 2014). Interestingly, this group also determined that pharmacological activation of HH signaling via SAG21k increases stromal proliferation and decreases epithelial proliferation/PanIN abundance. Together, these data indicate that HH signaling can have tumor-restricting roles in PDA.

While these data partially explained why clinical trials failed, they did not resolve the conflicting reports of tumor-promoting and tumor-restricting roles for HH signaling in PDA.

However, one important caveat to these studies is that they reduce, but not fully ablate HH signaling. *Ihh* expression is maintained in KPC lacking *Shh* (Rhim et al. 2014), enabling a HH response in fibroblasts. Further, vismodegib-treated KIC mice retain a small population of *Gli1*+ cells in the stroma (Lee et al. 2014), indicating that a low level of HH response persists in these mice. It is therefore possible that different levels of HH response can have different effects on tumor growth. To test this directly, fibroblasts lacking HH co-receptors *Gas1*, *Cdon*, and *Boc* were utilized in tumor implantation studies. Deleting two of these co-receptors reduces the levels of HH signaling, while deletion of all three leads to near-complete elimination of a HH response (Allen et al. 2011). WT fibroblasts co-implanted with tumor cells promote tumor growth, and this promotion is enhanced with $Gas1^{-/-};Boc^{-/-}$ fibroblasts (Mathew et al. 2014b). In contrast, $Gas1^{-/-};Boc^{-/-};Cdon^{-/-}$ fibroblasts fail to promote tumor growth, and the resulting tumors are equivalent in size to tumor cells injected alone (Mathew et al. 2014b). These data indicate that inhibiting HH signaling can restrict tumor growth, but only in the context of highly effective inhibition. Consistent with this idea, KPC tumor cells that lack effective *Ihh* and *Shh* expression have reduced growth in $Gli1^{lacZ/+}$ hosts (Steele et al. 2021). In spontaneous KPC tumors, administration of SMO inhibitor LDE225 fully eliminates *Gli1* expression, and this highly effective inhibition coincides with reduced tumor growth (Steele et al. 2021). Together, these data support a model in which the role of HH signaling in PDA depends on the levels of HH-response. Reducing HH response (loss of one ligand, incomplete pharmacological inhibition, or deletion of two co-receptors) promotes tumor progression, while near complete abrogation of HH signaling (deletion of three co-receptors, total pharmacological inhibition) restrains it.

Beyond affecting tumor growth, HH signaling is also intimately linked with the TME. One compartment of particular clinical interest is the vasculature. As discussed above, the high

interstitial pressure of pancreatic tumors collapses vasculature, limiting the perfusion of therapeutic agents into the tumors (Provenzano et al. 2012; Jacobetz et al. 2013). One clinical strategy currently being explored is whether treatments that increase vascular perfusion of tumors can improve drug delivery and survival in PDA patients. The pre-clinical study testing IPI-926 in combination with gemcitabine in KPC mice found that IPI-926-treatment temporarily improves endothelial abundance and drug delivery (Olive et al. 2009). This increase in vessel density was consistently observed in later studies, both in *Shh*-deleted as well as IPI-926 treated KPC (Lee et al. 2014; Rhim et al. 2014). However, KPC mice treated with LDE225 show no difference in tumor vasculature compared to vehicle-treated controls, and fibroblasts isolated from LDE225-treated KPC tumors express less *Angpt4* and *Vegfa* (Steele et al. 2021). This discrepancy might again reflect a difference in HH signaling levels. In line with this idea, *Gas1*$^{-/-}$*;Boc*$^{-/-}$ fibroblasts (reduced HH response) promote angiogenesis in tumor implantation experiments, while *Gas1*$^{-/-}$*;Boc*$^{-/-}$*;Cdon*$^{-/-}$ fibroblasts (ablated HH response) do not (Mathew et al. 2014b). Thus, distinct levels of HH signaling drive changes in multiple compartments in the TME.

In addition to affecting vasculature, growing evidence indicates that HH signaling regulates immune infiltration in the TME. Following activation of oncogenic *Kras* for 3 weeks, iKras* mice lacking one copy of *Gli1* (iKras*;*Gli1*$^{lacZ/+}$) express reduced levels of *Il6*, *Ccl2* (aka *Mcp-1*), *Cxcl15* (aka *mIL8*), and *Csf1* (aka *M-csf*) when compared to iKras* mice (Mathew et al. 2014a). Treating pancreatic fibroblasts with HH-inhibitors mitigates the expression of these cytokines in response to tumor-conditioned media (Mathew et al. 2014a). Further, chromatin immunoprecipitation (ChIP) analysis has revealed that GLI1 binds to an array of cytokine

promoter sequences (Mills et al. 2013; Mathew et al. 2014a; Mills et al. 2014), indicating that canonical HH signaling regulates cytokine expression by fibroblasts.

To widely assess the contribution of HH signaling to immune infiltration in PDA, immune populations have been analyzed with cytometry by time-of-flight (CyTOF) in LDE225 vs. vehicle treated KPC mice. Eliminating HH signaling in tumor-bearing KPC mice promotes immunosuppressive immune cell infiltration (Steele et al. 2021). Specifically, LDE225 treatment leads to an increase in immunosuppressive macrophages (PD-L1+ and CD206+ populations), Mo-MDSCs, and Tregs, while reducing the relative abundance of CD8+ T cells (Steele et al. 2021). Interestingly, these changes in immune infiltration coincide with a shift in fibroblast populations: a relative decrease in myCAFs and an increase in iCAFs (Steele et al. 2021). Together, these indicate indicating that HH signaling regulates fibroblast-immune crosstalk during PDA progression.

The broad impacts of HH signaling throughout the TME are striking, particularly considering that canonical HH signaling is restricted to fibroblasts. However, despite the extensive research exploring the roles of ligands and receptors in PDA, comparatively little is known about how HH signaling in PDA is regulated on a transcriptional level. Specifically, the roles of GLI1-3 in PDA remain poorly understood. Given that these proteins are the transcriptional effectors of the HH signaling pathway, uncovering their individual and combined functions is essential to fully elucidating the role of HH in PDA.

In the context of PDA, most of the data surrounding the role of GLIs has focused on GLI1. As described above, GLI1 has been shown to regulate the expression of cytokines in pancreatic fibroblasts (Mills et al. 2013; Mathew et al. 2014a; Mills et al. 2014). In addition to these roles in immune regulation, GLI1 also regulates multiple stages of disease progression.

Genetic loss of *Gli1* in KC mice restrains spontaneous PanIN progression and prevents the formation of high grade PanIN lesions (Mills et al. 2013), while *Gli1*$^{-/-}$;KPC mice display more rapid lesion formation and reduced survival (Mills et al. 2014). These data indicate that GLI1 may play opposing roles at pre-cancerous vs. PDA stages of tumor progression. Interestingly, GLI1 also appears to play a role in recovery from *Kras*^{G12D}-driven lesions. iKras* and *Gli1*$^{+/-}$;iKras* mice form comparable PanIN lesions after 3 weeks of oncogenic *Kras* expression (Mathew et al. 2014a). Following inactivation of oncogenic *Kras,* iKras* mice are largely able to recover within 2 weeks, whereas *Gli1*$^{+/-}$;iKras* mice have enduring lesions and fibrosis (Mathew et al. 2014a). Thus, GLI1 has multifaceted roles in the context of neoplasia, in both disease development as well as tissue recovery

While multiple roles have been identified for GLI1, the roles of GLI2 and GLI3 in HH signal transduction during PDA progression are virtually unknown. The few roles that have been described for GLI2 and GLI3 in PDA are in the context of non-canonical HH signaling. For example, conditionally deleting *Smo* in pancreatic fibroblasts effectively eliminates HH response to SHH stimulation (Liu et al. 2016). Despite this lack of canonical HH response, these fibroblasts upregulate *Gli2,* and promote tumor growth through GLI2-mediated upregulation of *Tgfα* (Liu et al. 2016). In addition to fibroblasts, non-canonical GLI activity can also affect epithelial cells. Expressing ectopic *Gli1* or a constitutively active form of *Gli2* (*Gli2ΔN*) in epithelial cells accelerates PanIN lesion formation in *Kras*^{G12D}-expressing mice (Pasca di Magliano et al. 2006; Rajurkar et al. 2012). Further, treating human PDA cell lines with a shRNA targeting *GLI1* increases tumor cell apoptosis and reduces colony formation (Nolan-Stevaux et al. 2009). Aberrant activation of GLI by tumor cells has also been associated with changing tumor subtype identity. Expression analysis of human PDA cell lines revealed that

tumor cells with a basal-like phenotype upregulate *GLI2* independent from *SHH* expression (Adams et al. 2019). Over-expressing *GLI2* in classical-like tumor cells leads to the upregulation of EMT-related genes and a downregulation of epithelial markers (Adams et al. 2019), indicating that non-canonical *GLI2* activity can induce a basal-like phenotype in tumor cells. While driving ectopic GLI-A in epithelial cells can support PDA, ectopic GLI-R cells can suppress PDA progression. Expressing a transgenic, constitutive repressor form of GLI3 (*Gli3-T*) in KC mice reduces spontaneous PanIN formation, and prolongs survival in KPC mice (Rajurkar et al. 2012).

Although these studies reveal striking effects of GLI activity on tumor cell progression, they rely heavily on the use of immortalized cancer cell lines or transgenic overexpression models. Since the consequences of GLI activity are highly dependent on the levels of GLI-A versus GLI-R, these data may not be reflective of endogenous GLI function during PDA progression *in vivo*. Further, these data describe roles for GLIs independent of HH stimulation. Since canonical HH signaling is a pervasive feature of human PDA (Jones et al. 2008), the role of endogenous GLI1-3 in mediating HH signaling remains an essential, unanswered question.

1.5 Conclusion

The GLI family of transcription factors play diverse roles in transducing HH signaling in embryogenesis as well as disease. While aberrant HH signaling is common in PDA, the roles of GLI1, GLI2, and GLI3 in the pancreas remain poorly understood. In this dissertation, my main objectives were to: 1) Determine the contribution of GLI1-3 to disease progression in PDA, and 2) Investigate the roles of GLI1-3 in pancreas development. Chapter two will determine the expression and function of GLI1-3 in pancreatic fibroblasts during PDA progression. In this chapter, I demonstrate that *Gli1*, *Gli2,* and *Gli3* are expressed by pancreatic fibroblasts in both mouse models of PDA as well as human PDA patients. I also show that GLIs regulate immune

cell infiltration during PDA progression, and that GLI-mediated effects on immune cells determine tumor growth. Chapter three describes the roles of GLI transcription factors during pancreas development. Specifically, I demonstrate that *Gli2* and *Gli3* are expressed extensively throughout the mesenchyme of the developing pancreas. I also provide evidence that fibroblast-specific GLI3 regulates pancreas organogenesis, as deleting mesenchymal *Gli3* disrupts pancreas morphology. In Chapter 4, I summarize my findings and discuss how these data shape our understanding of HH signaling in the pancreas. I also propose potential future directions for this work. Overall, the data presented in this thesis indicate that the GLIs are essential regulators of the pancreas microenvironment, and combinatorial GLI activity regulates pancreas development and disease progression.

1.6 Figures

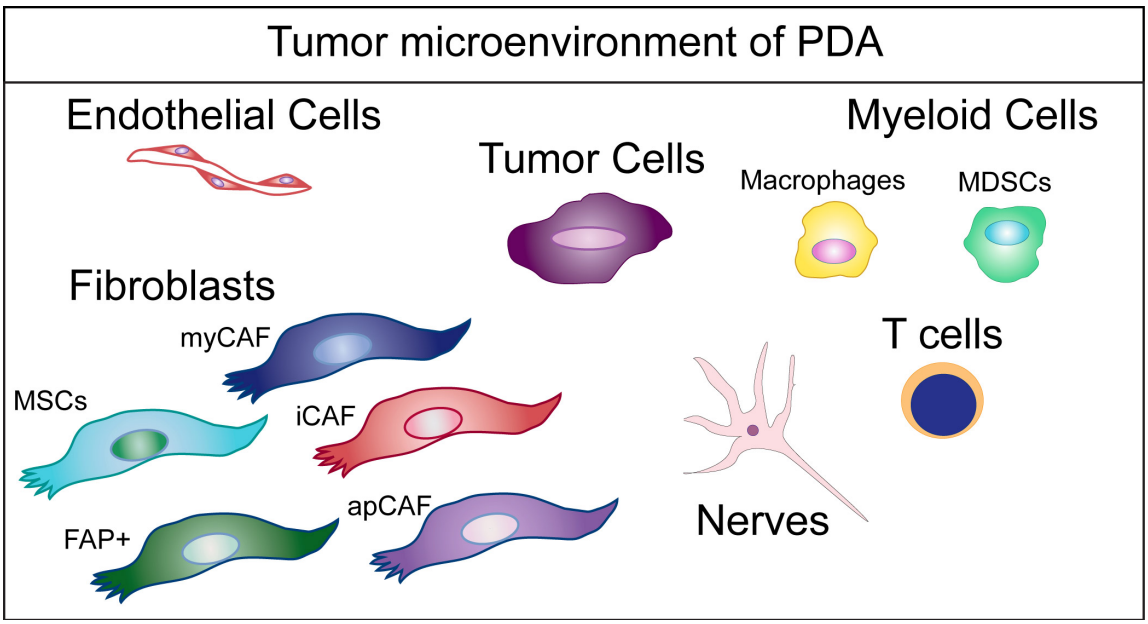

Figure 1.1 Tumor microenvironment of PDA.
Cell types found in the TME, including tumor cells, fibroblasts (myCAFs, iCAFs, apCAFs, MSCs, and FAP+ populations), nerves, myeloid cells (macrophages and MDSCs), and T cells.

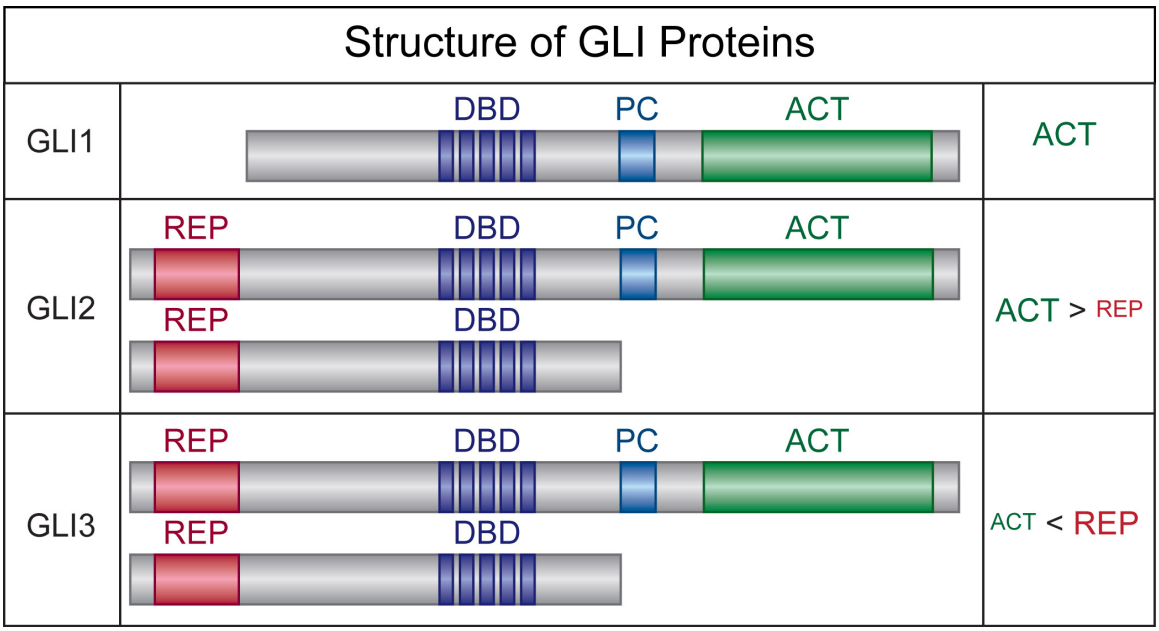

Figure 1.2 Structure of GLI proteins.
All three GLI proteins include a DNA binding domain (DBD), a phosphorylation cluster (PC), and a C-terminal activator domain (ACT). GLI1 (Top panel) functions exclusively as an activator, while GLI2 (Middle panel) and GLI3 (Bottom panel) both possess an N-terminal repressor domain, giving them dual functions as transcriptional activators or repressors. In the absence of HH signaling, GLI2 and GLI3 are phosphorylated at their phosphorylation cluster, leading to either their degradation or proteolytic processing into a truncated repressor. GLI2 primarily acts as an activator, while GLI3 primarily acts as a repressor.

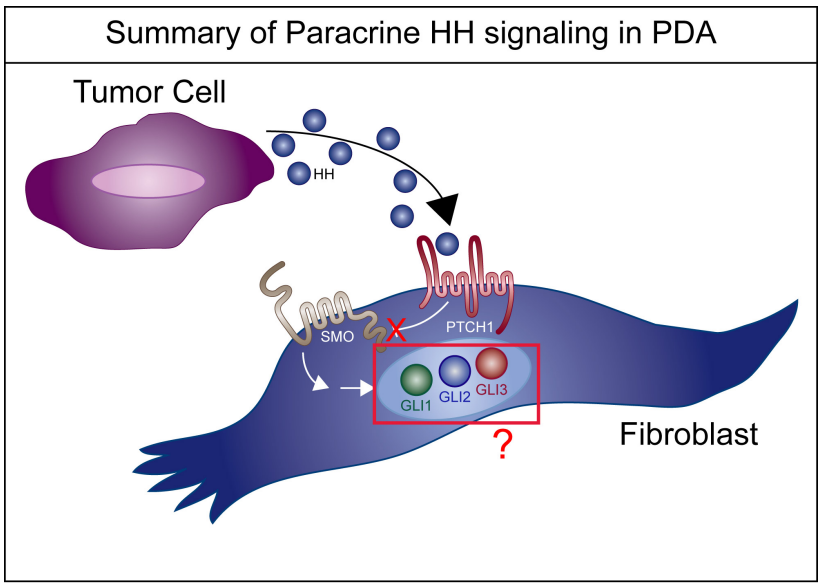

Figure 1.3 Summary of Paracrine HH signaling in PDA.
HH Ligands (SHH and IHH) are secreted by tumor cells and signal exclusively to the surrounding fibroblasts. HH ligands bind to the inhibitory receptor PTCH1, leading to its inactivation. In canonical HH signaling, the inactivation of PTCH1 leads to the de-repression of SMO, which leads to activation of GLI transcription factors. Activated GLIs then translocate to the nucleus, where they activate HH target genes. However, the role of GLIs in the context of PDA remains largely unknown.

1.7 References

Adams CR, Htwe HH, Marsh T, Wang AL, Montoya ML, Subbaraj L, Tward AD, Bardeesy N, Perera RM. 2019. Transcriptional control of subtype switching ensures adaptation and growth of pancreatic cancer. *Elife* **8**.

Aguirre AJ, Bardeesy N, Sinha M, Lopez L, Tuveson DA, Horner J, Redston MS, DePinho RA. 2003. Activated Kras and Ink4a/Arf deficiency cooperate to produce metastatic pancreatic ductal adenocarcinoma. *Genes Dev* **17**: 3112-3126.

Alcedo J, Ayzenzon M, Von Ohlen T, Noll M, Hooper JE. 1996. The Drosophila smoothened Gene Encodes a Seven-Pass Membrane Protein, a Putative Receptor for the Hedgehog Signal. *Cell* **86**: 221-232.

Allen BL, Song JY, Izzi L, Althaus IW, Kang JS, Charron F, Krauss RS, McMahon AP. 2011. Overlapping roles and collective requirement for the coreceptors GAS1, CDO, and BOC in SHH pathway function. *Dev Cell* **20**: 775-787.

Allen BL, Tenzen T, McMahon AP. 2007. The Hedgehog-binding proteins Gas1 and Cdo cooperate to positively regulate Shh signaling during mouse development. *Genes Dev* **21**: 1244-1257.

Almaca J, Weitz J, Rodriguez-Diaz R, Pereira E, Caicedo A. 2018. The Pericyte of the Pancreatic Islet Regulates Capillary Diameter and Local Blood Flow. *Cell Metab* **27**: 630-644 e634.

Apte MV, Haber PS, Applegate TL, Norton ID, McCaughan GW, Korsten MA, Pirola RC, Wilson JS. 1998. Periacinar stellate shaped cells in rat pancreas: identification, isolation, and culture. *Gut* **43**: 128-133.

Apte MV, Haber PS, Darby SJ, Rodgers SC, McCaughan GW, Korsten MA, Pirola RC, Wilson JS. 1999. Pancreatic stellate cells are activated by proinflammatory cytokines: implications for pancreatic fibrogenesis. *Gut* **44**: 534-541.

Apte MV, Park S, Phillips PA, Santucci N, Goldstein D, Kumar RK, Ramm GA, Buchler M, Friess H, McCarroll JA et al. 2004. Desmoplastic reaction in pancreatic cancer: role of pancreatic stellate cells. *Pancreas* **29**: 179-187.

Apte MV, Wilson JS. 2012. Dangerous liaisons: pancreatic stellate cells and pancreatic cancer cells. *J Gastroenterol Hepatol* **27 Suppl 2**: 69-74.

Bachem MG, Schneider E, Groß H, Weidenbach H, Schmid RM, Menke A, Siech M, Beger H, Grünert A, Adler G. 1998. Identification, culture, and characterization of pancreatic stellate cells in rats and humans. *Gastroenterology* **115**: 421-432.

Baertschiger RM, Bosco D, Morel P, Serre-Beinier V, Berney T, Buhler LH, Gonelle-Gispert C. 2008. Mesenchymal stem cells derived from human exocrine pancreas express transcription factors implicated in beta-cell development. *Pancreas* **37**: 75-84.

Bai CB, Auerbach W, Lee JS, Stephen D, Joyner AL. 2002. Gli2, but not Gli1, is required for initial Shh signaling and ectopic activation of the Shh pathway. *Development* **129**: 4753-4761.

Bai CB, Stephen D, Joyner AL. 2004. All Mouse Ventral Spinal Cord Patterning by Hedgehog Is Gli Dependent and Involves an Activator Function of Gli3. *Developmental Cell* **6**: 103-115.

Bailey JM, Hendley AM, Lafaro KJ, Pruski MA, Jones NC, Alsina J, Younes M, Maitra A, McAllister F, Iacobuzio-Donahue CA et al. 2016. p53 mutations cooperate with oncogenic Kras to promote adenocarcinoma from pancreatic ductal cells. *Oncogene* **35**: 4282-4288.

Bailey JM, Mohr AM, Hollingsworth MA. 2009. Sonic hedgehog paracrine signaling regulates metastasis and lymphangiogenesis in pancreatic cancer. *Oncogene* **28**: 3513-3525.

Bailey JM, Swanson BJ, Hamada T, Eggers JP, Singh PK, Caffery T, Ouellette MM, Hollingsworth MA. 2008. Sonic hedgehog promotes desmoplasia in pancreatic cancer. *Clin Cancer Res* **14**: 5995-6004.

Bakhti M, Bottcher A, Lickert H. 2019. Modelling the endocrine pancreas in health and disease. *Nat Rev Endocrinol* **15**: 155-171.

Baron M, Veres A, Wolock SL, Faust AL, Gaujoux R, Vetere A, Ryu JH, Wagner BK, Shen-Orr SS, Klein AM et al. 2016. A Single-Cell Transcriptomic Map of the Human and Mouse Pancreas Reveals Inter- and Intra-cell Population Structure. *Cell Syst* **3**: 346-360 e344.

Bayne LJ, Beatty GL, Jhala N, Clark CE, Rhim AD, Stanger BZ, Vonderheide RH. 2012. Tumor-derived granulocyte-macrophage colony-stimulating factor regulates myeloid inflammation and T cell immunity in pancreatic cancer. *Cancer Cell* **21**: 822-835.

Bengsch F, Knoblock DM, Liu A, McAllister F, Beatty GL. 2017. CTLA-4/CD80 pathway regulates T cell infiltration into pancreatic cancer. *Cancer Immunol Immunother* **66**: 1609-1617.

Berman DM, Karhadkar SS, Maitra A, Montes De Oca R, Gerstenblith MR, Briggs K, Parker AR, Shimada Y, Eshleman JR, Watkins DN et al. 2003. Widespread requirement for Hedgehog ligand stimulation in growth of digestive tract tumours. *Nature* **425**: 846-851.

Biffi G, Oni TE, Spielman B, Hao Y, Elyada E, Park Y, Preall J, Tuveson DA. 2019. IL1-Induced JAK/STAT Signaling Is Antagonized by TGFbeta to Shape CAF Heterogeneity in Pancreatic Ductal Adenocarcinoma. *Cancer Discov* **9**: 282-301.

Biffi G, Tuveson DA. 2021. Diversity and Biology of Cancer-Associated Fibroblasts. *Physiol Rev* **101**: 147-176.

Biswas SK, Mantovani A. 2010. Macrophage plasticity and interaction with lymphocyte subsets: cancer as a paradigm. *Nat Immunol* **11**: 889-896.

Bitgood MJ, McMahon AP. 1995. Hedgehog and Bmp genes are coexpressed at many diverse sites of cell-cell interaction in the mouse embryo. *Dev Biol* **172**: 126-138.

Brahmer JR, Tykodi SS, Chow LQ, Hwu WJ, Topalian SL, Hwu P, Drake CG, Camacho LH, Kauh J, Odunsi K et al. 2012. Safety and activity of anti-PD-L1 antibody in patients with advanced cancer. *N Engl J Med* **366**: 2455-2465.

Briscoe J, Therond PP. 2013. The mechanisms of Hedgehog signalling and its roles in development and disease. *Nat Rev Mol Cell Biol* **14**: 416-429.

Brissova M, Shostak A, Shiota M, Wiebe PO, Poffenberger G, Kantz J, Chen Z, Carr C, Jerome WG, Chen J et al. 2006. Pancreatic islet production of vascular endothelial growth factor--a is essential for islet vascularization, revascularization, and function. *Diabetes* **55**: 2974-2985.

Bronte V, Brandau S, Chen SH, Colombo MP, Frey AB, Greten TF, Mandruzzato S, Murray PJ, Ochoa A, Ostrand-Rosenberg S et al. 2016. Recommendations for myeloid-derived suppressor cell nomenclature and characterization standards. *Nat Commun* **7**: 12150.

Bronte V, Zanovello P. 2005. Regulation of immune responses by L-arginine metabolism. *Nat Rev Immunol* **5**: 641-654.

Brunner-Weinzierl MC, Rudd CE. 2018. CTLA-4 and PD-1 Control of T-Cell Motility and Migration: Implications for Tumor Immunotherapy. *Front Immunol* **9**: 2737.

Buchler P, Reber HA, Buchler MW, Friess H, Hines OJ. 2002. VEGF-RII influences the prognosis of pancreatic cancer. *Ann Surg* **236**: 738-749; discussion 749.

Bumcrot DA, Takada R, McMahon AP. 1995. Proteolytic processing yields two secreted forms of sonic hedgehog. *Mol Cell Biol* **15**: 2294-2303.

Burris HA, 3rd, Moore MJ, Andersen J, Green MR, Rothenberg ML, Modiano MR, Cripps MC, Portenoy RK, Storniolo AM, Tarassoff P et al. 1997. Improvements in survival and clinical benefit with gemcitabine as first-line therapy for patients with advanced pancreas cancer: a randomized trial. *J Clin Oncol* **15**: 2403-2413.

Buscail L, Bournet B, Cordelier P. 2020. Role of oncogenic KRAS in the diagnosis, prognosis and treatment of pancreatic cancer. *Nat Rev Gastroenterol Hepatol* **17**: 153-168.

Callahan MK, Kluger H, Postow MA, Segal NH, Lesokhin A, Atkins MB, Kirkwood JM, Krishnan S, Bhore R, Horak C et al. 2018. Nivolumab Plus Ipilimumab in Patients With

Advanced Melanoma: Updated Survival, Response, and Safety Data in a Phase I Dose-Escalation Study. *J Clin Oncol* **36**: 391-398.

Carpenter BS, Barry RL, Verhey KJ, Allen BL. 2015. The heterotrimeric kinesin-2 complex interacts with and regulates GLI protein function. *J Cell Sci* **128**: 1034-1050.

Carpenter D, Stone DM, Brush J, Ryan A, Armanini M, Frantz G, Rosenthal A, de Sauvage FJ. 1998. Characterization of two patched receptors for the vertebrate hedgehog protein family. *Proc Natl Acad Sci U S A* **95**: 13630-13634.

Carpenter E, Nelson S, Bednar F, Cho C, Nathan H, Sahai V, di Magliano MP, Frankel TL. 2021. Immunotherapy for pancreatic ductal adenocarcinoma. *J Surg Oncol* **123**: 751-759.

Catenacci DV, Junttila MR, Karrison T, Bahary N, Horiba MN, Nattam SR, Marsh R, Wallace J, Kozloff M, Rajdev L et al. 2015. Randomized Phase Ib/II Study of Gemcitabine Plus Placebo or Vismodegib, a Hedgehog Pathway Inhibitor, in Patients With Metastatic Pancreatic Cancer. *J Clin Oncol* **33**: 4284-4292.

Chan TS, Hsu CC, Pai VC, Liao WY, Huang SS, Tan KT, Yen CJ, Hsu SC, Chen WY, Shan YS et al. 2016. Metronomic chemotherapy prevents therapy-induced stromal activation and induction of tumor-initiating cells. *J Exp Med* **213**: 2967-2988.

Chauhan VP, Martin JD, Liu H, Lacorre DA, Jain SR, Kozin SV, Stylianopoulos T, Mousa AS, Han X, Adstamongkonkul P et al. 2013. Angiotensin inhibition enhances drug delivery and potentiates chemotherapy by decompressing tumour blood vessels. *Nat Commun* **4**: 2516.

Chen Y, LeBleu VS, Carstens JL, Sugimoto H, Zheng X, Malasi S, Saur D, Kalluri R. 2018. Dual reporter genetic mouse models of pancreatic cancer identify an epithelial-to-mesenchymal transition-independent metastasis program. *EMBO Mol Med* **10**.

Chen Y, Struhl G. 1996. Dual Roles for Patched in Sequestering and Transducing Hedgehog. *Cell* **87**: 553-563.

Chu LC, Goggins MG, Fishman EK. 2017. Diagnosis and Detection of Pancreatic Cancer. *Cancer J* **23**: 333-342.

Chuang PT, McMahon AP. 1999. Vertebrate Hedgehog signalling modulated by induction of a Hedgehog-binding protein. *Nature* **397**: 617-621.

Clark CE, Hingorani SR, Mick R, Combs C, Tuveson DA, Vonderheide RH. 2007. Dynamics of the immune reaction to pancreatic cancer from inception to invasion. *Cancer Res* **67**: 9518-9527.

Collins MA, Bednar F, Zhang Y, Brisset JC, Galban S, Galban CJ, Rakshit S, Flannagan KS, Adsay NV, Pasca di Magliano M. 2012. Oncogenic Kras is required for both the initiation and maintenance of pancreatic cancer in mice. *J Clin Invest* **122**: 639-653.

Commisso C, Davidson SM, Soydaner-Azeloglu RG, Parker SJ, Kamphorst JJ, Hackett S, Grabocka E, Nofal M, Drebin JA, Thompson CB et al. 2013. Macropinocytosis of protein is an amino acid supply route in Ras-transformed cells. *Nature* **497**: 633-637.

Conroy T, Desseigne F, Ychou M, Bouche O, Guimbaud R, Becouarn Y, Adenis A, Raoul JL, Gourgou-Bourgade S, de la Fouchardiere C et al. 2011. FOLFIRINOX versus gemcitabine for metastatic pancreatic cancer. *N Engl J Med* **364**: 1817-1825.

Conroy T, Hammel P, Hebbar M, Ben Abdelghani M, Wei AC, Raoul JL, Chone L, Francois E, Artru P, Biagi JJ et al. 2018. FOLFIRINOX or Gemcitabine as Adjuvant Therapy for Pancreatic Cancer. *N Engl J Med* **379**: 2395-2406.

Coquenlorge S, Yin WC, Yung T, Pan J, Zhang X, Mo R, Belik J, Hui CC, Kim TH. 2019. GLI2 Modulated by SUFU and SPOP Induces Intestinal Stem Cell Niche Signals in Development and Tumorigenesis. *Cell Rep* **27**: 3006-3018 e3004.

Corbit KC, Aanstad P, Singla V, Norman AR, Stainier DY, Reiter JF. 2005. Vertebrate Smoothened functions at the primary cilium. *Nature* **437**: 1018-1021.

Creanga A, Glenn TD, Mann RK, Saunders AM, Talbot WS, Beachy PA. 2012. Scube/You activity mediates release of dually lipid-modified Hedgehog signal in soluble form. *Genes Dev* **26**: 1312-1325.

Dai P, Akimaru H, Tanaka Y, Maekawa T, Nakafuku M, Ishii S. 1999. Sonic Hedgehog-induced activation of the Gli1 promoter is mediated by GLI3. *J Biol Chem* **274**: 8143-8152.

Dai P, Shinagawa T, Nomura T, Harada J, Kaul SC, Wadhwa R, Khan MM, Akimaru H, Sasaki H, Colmenares C et al. 2002. Ski is involved in transcriptional regulation by the repressor and full-length forms of Gli3. *Genes Dev* **16**: 2843-2848.

Del Fresno C, Sancho D. 2021. Myeloid cells in sensing of tissue damage. *Curr Opin Immunol* **68**: 34-40.

Dessaud E, McMahon AP, Briscoe J. 2008. Pattern formation in the vertebrate neural tube: a sonic hedgehog morphogen-regulated transcriptional network. *Development* **135**: 2489-2503.

Ding Q, Motoyama J, Gasca S, Mo R, Sasaki H, Rossant J, Hui CC. 1998. Diminished Sonic hedgehog signaling and lack of floor plate differentiation in Gli2 mutant mice. *Development* **125**: 2533-2543.

Djurec M, Grana O, Lee A, Troule K, Espinet E, Cabras L, Navas C, Blasco MT, Martin-Diaz L, Burdiel M et al. 2018. Saa3 is a key mediator of the protumorigenic properties of cancer-associated fibroblasts in pancreatic tumors. *Proc Natl Acad Sci U S A* **115**: E1147-E1156.

Doherty GJ, Tempero M, Corrie PG. 2018. HALO-109-301: a Phase III trial of PEGPH20 (with gemcitabine and nab-paclitaxel) in hyaluronic acid-high stage IV pancreatic cancer. *Future Oncol* **14**: 13-22.

Dominguez CX, Muller S, Keerthivasan S, Koeppen H, Hung J, Gierke S, Breart B, Foreman O, Bainbridge TW, Castiglioni A et al. 2020. Single-Cell RNA Sequencing Reveals Stromal Evolution into LRRC15(+) Myofibroblasts as a Determinant of Patient Response to Cancer Immunotherapy. *Cancer Discov* **10**: 232-253.

Duffield JS, Forbes SJ, Constandinou CM, Clay S, Partolina M, Vuthoori S, Wu S, Lang R, Iredale JP. 2005. Selective depletion of macrophages reveals distinct, opposing roles during liver injury and repair. *Journal of Clinical Investigation* **115**: 56-65.

Echelard Y, Epstein DJ, St-Jacques B, Shen L, Mohler J, McMahon JA, McMahon AP. 1993. Sonic hedgehog, a member of a family of putative signaling molecules, is implicated in the regulation of CNS polarity. *Cell* **75**: 1417-1430.

Echevarria-Andino ML, Allen BL. 2020. The hedgehog co-receptor BOC differentially regulates SHH signaling during craniofacial development. *Development* **147**.

Elyada E, Bolisetty M, Laise P, Flynn WF, Courtois ET, Burkhart RA, Teinor JA, Belleau P, Biffi G, Lucito MS et al. 2019. Cross-Species Single-Cell Analysis of Pancreatic Ductal Adenocarcinoma Reveals Antigen-Presenting Cancer-Associated Fibroblasts. *Cancer Discov* **9**: 1102-1123.

Endoh-Yamagami S, Evangelista M, Wilson D, Wen X, Theunissen JW, Phamluong K, Davis M, Scales SJ, Solloway MJ, de Sauvage FJ et al. 2009. The mammalian Cos2 homolog Kif7 plays an essential role in modulating Hh signal transduction during development. *Curr Biol* **19**: 1320-1326.

Faber CL, Deem JD, Campos CA, Taborsky GJ, Jr., Morton GJ. 2020. CNS control of the endocrine pancreas. *Diabetologia* **63**: 2086-2094.

Farhood B, Najafi M, Mortezaee K. 2019. CD8(+) cytotoxic T lymphocytes in cancer immunotherapy: A review. *J Cell Physiol* **234**: 8509-8521.

Farran B, Nagaraju GP. 2019. The dynamic interactions between the stroma, pancreatic stellate cells and pancreatic tumor development: Novel therapeutic targets. *Cytokine Growth Factor Rev* **48**: 11-23.

Feig C, Jones JO, Kraman M, Wells RJ, Deonarine A, Chan DS, Connell CM, Roberts EW, Zhao Q, Caballero OL et al. 2013. Targeting CXCL12 from FAP-expressing carcinoma-associated fibroblasts synergizes with anti-PD-L1 immunotherapy in pancreatic cancer. *Proc Natl Acad Sci U S A* **110**: 20212-20217.

Ferreira RMM, Sancho R, Messal HA, Nye E, Spencer-Dene B, Stone RK, Stamp G, Rosewell I, Quaglia A, Behrens A. 2017. Duct- and Acinar-Derived Pancreatic Ductal Adenocarcinomas Show Distinct Tumor Progression and Marker Expression. *Cell Rep* **21**: 966-978.

Francescone R, Barbosa Vendramini-Costa D, Franco-Barraza J, Wagner J, Muir A, Lau AN, Gabitova L, Pazina T, Gupta S, Luong T et al. 2021. Netrin G1 Promotes Pancreatic

Tumorigenesis through Cancer-Associated Fibroblast-Driven Nutritional Support and Immunosuppression. *Cancer Discov* **11**: 446-479.

Froeling FE, Feig C, Chelala C, Dobson R, Mein CE, Tuveson DA, Clevers H, Hart IR, Kocher HM. 2011. Retinoic acid-induced pancreatic stellate cell quiescence reduces paracrine Wnt-beta-catenin signaling to slow tumor progression. *Gastroenterology* **141**: 1486-1497, 1497 e1481-1414.

Garcia PE, Adoumie M, Kim EC, Zhang Y, Scales MK, El-Tawil YS, Shaikh AZ, Wen HJ, Bednar F, Allen BL et al. 2020a. Differential Contribution of Pancreatic Fibroblast Subsets to the Pancreatic Cancer Stroma. *Cell Mol Gastroenterol Hepatol* **10**: 581-599.

Garcia PE, Scales MK, Allen BL, Pasca di Magliano M. 2020b. Pancreatic Fibroblast Heterogeneity: From Development to Cancer. *Cells* **9**.

Geiger R, Rieckmann JC, Wolf T, Basso C, Feng Y, Fuhrer T, Kogadeeva M, Picotti P, Meissner F, Mann M et al. 2016. L-Arginine Modulates T Cell Metabolism and Enhances Survival and Anti-tumor Activity. *Cell* **167**: 829-842 e813.

Goetz SC, Anderson KV. 2010. The primary cilium: a signalling centre during vertebrate development. *Nat Rev Genet* **11**: 331-344.

Gorchs L, Ahmed S, Mayer C, Knauf A, Fernandez Moro C, Svensson M, Heuchel R, Rangelova E, Bergman P, Kaipe H. 2020. The vitamin D analogue calcipotriol promotes an anti-tumorigenic phenotype of human pancreatic CAFs but reduces T cell mediated immunity. *Sci Rep* **10**: 17444.

Griesmann H, Drexel C, Milosevic N, Sipos B, Rosendahl J, Gress TM, Michl P. 2017. Pharmacological macrophage inhibition decreases metastasis formation in a genetic model of pancreatic cancer. *Gut* **66**: 1278-1285.

Haeberle L, Steiger K, Schlitter AM, Safi SA, Knoefel WT, Erkan M, Esposito I. 2018. Stromal heterogeneity in pancreatic cancer and chronic pancreatitis. *Pancreatology* **18**: 536-549.

Halbrook CJ, Lyssiotis CA. 2017. Employing Metabolism to Improve the Diagnosis and Treatment of Pancreatic Cancer. *Cancer Cell* **31**: 5-19.

Hall ET, Dillard ME, Stewart DP, Zhang Y, Wagner B, Levine RM, Pruett-Miller SM, Sykes A, Temirov J, Cheney RE et al. 2021. Cytoneme delivery of Sonic Hedgehog from ligand-producing cells requires Myosin 10 and a Dispatched-BOC/CDON co-receptor complex. *Elife* **10**.

Hallikas O, Palin K, Sinjushina N, Rautiainen R, Partanen J, Ukkonen E, Taipale J. 2006. Genome-wide prediction of mammalian enhancers based on analysis of transcription-factor binding affinity. *Cell* **124**: 47-59.

Haycraft CJ, Banizs B, Aydin-Son Y, Zhang Q, Michaud EJ, Yoder BK. 2005. Gli2 and Gli3 localize to cilia and require the intraflagellar transport protein polaris for processing and function. *PLoS Genet* **1**: e53.

Heldin CH, Rubin K, Pietras K, Ostman A. 2004. High interstitial fluid pressure - an obstacle in cancer therapy. *Nat Rev Cancer* **4**: 806-813.

Helms E, Onate MK, Sherman MH. 2020. Fibroblast Heterogeneity in the Pancreatic Tumor Microenvironment. *Cancer Discov* **10**: 648-656.

Henderson JR, Moss MC. 1985. A morphometric study of the endocrine and exocrine capillaries of the pancreas. *Q J Exp Physiol* **70**: 347-356.

Hessmann E, Patzak MS, Klein L, Chen N, Kari V, Ramu I, Bapiro TE, Frese KK, Gopinathan A, Richards FM et al. 2018. Fibroblast drug scavenging increases intratumoural gemcitabine accumulation in murine pancreas cancer. *Gut* **67**: 497-507.

Hilmi M, Bartholin L, Neuzillet C. 2018. Immune therapies in pancreatic ductal adenocarcinoma: Where are we now? *World J Gastroenterol* **24**: 2137-2151.

Hingorani SR, Petricoin EF, Maitra A, Rajapakse V, King C, Jacobetz MA, Ross S, Conrads TP, Veenstra TD, Hitt BA et al. 2003. Preinvasive and invasive ductal pancreatic cancer and its early detection in the mouse. *Cancer Cell* **4**: 437-450.

Hingorani SR, Wang L, Multani AS, Combs C, Deramaudt TB, Hruban RH, Rustgi AK, Chang S, Tuveson DA. 2005. Trp53R172H and KrasG12D cooperate to promote chromosomal instability and widely metastatic pancreatic ductal adenocarcinoma in mice. *Cancer Cell* **7**: 469-483.

Hingorani SR, Zheng L, Bullock AJ, Seery TE, Harris WP, Sigal DS, Braiteh F, Ritch PS, Zalupski MM, Bahary N et al. 2018. HALO 202: Randomized Phase II Study of PEGPH20 Plus Nab-Paclitaxel/Gemcitabine Versus Nab-Paclitaxel/Gemcitabine in Patients With Untreated, Metastatic Pancreatic Ductal Adenocarcinoma. *J Clin Oncol* **36**: 359-366.

Hirayama K, Kono H, Nakata Y, Akazawa Y, Wakana H, Fukushima H, Fujii H. 2018. Expression of podoplanin in stromal fibroblasts plays a pivotal role in the prognosis of patients with pancreatic cancer. *Surg Today* **48**: 110-118.

Holtz AM, Peterson KA, Nishi Y, Morin S, Song JY, Charron F, McMahon AP, Allen BL. 2013. Essential role for ligand-dependent feedback antagonism of vertebrate hedgehog signaling by PTCH1, PTCH2 and HHIP1 during neural patterning. *Development* **140**: 3423-3434.

Homma T, Tsuchiya R. 1991. The study of the mass screening of persons without symptoms and of the screening of outpatients with gastrointestinal complaints or icterus for pancreatic cancer in Japan, using CA19-9 and elastase-1 or ultrasonography. *Int J Pancreatol* **9**: 119-124.

Horn L, Spigel DR, Vokes EE, Holgado E, Ready N, Steins M, Poddubskaya E, Borghaei H, Felip E, Paz-Ares L et al. 2017. Nivolumab Versus Docetaxel in Previously Treated Patients With Advanced Non-Small-Cell Lung Cancer: Two-Year Outcomes From Two Randomized, Open-Label, Phase III Trials (CheckMate 017 and CheckMate 057). *J Clin Oncol* **35**: 3924-3933.

Hosein AN, Huang H, Wang Z, Parmar K, Du W, Huang J, Maitra A, Olson E, Verma U, Brekken RA. 2019. Cellular heterogeneity during mouse pancreatic ductal adenocarcinoma progression at single-cell resolution. *JCI Insight* **5**.

Huang H, Cotton JL, Wang Y, Rajurkar M, Zhu LJ, Lewis BC, Mao J. 2013. Specific requirement of Gli transcription factors in Hedgehog-mediated intestinal development. *J Biol Chem* **288**: 17589-17596.

Huangfu D, Anderson KV. 2005. Cilia and Hedgehog responsiveness in the mouse. *Proc Natl Acad Sci U S A* **102**: 11325-11330.

Hui CC, Angers S. 2011. Gli proteins in development and disease. *Annu Rev Cell Dev Biol* **27**: 513-537.

Hui CC, Joyner AL. 1993. A mouse model of greig cephalopolysyndactyly syndrome: the extra-toesJ mutation contains an intragenic deletion of the Gli3 gene. *Nat Genet* **3**: 241-246.

Hui CC, Slusarski D, Platt KA, Holmgren R, Joyner AL. 1994. Expression of three mouse homologs of the Drosophila segment polarity gene cubitus interruptus, Gli, Gli-2, and Gli-3, in ectoderm- and mesoderm-derived tissues suggests multiple roles during postimplantation development. *Dev Biol* **162**: 402-413.

Humke EW, Dorn KV, Milenkovic L, Scott MP, Rohatgi R. 2010. The output of Hedgehog signaling is controlled by the dynamic association between Suppressor of Fused and the Gli proteins. *Genes Dev* **24**: 670-682.

Hwang RF, Moore T, Arumugam T, Ramachandran V, Amos KD, Rivera A, Ji B, Evans DB, Logsdon CD. 2008. Cancer-associated stromal fibroblasts promote pancreatic tumor progression. *Cancer Res* **68**: 918-926.

Ingham PW, Hidalgo A. 1993. Regulation of wingless transcription in the Drosophila embryo. *Development* **117**: 283-291.

Ingham PW, Taylor AM, Nakano Y. 1991. Role of the Drosophila patched gene in positional signalling. *Nature* **353**: 184-187.

Ireland L, Santos A, Ahmed MS, Rainer C, Nielsen SR, Quaranta V, Weyer-Czernilofsky U, Engle DD, Perez-Mancera PA, Coupland SE et al. 2016. Chemoresistance in Pancreatic Cancer Is Driven by Stroma-Derived Insulin-Like Growth Factors. *Cancer Res* **76**: 6851-6863.

Jacobetz MA, Chan DS, Neesse A, Bapiro TE, Cook N, Frese KK, Feig C, Nakagawa T, Caldwell ME, Zecchini HI et al. 2013. Hyaluronan impairs vascular function and drug delivery in a mouse model of pancreatic cancer. *Gut* **62**: 112-120.

Jeon S, Seong RH. 2016. Anteroposterior Limb Skeletal Patterning Requires the Bifunctional Action of SWI/SNF Chromatin Remodeling Complex in Hedgehog Pathway. *PLoS Genet* **12**: e1005915.

Jonckheere N, Vasseur R, Van Seuningen I. 2017. The cornerstone K-RAS mutation in pancreatic adenocarcinoma: From cell signaling network, target genes, biological processes to therapeutic targeting. *Crit Rev Oncol Hematol* **111**: 7-19.

Jones S, Zhang X, Parsons DW, Lin JC, Leary RJ, Angenendt P, Mankoo P, Carter H, Kamiyama H, Jimeno A et al. 2008. Core signaling pathways in human pancreatic cancers revealed by global genomic analyses. *Science* **321**: 1801-1806.

Kamphorst JJ, Nofal M, Commisso C, Hackett SR, Lu W, Grabocka E, Vander Heiden MG, Miller G, Drebin JA, Bar-Sagi D et al. 2015. Human pancreatic cancer tumors are nutrient poor and tumor cells actively scavenge extracellular protein. *Cancer Res* **75**: 544-553.

Katsarou A, Gudbjornsdottir S, Rawshani A, Dabelea D, Bonifacio E, Anderson BJ, Jacobsen LM, Schatz DA, Lernmark A. 2017. Type 1 diabetes mellitus. *Nat Rev Dis Primers* **3**: 17016.

Kemp SB, Pasca di Magliano M, Crawford HC. 2021. Myeloid Cell Mediated Immune Suppression in Pancreatic Cancer. *Cell Mol Gastroenterol Hepatol* **12**: 1531-1542.

Kim EJ, Sahai V, Abel EV, Griffith KA, Greenson JK, Takebe N, Khan GN, Blau JL, Craig R, Balis UG et al. 2014. Pilot clinical trial of hedgehog pathway inhibitor GDC-0449 (vismodegib) in combination with gemcitabine in patients with metastatic pancreatic adenocarcinoma. *Clin Cancer Res* **20**: 5937-5945.

Kim J, Kato M, Beachy PA. 2009. Gli2 trafficking links Hedgehog-dependent activation of Smoothened in the primary cilium to transcriptional activation in the nucleus. *Proc Natl Acad Sci U S A* **106**: 21666-21671.

Kim JE, Lee KT, Lee JK, Paik SW, Rhee JC, Choi KW. 2004. Clinical usefulness of carbohydrate antigen 19-9 as a screening test for pancreatic cancer in an asymptomatic population. *J Gastroenterol Hepatol* **19**: 182-186.

Kindler HL, Ioka T, Richel DJ, Bennouna J, Létourneau R, Okusaka T, Funakoshi A, Furuse J, Park YS, Ohkawa S et al. 2011. Axitinib plus gemcitabine versus placebo plus gemcitabine in patients with advanced pancreatic adenocarcinoma: a double-blind randomised phase 3 study. *The Lancet Oncology* **12**: 256-262.

Kindler HL, Niedzwiecki D, Hollis D, Sutherland S, Schrag D, Hurwitz H, Innocenti F, Mulcahy MF, O'Reilly E, Wozniak TF et al. 2010. Gemcitabine plus bevacizumab compared with

gemcitabine plus placebo in patients with advanced pancreatic cancer: phase III trial of the Cancer and Leukemia Group B (CALGB 80303). *J Clin Oncol* **28**: 3617-3622.

Kinzler KW, Vogelstein B. 1990. The GLI gene encodes a nuclear protein which binds specific sequences in the human genome. *Mol Cell Biol* **10**: 634-642.

Kleeff J, Korc M, Apte M, La Vecchia C, Johnson CD, Biankin AV, Neale RE, Tempero M, Tuveson DA, Hruban RH et al. 2016. Pancreatic cancer. *Nat Rev Dis Primers* **2**: 16022.

Ko AH, LoConte N, Tempero MA, Walker EJ, Kate Kelley R, Lewis S, Chang WC, Kantoff E, Vannier MW, Catenacci DV et al. 2016. A Phase I Study of FOLFIRINOX Plus IPI-926, a Hedgehog Pathway Inhibitor, for Advanced Pancreatic Adenocarcinoma. *Pancreas* **45**: 370-375.

Kolterud A, Grosse AS, Zacharias WJ, Walton KD, Kretovich KE, Madison BB, Waghray M, Ferris JE, Hu C, Merchant JL et al. 2009. Paracrine Hedgehog signaling in stomach and intestine: new roles for hedgehog in gastrointestinal patterning. *Gastroenterology* **137**: 618-628.

Kool M, Jones DT, Jager N, Northcott PA, Pugh TJ, Hovestadt V, Piro RM, Esparza LA, Markant SL, Remke M et al. 2014. Genome sequencing of SHH medulloblastoma predicts genotype-related response to smoothened inhibition. *Cancer Cell* **25**: 393-405.

Kool M, Korshunov A, Remke M, Jones DT, Schlanstein M, Northcott PA, Cho YJ, Koster J, Schouten-van Meeteren A, van Vuurden D et al. 2012. Molecular subgroups of medulloblastoma: an international meta-analysis of transcriptome, genetic aberrations, and clinical data of WNT, SHH, Group 3, and Group 4 medulloblastomas. *Acta Neuropathol* **123**: 473-484.

Kopp JL, Dubois CL, Schaeffer DF, Samani A, Taghizadeh F, Cowan RW, Rhim AD, Stiles BL, Valasek M, Sander M. 2018. Loss of Pten and Activation of Kras Synergistically Induce Formation of Intraductal Papillary Mucinous Neoplasia From Pancreatic Ductal Cells in Mice. *Gastroenterology* **154**: 1509-1523 e1505.

Kopp JL, von Figura G, Mayes E, Liu FF, Dubois CL, Morris JPt, Pan FC, Akiyama H, Wright CV, Jensen K et al. 2012. Identification of Sox9-dependent acinar-to-ductal reprogramming as the principal mechanism for initiation of pancreatic ductal adenocarcinoma. *Cancer Cell* **22**: 737-750.

Kraman M, Bambrough PJ, Arnold JN, Roberts EW, Magiera L, Jones JO, Gopinathan A, Tuveson DA, Fearon DT. 2010. Suppression of antitumor immunity by stromal cells expressing fibroblast activation protein-alpha. *Science* **330**: 827-830.

Krauss S, Concordet JP, Ingham PW. 1993. A functionally conserved homolog of the Drosophila segment polarity gene hh is expressed in tissues with polarizing activity in zebrafish embryos. *Cell* **75**: 1431-1444.

Kurahara H, Shinchi H, Mataki Y, Maemura K, Noma H, Kubo F, Sakoda M, Ueno S, Natsugoe S, Takao S. 2011. Significance of M2-polarized tumor-associated macrophage in pancreatic cancer. *J Surg Res* **167**: e211-219.

Lai X, Wang M, McElyea SD, Sherman S, House M, Korc M. 2017. A microRNA signature in circulating exosomes is superior to exosomal glypican-1 levels for diagnosing pancreatic cancer. *Cancer Lett* **393**: 86-93.

Larsen BM, Hrycaj SM, Newman M, Li Y, Wellik DM. 2015. Mesenchymal Hox6 function is required for mouse pancreatic endocrine cell differentiation. *Development* **142**: 3859-3868.

Leal F, Cohn MJ. 2016. Loss and Re-emergence of Legs in Snakes by Modular Evolution of Sonic hedgehog and HOXD Enhancers. *Curr Biol* **26**: 2966-2973.

LeBleu VS, Kalluri R. 2018. A peek into cancer-associated fibroblasts: origins, functions and translational impact. *Dis Model Mech* **11**.

Lee CS, Buttitta L, Fan CM. 2001. Evidence that the WNT-inducible growth arrest-specific gene 1 encodes an antagonist of sonic hedgehog signaling in the somite. *Proc Natl Acad Sci U S A* **98**: 11347-11352.

Lee JJ, Perera RM, Wang H, Wu DC, Liu XS, Han S, Fitamant J, Jones PD, Ghanta KS, Kawano S et al. 2014. Stromal response to Hedgehog signaling restrains pancreatic cancer progression. *Proc Natl Acad Sci U S A* **111**: E3091-3100.

Lee JJ, Rothenberg ME, Seeley ES, Zimdahl B, Kawano S, Lu WJ, Shin K, Sakata-Kato T, Chen JK, Diehn M et al. 2016. Control of inflammation by stromal Hedgehog pathway activation restrains colitis. *Proc Natl Acad Sci U S A* **113**: E7545-E7553.

Lee JJ, von Kessler DP, Parks S, Beachy PA. 1992. Secretion and localized transcription suggest a role in positional signaling for products of the segmentation gene hedgehog. *Cell* **71**: 33-50.

Lees CW, Zacharias WJ, Tremelling M, Noble CL, Nimmo ER, Tenesa A, Cornelius J, Torkvist L, Kao J, Farrington S et al. 2008. Analysis of germline GLI1 variation implicates hedgehog signalling in the regulation of intestinal inflammatory pathways. *PLoS Med* **5**: e239.

Lex RK, Ji Z, Falkenstein KN, Zhou W, Henry JL, Ji H, Vokes SA. 2020. GLI transcriptional repression regulates tissue-specific enhancer activity in response to Hedgehog signaling. *Elife* **9**.

Li J, Yuan S, Norgard RJ, Yan F, Sun YH, Kim IK, Merrell AJ, Sela Y, Jiang Y, Bhanu NV et al. 2021. Epigenetic and Transcriptional Control of the Epidermal Growth Factor Receptor Regulates the Tumor Immune Microenvironment in Pancreatic Cancer. *Cancer Discov* **11**: 736-753.

Liem KF, Jr., He M, Ocbina PJ, Anderson KV. 2009. Mouse Kif7/Costal2 is a cilia-associated protein that regulates Sonic hedgehog signaling. *Proc Natl Acad Sci U S A* **106**: 13377-13382.

Liou GY, Doppler H, Necela B, Edenfield B, Zhang L, Dawson DW, Storz P. 2015. Mutant KRAS-induced expression of ICAM-1 in pancreatic acinar cells causes attraction of macrophages to expedite the formation of precancerous lesions. *Cancer Discov* **5**: 52-63.

Liou GY, Doppler H, Necela B, Krishna M, Crawford HC, Raimondo M, Storz P. 2013. Macrophage-secreted cytokines drive pancreatic acinar-to-ductal metaplasia through NF-kappaB and MMPs. *J Cell Biol* **202**: 563-577.

Litingtung Y, Dahn RD, Li Y, Fallon JF, Chiang C. 2002. Shh and Gli3 are dispensable for limb skeleton formation but regulate digit number and identity. *Nature* **418**: 979-983.

Liu A, Wang B, Niswander LA. 2005. Mouse intraflagellar transport proteins regulate both the activator and repressor functions of Gli transcription factors. *Development* **132**: 3103-3111.

Liu JA, Lai FP, Gui HS, Sham MH, Tam PK, Garcia-Barcelo MM, Hui CC, Ngan ES. 2015. Identification of GLI Mutations in Patients With Hirschsprung Disease That Disrupt Enteric Nervous System Development in Mice. *Gastroenterology* **149**: 1837-1848 e1835.

Liu X, Pitarresi JR, Cuitino MC, Kladney RD, Woelke SA, Sizemore GM, Nayak SG, Egriboz O, Schweickert PG, Yu L et al. 2016. Genetic ablation of Smoothened in pancreatic fibroblasts increases acinar-ductal metaplasia. *Genes Dev* **30**: 1943-1955.

Lo A, Wang LS, Scholler J, Monslow J, Avery D, Newick K, O'Brien S, Evans RA, Bajor DJ, Clendenin C et al. 2015. Tumor-Promoting Desmoplasia Is Disrupted by Depleting FAP-Expressing Stromal Cells. *Cancer Res* **75**: 2800-2810.

Lyssiotis CA, Kimmelman AC. 2017. Metabolic Interactions in the Tumor Microenvironment. *Trends Cell Biol* **27**: 863-875.

Madison BB, McKenna LB, Dolson D, Epstein DJ, Kaestner KH. 2009. FoxF1 and FoxL1 link hedgehog signaling and the control of epithelial proliferation in the developing stomach and intestine. *J Biol Chem* **284**: 5936-5944.

Maitra A, Hruban RH. 2008. Pancreatic cancer. *Annu Rev Pathol* **3**: 157-188.

Mantoni TS, Lunardi S, Al-Assar O, Masamune A, Brunner TB. 2011. Pancreatic stellate cells radioprotect pancreatic cancer cells through beta1-integrin signaling. *Cancer Res* **71**: 3453-3458.

Marcucio RS, Cordero DR, Hu D, Helms JA. 2005. Molecular interactions coordinating the development of the forebrain and face. *Dev Biol* **284**: 48-61.

Marigo V, Davey RA, Zuo Y, Cunningham JM, Tabin CJ. 1996. Biochemical evidence that patched is the Hedgehog receptor. *Nature* **384**: 176-179.

Martinelli DC, Fan CM. 2007. Gas1 extends the range of Hedgehog action by facilitating its signaling. *Genes Dev* **21**: 1231-1243.

Masamune A, Kikuta K, Watanabe T, Satoh K, Hirota M, Shimosegawa T. 2008. Hypoxia stimulates pancreatic stellate cells to induce fibrosis and angiogenesis in pancreatic cancer. *Am J Physiol Gastrointest Liver Physiol* **295**: G709-717.

Mathew E, Brannon AL, Del Vecchio A, Garcia PE, Penny MK, Kane KT, Vinta A, Buckanovich RJ, di Magliano MP. 2016. Mesenchymal Stem Cells Promote Pancreatic Tumor Growth by Inducing Alternative Polarization of Macrophages. *Neoplasia* **18**: 142-151.

Mathew E, Collins MA, Fernandez-Barrena MG, Holtz AM, Yan W, Hogan JO, Tata Z, Allen BL, Fernandez-Zapico ME, di Magliano MP. 2014a. The transcription factor GLI1 modulates the inflammatory response during pancreatic tissue remodeling. *J Biol Chem* **289**: 27727-27743.

Mathew E, Zhang Y, Holtz AM, Kane KT, Song JY, Allen BL, Pasca di Magliano M. 2014b. Dosage-dependent regulation of pancreatic cancer growth and angiogenesis by hedgehog signaling. *Cell Rep* **9**: 484-494.

Matise MP, Epstein DJ, Park HL, Platt KA, Joyner AL. 1998. Gli2 is required for induction of floor plate and adjacent cells, but not most ventral neurons in the mouse central nervous system. *Development* **125**: 2759-2770.

Matus DQ, Magie CR, Pang K, Martindale MQ, Thomsen GH. 2008. The Hedgehog gene family of the cnidarian, Nematostella vectensis, and implications for understanding metazoan Hedgehog pathway evolution. *Dev Biol* **313**: 501-518.

May SR, Ashique AM, Karlen M, Wang B, Shen Y, Zarbalis K, Reiter J, Ericson J, Peterson AS. 2005. Loss of the retrograde motor for IFT disrupts localization of Smo to cilia and prevents the expression of both activator and repressor functions of Gli. *Dev Biol* **287**: 378-389.

McCarroll JA, Naim S, Sharbeen G, Russia N, Lee J, Kavallaris M, Goldstein D, Phillips PA. 2014. Role of pancreatic stellate cells in chemoresistance in pancreatic cancer. *Front Physiol* **5**: 141.

Melo SA, Luecke LB, Kahlert C, Fernandez AF, Gammon ST, Kaye J, LeBleu VS, Mittendorf EA, Weitz J, Rahbari N et al. 2015. Glypican-1 identifies cancer exosomes and detects early pancreatic cancer. *Nature* **523**: 177-182.

Mills LD, Zhang L, Marler R, Svingen P, Fernandez-Barrena MG, Dave M, Bamlet W, McWilliams RR, Petersen GM, Faubion W et al. 2014. Inactivation of the transcription factor GLI1 accelerates pancreatic cancer progression. *J Biol Chem* **289**: 16516-16525.

Mills LD, Zhang Y, Marler RJ, Herreros-Villanueva M, Zhang L, Almada LL, Couch F, Wetmore C, Pasca di Magliano M, Fernandez-Zapico ME. 2013. Loss of the transcription factor GLI1 identifies a signaling network in the tumor microenvironment mediating KRAS oncogene-induced transformation. *J Biol Chem* **288**: 11786-11794.

Mitchem JB, Brennan DJ, Knolhoff BL, Belt BA, Zhu Y, Sanford DE, Belaygorod L, Carpenter D, Collins L, Piwnica-Worms D et al. 2013. Targeting tumor-infiltrating macrophages decreases tumor-initiating cells, relieves immunosuppression, and improves chemotherapeutic responses. *Cancer Res* **73**: 1128-1141.

Mo R, Freer AM, Zinyk DL, Crackower MA, Michaud J, Heng HH, Chik KW, Shi XM, Tsui LC, Cheng SH et al. 1997. Specific and redundant functions of Gli2 and Gli3 zinc finger genes in skeletal patterning and development. *Development* **124**: 113-123.

Monti P, Leone BE, Marchesi F, Balzano G, Zerbi A, Scaltrini F, Pasquali C, Calori G, Pessi F, Sperti C et al. 2003. The CC chemokine MCP-1/CCL2 in pancreatic cancer progression: regulation of expression and potential mechanisms of antimalignant activity. *Cancer Res* **63**: 7451-7461.

Morton JP, Mongeau ME, Klimstra DS, Morris JP, Lee YC, Kawaguchi Y, Wright CV, Hebrok M, Lewis BC. 2007. Sonic hedgehog acts at multiple stages during pancreatic tumorigenesis. *Proc Natl Acad Sci U S A* **104**: 5103-5108.

Movahedi K, Guilliams M, Van den Bossche J, Van den Bergh R, Gysemans C, Beschin A, De Baetselier P, Van Ginderachter JA. 2008. Identification of discrete tumor-induced myeloid-derived suppressor cell subpopulations with distinct T cell-suppressive activity. *Blood* **111**: 4233-4244.

Muranen T, Iwanicki MP, Curry NL, Hwang J, DuBois CD, Coloff JL, Hitchcock DS, Clish CB, Brugge JS, Kalaany NY. 2017. Starved epithelial cells uptake extracellular matrix for survival. *Nat Commun* **8**: 13989.

Murtaugh LC, Keefe MD. 2015. Regeneration and repair of the exocrine pancreas. *Annu Rev Physiol* **77**: 229-249.

Nakano Y, Guerrero I, Hidalgo A, Taylor A, Whittle JR, Ingham PW. 1989. A protein with several possible membrane-spanning domains encoded by the Drosophila segment polarity gene patched. *Nature* **341**: 508-513.

Neoptolemos JP, Kleeff J, Michl P, Costello E, Greenhalf W, Palmer DH. 2018. Therapeutic developments in pancreatic cancer: current and future perspectives. *Nat Rev Gastroenterol Hepatol* **15**: 333-348.

Neoptolemos JP, Palmer DH, Ghaneh P, Psarelli EE, Valle JW, Halloran CM, Faluyi O, O'Reilly DA, Cunningham D, Wadsley J et al. 2017. Comparison of adjuvant gemcitabine and capecitabine with gemcitabine monotherapy in patients with resected pancreatic cancer (ESPAC-4): a multicentre, open-label, randomised, phase 3 trial. *The Lancet* **389**: 1011-1024.

Nielsen MFB, Mortensen MB, Detlefsen S. 2017. Identification of markers for quiescent pancreatic stellate cells in the normal human pancreas. *Histochem Cell Biol* **148**: 359-380.

Niewiadomski P, Kong JH, Ahrends R, Ma Y, Humke EW, Khan S, Teruel MN, Novitch BG, Rohatgi R. 2014. Gli protein activity is controlled by multisite phosphorylation in vertebrate Hedgehog signaling. *Cell Rep* **6**: 168-181.

Nolan-Stevaux O, Lau J, Truitt ML, Chu GC, Hebrok M, Fernandez-Zapico ME, Hanahan D. 2009. GLI1 is regulated through Smoothened-independent mechanisms in neoplastic pancreatic ducts and mediates PDAC cell survival and transformation. *Genes Dev* **23**: 24-36.

Northcott PA, Robinson GW, Kratz CP, Mabbott DJ, Pomeroy SL, Clifford SC, Rutkowski S, Ellison DW, Malkin D, Taylor MD et al. 2019. Medulloblastoma. *Nat Rev Dis Primers* **5**: 11.

Nusslein-Volhard C, Wieschaus E. 1980. Mutations affecting segment number and polarity in Drosophila. *Nature* **287**: 795-801.

O'Reilly EM, Oh DY, Dhani N, Renouf DJ, Lee MA, Sun W, Fisher G, Hezel A, Chang SC, Vlahovic G et al. 2019. Durvalumab With or Without Tremelimumab for Patients With Metastatic Pancreatic Ductal Adenocarcinoma: A Phase 2 Randomized Clinical Trial. *JAMA Oncol* **5**: 1431-1438.

Oba A, Ho F, Bao QR, Al-Musawi MH, Schulick RD, Del Chiaro M. 2020. Neoadjuvant Treatment in Pancreatic Cancer. *Front Oncol* **10**: 245.

Ocbina PJ, Anderson KV. 2008. Intraflagellar transport, cilia, and mammalian Hedgehog signaling: analysis in mouse embryonic fibroblasts. *Dev Dyn* **237**: 2030-2038.

Ohlund D, Handly-Santana A, Biffi G, Elyada E, Almeida AS, Ponz-Sarvise M, Corbo V, Oni TE, Hearn SA, Lee EJ et al. 2017. Distinct populations of inflammatory fibroblasts and myofibroblasts in pancreatic cancer. *J Exp Med* **214**: 579-596.

Olive KP, Jacobetz MA, Davidson CJ, Gopinathan A, McIntyre D, Honess D, Madhu B, Goldgraben MA, Caldwell ME, Allard D et al. 2009. Inhibition of Hedgehog signaling enhances delivery of chemotherapy in a mouse model of pancreatic cancer. *Science* **324**: 1457-1461.

Omary MB, Lugea A, Lowe AW, Pandol SJ. 2007. The pancreatic stellate cell: a star on the rise in pancreatic diseases. *J Clin Invest* **117**: 50-59.

Ostrom QT, Gittleman H, Truitt G, Boscia A, Kruchko C, Barnholtz-Sloan JS. 2018. CBTRUS Statistical Report: Primary Brain and Other Central Nervous System Tumors Diagnosed in the United States in 2011-2015. *Neuro Oncol* **20**: iv1-iv86.

Ozdemir BC, Pentcheva-Hoang T, Carstens JL, Zheng X, Wu CC, Simpson TR, Laklai H, Sugimoto H, Kahlert C, Novitskiy SV et al. 2014. Depletion of carcinoma-associated fibroblasts and fibrosis induces immunosuppression and accelerates pancreas cancer with reduced survival. *Cancer Cell* **25**: 719-734.

Pan Y, Bai CB, Joyner AL, Wang B. 2006. Sonic hedgehog signaling regulates Gli2 transcriptional activity by suppressing its processing and degradation. *Mol Cell Biol* **26**: 3365-3377.

Park HL, Bai C, Platt KA, Matise MP, Beeghly A, Hui CC, Nakashima M, Joyner AL. 2000. Mouse Gli1 mutants are viable but have defects in SHH signaling in combination with a Gli2 mutation. *Development* **127**: 1593-1605.

Pasca di Magliano M, Sekine S, Ermilov A, Ferris J, Dlugosz AA, Hebrok M. 2006. Hedgehog/Ras interactions regulate early stages of pancreatic cancer. *Genes Dev* **20**: 3161-3173.

Pepinsky RB, Zeng C, Wen D, Rayhorn P, Baker DP, Williams KP, Bixler SA, Ambrose CM, Garber EA, Miatkowski K et al. 1998. Identification of a palmitic acid-modified form of human Sonic hedgehog. *J Biol Chem* **273**: 14037-14045.

Persson M, Stamataki D, te Welscher P, Andersson E, Bose J, Ruther U, Ericson J, Briscoe J. 2002. Dorsal-ventral patterning of the spinal cord requires Gli3 transcriptional repressor activity. *Genes Dev* **16**: 2865-2878.

Peterson KA, Nishi Y, Ma W, Vedenko A, Shokri L, Zhang X, McFarlane M, Baizabal JM, Junker JP, van Oudenaarden A et al. 2012. Neural-specific Sox2 input and differential Gli-binding affinity provide context and positional information in Shh-directed neural patterning. *Genes Dev* **26**: 2802-2816.

Platt KA, Michaud J, Joyner AL. 1997. Expression of the mouse Gli and Ptc genes is adjacent to embryonic sources of hedgehog signals suggesting a conservation of pathways between flies and mice. *Mechanisms of Development* **62**: 121-135.

Porter JA, Young KE, Beachy PA. 1996. Cholesterol modification of hedgehog signaling proteins in animal development. *Science* **274**: 255-259.

Poruk KE, Gay DZ, Brown K, Mulvihill JD, Boucher KM, Scaife CL, Firpo MA, Mulvihill SJ. 2013. The clinical utility of CA 19-9 in pancreatic adenocarcinoma: diagnostic and prognostic updates. *Curr Mol Med* **13**: 340-351.

Provenzano PP, Cuevas C, Chang AE, Goel VK, Von Hoff DD, Hingorani SR. 2012. Enzymatic targeting of the stroma ablates physical barriers to treatment of pancreatic ductal adenocarcinoma. *Cancer Cell* **21**: 418-429.

Provenzano PP, Hingorani SR. 2013. Hyaluronan, fluid pressure, and stromal resistance in pancreas cancer. *Br J Cancer* **108**: 1-8.

Pylayeva-Gupta Y, Lee KE, Hajdu CH, Miller G, Bar-Sagi D. 2012. Oncogenic Kras-induced GM-CSF production promotes the development of pancreatic neoplasia. *Cancer Cell* **21**: 836-847.

Qian BZ, Pollard JW. 2010. Macrophage diversity enhances tumor progression and metastasis. *Cell* **141**: 39-51.

Raber P, Ochoa AC, Rodriguez PC. 2012. Metabolism of L-arginine by myeloid-derived suppressor cells in cancer: mechanisms of T cell suppression and therapeutic perspectives. *Immunol Invest* **41**: 614-634.

Rajurkar M, De Jesus-Monge WE, Driscoll DR, Appleman VA, Huang H, Cotton JL, Klimstra DS, Zhu LJ, Simin K, Xu L et al. 2012. The activity of Gli transcription factors is essential for Kras-induced pancreatic tumorigenesis. *Proc Natl Acad Sci U S A* **109**: E1038-1047.

Ramalho-Santos M, Melton DA, McMahon AP. 2000. Hedgehog signals regulate multiple aspects of gastrointestinal development. *Development* **127**: 2763-2772.

Raskov H, Orhan A, Christensen JP, Gogenur I. 2021. Cytotoxic CD8(+) T cells in cancer and cancer immunotherapy. *Br J Cancer* **124**: 359-367.

Renz BW, Takahashi R, Tanaka T, Macchini M, Hayakawa Y, Dantes Z, Maurer HC, Chen X, Jiang Z, Westphalen CB et al. 2018. beta2 Adrenergic-Neurotrophin Feedforward Loop Promotes Pancreatic Cancer. *Cancer Cell* **33**: 75-90 e77.

Rhim AD, Oberstein PE, Thomas DH, Mirek ET, Palermo CF, Sastra SA, Dekleva EN, Saunders T, Becerra CP, Tattersall IW et al. 2014. Stromal elements act to restrain, rather than support, pancreatic ductal adenocarcinoma. *Cancer Cell* **25**: 735-747.

Riddle RD, Johnson RL, Laufer E, Tabin C. 1993. Sonic hedgehog mediates the polarizing activity of the ZPA. *Cell* **75**: 1401-1416.

Rivera A, Siracusa MC, Yap GS, Gause WC. 2016. Innate cell communication kick-starts pathogen-specific immunity. *Nat Immunol* **17**: 356-363.

Robert C, Ribas A, Schachter J, Arance A, Grob J-J, Mortier L, Daud A, Carlino MS, McNeil CM, Lotem M et al. 2019. Pembrolizumab versus ipilimumab in advanced melanoma (KEYNOTE-006): post-hoc 5-year results from an open-label, multicentre, randomised, controlled, phase 3 study. *The Lancet Oncology* **20**: 1239-1251.

Roberts EW, Deonarine A, Jones JO, Denton AE, Feig C, Lyons SK, Espeli M, Kraman M, McKenna B, Wells RJ et al. 2013. Depletion of stromal cells expressing fibroblast activation protein-alpha from skeletal muscle and bone marrow results in cachexia and anemia. *J Exp Med* **210**: 1137-1151.

Rodriguez PC, Quiceno DG, Zabaleta J, Ortiz B, Zea AH, Piazuelo MB, Delgado A, Correa P, Brayer J, Sotomayor EM et al. 2004. Arginase I production in the tumor

microenvironment by mature myeloid cells inhibits T-cell receptor expression and antigen-specific T-cell responses. *Cancer Res* **64**: 5839-5849.

Rohatgi R, Milenkovic L, Scott MP. 2007. Patched1 regulates hedgehog signaling at the primary cilium. *Science* **317**: 372-376.

Royal RE, Levy C, Turner K, Mathur A, Hughes M, Kammula US, Sherry RM, Topalian SL, Yang JC, Lowy I et al. 2010. Phase 2 trial of single agent Ipilimumab (anti-CTLA-4) for locally advanced or metastatic pancreatic adenocarcinoma. *J Immunother* **33**: 828-833.

Saloman JL, Albers KM, Li D, Hartman DJ, Crawford HC, Muha EA, Rhim AD, Davis BM. 2016. Ablation of sensory neurons in a genetic model of pancreatic ductal adenocarcinoma slows initiation and progression of cancer. *Proc Natl Acad Sci U S A* **113**: 3078-3083.

Sanders TA, Llagostera E, Barna M. 2013. Specialized filopodia direct long-range transport of SHH during vertebrate tissue patterning. *Nature* **497**: 628-632.

Sanford DE, Belt BA, Panni RZ, Mayer A, Deshpande AD, Carpenter D, Mitchem JB, Plambeck-Suess SM, Worley LA, Goetz BD et al. 2013. Inflammatory monocyte mobilization decreases patient survival in pancreatic cancer: a role for targeting the CCL2/CCR2 axis. *Clin Cancer Res* **19**: 3404-3415.

Sasaki H, Hui C, Nakafuku M, Kondoh H. 1997. A binding site for Gli proteins is essential for HNF-3beta floor plate enhancer activity in transgenics and can respond to Shh in vitro. *Development* **124**: 1313-1322.

Sasaki H, Nishizaki Y, Hui C, Nakafuku M, Kondoh H. 1999. Regulation of Gli2 and Gli3 activities by an amino-terminal repression domain: implication of Gli2 and Gli3 as primary mediators of Shh signaling. *Development* **126**: 3915-3924.

Sasson A, Rachi E, Sakhneny L, Baer D, Lisnyansky M, Epshtein A, Landsman L. 2016. Islet Pericytes Are Required for beta-Cell Maturity. *Diabetes* **65**: 3008-3014.

Scarlett CJ, Colvin EK, Pinese M, Chang DK, Morey AL, Musgrove EA, Pajic M, Apte M, Henshall SM, Sutherland RL et al. 2011. Recruitment and activation of pancreatic stellate cells from the bone marrow in pancreatic cancer: a model of tumor-host interaction. *PLoS One* **6**: e26088.

Schimmang T, Lemaistre M, Vortkamp A, Ruther U. 1992. Expression of the zinc finger gene Gli3 is affected in the morphogenetic mouse mutant extra-toes (Xt). *Development* **116**: 799-804.

Seeberger KL, Dufour JM, Shapiro AM, Lakey JR, Rajotte RV, Korbutt GS. 2006. Expansion of mesenchymal stem cells from human pancreatic ductal epithelium. *Lab Invest* **86**: 141-153.

Seo Y, Baba H, Fukuda T, Takashima M, Sugimachi K. 2000. High expression of vascular endothelial growth factor is associated with liver metastasis and a poor prognosis for patients with ductal pancreatic adenocarcinoma. *Cancer* **88**: 2239-2245.

Shek FW-T, Benyon RC, Walker FM, McCrudden PR, Pender SLF, Williams EJ, Johnson PA, Johnson CD, Bateman AC, Fine DR et al. 2002. Expression of Transforming Growth Factor-β1 by Pancreatic Stellate Cells and Its Implications for Matrix Secretion and Turnover in Chronic Pancreatitis. *The American Journal of Pathology* **160**: 1787-1798.

Sherman MH, Yu RT, Engle DD, Ding N, Atkins AR, Tiriac H, Collisson EA, Connor F, Van Dyke T, Kozlov S et al. 2014. Vitamin D receptor-mediated stromal reprogramming suppresses pancreatitis and enhances pancreatic cancer therapy. *Cell* **159**: 80-93.

Siegel RL, Miller KD, Fuchs HE, Jemal A. 2022. Cancer statistics, 2022. *CA Cancer J Clin* **72**: 7-33.

Son J, Lyssiotis CA, Ying H, Wang X, Hua S, Ligorio M, Perera RM, Ferrone CR, Mullarky E, Shyh-Chang N et al. 2013. Glutamine supports pancreatic cancer growth through a KRAS-regulated metabolic pathway. *Nature* **496**: 101-105.

Stamataki D, Ulloa F, Tsoni SV, Mynett A, Briscoe J. 2005. A gradient of Gli activity mediates graded Sonic Hedgehog signaling in the neural tube. *Genes Dev* **19**: 626-641.

Steele NG, Biffi G, Kemp SB, Zhang Y, Drouillard D, Syu L, Hao Y, Oni TE, Brosnan E, Elyada E et al. 2021. Inhibition of Hedgehog Signaling Alters Fibroblast Composition in Pancreatic Cancer. *Clin Cancer Res* **27**: 2023-2037.

Steele NG, Carpenter ES, Kemp SB, Sirihorachai V, The S, Delrosario L, Lazarus J, Amir ED, Gunchick V, Espinoza C et al. 2020. Multimodal Mapping of the Tumor and Peripheral Blood Immune Landscape in Human Pancreatic Cancer. *Nat Cancer* **1**: 1097-1112.

Stone DM, Hynes M, Armanini M, Swanson TA, Gu Q, Johnson RL, Scott MP, Pennica D, Goddard A, Phillips H et al. 1996. The tumour-suppressor gene patched encodes a candidate receptor for Sonic hedgehog. *Nature* **384**: 129-134.

Stromnes IM, Brockenbrough JS, Izeradjene K, Carlson MA, Cuevas C, Simmons RM, Greenberg PD, Hingorani SR. 2014. Targeted depletion of an MDSC subset unmasks pancreatic ductal adenocarcinoma to adaptive immunity. *Gut* **63**: 1769-1781.

Stylianopoulos T, Martin JD, Chauhan VP, Jain SR, Diop-Frimpong B, Bardeesy N, Smith BL, Ferrone CR, Hornicek FJ, Boucher Y et al. 2012. Causes, consequences, and remedies for growth-induced solid stress in murine and human tumors. *Proc Natl Acad Sci U S A* **109**: 15101-15108.

Sugimoto H, Mundel TM, Kieran MW, Kalluri R. 2006. Identification of fibroblast heterogeneity in the tumor microenvironment. *Cancer Biol Ther* **5**: 1640-1646.

Taipale J, Cooper MK, Maiti T, Beachy PA. 2002. Patched acts catalytically to suppress the activity of Smoothened. *Nature* **418**: 892-897.

Tao J, Yang G, Zhou W, Qiu J, Chen G, Luo W, Zhao F, You L, Zheng L, Zhang T et al. 2021. Targeting hypoxic tumor microenvironment in pancreatic cancer. *J Hematol Oncol* **14**: 14.

Tape CJ, Ling S, Dimitriadi M, McMahon KM, Worboys JD, Leong HS, Norrie IC, Miller CJ, Poulogiannis G, Lauffenburger DA et al. 2016. Oncogenic KRAS Regulates Tumor Cell Signaling via Stromal Reciprocation. *Cell* **165**: 910-920.

Taylor AM, Nakano Y, Mohler J, Ingham PW. 1993. Contrasting distributions of patched and hedgehog proteins in the Drosophila embryo. *Mechanisms of Development* **42**: 89-96.

te Welscher P, Zuniga A, Kuijper S, Drenth T, Goedemans HJ, Meijlink F, Zeller R. 2002. Progression of vertebrate limb development through SHH-mediated counteraction of GLI3. *Science* **298**: 827-830.

Tenzen T, Allen BL, Cole F, Kang JS, Krauss RS, McMahon AP. 2006. The cell surface membrane proteins Cdo and Boc are components and targets of the Hedgehog signaling pathway and feedback network in mice. *Dev Cell* **10**: 647-656.

Thayer SP, di Magliano MP, Heiser PW, Nielsen CM, Roberts DJ, Lauwers GY, Qi YP, Gysin S, Fernandez-del Castillo C, Yajnik V et al. 2003. Hedgehog is an early and late mediator of pancreatic cancer tumorigenesis. *Nature* **425**: 851-856.

Tian H, Callahan CA, DuPree KJ, Darbonne WC, Ahn CP, Scales SJ, de Sauvage FJ. 2009. Hedgehog signaling is restricted to the stromal compartment during pancreatic carcinogenesis. *Proc Natl Acad Sci U S A* **106**: 4254-4259.

Toole BP, Slomiany MG. 2008. Hyaluronan: a constitutive regulator of chemoresistance and malignancy in cancer cells. *Semin Cancer Biol* **18**: 244-250.

Trovato R, Fiore A, Sartori S, Cane S, Giugno R, Cascione L, Paiella S, Salvia R, De Sanctis F, Poffe O et al. 2019. Immunosuppression by monocytic myeloid-derived suppressor cells in patients with pancreatic ductal carcinoma is orchestrated by STAT3. *J Immunother Cancer* **7**: 255.

Tukachinsky H, Kuzmickas RP, Jao CY, Liu J, Salic A. 2012. Dispatched and scube mediate the efficient secretion of the cholesterol-modified hedgehog ligand. *Cell Rep* **2**: 308-320.

Tukachinsky H, Lopez LV, Salic A. 2010. A mechanism for vertebrate Hedgehog signaling: recruitment to cilia and dissociation of SuFu-Gli protein complexes. *J Cell Biol* **191**: 415-428.

Van Cutsem E, Tempero MA, Sigal D, Oh DY, Fazio N, Macarulla T, Hitre E, Hammel P, Hendifar AE, Bates SE et al. 2020. Randomized Phase III Trial of Pegvorhyaluronidase

Alfa With Nab-Paclitaxel Plus Gemcitabine for Patients With Hyaluronan-High Metastatic Pancreatic Adenocarcinoma. *J Clin Oncol* **38**: 3185-3194.

van den Heuvel M, Ingham PW. 1996. smoothened encodes a receptor-like serpentine protein required for hedgehog signalling. *Nature* **382**: 547-551.

Velez-Delgado A, Donahue KL, Brown KL, Du W, Irizarry-Negron V, Menjivar RE, Lasse Opsahl EL, Steele NG, The S, Lazarus J et al. 2022. Extrinsic KRAS Signaling Shapes the Pancreatic Microenvironment Through Fibroblast Reprogramming. *Cell Mol Gastroenterol Hepatol*.

Vokes SA, Ji H, McCuine S, Tenzen T, Giles S, Zhong S, Longabaugh WJ, Davidson EH, Wong WH, McMahon AP. 2007. Genomic characterization of Gli-activator targets in sonic hedgehog-mediated neural patterning. *Development* **134**: 1977-1989.

Vokes SA, Ji H, Wong WH, McMahon AP. 2008. A genome-scale analysis of the cis-regulatory circuitry underlying sonic hedgehog-mediated patterning of the mammalian limb. *Genes Dev* **22**: 2651-2663.

Von Hoff DD, Ervin T, Arena FP, Chiorean EG, Infante J, Moore M, Seay T, Tjulandin SA, Ma WW, Saleh MN et al. 2013. Increased survival in pancreatic cancer with nab-paclitaxel plus gemcitabine. *N Engl J Med* **369**: 1691-1703.

Vonderheide RH. 2018. The Immune Revolution: A Case for Priming, Not Checkpoint. *Cancer Cell* **33**: 563-569.

Vortkamp A, Gessler M, Grzeschik KH. 1995. Identification of optimized target sequences for the GLI3 zinc finger protein. *DNA Cell Biol* **14**: 629-634.

Waghray M, Yalamanchili M, Dziubinski M, Zeinali M, Erkkinen M, Yang H, Schradle KA, Urs S, Pasca Di Magliano M, Welling TH et al. 2016. GM-CSF Mediates Mesenchymal-Epithelial Cross-talk in Pancreatic Cancer. *Cancer Discov* **6**: 886-899.

Wainberg ZA, Hochster HS, Kim EJ, George B, Kaylan A, Chiorean EG, Waterhouse DM, Guiterrez M, Parikh A, Jain R et al. 2020. Open-label, Phase I Study of Nivolumab Combined with nab-Paclitaxel Plus Gemcitabine in Advanced Pancreatic Cancer. *Clin Cancer Res* **26**: 4814-4822.

Walton KD, Gumucio DL. 2021. Hedgehog Signaling in Intestinal Development and Homeostasis. *Annu Rev Physiol* **83**: 359-380.

Walton KD, Kolterud A, Czerwinski MJ, Bell MJ, Prakash A, Kushwaha J, Grosse AS, Schnell S, Gumucio DL. 2012. Hedgehog-responsive mesenchymal clusters direct patterning and emergence of intestinal villi. *Proc Natl Acad Sci U S A* **109**: 15817-15822.

Wang B, Fallon JF, Beachy PA. 2000. Hedgehog-Regulated Processing of Gli3 Produces an Anterior/Posterior Repressor Gradient in the Developing Vertebrate Limb. *Cell* **100**: 423-434.

Wang B, Li Y. 2006. Evidence for the direct involvement of {beta}TrCP in Gli3 protein processing. *Proc Natl Acad Sci U S A* **103**: 33-38.

Wang Y, Zhou Z, Walsh CT, McMahon AP. 2009. Selective translocation of intracellular Smoothened to the primary cilium in response to Hedgehog pathway modulation. *Proc Natl Acad Sci U S A* **106**: 2623-2628.

Wen X, Lai CK, Evangelista M, Hongo JA, de Sauvage FJ, Scales SJ. 2010. Kinetics of hedgehog-dependent full-length Gli3 accumulation in primary cilia and subsequent degradation. *Mol Cell Biol* **30**: 1910-1922.

West H, McCleod M, Hussein M, Morabito A, Rittmeyer A, Conter HJ, Kopp H-G, Daniel D, McCune S, Mekhail T et al. 2019. Atezolizumab in combination with carboplatin plus nab-paclitaxel chemotherapy compared with chemotherapy alone as first-line treatment for metastatic non-squamous non-small-cell lung cancer (IMpower130): a multicentre, randomised, open-label, phase 3 trial. *The Lancet Oncology* **20**: 924-937.

Williams JA. 2019. Cholecystokinin (CCK) Regulation of Pancreatic Acinar Cells: Physiological Actions and Signal Transduction Mechanisms. *Compr Physiol* **9**: 535-564.

Williams PG, Hersh JH, Yen FF, Barch MJ, Kleinert HE, Kunz J, Kalff-Suske M. 1997. Greig cephalopolysyndactyly syndrome: altered phenotype of a microdeletion syndrome due to the presence of a cytogenetic abnormality. *Clin Genet* **52**: 436-441.

Wilson CW, Chuang PT. 2010. Mechanism and evolution of cytosolic Hedgehog signal transduction. *Development* **137**: 2079-2094.

Winograd R, Byrne KT, Evans RA, Odorizzi PM, Meyer AR, Bajor DL, Clendenin C, Stanger BZ, Furth EE, Wherry EJ et al. 2015. Induction of T-cell Immunity Overcomes Complete Resistance to PD-1 and CTLA-4 Blockade and Improves Survival in Pancreatic Carcinoma. *Cancer Immunol Res* **3**: 399-411.

Yang S, Che SP, Kurywchak P, Tavormina JL, Gansmo LB, Correa de Sampaio P, Tachezy M, Bockhorn M, Gebauer F, Haltom AR et al. 2017. Detection of mutant KRAS and TP53 DNA in circulating exosomes from healthy individuals and patients with pancreatic cancer. *Cancer Biol Ther* **18**: 158-165.

Yauch RL, Gould SE, Scales SJ, Tang T, Tian H, Ahn CP, Marshall D, Fu L, Januario T, Kallop D et al. 2008. A paracrine requirement for hedgehog signalling in cancer. *Nature* **455**: 406-410.

Ying H, Kimmelman AC, Lyssiotis CA, Hua S, Chu GC, Fletcher-Sananikone E, Locasale JW, Son J, Zhang H, Coloff JL et al. 2012. Oncogenic Kras maintains pancreatic tumors through regulation of anabolic glucose metabolism. *Cell* **149**: 656-670.

Youn JI, Nagaraj S, Collazo M, Gabrilovich DI. 2008. Subsets of myeloid-derived suppressor cells in tumor-bearing mice. *J Immunol* **181**: 5791-5802.

Yuzawa S, Kano MR, Einama T, Nishihara H. 2012. PDGFRbeta expression in tumor stroma of pancreatic adenocarcinoma as a reliable prognostic marker. *Med Oncol* **29**: 2824-2830.

Zhang L, Sanagapalli S, Stoita A. 2018. Challenges in diagnosis of pancreatic cancer. *World J Gastroenterol* **24**: 2047-2060.

Zhang Y, Crawford HC, Pasca di Magliano M. 2019. Epithelial-Stromal Interactions in Pancreatic Cancer. *Annu Rev Physiol* **81**: 211-233.

Zhang Y, Lazarus J, Steele NG, Yan W, Lee HJ, Nwosu ZC, Halbrook CJ, Menjivar RE, Kemp SB, Sirihorachai VR et al. 2020. Regulatory T-cell Depletion Alters the Tumor Microenvironment and Accelerates Pancreatic Carcinogenesis. *Cancer Discov* **10**: 422-439.

Zhang Y, Velez-Delgado A, Mathew E, Li D, Mendez FM, Flannagan K, Rhim AD, Simeone DM, Beatty GL, Pasca di Magliano M. 2017a. Myeloid cells are required for PD-1/PD-L1 checkpoint activation and the establishment of an immunosuppressive environment in pancreatic cancer. *Gut* **66**: 124-136.

Zhang Y, Yan W, Mathew E, Kane KT, Brannon A, 3rd, Adoumie M, Vinta A, Crawford HC, Pasca di Magliano M. 2017b. Epithelial-Myeloid cell crosstalk regulates acinar cell plasticity and pancreatic remodeling in mice. *Elife* **6**.

Zhu Y, Knolhoff BL, Meyer MA, Nywening TM, West BL, Luo J, Wang-Gillam A, Goedegebuure SP, Linehan DC, DeNardo DG. 2014. CSF1/CSF1R blockade reprograms tumor-infiltrating macrophages and improves response to T-cell checkpoint immunotherapy in pancreatic cancer models. *Cancer Res* **74**: 5057-5069.

Chapter 2 Combinatorial *Gli* activity directs immune infiltration and tumor growth in pancreatic cancer[2]

2.1 Abstract

Proper Hedgehog (HH) signaling is essential for embryonic development, while aberrant HH signaling drives pediatric and adult cancers. HH signaling is frequently dysregulated in pancreatic cancer, yet its role remains controversial, with both tumor-promoting and tumor-restraining functions reported. Notably, the GLI family of HH transcription factors (GLI1, GLI2, GLI3), remain largely unexplored in pancreatic cancer. We therefore investigated the individual and combined contributions of GLI1-3 to pancreatic cancer progression. At pre-cancerous stages, fibroblast-specific *Gli2/Gli3* deletion decreases immunosuppressive macrophage infiltration and promotes T cell infiltration. Strikingly, combined loss of *Gli1/Gli2/Gli3* promotes macrophage infiltration, indicating that subtle changes in *Gli* expression differentially regulate immune infiltration. In invasive tumors, *Gli2/Gli3* KO fibroblasts exclude immunosuppressive myeloid cells and suppress tumor growth by recruiting natural killer cells. Finally, we demonstrate that fibroblasts directly regulate macrophage and T cell migration through the expression of *Gli*-dependent cytokines. Thus, the coordinated activity of GLI1-3 directs the fibroinflammatory response throughout pancreatic cancer progression.

[2] This chapter has been accepted for publication: Scales, M.K., Velez-Delgado, A., Steele, N.G., Schrader, H.E., Stabnick, A.M., Yan, W., Mercado Soto, N.M., Nwosu, Z.C., Johnson, C., Zhang, Y., Salas-Escabillas, D.J., Menjivar, R.E., Maurer, H.C., Crawford, H.C., Bednar., F., Olive, K.P., Pasca di Magliano, M., and Allen, B.L. 2022. Combinatorial *Gli* activity directs immune infiltration and tumor growth in pancreatic cancer. *PLOS Genetics.* In press.

2.2 Introduction

Pancreatic ductal adenocarcinoma (PDA) remains a deadly malignancy, with a 5-year survival rate of 11% (Siegel et al. 2022). One contributing factor to this low survival rate is a lack of effective therapies. Although the mechanisms driving resistance to treatment are complex, one major barrier is the tumor microenvironment (TME). The TME of PDA is extremely heterogeneous, involving a complex network of endothelial cells, nerves, fibroblasts, and immune cells (Zhang et al. 2019). Within this network, fibroblasts function as critical nodes for intercellular signaling. Pancreatic fibroblasts contribute to pancreatic disease through a variety of means, including the production of extracellular matrix (ECM) and the secretion of pro-tumorigenic factors (Apte et al. 1999; Apte et al. 2000; Mews et al. 2002; Shek et al. 2002; Hwang et al. 2008). Fibroblasts also provide metabolic support (Halbrook and Lyssiotis 2017; Muranen et al. 2017; Francescone et al. 2021), confer chemoresistance (Hwang et al. 2008; Ireland et al. 2016; Hessmann et al. 2018), facilitate immunosuppression (Kraman et al. 2010; Feig et al. 2013), and restrict tumor perfusion via ECM deposition (Olive et al. 2009; Provenzano et al. 2012; Jacobetz et al. 2013). However, fibroblasts also have tumor-restricting roles (Lee et al. 2014; Mathew et al. 2014b; Ozdemir et al. 2014; Rhim et al. 2014). These seemingly disparate functions could be explained by the observation that cancer-associated fibroblasts are heterogeneous (Biffi et al. 2019; Garcia et al. 2020b; Helms et al. 2020), with different populations having different, potentially opposing functions. However, the mechanisms and signals used by fibroblast populations to affect disease progression are not fully understood.

Work from our lab and others has identified aberrant HH signaling as a feature of PDA (Berman et al. 2003; Thayer et al. 2003; Jones et al. 2008). In the context of PDA, HH ligands (primarily sonic hedgehog [SHH] and indian hedgehog [IHH]) are secreted by tumor cells and

bind to the canonical receptor patched 1 (PTCH1) on fibroblasts (Bailey et al. 2008; Yauch et al. 2008; Tian et al. 2009). Following ligand binding, the repressive activity of PTCH1 is inhibited, leading to the activation of smoothened (SMO), which in turn modulates the GLI family of HH transcription factors (Briscoe and Therond 2013). Although this paracrine model of HH signaling in pancreatic cancer is well-established, the contribution of HH signaling to pancreatic cancer progression remains controversial.

Previous mouse studies indicated that HH pathway inhibition improves chemotherapy delivery and extends survival (Olive et al. 2009). However, clinical trials employing SMO inhibitors provided no clinical benefit or, in some cases, led to worse outcomes (Kim et al. 2014; Catenacci et al. 2015; Ko et al. 2016). Further, genetic loss of *Shh* shortens survival in mouse models of PDA, suggesting that HH signaling has tumor-restraining roles (Lee et al. 2014; Rhim et al. 2014). One explanation for these contradictory results is that the level of HH pathway activity influences pancreatic tumor growth. Combinatorial targeting of HH pathway co-receptors revealed that partial reduction of HH signaling in fibroblasts promotes tumor growth, while near complete ablation of the stromal HH response fails to promote tumorigenesis (Mathew et al. 2014b). More recent work demonstrated that pharmacologic HH pathway inhibition alters cancer-associated fibroblast (CAF) composition and immune infiltration in PDA, indicating that HH signaling impacts multiple cell types within the pancreatic TME (Steele et al. 2021). However, the downstream consequences of HH pathway activity on pancreatic tumor growth, specifically the transcriptional outcomes of HH signal transduction in the pancreatic stroma, remain unexplored.

The GLI family of proteins (GLI1, GLI2, GLI3) are the transcriptional effectors of the HH pathway. GLI1 exclusively functions as a transcriptional activator, while GLI2 and GLI3

contain both activator and repressor domains (Hui and Angers 2011). In multiple tissues, GLI2 primarily acts as a transcriptional activator (Bai and Joyner 2001), while GLI3 functions as a transcriptional repressor (Persson et al. 2002). Prior work from our group has demonstrated that GLI1 supports pancreatic tissue recovery following induction of acute pancreatitis or oncogenic *Kras*-driven injury (Mathew et al. 2014a). However, the expression and function of GLI2 and GLI3 in PDA remain largely unknown. Further, the combined role of multiple GLIs during PDA progression has not been explored.

In this study, we investigated the role of GLI1-3 in PDA progression. We have determined that *Gli1*, *Gli2*, and *Gli3* are expressed in the healthy pancreas, and expand throughout PDA progression. At pre-cancerous stages, genetic deletion of *Gli2* and *Gli3* in fibroblasts reduces collagen deposition and dramatically alters immune infiltration. Specifically, stromal depletion of *Gli2* and *Gli3* leads to a decrease in immunosuppressive macrophage infiltration and an increase in T cells. However, deleting all three *Glis* in fibroblasts leads to an increase in macrophage infiltration and the exclusion of T cells. Further, mice lacking *Gli1*, *Gli2*, and *Gli3* display a widespread loss of pancreatic tissue, suggesting that a baseline level of GLI activity is necessary to maintain tissue integrity during disease progression. In invasive tumors, we have determined that the loss of *Gli2* and *Gli3* in fibroblasts decreases myeloid-derived suppressor cells (MDSCs) and increases natural killer (NK) cells, which in turn antagonize tumor growth. In contrast, *Gli1/Gli2/Gli3* KO fibroblasts recruit MDSCs and exclude NK cells, leading to sustained tumor growth. Together, our data demonstrate that the activities of all three GLIs regulate immune infiltration throughout PDA progression, and these GLI-driven changes determine tumor growth.

2.3 Results

2.3.1 Gli1-3 are expressed in the pancreatic stroma and expand during PDA progression

To determine *GLI1-3* expression in human PDA, we analyzed epithelial and stromal samples isolated from PDA patients by laser-capture microdissection (Maurer et al. 2019). *GLI1-3* are predominantly expressed in the stroma (Figure 2.1A-C), while HH ligands are expressed in the epithelium (Figure 2.2A). HH receptors are also enriched in the stroma (Figure 2.2B-C), consistent with the paracrine manner of HH signaling in PDA (Berman et al. 2003; Thayer et al. 2003; Yauch et al. 2008; Nolan-Stevaux et al. 2009; Tian et al. 2009). Further, all three *GLI*s are expressed by multiple types of pre-cancerous lesions, including both pancreatic intraepithelial neoplasia (PanIN) and intraductal papillary mucinous neoplasms (IPMNs). Since the stroma consists of diverse cell types, we analyzed a recently published single-cell RNA sequencing dataset (Steele et al. 2020) to precisely determine which cellular compartments express *GLI1-3*. Gene expression analysis revealed that fibroblasts are the primary source of *GLI1-3* in PDA (Figure 2.1D).

$Kras^{LSL\text{-}G12D/+};Ptf1a^{Cre/+}$ (KC) (Hingorani et al. 2003) and $Kras^{LSL\text{-}G12D/+}; p53^{LSL\text{-}R172H/+};Ptf1a^{Cre/+}$ (KPC) (Hingorani et al. 2005) mouse models of PDA provide an opportunity to investigate disease progression in a system that faithfully recapitulates human disease. In both models, *Cre* expression by pancreatic progenitor cells activates oncogenic *Kras* (Hingorani et al. 2003; Hingorani et al. 2005). Induction of acute pancreatitis (via caeruelin injections) synergizes with oncogenic *Kras* to produce widespread PanIN lesions in KC mice (Carriere et al. 2009). In KPC mice, CRE also drives the expression of a mutant *p53* allele, leading to the spontaneous development of invasive pancreatic tumors (Hingorani et al. 2005). To determine if *Gli1-3* expression in mouse models is consistent with human disease, we utilized *Gli-lacZ* reporter mice

(Bai and Joyner 2001; Bai et al. 2002; Garcia et al. 2010). X-gal staining (Figure 2.1E) and immunofluorescent (IF) detection of Beta Galactosidase (β-GAL; Figures 2.1F, 2.2D-E) in healthy mouse pancreata revealed that *Gli1*, *Gli2*, and *Gli3* are all expressed by fibroblasts surrounding blood vessels and pancreatic ducts. Further, *Gli2*- and *Gli3*-expressing fibroblasts also surround acinar cell clusters (Figure 2.1E-F). *Gli-lacZ* reporter mice were then crossed into KC and KPC models of PDA. X-gal staining of *Gli1-lacZ;KC, Gli2-lacZ;KC,* and *Gli3-lacZ*;*KC* tissue revealed that all three *Glis* expand within the stroma at PanIN stages (Figure 2.1G), and immunofluorescent detection of β-GAL indicated that *Gli* expression remains restricted to pancreatic fibroblasts (Figure 2.2F-I). Further, *Gli1-3* are expressed broadly within the tumor stroma of *Gli-lacZ; KPC* mice (Figure 2.1H, Figure 2.2J). Together, these data demonstrate that the patterns of *Gli* expression observed in mouse models are consistent with human PDA.

2.3.2 Conditional Gli2 and Gli3 deletion in vivo restricts immunosuppressive macrophages and promotes T cell infiltration

The broad, stromal expression of *Gli1-3* throughout disease progression raised the question of *Gli* function in PDA. While *Gli1* has established roles in tissue recovery (Mathew et al. 2014a) and PanIN progression (Mills et al. 2013), the roles of stromal *Gli2* and *Gli3* during PDA progression are unknown. To target *Gli2* and *Gli3* in fibroblasts *in vivo*, we crossed the $Pdgfr\alpha^{CreER\text{-}T2}$ allele (Chung et al. 2018) into $Kras^{FSF\text{-}G12D/+};Ptf1a^{FlpO/+}$ (KF) (Garcia et al. 2020a) mice. In this combined $KF;Pdgfr\alpha^{CreER\text{-}T2}$ model (Figure 2.3A), $Ptf1a^{FlpO/+}$ drives oncogenic *Kras* expression and PanIN formation in the pancreatic epithelium, allowing us to utilize a CreER to inducibly delete *Gli* in pancreatic fibroblasts. Adult $KF;Pdgfr\alpha^{CreER\text{-}T2}$ mice were given tamoxifen daily for 5 days to induce recombination, followed by two days of caerulein injections to drive acute pancreatitis and initiate PanIN formation (Morris et al. 2010). Mice were then

harvested 3 weeks later once PanIN lesions established throughout the pancreas. Lineage tracing revealed that the *Pdgfrα*$^{CreER-T2}$ allele effectively labels the neoplastic stroma (Figure 2.4A), and reduces *Gli2* and *Gli3* expression by approximately 70% each in *KF; Pdgfrα*$^{CreER-T2}$*; Gli2*$^{fl/fl}$*; Gli3*$^{fl/fl}$ (*KF;Gli2/Gli3* cKO) mice (Figure 2.4B). Histologic analysis of *KF;Gli2/Gli3* cKO mice revealed a disrupted stroma, including an increased number of stromal cells and a decrease in collagen deposition compared to *KF; Gli2*$^{fl/fl}$*; Gli3*$^{fl/fl}$ (*KF;Gli2/Gli3* WT) mice (Figure 2.3B-C). However, initial characterization of fibroblasts from *KF;Gli2/Gli3* cKO mice revealed no inherent differences in proliferation compared to *KF;Gli2/Gli3* WT mice (Figure 2.4C). To determine which stromal cell types change as a result of *Gli2/Gli3* deletion, we performed flow cytometry analysis on *KF;Gli2/Gli3* cKO and *KF;Gli2/Gli3* WT tissue. Interestingly, we found that total immune cells increase following loss of *Gli2* and *Gli3*, yet total myeloid cells decrease (Figure 2.3D, Figure 2.4D-E). When we examined different subpopulations of immune cells (Figure 2.3E-I, Figure 2.4D, F-J), we found a significant reduction in macrophages in *KF;Gli2/Gli3* cKO mice (Figure 2.3E). To assess which types of macrophages are impacted by the loss of *Gli2/Gli3*, we evaluated the expression of arginase 1 (ARG1), a marker of immunosuppressive tumor-associated macrophages (TAMs). Co-staining with ARG1 and the general macrophage marker F4/80 revealed a decrease in TAMs following the loss of *Gli2* and *Gli3* (Figure 2.3F). In contrast to this decrease in immunosuppressive TAMs, we found an increase in total T cells in *KF;Gli2/Gli3* cKO mice (Figure 2.3G, Figure 2.4D). Analysis of different T cell populations (Figure 2.3H-I, Figure 2.4D, H-J) revealed that both CD4+ and CD8+ T cells increased following the loss of *Gli2* and *Gli3* (Figure 2.3H-I, Figure 2.4D). Together, these data suggest that fibroblast-specific *Gli2*/*Gli3* deletion disrupts the immunosuppressive microenvironment in pancreatic neoplasia.

Since immune suppression plays a crucial role in PDA (Feig et al. 2013), we investigated whether loss of *Gli2/Gli3* affects PanIN progression. However, caerulein administration in mutant *Kras* mice can synchronize and accelerate PanIN lesions (Carriere et al. 2009). We therefore utilized a spontaneous model in which *KF;Gli2/Gli3* cKO mice were aged to 20 weeks, when spontaneous PanIN formation is expected (Figure 2.5A-B). *KF;Gli2/Gli3* cKO mice present with reduced collagen deposition (Figure 2.5C, G) and a reduction in macrophage infiltration (Figure 2.5E, I). We also observed a trend toward increased cytoplasmic mucin, a feature of low-grade PanIN (Cornish and Hruban 2011), in a majority of *KF;Gli2/Gli3* cKO mice (Figure 2.5D, H). However, histopathological analysis of the PanIN lesions indicated no difference in PanIN progression between *KF;Gli2/Gli3* cKO and *KF;Gli2/Gli3* WT mice (Figure 2.5F). Thus, while loss of *Gli2* and *Gli3* in the fibroblasts significantly impairs ECM accumulation and reduces the relative proportion of macrophages, it is not sufficient to alter PanIN progression.

2.3.3 Combined Gli1-3 deletion drives widespread tissue loss during PanIN progression

While validating our *KF;Gli2/Gli3* cKO model, we were surprised to find that *Gli1* expression is maintained following the loss of *Gli2/Gli3* (Figure 2.5J). This contrasts with *Gli2;Gli3* double mutant embryos, which lack *Gli1* expression across multiple developing tissues (Bai et al. 2004). We hypothesized that *Gli1* could be functioning partially redundantly with *Gli2* and *Gli3*, and that deleting all three *Glis* would accentuate the phenotypes we observed in *KF;Gli2/Gli3* cKO mice. To test this, we utilized $Gli1^{CreERT2}$ mice (Ahn and Joyner 2004), in which a *CreER-t2* allele knocked into the endogenous *Gli1* locus abolishes *Gli1* expression while driving recombination in pancreatic fibroblasts (Garcia et al. 2020a). Crossing this allele into *KF* mice enabled us to target *Gli2* and *Gli3* expression in *Gli1*-expressing fibroblasts during PanIN

progression (Figure 2.6A). RNAscope analysis of *KF; Gli1*$^{CreERT2/CreERT2}$*; Gli2*$^{fl/fl}$*; Gli3*$^{fl/fl}$ (*KF;Gli1/Gli2/Gli3* KO) mice confirmed complete elimination of *Gli1* (Figure 2.7A) and efficient conditional reduction of *Gli3* (Figure 2.7B). Once validated, *KF;Gli1/Gli2/Gli3* KO mice were aged to 20 weeks to evaluate spontaneous PanIN progression in the absence of *Gli1-3*.

Strikingly, combined *Gli1/Gli2/Gli3* depletion leads to a dramatic loss of pancreas parenchyma, with concurrent pancreatic lipomatosis, or adipocyte accumulation in the pancreas (Figure 2.6B-E, Figure 2.7C). Pancreatic lipomatosis is observed following extensive acinar cell death (Cano et al. 2006; Criscimanna et al. 2011). Although no differences in cell death are detected between *KF;Gli1/Gli2/Gli3* WT and *KF;Gli1/Gli2/Gli3* KO tissue at the time of dissection (Figure 2.7C), the loss of acinar tissue likely occurred earlier in disease progression, resulting in the disrupted state of the pancreas following *Gli* deletion. Interestingly, the pancreata of *Gli1/Gli2/Gli3* KO mice that do not express oncogenic *Kras* are grossly normal, and do not show any evidence of tissue loss or pancreatic lipomatosis (Figure 2.6D-E). Thus, the combined loss of *Gli1/Gli2/Gli3* only compromises tissue integrity in the context of pancreatic carcinogenesis.

In addition to disrupted tissue architecture, the pancreata of *KF;Gli1/Gli2/Gli3* KO mice feature an increase in macrophages compared to *KF;Gli1/Gli2/Gli3* WT mice (Figure 2.6F-G), in contrast to the decrease in macrophages observed in *KF;Gli2/Gli3* cKO tissue (cf. Figure 2.3E). We did not find any difference in T cell number between *KF;Gli1/Gli2/Gli3* KO and *KF;Gli1/Gli2/Gli3* WT mice (Figure 2.6F, H). Thus, a baseline level of *Gli* activity is necessary to maintain pancreas integrity during PanIN progression. Further, total ablation of *Gli* promotes macrophage infiltration, suggesting that macrophages are sensitive to subtle changes in GLI activity in fibroblasts.

2.3.4 Loss of Gli2 and Gli3 reduces tumor growth through the recruitment of NK cells

To study the role of *Gli1/Gli2/Gli3* in tumor growth, we performed tumor implantation experiments with *Gli* KO pancreatic fibroblasts (Figure 2.8A). Since germline *Gli2* and *Gli3* mutants die perinatally (Hui and Joyner 1993; Mo et al. 1997), we utilized $Gli^{fl/fl}$ mice to derive fibroblast lines from the adult pancreas. Once established, fibroblast lines were infected with either a GFP-expressing adenovirus (WT lines) or a Cre-expressing adenovirus (*Gli* KO), and *Gli* deletion was validated by qPCR and western blot (Figure 2.9A-D). Both *Gli2/Gli3* KO and *Gli1/Gli2/Gli3* KO pancreatic fibroblasts are unresponsive to HH stimulation, while parental line controls remain HH responsive (Figure 2.9E-F). *Gli* KO fibroblasts were co-injected with KPC-derived tumor cells (Long et al. 2016) into the flanks of nude mice, which lack functional T and B cells. Consistent with previous findings (Xu et al. 2010; Mathew et al. 2014b), co-injecting tumor cells with WT fibroblasts produces larger tumors than tumor cells alone (Figure 2.8B). In contrast, co-injecting *Gli2/Gli3* KO fibroblasts with tumor cells fails to promote tumor growth, and produces tumors that are significantly smaller than tumors co-injected with WT fibroblasts (Figure 2.8B). Given the detrimental effects observed when *Gli1*, *Gli2*, and *Gli3* are deleted at PanIN stages (Figure 2.6), we next tested how *Gli1/Gli2/Gli3* KO fibroblasts impact invasive tumor growth. Strikingly, co-injection of tumor cells with *Gli1/Gli2/Gli3* KO fibroblasts promotes tumor growth to the same degree as parental *Gli1* KO fibroblasts and WT control fibroblasts (Figure 2.8C, cf. Figure 2.8B). Thus, while reduction of *Gli* restrains tumor growth, total ablation of *Gli* promotes tumor growth.

We next wanted to determine why *Gli2/Gli3* KO fibroblasts fail to promote tumor growth. To confirm that *Gli2/Gli3* KO fibroblasts persist in this transplantation model, we analyzed harvested tumors for the presence of a tdTomato reporter allele expressed by *Gli2/Gli3*

KO fibroblasts. TdTomato expression was detected by IF in tumors from our *Gli2/Gli3* KO condition (Figure 2.10A), confirming that the decrease in tumor growth was not simply due to the death of injected fibroblasts. We next assessed whether *Gli2/Gli3* KO fibroblasts impacted the growth of tumor cells directly. However, we found no differences in tumor cell proliferation nor cell death between *Gli2/Gli3* KO and WT conditions (Figure 2.10B-C). We also did not find any differences between fibroblast nor endothelial cell abundance across our experimental conditions (Figure 2.10D-E). Given the connection between *Gli* expression and immune infiltration that we observed at PanIN stages, we next investigated whether this reduction in tumor growth was due to altered recruitment of immune cells. We found no difference in total immune cells between our different experimental conditions (Figure 2.8D). However, when we analyzed different subpopulations of immune cells (Figure 2.8E-F, Figure 2.10F-G), we determined that *Gli2/Gli3* deletion in fibroblasts leads to a decrease in MDSCs and an increase in NK cells (Figure 2.8E-F). Interestingly, *Gli2* KO, *Gli3* KO, and *Gli1/Gli2/Gli3* KO fibroblasts do not impact MDSC nor NK cell infiltration (Figure 2.10H-J, Figure 2.11A-L), indicating that this effect on immune infiltration is specific to *Gli2/Gli3* KO fibroblasts.

We were surprised to find that total myeloid cells and macrophages do not change following the loss of *Gli2/Gli3* in our tumor implantation experiments (Figure 2.10F-G), in contrast to our *KF;Gli2/Gli3* cKO model (cf. Figure 2.3E, Figure 2.4E). We wondered if this difference could be due to the different genetic strains between our experimental systems, as *KF;Gli2/Gli3* cKO mice are fully immune competent and possess functional T cells, while nude mice do not. We hypothesized that the loss of *Gli2/Gli3* leads to a decrease in immunosuppressive myeloid cells (MDSCs/macrophages) and an increase in cytotoxic immune cells (T cells/NK cells), and the exact cell types involved depend on the model system. We

therefore suspected that in the absence of T cells, the enhanced NK cell recruitment in our *Gli2/Gli3* KO condition was responsible for antagonizing tumor growth. To test whether this infiltration of NK cells suppresses tumor growth, tumor-bearing mice were treated with an NK cell-depleting antibody (anti-asialo GM1; Figure 2.8G, Figure 2.11M-P). Tumor growth following co-injection with WT fibroblasts is unaffected by NK cell depletion (Figure 2.8H), presumably due to NK cells already being excluded from the microenvironment. In contrast, depleting NK cells in tumors co-injected with *Gli2/Gli3* KO fibroblasts rescues tumor growth, and the resulting tumors are equivalent in size to tumors co-injected with WT fibroblasts (Figure 2.8H). These data reveal that the loss of *Gli2/Gli3* in fibroblasts restricts tumor growth through the recruitment of NK cells.

2.3.5 Gli activity in fibroblasts directly controls macrophage and T cell migration

To further investigate GLI2/GLI3 function in the pancreatic TME, we transcriptionally profiled *Gli2/Gli3* KO pancreatic fibroblasts by RNA sequencing (RNAseq). RNAseq analysis identified over 2,200 differentially expressed genes in *Gli2/Gli3* KO fibroblasts compared to WT fibroblasts. When we filtered the data for membrane-bound and secreted factors (Zhang et al. 2020), we detected a number of differentially expressed ECM components and receptors (Figure 2.12A-B), consistent with the impaired ECM deposition we observe following the loss of *Gli2* and *Gli3 in vivo* (cf. Figure 2.3C). Further, we detected several cytokines that are upregulated in *Gli2/Gli3* KO fibroblasts (Figure 2.13A, Figure 2.12A). Specifically, *Ccl5* and *Cxcl10*, two genes encoding T cell and NK cell chemoattractants (Maghazachi et al. 1996; Tan et al. 2009; Karin and Razon 2018), are increased in *Gli2/Gli3* KO fibroblasts (Figure 2.13A). Further, two myeloid-modulating cytokines, *Il6* and *Il11*, (Putoczki and Ernst 2010; Fernando et al. 2014) are reduced in *Gli2/Gli3* KO fibroblasts. We validated these changes in cytokine expression by

qPCR (Figure 2.13B). To determine if these transcriptional changes in *Gli2/Gli3* KO fibroblasts are maintained *in vivo,* we analyzed cytokine expression in *KF;Gli2/Gli3* cKO mice by RNAscope. While *Il6* expression in fibroblasts is heterogeneous (as expected from previous work (Ohlund et al. 2017)), we detected PDPN+ fibroblasts with high *Il6* expression in our *KF;Gli2/Gli3* WT mice (Figure 2.13C-D). In contrast, no PDPN+ fibroblasts with high *Il6* expression were detected in *KF;Gli2/Gli3* cKO mice (Figure 2.13C-D), indicating that *Gli2* and *Gli3* deletion restricts *Il6* expression *in vivo.*

Although these changes in cytokine expression are consistent with the decrease in macrophages and increase in T cells observed *in vivo*, it remained unclear whether *Gli2/Gli3* deletion in fibroblasts impacted the function of these immune cells directly. To investigate the interaction between fibroblasts and macrophages mechanistically, we performed macrophage migration assays (Sakamoto et al. 2021), in which macrophages were placed above fibroblasts on a transwell membrane and allowed to migrate for 12 hours (Figure 2.13E). WT fibroblasts consistently promote macrophage migration compared to media alone (Figure 2.13F-I). Loss of *Gli2* alone does not affect macrophage migration (Figure 2.13F), while loss of *Gli3* alone leads to a partial reduction of macrophage migration (Figure 2.13G). In contrast, *Gli2/Gli3* KO fibroblasts reduce macrophage migration to near baseline levels (Figure 2.13H). This reduction in macrophage migration is consistent across multiple macrophage phenotypes, including M0, M1, M2, and TAMs (Figure 2.12C). Interestingly, *Gli1/Gli2/Gli3* KO fibroblasts promote macrophage migration to a significantly greater degree than either WT or *Gli1* KO parental line control fibroblasts (Figure 2.13I). These data are consistent with what we observe *in vivo* (cf. Figure 2.6G), indicating that the increase in macrophage infiltration in *KF;Gli1/Gli2/Gli3* KO mice is directly due to the loss of *Gli1/Gli2/Gli3* in fibroblasts. Further, these *Gli*-dependent

effects on macrophages are mediated by secreted factors, as conditioned media from WT and *Gli* KO fibroblasts recapitulate the effects observed in fibroblast co-culture experiments (Figure 2.12D). Together, our data indicate that *Gli*-mediated cytokine expression directly regulates macrophage infiltration in PDA.

To determine if this effect is conserved in human fibroblasts, we performed macrophage migration assays with human pancreatic stellate cells (hPSCs) (Hwang et al. 2008). We confirmed that hPSCs are HH-responsive, and upregulate the HH target genes *GLI1* and *PTCH1* in response to HH stimulation (Figure 2.12E-F). In addition, hPSCs promote macrophage migration to a similar degree as WT mouse fibroblasts (Figure 2.12G). Thus, human pancreatic fibroblasts are both HH-responsive and directly promote macrophage migration.

We next investigated the consequence of fibroblast-specific *Gli* deletion on T cells. We first evaluated whether *Gli* expression regulates T cell differentiation and polarization. Our *in vivo* data indicate that fibroblast-specific *Gli2/Gli3* deletion leads to a subtle (and not statistically significant) increase in regulatory T cells (Tregs, Figure 2.4H). Since Tregs regulate immune suppression in PDA through cross-talk with fibroblasts (Zhang et al. 2020), we investigated whether loss of *Gli* in fibroblasts impacts Treg differentiation. While T cells co-cultured with *Gli2/Gli3* KO fibroblasts do not significantly increase expression of the Treg marker *Foxp3*, T cells co-cultured with *Gli1/Gli2/Gli3* KO fibroblasts do significantly upregulate *Foxp3* (Figure 2.14A). These data are consistent with the notion that *Gli1/Gli2/Gli3* KO fibroblasts promote immune suppression, as suggested by enhanced macrophage infiltration both *in vitro* and *in vivo* (Figures 2.6G and 2.13I). Notably, the expression of functional Treg markers associated with an immunosuppressive phenotype (including *Il10* and *Tgfb*) is not significantly altered across our different *Gli* KO fibroblast lines (Figure 2.14B-C). These data indicate that fibroblasts regulate T

cell differentiation into Tregs in a GLI-dependent fashion, but do not affect the gene expression pattern of established Tregs.

To determine if the loss of *Gli* in fibroblasts directly regulates T cell infiltration, we performed transwell T cell migration assays with our *Gli* KO fibroblast lines. While WT fibroblasts do not impact T cell migration, *Gli2/Gli3* KO fibroblasts promote T cell migration to the same degree as a potent T cell chemoattractant, CXCL12 (SDF1α) (Fig 2.13J). In contrast, *Gli1/Gli2/Gli3* KO fibroblasts do not promote T cell migration, as the degree of migration is comparable to media alone (Fig 2.13J). Together, these data corroborate the phenotypes we observe *in vivo,* and reveal that fibroblasts directly regulate the migration of both macrophages and T cells through GLI-dependent expression of cytokines.

2.4 Discussion

In this study, we investigated the individual and combined roles of *Gli1-3* throughout PDA progression. We determined that *Gli1-3* are expressed by fibroblasts in the healthy pancreas, and that expression of all *Glis* expands in PanIN and PDA stages of disease. Through a combination of genetic mouse models and *ex vivo* approaches, we found that GLIs direct the fibroinflammatory response during PanIN progression and in PDA (Figure 2.15). Reducing *Gli* activity through loss of *Gli2* and *Gli3* decreases collagen and reduces the infiltration of immunosuppressive myeloid cells, and at the same time promotes T cell infiltration. In a PDA transplantation model, where T cells are absent in the host, we observe an increase in NK cell infiltration, that in turn reduces tumor growth. However, a baseline level of *Gli* activity is necessary, as deleting all three *Glis* leads to a dramatic loss of pancreas tissue, an increase in macrophage infiltration, sustained T cell exclusion, and enhanced tumor growth. Together, these

data demonstrate that differing levels of *Gli* activity have opposing functions throughout PDA progression, and that *Gli*-driven changes in immune infiltration determine tumor growth.

2.4.1 Tumor-supporting and tumor-restricting roles for HH in PDA

Unraveling the role of HH signaling in PDA has proven challenging, as reports have described contradictory roles for the pathway in pancreatic cancer. However, these seemingly conflicting findings may be an accurate reflection of the complicated and nuanced biology at play in this disease. Our data support a model in which reduced HH signaling promotes tumor growth, while total ablation of HH pathway activity reduces it. Subtle differences in how the pathway is manipulated alter the levels of HH signaling and tip the scales towards tumor-promoting or tumor-restricting effects.

Our data provide evidence that the activity of multiple transcription factors regulate PDA progression, a theme that has been seen at all levels of the HH signaling pathway. For example, multiple HH ligands (*Shh* and *Ihh*) are expressed in PDA (Yauch et al. 2008; Rhim et al. 2014; Steele et al. 2021), and while loss of a single ligand promotes tumor growth (Lee et al. 2014; Rhim et al. 2014), the absence of both *Ihh* and *Shh* reduces tumor growth (Steele et al. 2021). Importantly, this decrease in tumor growth is only seen in a HH-sensitized model (when host mice lack one copy of *Gli1*), further demonstrating that severe inhibition of HH, not slight reduction, is necessary to reduce tumor growth. Similarly, multiple HH co-receptors (*Gas1*, *Boc*, *Cdon*) regulate pancreatic tumor growth (Mathew et al. 2014b). While loss of two receptors (*Gas1* and *Boc*) promote tumor growth, deleting all three co-receptors reduces tumor growth (Mathew et al. 2014b). These patterns of tumor growth in $Gas^{-/-};Boc^{-/-}$ and $Gas1^{-/-};Boc^{-/-};Cdon^{-/-}$ tumors also coincide with increased and decreased vasculature, respectively, indicating that subtle differences in HH signaling levels impact multiple compartments within the TME.

Together, these data from throughout the pathway indicate that slight reduction of HH signaling promotes disease progression, while severe inhibition restrains it.

Taken alone, the reduction of tumor growth following severe inhibition of HH signaling would indicate that HH solely supports tumor growth. However, our data also indicate that activation of HH can be protective. Loss of GLI repressor (via *Gli3* deletion) reduces the migration of macrophages and decreases tumor growth, demonstrating that HH activation can antagonize PDA. This finding is consistent with previous work, in which pharmacological activation of HH signaling via Smoothened agonist (SAG21k) led to decreased proliferation/abundance of PanIN lesions (Lee et al. 2014). Thus, HH has the ability to both promote and restrict tumor growth, and the net effect depends on the levels of HH pathway activity.

Beyond the importance of signaling levels, HH pathway components have functions outside of canonical signal transduction. While the primary role of GLIs is to regulate levels of HH signaling, growing evidence indicates that GLIs also influence PDA through HH-independent mechanisms. Although the canonical HH response is restricted to fibroblasts, tumor cells can aberrantly activate GLIs. Non-canonical upregulation of GLI2 causes tumor cells to adopt a more basal subtype, leading to an increase in mesenchymal markers and a decrease in epithelial markers (Adams et al. 2019). This finding is consistent with previous work from our group, where ectopic expression of constitutively active GLI2 drove the formation of undifferentiated tumors (Pasca di Magliano et al. 2006). Conversely, antagonizing GLI targets in tumor cells either by knocking down *Gli1* (Nolan-Stevaux et al. 2009) or over-expressing a constitutive GLI3 repressor (Rajurkar et al. 2012) increases tumor cell death and reduces colony

formation. Thus, GLI activity can promote tumor growth in epithelial cells in a cell-autonomous, HH-independent manner.

While aberrant upregulation of GLI promotes tumor cell growth, our single-cell and laser capture RNA sequencing analysis indicate that GLIs are predominantly expressed in the stroma. Therefore, in this study we focused our attention on the role of GLI1-3 in the stroma. However, even within the stroma there are non-canonical functions for HH pathway components. For example, genetic deletion of *Smo* in pancreatic fibroblasts eliminates the HH-response but leads to the aberrant activation of AKT (Liu et al. 2016; Pitarresi et al. 2018). AKT is then able to stabilize GLI2 in fibroblasts, which in turn promotes epithelial cell growth via TGF-α secretion (Liu et al. 2016). These HH-independent roles for GLIs open up the possibility that the phenotypes we observe in *Gli* KO fibroblasts could be due to a combination of both canonical as well as non-canonical GLI functions. Exploring this possibility requires a deeper investigation into GLI targets in PDA.

Here we describe the coordinated roles of all three GLIs *in vivo* within the context of PDA progression. Our data demonstrate that manipulating GLI has both tumor-promoting and tumor-restricting effects, depending on their combinatorial activity. However, the transcriptional mechanisms driving these different phenotypes remain unclear. Our RNA sequencing analysis of *Gli2/Gli3* KO fibroblasts indicates that the coordinated activity of GLI2 and GLI3 drive a transcriptional program that shapes the extracellular and immune landscape of PDA. Further, pervious work has identified a number of transcriptional targets of GLI1 in pancreatic fibroblasts, including *Il6, Il8*, *Mcp-1, M-csf* (Mills et al. 2013; Mathew et al. 2014a). However, the degree of overlap between GLI1, GLI2, and GLI3 transcriptional targets in PDA is still unknown. In addition, it is possible that GLI target genes may change at different stages of

disease progression. Fortunately, the development of ChIP-capable tags on endogenous *Gli* alleles (e.g., 3x*Flag*-*Gli3*) (Elliott et al. 2020) provides an opportunity to define GLI target genes *in vivo*. Future studies could utilize ChIP-capable GLI1-3 proteins to define shared and unique GLI target genes and evaluate how GLI-driven transcriptional programs change throughout PDA progression. Building out this transcriptional roadmap could help identify the HH targets responsible for driving tumor-promoting versus tumor-restricting programs in PDA, opening up new, more targeted avenues for potential therapies.

2.4.2 Hedgehog-Immune Crosstalk

Fibroblasts play a crucial role in regulating immune infiltration in PDA and are essential in driving immune-suppression (Kraman et al. 2010; Feig et al. 2013; Zhang et al. 2020). Further, growing evidence supports the notion that HH signaling regulates immune infiltration in pancreatic cancer. Prior work has demonstrated that *Gli1* drives the expression of immune-modulatory cytokines (Mills et al. 2013; Mathew et al. 2014a). More recently, pharmacological inhibition of SMO (via LDE225) in tumor-bearing mice was shown to increase the recruitment of immunosuppressive macrophages and decrease the relative proportion of cytotoxic T cells (Steele et al. 2021). Our data confirms that disrupting HH signaling dramatically alters immune infiltration in the context of PDA progression. However, combined loss of *Gli2* and *Gli3* decreases the recruitment immunosuppressive macrophages and increases the recruitment of cytotoxic T cells. At first glance these results seem surprising, as both LDE225-treated and *Gli2/Gli3* KO fibroblasts do not respond to HH. This discrepancy raises the question: why does SMO inhibition and *Gli* deletion drive such divergent immune phenotypes?

One essential difference between these two experimental systems is the combinatorial activity of the GLIs. Although *Gli2/Gli3* KO pancreatic fibroblasts do not upregulate target

genes following HH stimulation, we found that a baseline level of *Gli1* expression is maintained in these cells. As a result, some GLI target genes could still be bound by this baseline level of GLI-activator in the absence of *Gli2* and *Gli3*. In contrast, LDE225 treatment effectively eliminates *Gli1* expression in pancreatic fibroblasts (Steele et al. 2021), leading to a fully "HH Off" state. Thus, genetic loss of *Gli2* and *Gli3* represents a different level of HH pathway activity compared to LDE225-treated pancreatic fibroblasts. Given the evidence that different levels of HH activity drive radically different phenotypes in PDA (Mathew et al. 2014b), it is not surprising that we see distinct immune phenotypes between *Gli2/Gli3* cKO and LDE225-treated mice. Notably, when we eliminate all three *Glis*, we observe patterns of immune infiltration that are more consistent with LDE225 treatment, presumably due to the elimination of redundant GLI-activator.

Beyond the compensatory actions of GLI-activators, *Gli2/Gli3* KO fibroblasts fundamentally differ from LDE225-treated cells due to the loss of *Gli3*. We see in our system that loss of *Gli3* alone is sufficient to partially reduce the migration of macrophages. This indicates that in the context of PDA progression, de-repression of GLI target genes is an important force in regulating immune infiltration. In our *Gli2/Gli3* KO fibroblasts, the absence of a repressor combined with the presence of an activator (GLI1) has the potential to drive substantial transcriptional activity, even in the absence of a HH response. Together, these data emphasize the importance of combinatorial GLI activity in regulating disease progression, and reveal how subtle differences in HH transcriptional activity can dramatically shape the immune landscape of PDA. These findings also provide further rationale for defining GLI-activator versus GLI-repressor transcriptional targets throughout PDA progression.

In addition to demonstrating the differences between pharmacological and genetic manipulation of HH signaling, these studies reveal how the role of HH in regulating immune infiltration changes at different stages of disease. In the present study, *Gli* was deleted in fibroblasts prior to the formation of PanIN lesions (KF mice) or before exposure to tumor cells (tumor implantation experiments). Therefore, our data reveal how the immune landscape of PDA develops in the absence of normal HH activity. In contrast, pharmacological inhibition in tumor-bearing mice demonstrate the impact of removing HH signaling from an established disease (Steele et al. 2021). Prior research has demonstrated that disrupting HH signaling in fibroblasts has different consequences on PDA progression depending on the stage of disease studied (Mills et al. 2013; Mills et al. 2014). It is therefore likely that the role of HH on the immune system also evolves throughout PDA progression, and that some of the differences we observe reflect a shift in HH's role. Fortunately, the inducible nature of the *KF; Pdgfr*$\alpha^{CreER\text{-}T2}$*;Gli2*$^{fl/fl}$*; Gli3*$^{fl/fl}$ mouse model could be leveraged to delete *Gli* after the formation of PanIN lesions, directly testing the role of *Gli* in established pancreatic disease. Thus, this experimental system provides new opportunities to evaluate the role of HH signaling at multiple stages of PDA.

Although our study provides new insight into *Gli*-mediated regulation of immune infiltration in PDA, many open questions remain. One outstanding question is how GLIs regulate the balance of CAF subtypes in PDA. A growing body of work is revealing the heterogeneity of pancreatic fibroblasts and demonstrating that different populations have distinct roles in the context of pancreatic cancer (Ohlund et al. 2017; Biffi et al. 2019; Elyada et al. 2019; Hosein et al. 2019). Further, pharmacological inhibition of HH changes the balance of inflammatory CAFs (iCAFs) and myofibroblastic CAFs (myCAFs) *in vivo,* resulting in a more immunosuppressive microenvironment (Steele et al. 2021). Given the ability of GLIs to fine-tune HH responses in

pancreatic fibroblasts, a natural next question is how different GLIs influence the relative proportion of CAFs in PDA. Our expression analysis *in vitro* and *in vivo* demonstrates that loss of *Gli2/Gli3* reduces *Il6* expression, a key marker of iCAFs. A reduction in iCAFs would be consistent with the reduction in immunosuppressive immune cells that we observe *in vivo*. However, more in-depth analysis will be necessary to explore the potential connections between GLIs and fibroblast heterogeneity.

Overall, our data indicate that all three GLIs play a central role in PDA progression. The reduction in immunosuppression following *Gli2/Gli3* deletion warrants further exploration into the transcriptional networks downstream of *Gli*. Identifying and targeting these mechanisms of immunosuppression could provide new avenues for future therapies, potentially enhancing the efficacy of immunotherapy in this challenging disease.

2.5 Materials and methods

Laser-capture microdissection and RNA sequencing (LCM-RNAseq)

LCM-RNAseq was performed and analyzed by Maurer and colleagues (Maurer et al. 2019). Briefly, samples underwent laser capture microdissection using a PALM MicroBeam microscope (Zeiss). RNA libraries were generated using the Obation RNAseq System V2 kit (NuGEN), and sequenced to a depth of 30 million, 100 bp, single-end reads.

Single-cell RNA sequencing (scRNAseq)

scRNAseq data were generated and processed as previously described (Steele et al. 2020). Briefly, processed data were normalized using the Seurat (V4) (Hao et al. 2021) pipeline in R with a scale factor of 10,000 and the LogNormalize normalization method. Variable genes were identified using FindVariableFeatures. Data were scaled and centered using linear

regression and principal component analysis (PCA) was run with the RunPCA function using the defined variable genes. Genes in the HH pathway were displayed as a Dot Plot analysis.

X-gal Staining

Pancreata were dissected in chilled 1x PBS (pH 7.4). Tissue samples were collected for RNA isolation and histology, and the remaining tissue was fixed (4% PFA) on ice for 1h. Pancreata were washed 3x5min in PBS and transferred to a PBS+30% sucrose solution overnight at 4°C. The next day, half of the 30% sucrose was removed and replaced with OCT embedding medium, and placed on a rocker at 4°C for 1h. This process was repeated twice, and then the tissue was transferred to 100% OCT for 1h. Tissues were embedded in OCT and sectioned on a Leica CM1950 cryostat (12μm sections). β-Galactosidase activity was detected with X-gal staining solution [5 mM K3Fe(CN)6, 5 mM K4Fe(CN)6, 2 mM MgCl2, 0.01% Na deoxycholate, 0.02% NP-40, 1 mg/ml X-gal] and stained for 2 – 36h at 37°C. After staining, the sections were washed 3x5min in PBS and counterstained with Nuclear Fast Red for 5min. Sections were dehydrated 70% ethanol, 95% ethanol, 100% ethanol and 100% xylene) and mounted with coverslips using Permount Mounting Medium (Thermo Fisher Scientific).

Immunofluorescence

Tissues were dissected/processed as described above. Frozen sections were warmed to room temperature (RT), then baked at 60°C for 10min. Sections were washed 3x5min in PBS and blocked in blocking buffer [3% bovine serum albumin, 1% heat-inactivated sheep serum, 0.1% Triton X-100 in PBS] for 1h at RT. Paraffin sections were rehydrated (100% xylene, 100% ethanol, 95% ethanol, DI water) and underwent citric acid antigen retrieval (Vector Laboratories,

H-3300) for 10min at 92°C. Paraffin sections were washed 3x5min with DI water, 3x5min with PBS, and blocked for 1h at RT in PBS+1% BSA. All sections were incubated with primary antibodies overnight at 4°C in a humidified chamber. Primary antibodies are listed in Table 2.1. Secondary antibodies were diluted in blocking buffer and incubated for 1h at RT, followed by 3x5min washes in PBS. All secondary antibodies were used at a 1:500 dilution. Nuclei were labeled with DAPI for 10min at RT. Slides were mounted with coverslips using Immu-mount aqueous mounting medium (for frozen sections) or Permount Mounting Medium (for paraffin sections). Sections were visualized on a Leica SP5X upright confocal or a Nikon E800 epifluorescent microscope. For quantitation, 3 – 5 fields of view were imaged per section and analyzed using FIJI (version 2.0.0-rc-69/1.52p).

Subcutaneous Tumor Growth Assays

1 x 10^5 7940b tumor cells were mixed with 5 x 10^5 fibroblasts, resuspended in a 50:50 mix of serum-free media [DMEM+1% Pen/Step] and Matrigel (Corning 354234). Two fibroblast clones (in equal numbers) were used in each injection to reduce the impact of clonal variability. Cells were injected subcutaneously into the flanks of NU/J mice (Jackson Laboratory Stock No: 002019). Tumors were measured every other day with calipers, and animals were sacrificed after 10 days. For NK cell depletion experiments, 10µl of anti-asialo GM1 (Wako 986-10001) or an equivalent volume of normal Rabbit IgG control (R&D AB-105-C) was diluted 1:10 in sterile PBS and injected intraperitoneally. Injections were given 24h before tumor implantation, on the day of tumor implantation, and once every three days for the remainder of the experiment.

Flow Cytometry

Single-cell suspensions of tissue were prepared as previously described (Zhang et al. 2014). Flow cytometry was performed either on a BioRad Ze5 Analyzer or a MoFLo Astrios cell sorter, and data were analyzed with FlowJo v10 Software. Values for all flow cytometry data displayed as a percentage of total cells. Antibodies used for flow cytometry are listed in Table 2.2.

Histology

Tissue samples were fixed in 10% neutral buffered formalin (Thermo Fisher 245-685) overnight at RT. Samples were washed 3x5min in PBS, moved to 70% ethanol, and then processed for paraffin embedding. 5μm sections were collected and used for histological analysis. Hematoxylin and eosin (H&E) and Gomori Trichrome stain were performed according to standard protocols.

Macrophage Migration Assays

Bone marrow cells were isolated as described previously (Zhang et al. 2008) and plated in a 50-50 mixture of complete media [DMEM F12 + 10% Calf Serum + 1% Pen/Step] and tumor cell (7940b) conditioned media. Cells were supplemented with 750μl of 50-50 media every other day for a total of 6 days. On day 5, 2.5 x 10^5 total fibroblasts were plated into each well of a 12-well plate. Two fibroblast clones (in equal numbers) were used for all conditions. Once cells adhered to the plates (after 8h), the media was replaced with low (0.1%) serum media. On day 6, macrophages were removed from plates with 0.25% Trypsin-EDTA (Gibco 25200-056) and scraping, and resuspended in low serum media. 4 x 10^5 macrophages were plated onto

each transwell insert (8μm pore size, Thermo Scientific 140656) above fibroblast wells. After 12h, remaining macrophages were removed from the top of the transwells with a cotton swab, and the membranes were fixed (4% PFA) for 10min at RT, followed by 3x5 min PBS washes. Membranes were stained with DAPI for 10min at RT, washed 3x5 min in PBS, and removed from the transwells with a scalpel. Membranes were then mounted onto slides with Immu-mount aqueous mounting medium, coverslipped, and imaged as described above.

T Cell Differentiation and Migration Assays

1 x 10^5 total fibroblasts were plated into each well of a 24-well plate in complete media [DMEM + 10% CS + 1% Pen/Strep]. Two fibroblast clones (in equal numbers) were used for all conditions. 8 h later, the media was replaced with 1% serum media [DMEM + 1% CS + 1% Pen/Strep]. The next morning, single cell suspensions were made from the spleens of BL6 mice, and total T cells were isolated by MACS according to the manufacturer's instructions (Miltenyi Biotec 130-042-401). T cells in suspension were bound by Biotin-conjugated anti-CD3 antibody (R&D BAM4841), and captured in a magnetic column with anti-Biotin microbeads. Isolated T cells were resuspended in 1% serum media and 2.5 x 10^5 T cells were added to the top of each transwell. For differentiation assays, 0.4μm pore transwell membranes were used. For migration assays, 5μm pore transwell membranes were used. 100 ng/ml CXCL12 (SDF1α) R&D 460-SD-010) added to the bottom chamber was used as a positive control in migration assays. Plates were returned to the cell culture incubator under standard cell culture conditions for 6.5 h. At the end of differentiation assays, T cells were collected from the top chamber and lysed for RNA isolation (see below). At the end of migration assays, migrated T cells were collected from the bottom chamber, spun down, and counted with a hemocytometer.

RNAscope

RNAscope was performed as described previously (Holloway et al. 2021). Briefly, paraffin sections were baked at 60°C for 1h, and then stored overnight at RT. Fluorescent RNAscope was performed according to the manufacturer's protocol (ACD: 323100-USM). Samples underwent antigen retrieval for 15min, followed by a 12min protease digestion. TSA fluorophores (Akoya biosciences NEL744001KT and NEL745E001KT) were diluted 1:2000 in TSA dilution buffer. Following HRP blocking, slides were washed 3x5 min in PBS and blocked in 0.1% PBS-Tween20 + 5% Normal Donkey Serum for 1h at RT. Primary antibody incubation, secondary antibody incubation, and the subsequent processing, imaging, and quantitation was performed as described above.

Western Blot Analysis

20μg of protein was separated on an SDS-polyacrylamide gel (5% GLI2, 7.5% GLI3) for 30min at 80V followed by 90min at 100V. Gels were transferred to an Immuno-Blot PVDF membrane (Bio-Rad; Cat #1620177), blocked with western blocking buffer (30g BSA, 2ml 10% NaN3, Q.S. 1L TBST) for 5min, and probed with antibody diluted in western blocking buffer. Membranes were washed for 3x5min in TBST and then probed with secondary antibody for 1h at RT. Membranes were then washed 12x5min at RT. Protein was detected by fluorescence, using ECL Primer Western Blotting Detection Reagents (RPN2232) developed on a Konica Minolta SRX-101A Medical Film Processor. All primary and secondary antibodies are listed in Tables 2.3 and 2.4, respectively.

Cell culture

All cell lines were maintained at 37°C and 5% CO_2, and were kept in standard media (DMEM + 10% Calf Serum + 1% Pen/Strep) unless noted otherwise. The human pancreatic stellate cell (hPSC) line has been previously published (Hwang et al. 2008), and was generously provided by C.A. Lyssiotis. Mouse fibroblast lines were established through the outgrowth method (Todaro and Green 1963). Briefly, pancreata were isolated from adult mice under sterile conditions. Pancreata were minced mechanically and digested for 15min at 37°C in 1 mg/ml collagenase (Sigma C9263, diluted in sterile Hank's Balanced Salt Solution - HBSS). Standard media was added to inactivate the enzymatic digestion, and samples were passed through a 70μm cell strainer, resuspended in standard media, and plated onto tissue culture plates coated in 0.1% gelatin. Primary cells (less than 3 passages) were frozen and stored, and kept separate from immortalized lines. Following immortalization, fibroblasts were infected with adenovirus (Control: Ad5 CMV-eGFP and Lenti dsRed; cKO: Ad5 CMV-eGFP and Ad5 CMV-Cre) at an MOI of 500 – 2000. Successfully infected cells were isolated by flow cytometry and screened by qPCR and western blot for recombination efficacy. Cell lines were tested for mycoplasma before running experiments. For HH signaling assays, 5 x 10^5 fibroblasts were plated in each well of a 6-well plate in standard media. 24h after plating, the media was replaced with low (0.1%) serum media. 24h later, the media was replaced with 1.5ml of low serum media + 600 nM of Smoothened agonist (SAG) or vehicle control (DMSO). 24h later, a supplemental dose of SAG/vehicle was added directly to each well to a final concentration of 600 nM. 24h later, the cells were lysed and analyzed for HH target gene expression.

RNA isolation

Snap-frozen tissue samples were pre-treated with RNA*later*-ICE (Invitrogen AM7030) according to the manufacturer's instructions. Tissue samples and bulk RNA sequencing samples were lysed in Buffer RLT + 1% BME and processed with the Qiagen RNeasy Mini Kit (Qiagen 74104) according to the manufacturer's instructions. For all other applications, RNA isolation was performed using the PureLink RNA Mini Kit (Invitrogen 12183025) according to the manufacturer's instructions. All samples were eluted in ultrapure water, and RNA quality was determined using a NanoDrop One (Thermo Scientific ND-ONE-W).

qPCR

cDNA was generated from 0.5 – 2μg of RNA using the Applied Biosystems High Capacity cDNA Reverse Transcription Kit (Thermo Fisher 4368814) according to the manufacturer's instructions. qPCR reactions were run using PowerUp SYBR Green Master Mix (Applied Biosystems A25742) and the primers listed in Table 2.5 in a StepOnePlus Real-time PCR System (Applied Biosystems 4376600). Gene expression was normalized to Cyclophilin unless stated otherwise. Relative expression was calculated using the $2(^{-ddCT})$ method.

Animal models

All mice were housed in specific pathogen-free facilities at the University of Michigan. This study was approved by the University of Michigan Institutional Animal Care and Use Committee (IACUC). *Gli1*^{lacZ} (Bai et al. 2002), *Gli2*^{lacZ} (Bai and Joyner 2001), *Gli3*^{lacZ} (Garcia et al. 2010), *Ptf1a*^{Cre} (*p48*^{Cre}) (Kawaguchi et al. 2002), *Kras*$^{LSL\text{-}G12D}$ (Hingorani et al. 2003), *Ptf1a*^{FlpO} (*p48*^{FlpO}) (Wen et al. 2019), *Kras*$^{FSF\text{-}G12D}$ (Schonhuber et al. 2014), *Pdgfrα*^{CreERt2}

(Chung et al. 2018), *Gli2*$^{fl/fl}$ (Corrales et al. 2006), *Gli3*$^{fl/fl}$ (Blaess et al. 2008), *LSL*-tdTomato (Madisen et al. 2010), *Gli1*^{CreERt2} (Ahn and Joyner 2004)mice have all been described previously. To induce Cre recombination, tamoxifen (Sigma T5648) was administered to mice at a dose of 200 mg/kg once per day for 5 days by oral gavage. To induce acute pancreatitis in 6 – 8 week old KC and KF mice, 8 hourly i.p. injections of caerulein (Sigma C9026) were administered at a dose of 75μg/kg over two consecutive days. Caerulein-treated mice were harvested 3 weeks after their final dose. KF mice used in aging experiments were not given caerulein, and were dissected once the mice reached 20 weeks of age. KPC mice were monitored daily by abdominal palpitation and dissected once the mice reached humane endpoint.

Statistical Analysis

All statistical analysis was performed using Graphpad Prism software. For quantitative analysis, each data point represents an independent biological replicate. Information such as sample size, P value, and the statistical test used is stated in the figure legend. Significant P-values are indicated with one or multiple asterisks according to the following convention: * = $p \leq 0.05$, ** = $p \leq 0.01$, *** = $p \leq 0.001$, **** = $p \leq 0.0001$, ns = $p > 0.05$.

2.6 Acknowledgements

We thank members of the Allen and Pasca di Magliano Labs, as well as the Developmental Genetics and Pancreatic Cancer research groups. We acknowledge members of the Department of Cell and Developmental Biology who provided access to equipment, including the O'Shea, Engel, and Spence labs. We also acknowledge Daniel Long and Michael Mattea for providing histology services. We thank Katelyn Donahue for valuable input regarding macrophage and

fibroblast cross-talk. We thank Costas Lyssiotis and the members of the Lyssiotis Lab for generously providing hPSCs. We thank Ethan Tyler and Dr. L. Kravitz for providing the mouse drawing used in our schematics (doi.org/10.5281/zenodo.3925901) through the opensiyrce repository Scidraw.io. Finally, we thank the University of Michigan Biomedical Research Core Facilities and the School of Dentistry Histology core, for providing access to research equipment and services.

2.7 Author Contributions

Conceptualization: MKS, MPM, BLA

Methodology: MKS, MPM, BLA

Software: MKS, ZCN, CJ, HCM, KPO

Validation: MKS, MPM, BLA

Formal Analysis: MKS, AVD, NGS, ZCN, CJ, YZ, HCM, KPO

Investigation: MKS, AVD, NGS, HES, AMS, WY, NMS, ZCN, CJ, YZ, DJSE, REM, HCM, HCC, FB, KPO, MPM, BLA

Resources: HCC, FB, KPO, MPM, BLA

Data Curation: MKS, CJ

Writing – Original Draft: MKS, MPM, BLA

Writing - Review & Editing: MKS, NGS, ZCN, MPM, BLA

Visualization: MKS, MPM, BLA

Supervision: MPM, BLA

Project Administration: MPM, BLA

Funding Acquisition: MKS, AVD, NGS, ZCN, YZ, REM, HCC, FB, KPO, MPM, BLA

2.8 Tables

Table 2.1 Antibodies used for immunofluorescence

Antibody	Host species	Catalog Number	Dilution
β-Gal	Chicken	Abcam ab9361	1:2500
β-Gal	Chicken	ICL Cgal-45A-Z	1:2000
Vimentin	Rabbit	Cell Signaling cs5741	1:500
CK19 (Troma-III)	Rat	DHSB AB_2133570	1:100
CD31	Rat	BD Biosciences 550274	1:500
Ecad	Mouse	BD Biosciences 610181	1:100
CD45	Rat	BD Biosciences 553076	1:100
F4/80	Rat	BMA Biomedicals T-2006	1:100
Arg1	Rabbit	Cell Signaling 93668	1:75 (TSA)
tdTomato (RFP)	Rabbit	Rockland 600-401-379	1:200
Pdgfrβ	Rabbit	Abcam ab32570	1:200
CD3	Rabbit	Abcam ab5690	1:500
CD8	Rabbit	Cell Signaling 98941S	1:500
Alpha-Amylase	Rabbit	Sigma A8273	1:100
pHH3	Mouse	Cell Signaling 9706S	1:100
Cleaved Caspase-3 (Asp175)	Rabbit	Cell Signaling 9661S	1:200

Table 2.2 Antibodies used for flow cytometry

Antibodies	Host species	Catalog Number	Clone	Dilution
CD45	Rat	BD Horizon 563891	30-F11	1:100
CD11b	Rat	BD Pharmingen 557657	M1/70	1:100
F4/80	Rat	eBioscience 15-4801-82	BM8	1:100
NKp46	Rat	BD Pharmingen 560757	29A1.4	1:100
GR1	Rat	BD Pharmingen 553127	R86-8C5	1:100
CD3	Rat	BD Pharmingen 555275	17A2	1:100
CD4	Rat	BD Pharmingen 558107	RM4-5	1:100
CD8	Rat	BD Pharmingen 557654	53-6.7	1:100
Foxp3	Rat	eBioscience 53-5773-82	FJK-16s	1:100
IFNγ	Rat	BD Pharmingen 557649	XMG1.2	1:100
IL4	Rat	BD Pharmingen 554436	11B11	1:100

Table 2.3 Antibodies used for western blotting

Antibody	Host species	Catalog Number	Dilution
GLI2	Goat IgG	R&D AF3635	1:1,000
GLI3	Goat IgG	R&D AF3690	1:1,000
Vinculin	Rabbit IgG	Cell Signaling 13901	1:1,000

Table 2.4 Secondary antibodies used for western blotting

Secondary Antibody	Host species	Catalog Number	Dilution
anti-goat IgG	Donkey IgG	R&D HAF109	1:10,000
anti-Rabbit IgG	Donkey IgG	Jackson ImmunoResearch 711-035-152	1:5,000

Table 2.5 Primers used for qPCR

Target Gene	Forward Primer Sequence (5' → 3')	Reverse Primer Sequence (5' → 3')
Il6	TTCCATCCAGTTGCCTTCTTGG	TTCTCATTTCCACGATTTCCCAG
Ccl5	GCCCACGTCAAGGAGTATTT	CTTGAACCCACTTCTTCTCTGG
Il11	CAGCCTGTGTTCGAGGATATG	TCACAGCCAGTCCTCTTACT
Ccl7	TCAAGAGCTACAGAAGGATCACC	ATAGCCTCCTCGACCCACTT
Gli1 (Mouse)	GTGCACGTTTGAAGGCTGTC	GAGTGGGTCCGATTCTGGTG
Gli2	CCTTCACCCACCTTCTTGG	CTTGTTCTGGTTGGCATCATTT
Gli3	CACATGCATCAACAGATCCTAAGC	AGGGATAGGTCTCTGTGTTGGAAAT
Ptch1 (Mouse)	GAAGCCACAGAAAACCCTGTC	GCCGCAAGCCTTCTCTAGG
GLI1 (human)	CCAACTCCACAGGCATACAGGAT	CACAGATTCAGGCTCACGCTTC
PTCH1 (human)	GGGTGGCACAGTCAAGAACAG	CGTACATTTGCTTGGGAGTCATT
Il10	GCTATGCTGCCTGCTCTTACT	CCTGCTGATCCTCATGCCA
Tgfb	TGACGTCACTGGAGTTGTACGG	GGTTCATGTCATGGATGGTGC

2.9 Figures

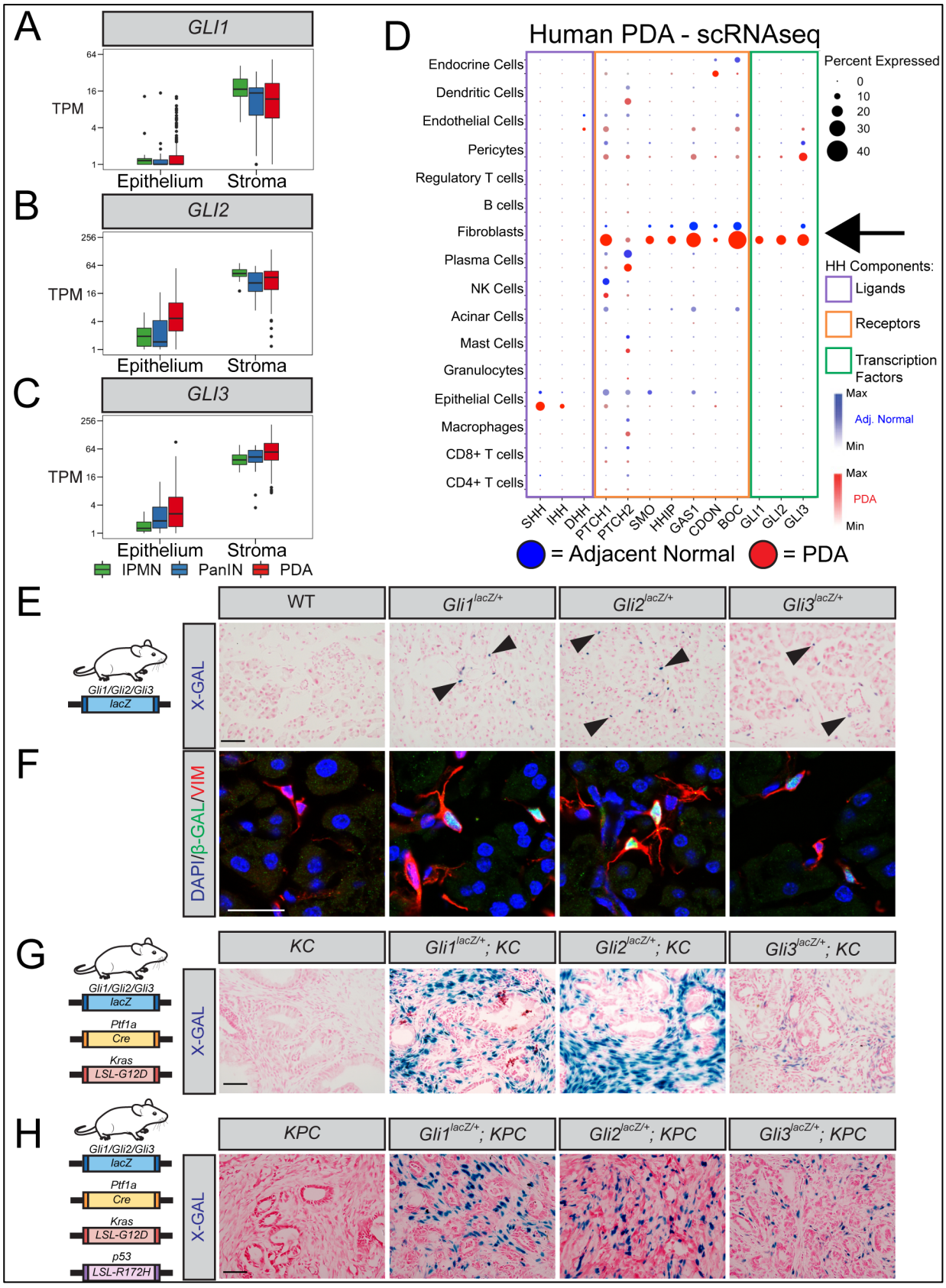
A
GLI1
TPM
64
16
4
1
Epithelium
Stroma
B
GLI2
256
64
16
4
1
C
GLI3
IPMN
PanIN
PDA
D
Human PDA - scRNAseq
Endocrine Cells
Dendritic Cells
Endothelial Cells
Pericytes
Regulatory T cells
B cells
Fibroblasts
Plasma Cells
NK Cells
Acinar Cells
Mast Cells
Granulocytes
Epithelial Cells
Macrophages
CD8+ T cells
CD4+ T cells
SHH
IHH
DHH
PTCH1
PTCH2
SMO
HHIP
GAS1
CDON
BOC
GLI1
GLI2
GLI3
Percent Expressed
0
10
20
30
40
HH Components:
Ligands
Receptors
Transcription Factors
Max
Adj. Normal
Min
Max
PDA
Min
= Adjacent Normal
= PDA
E
WT
Gli1lacZ/+
Gli2lacZ/+
Gli3lacZ/+
Gli1/Gli2/Gli3
lacZ
X-GAL
F
DAPI/β-GAL/VIM
G
KC
Gli1lacZ/+; KC
Gli2lacZ/+; KC
Gli3lacZ/+; KC
Ptf1a
Cre
Kras
LSL-G12D
H
KPC
Gli1lacZ/+; KPC
Gli2lacZ/+; KPC
Gli3lacZ/+; KPC
p53
LSL-R172H

Figure 2.1 *Gli1-3* are expressed in the pancreatic stroma and expand during PDA progression.
(**A – C**) Epithelial vs. Stromal *GLI* expression in human IPMN tissue (green, n = 19 Epithelial, n = 12 Stromal), PanIN (blue, n = 26 Epithelial, n = 23 Stromal), and PDA (red, n = 197 Epithelial, n = 124 Stromal), determined by LCM-RNAseq (Maurer et al. 2019) . (**D**) Expression of HH pathway components in human PDA (red, n = 16) and adjacent normal pancreas (blue, n = 3), determined by scRNAseq (Steele et al. 2021) . Dot size indicates frequency. Dot color intensity indicates expression level. Boxes outline ligands (purple), receptors (orange), and transcription factors (green). Arrow indicates *GLI* expression in fibroblasts. (**E – H**) Expression analysis of healthy (**E-F**), PanIN (**G**), and PDA (**H**) pancreata from Gli^{lacZ} reporter mice (n ≥ 3 for all genotypes). X-gal staining (**E, G, H**) in blue. Arrowheads indicate *lacZ*+ cells. Scale bar = 50μm. For immunofluorescent antibody analysis of healthy pancreata (**F**), antibodies detect β-Galactosidase (β-GAL, green) and fibroblasts (VIM, Red). DAPI (blue) denotes nuclei. Scale bar = 20 μm. Mouse drawing acquired from the open source repository SciDraw.io (doi.org/10.5281/zenodo.3925901).

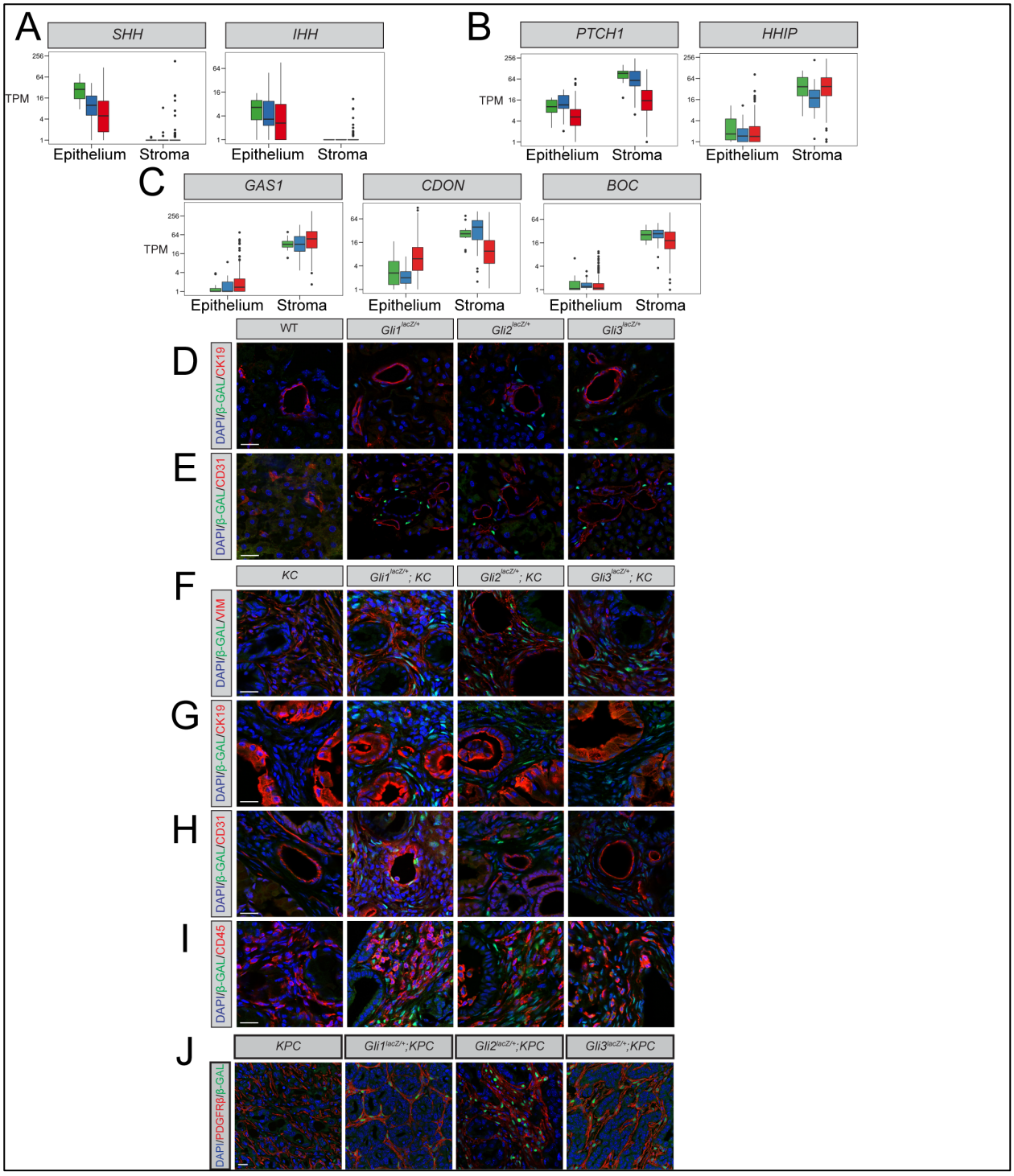
A
SHH
IHH
TPM
Epithelium
Stroma
B
PTCH1
HHIP
C
GAS1
CDON
BOC
WT
Gli1lacZ/+
Gli2lacZ/+
Gli3lacZ/+
D
DAPI/β-GAL/CK19
E
DAPI/β-GAL/CD31
KC
Gli1lacZ/+; KC
Gli2lacZ/+; KC
Gli3lacZ/+; KC
F
DAPI/β-GAL/VIM
G
H
I
DAPI/β-GAL/CD45
J
KPC
Gli1lacZ/+;KPC
Gli2lacZ/+;KPC
Gli3lacZ/+;KPC
DAPI/PDGFRβ/β-GAL

Figure 2.2 Characterization of *Gli* expression during human and mouse PDA progression. (**A-C**) Epithelial vs. Stromal expression of HH ligands (**A**) and receptors (**B-C**) in human IPMN (Green, n = 19 Epithelial samples, n = 12 Stromal Samples), PanIN (Blue, n = 26 Epithelial samples, n = 23 Stromal Samples), and PDA (Red, n = 197 Epithelial samples, n = 124 Stromal Samples) tissue, as determined by laser capture microdissection-RNA sequencing (40). (**D-J**) Immunofluorescent antibody analysis of healthy (**D-E**), PanIN (**F-I**), and tumor-bearing (**J**) *Gli-lacZ* reporter mice (n ≥ 3 for all genotypes). Antibodies detect β-Galactosidase (β-GAL, green), fibroblasts (VIM or PDGFβ, Red, **F,J**), ductal cells/PanIN (CK19, Red, **D, G**), blood vessels (CD31, Red, **E, H**), and immune cells (CD45, Red, **I**). DAPI staining in blue. Scale bar = 20μm.

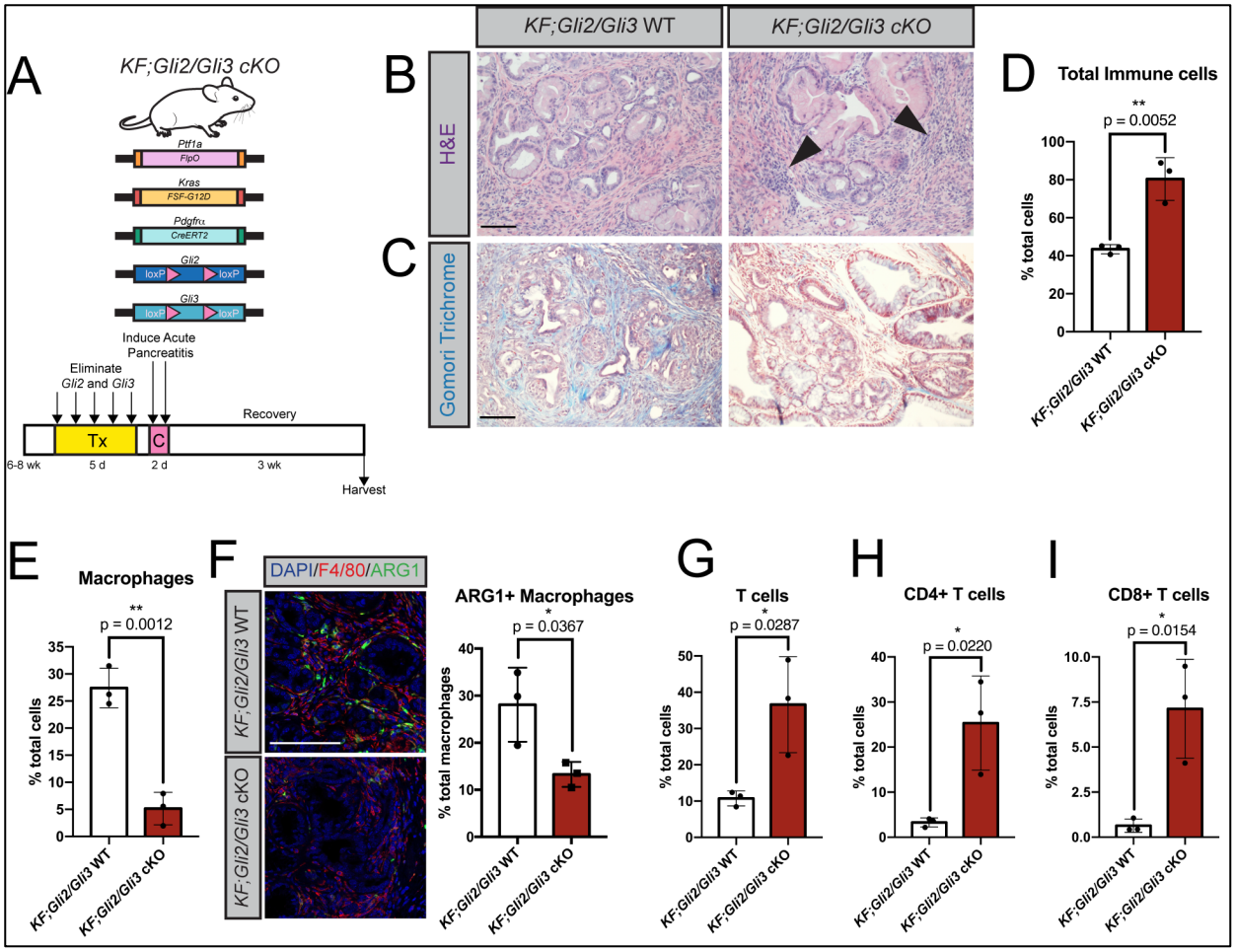

Figure 2.3 Conditional *Gli2* and *Gli3* deletion *in vivo* restricts immunosuppressive macrophages and promotes T cell infiltration.

A) Cartoon depicting experimental strategy. Adult *KF; Pdgfrα*$^{CreERt2/+}$*; Gli2*$^{fl/fl}$*; Gli3*$^{fl/fl}$ (*KF;Gli2/Gli3* cKO) mice were given tamoxifen (Tx, 200mg/kg) once a day for 5 days. Mice were then given 8 hourly injections of caerulein (C) over 2 days to induce pancreatitis. Pancreata were harvested 3 weeks later. **B-C**) H&E (**B**) and Gomori trichrome (**C**) staining of *KF;Gli2/Gli3* cKO mice (right) and *KF; Gli2*$^{fl/fl}$*; Gli3*$^{fl/fl}$ (*KF;Gli2/Gli3* WT) mice (left). Arrowheads indicate dense pockets of stromal cells. **D-E**) Flow cytometry analysis of total immune cells (**D**) and macrophages (**E**) in *KF;Gli2/Gli3* WT and *KF;Gli2/Gli3* cKO mice. **F**) Immunofluorescent antibody detection (left) and quantitation (right) of macrophages (F4/80, red) expressing arginase 1 (ARG1, green). DAPI staining in blue. **G-I**) Flow cytometry analysis of total T cells (**G**), CD4+ T cells (**H**), and CD8+ T Cells (**I**). N ≥ 3 for all genotypes. All P-values were determined by un-paired t-test. Scale bars = 100µm. Mouse drawing acquired from the open source repository SciDraw.io (doi.org/10.5281/zenodo.3925901).

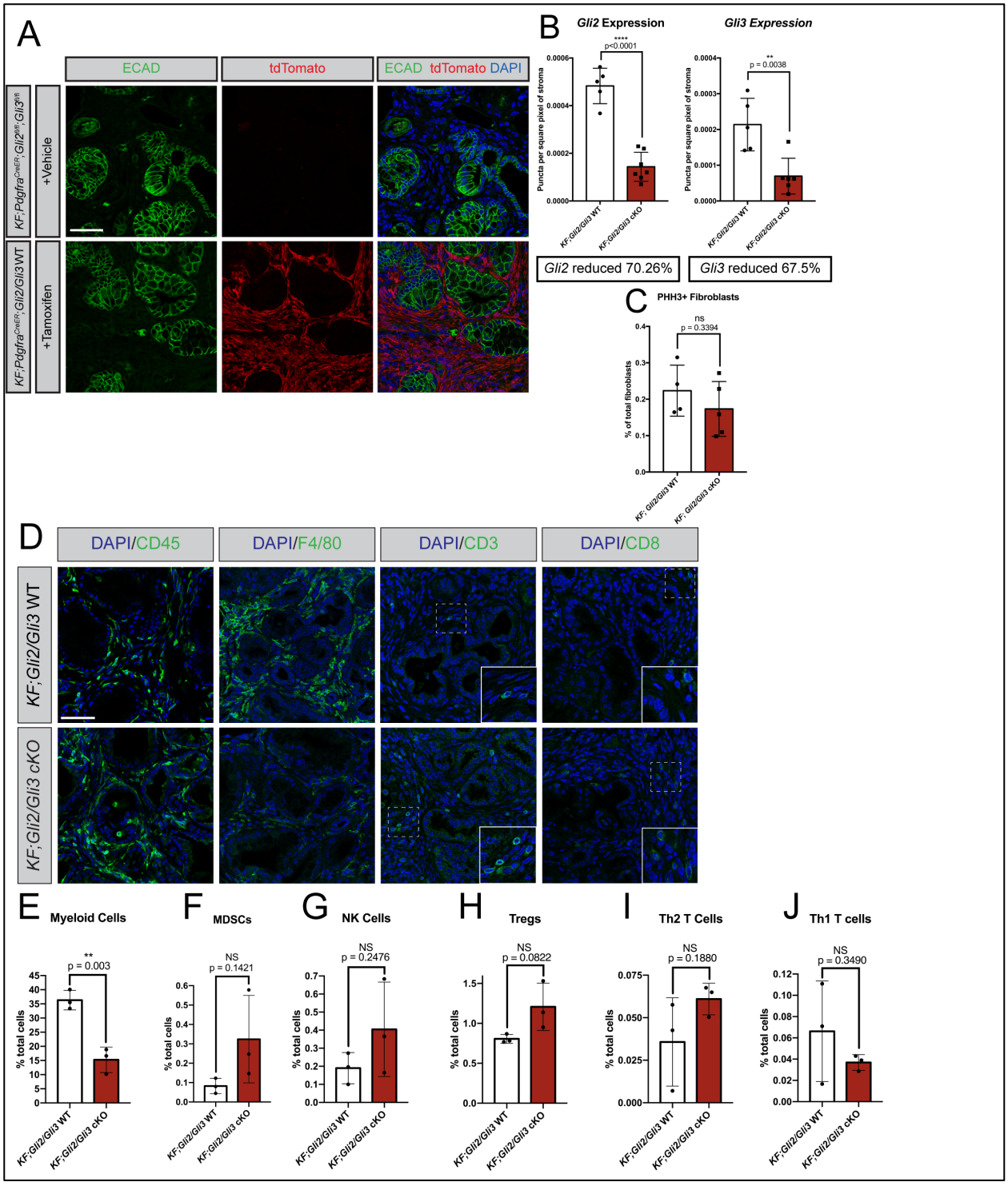
A
ECAD
tdTomato
ECAD tdTomato DAPI
KF;Pdgfra^CreER;Gli2^fl/fl;Gli3^fl/fl
+Vehicle
KF;Pdgfra^CreER;Gli2/Gli3 WT
+Tamoxifen
B
Gli2 Expression
Gli3 Expression
****
p<0.0001
**
p = 0.0038
Puncta per square pixel of stroma
KF;Gli2/Gli3 WT
KF;Gli2/Gli3 cKO
Gli2 reduced 70.26%
Gli3 reduced 67.5%
C
PHH3+ Fibroblasts
ns
p = 0.3394
% of total fibroblasts
KF; Gli2/Gli3 WT
KF; Gli2/Gli3 cKO
D
DAPI/CD45
DAPI/F4/80
DAPI/CD3
DAPI/CD8
KF;Gli2/Gli3 WT
KF;Gli2/Gli3 cKO
E
Myeloid Cells
**
p = 0.003
F
MDSCs
NS
p = 0.1421
G
NK Cells
NS
p = 0.2476
H
Tregs
NS
p = 0.0822
I
Th2 T Cells
NS
p = 0.1880
J
Th1 T cells
NS
p = 0.3490
% total cells

Figure 2.4 Validation and immune characterization of *KF;Gli2/Gli3* cKO mouse model. **A**) Immunofluorescent antibody detection of a tdTomato reporter (Red) and ECAD (Green) in *KF;Pdgrα$^{CreER/+}$;LSL-tdTomato/+* mice treated with either tamoxifen (Bottom, n = 4) or vehicle (Top, n = 2). **B**) Efficiency of *Gli2* (Left) and *Gli3* (Right) deletion in *KF;Gli2/Gli3* cKO mice, as determined by RNAscope. Puncta of *Gli* expression were counted and normalized to stromal area in each image. N ≥ 5 for each genotype. **C**) Proliferation (PHH3+) analysis of fibroblasts (PDGFRβ+) in *KF;Gli2/Gli3* cKO and *KF;Gli2/Gli3* WT mice (n ≥ 4 for each genotype). For (**B**) and (**C**), each point represents the average value for an animal, calculated from four independent fields of view. **D**) Immunofluorescent antibody detection of total immune cells (CD45), macrophages (F4/80), total T cells (CD3), and CD8+ T cells (CD8) in *KF;Gli2/Gli3* WT (Top) and *KF;Gli2/Gli3* cKO (Bottom) mice. DAPI staining in blue. Scale bar for all images = 50μm. **E-J**) Flow cytometry analysis of myeloid cells (**E**), MDSCs (**F**), NK cells (**G**), regulatory T cells (**H**), T helper 2 cells (IL4+) (**I**), and T helper 1 cells (IFNγ+) (**J**) in *KF;Gli2/Gli3* WT and *KF;Gli2/Gli3* cKO mice. For all immune analyses, n ≥ 3 for each genotype. For all quantitation, p-values were determined by un-paired t-test.

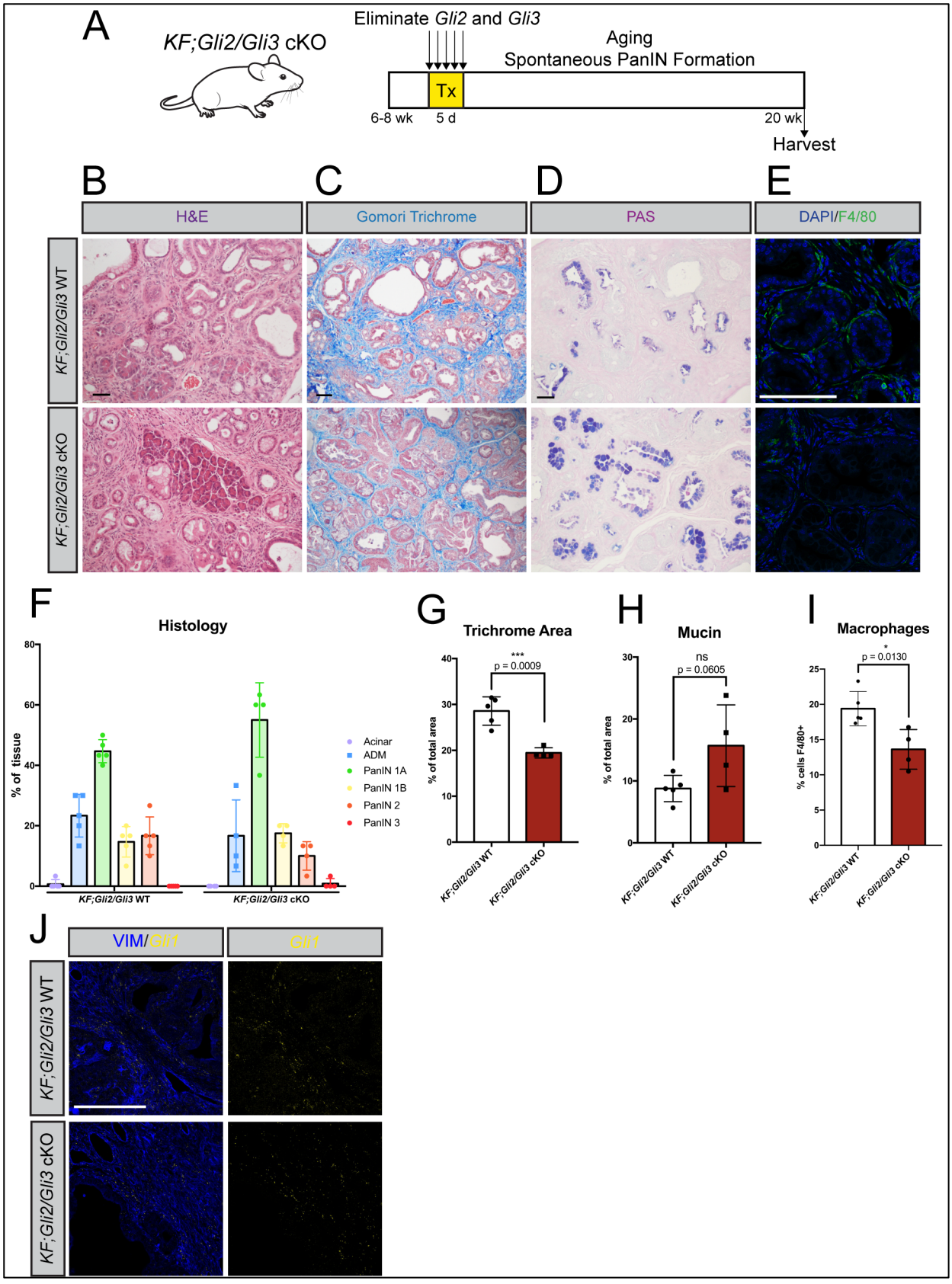
A
KF;Gli2/Gli3 cKO
Eliminate Gli2 and Gli3
Aging
Spontaneous PanIN Formation
Tx
6-8 wk
5 d
20 wk
Harvest
B
C
D
E
H&E
Gomori Trichrome
PAS
DAPI/F4/80
KF;Gli2/Gli3 WT
KF;Gli2/Gli3 cKO
F
Histology
% of tissue
Acinar
ADM
PanIN 1A
PanIN 1B
PanIN 2
PanIN 3
G
Trichrome Area
% of total area
p = 0.0009
H
Mucin
% of total area
ns
p = 0.0605
I
Macrophages
% cells F4/80+
p = 0.0130
J
VIM/Gli1
Gli1

Figure 2.5 Loss of stromal *Gli2* and *Gli3* reduces collagen deposition and macrophage infiltration in a spontaneous PanIN model.
A) Cartoon depicting experimental strategy. Adult *KF;Gli2/Gli3* cKO mice were given tamoxifen (Tx, 200 mg/kg) once a day for 5 days. Pancreata were harvested at 20 weeks of age. **B-D**) Histological analysis of *KF;Gli2/Gli3* cKO;*LSL-tdTomato/+* (bottom) pancreata compared to *KF;Gli2/Gli3* WT;*LSL-tdTomato/+* tissue (top), including H&E (**B**), Gomori Trichrome (**C**), and PAS (**D**) staining. **E**) Immunofluorescent antibody detection of macrophages (F4/80, green). DAPI staining in blue. **F**) Pathology analysis of PanIN progression in *KF;Gli2/Gli3* WT;*LSL-tdTomato/+* (left) and *KF;Gli2/Gli3* cKO;*LSL-tdTomato/+* (right) mice. **G-I**) Quantitation of collagen deposition (**G**), mucin (**H**), and macrophages (**I**) in *KF;Gli2/Gli3* WT;*LSL-tdTomato/+* and *KF;Gli2/Gli3* cKO;*LSL-tdTomato/+* mice. **J**) *Gli1* expression (yellow) in *KF;Gli2/Gli3* WT (top) and *KF;Gli2/Gli3* cKO mice (bottom), determined by RNAscope. Vimentin (VIM) staining in blue. Scale bar = 50 μm. N ≥ 3 for all genotypes. P-values were determined by un-paired t-test. Mouse drawing acquired from the open source repository SciDraw.io (doi.org/10.5281/zenodo.3925901).

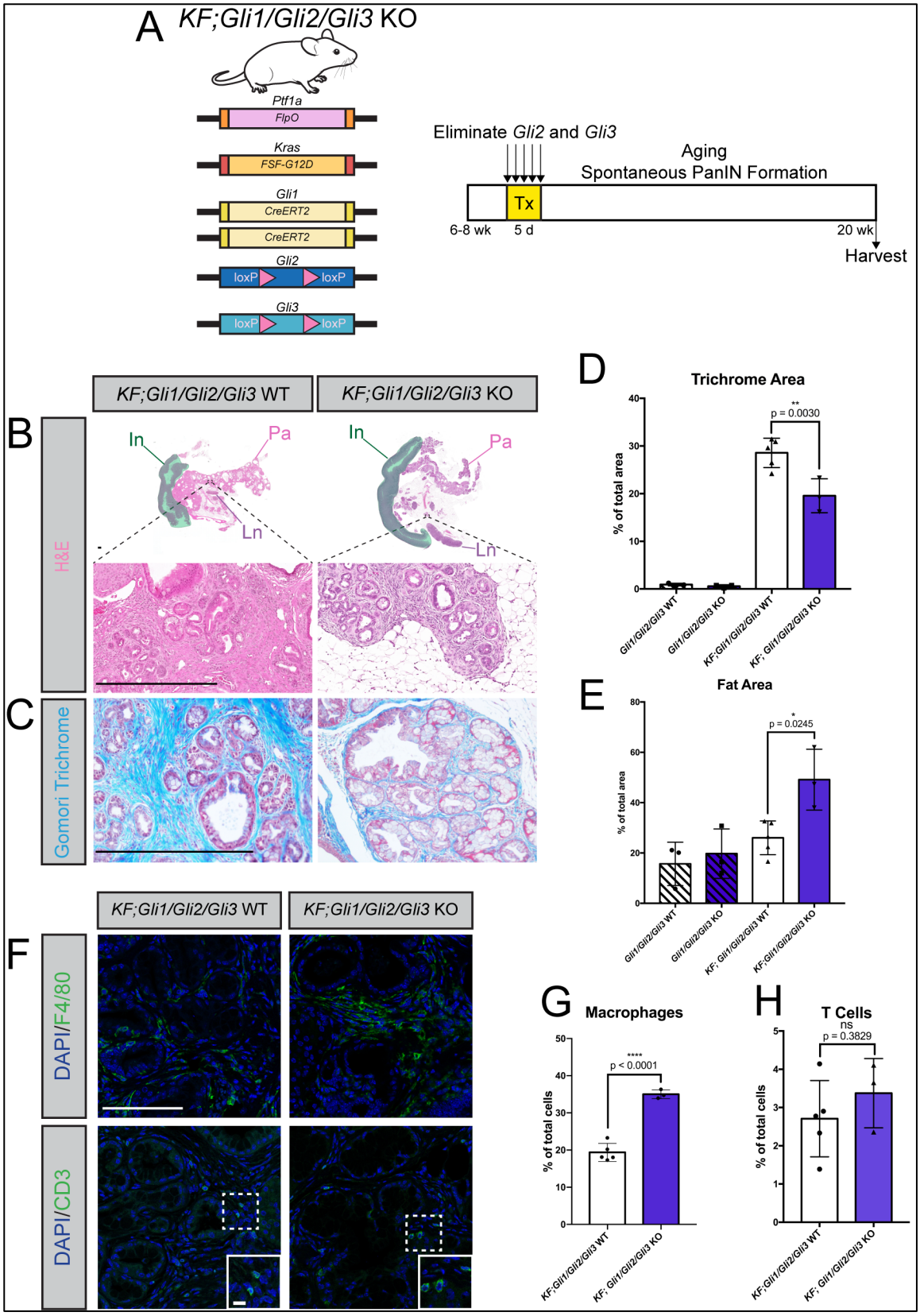
A
KF;Gli1/Gli2/Gli3 KO
Ptf1a
FlpO
Kras
FSF-G12D
Gli1
CreERT2
CreERT2
Gli2
loxP
loxP
Gli3
loxP
loxP
Eliminate Gli2 and Gli3
Aging
Spontaneous PanIN Formation
Tx
6-8 wk
5 d
20 wk
Harvest
B
H&E
C
Gomori Trichrome
KF;Gli1/Gli2/Gli3 WT
KF;Gli1/Gli2/Gli3 KO
In
Pa
Ln
D
Trichrome Area
p = 0.0030
% of total area
E
Fat Area
p = 0.0245
% of total area
F
DAPI/F4/80
DAPI/CD3
G
Macrophages
p < 0.0001
% of total cells
H
T Cells
ns
p = 0.3829
% of total cells

Figure 2.6 Combined *Gli1-3* deletion drives widespread tissue loss during PanIN progression.
A) Cartoon depicting experimental strategy. Adult *KF; Gli1*$^{CreERT2/CreERT2}$*; Gli2*$^{fl/fl}$*; Gli3*$^{fl/fl}$ (*KF;Gli1/Gli2/Gli3* KO) mice were given tamoxifen (Tx, 200mg/kg) once a day for 5 days. Pancreata were harvested at 20 weeks of age. **B-E**) Histological analysis of *KF; Gli2*$^{fl/fl}$*; Gli3*$^{fl/fl}$ (*KF;Gli1/Gli2/Gli3* WT) (left) and *KF;Gli1/Gli2/Gli3* KO (right) mice, including H&E staining (**B**), Gomori trichrome (**C,** quantified in **D**), and fat area (**E**). Green shaded area outlines intestinal tissue (In). Pancreas tissue (Pa) and Lymph nodes (Ln) annotated accordingly. Scale bar = 500μm. P-values determined by ordinary one-way ANOVA with Tukey's multiple comparisons test. **F-H**) Immunofluorescent antibody detection (**F**) and quantitation (**G-H**) of macrophages (F4/80) and T cells (CD3) in *KF;Gli1/Gli2/Gli3* WT and *KF;Gli1/Gli2/Gli3* KO mice. Inset scale bar = 10μm. All other scale bars = 100μm. P-values were determined by unpaired t-test. N ≥ 3 for all genotypes. Mouse drawing acquired from the open source repository SciDraw.io (doi.org/10.5281/zenodo.3925901).

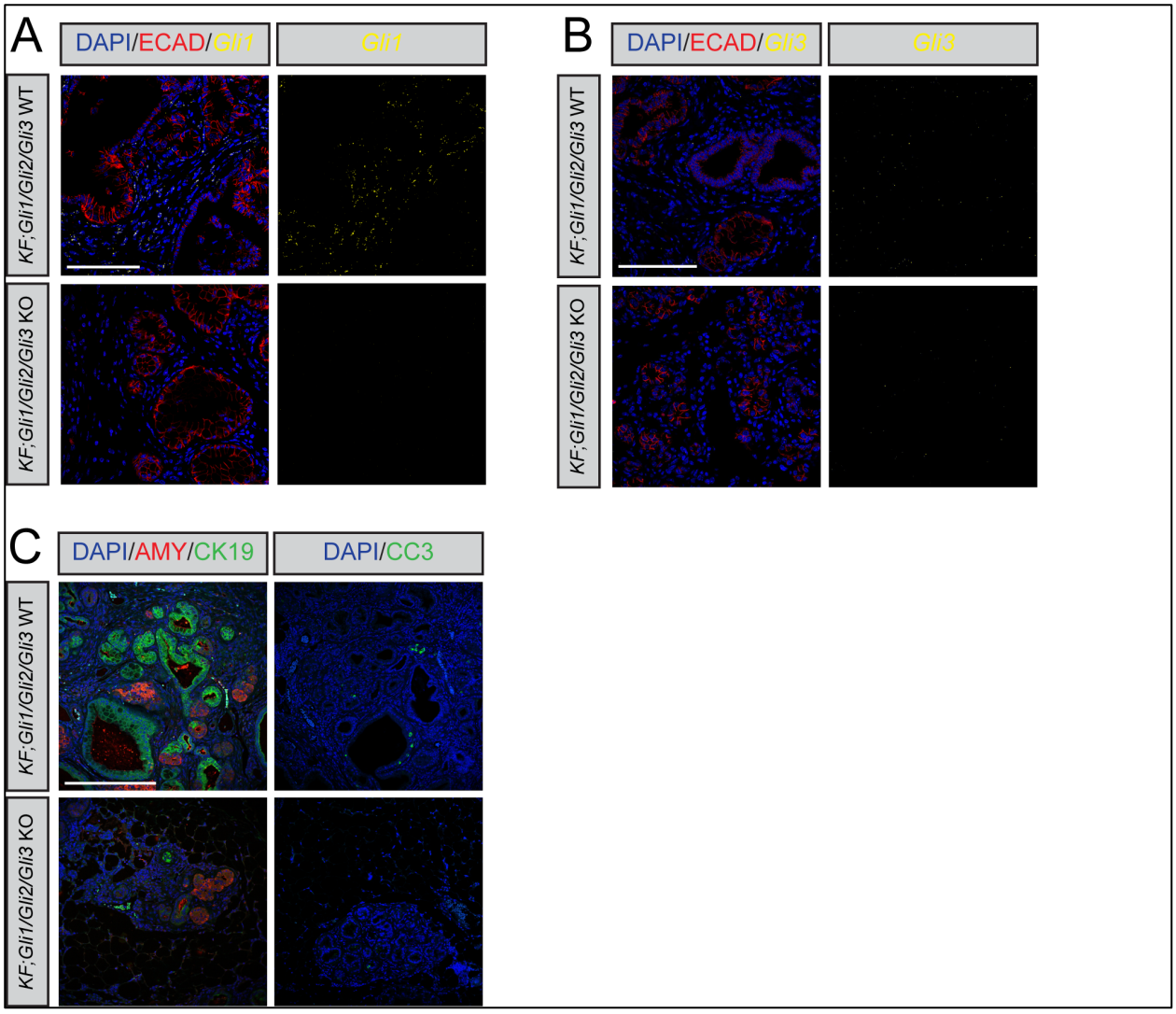

Figure 2.7 Validation and tissue analysis of *KF;Gli1/Gli2/Gli3* KO mice.
A-B) RNAscope analysis of *Gli1* (**A**, Yellow) and *Gli3* (**B**, Yellow) expression in *KF;Gli1/Gli2/Gli3* WT (Top) and *KF;Gli1/Gli2/Gli3* KO (Bottom) mice. E-Cadherin (ECAD) expressing epithelial cells in red. **C**) Immunofluorescent antibody detection of acinar cells (AMY, Red), PanIN lesions (CK19, Green), and cell death (CC3, Green) in *KF;Gli1/Gli2/Gli3* WT (Top) and *KF;Gli1/Gli2/Gli3* KO (Bottom) mice. DAPI staining in blue. Scale bar = 100 μm. N ≥ 3 for all genotypes.

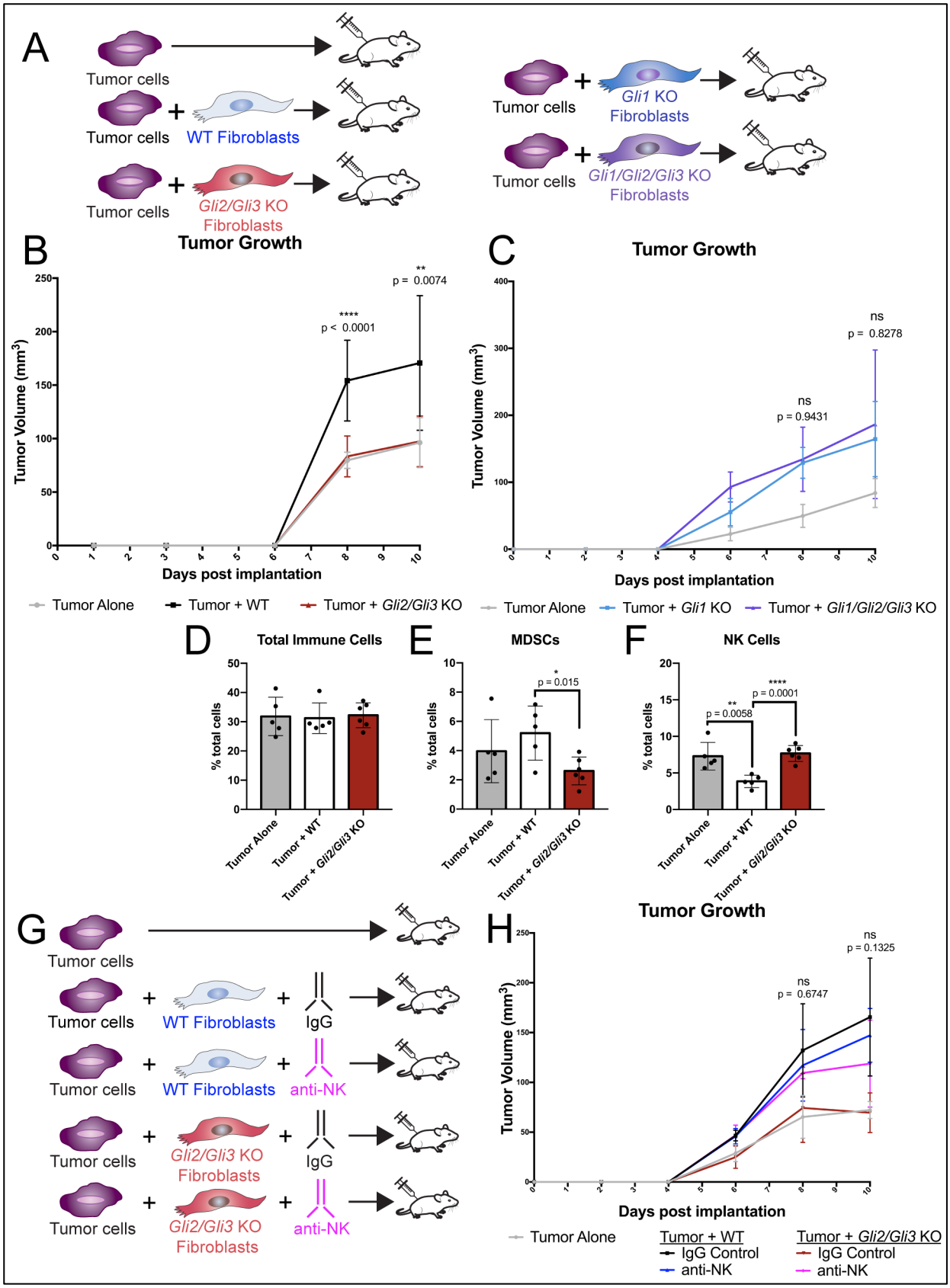
A
Tumor cells
Tumor cells
WT Fibroblasts
Tumor cells
Gli2/Gli3 KO Fibroblasts
Tumor cells
Gli1 KO Fibroblasts
Tumor cells
Gli1/Gli2/Gli3 KO Fibroblasts
B
Tumor Growth
Tumor Volume (mm3)
Days post implantation
p = 0.0074
p < 0.0001
Tumor Alone
Tumor + WT
Tumor + Gli2/Gli3 KO
C
Tumor Growth
Tumor Volume (mm3)
Days post implantation
ns
p = 0.8278
ns
p = 0.9431
Tumor Alone
Tumor + Gli1 KO
Tumor + Gli1/Gli2/Gli3 KO
D
Total Immune Cells
% total cells
Tumor Alone
Tumor + WT
Tumor + Gli2/Gli3 KO
E
MDSCs
% total cells
p = 0.015
Tumor Alone
Tumor + WT
Tumor + Gli2/Gli3 KO
F
NK Cells
% total cells
p = 0.0058
p = 0.0001
Tumor Alone
Tumor + WT
Tumor + Gli2/Gli3 KO
G
Tumor cells
Tumor cells
WT Fibroblasts
IgG
Tumor cells
WT Fibroblasts
anti-NK
Tumor cells
Gli2/Gli3 KO Fibroblasts
IgG
Tumor cells
Gli2/Gli3 KO Fibroblasts
anti-NK
H
Tumor Growth
Tumor Volume (mm3)
Days post implantation
ns
p = 0.1325
ns
p = 0.6747
Tumor Alone
Tumor + WT
IgG Control
anti-NK
Tumor + Gli2/Gli3 KO
IgG Control
anti-NK

Figure 2.8 Loss of *Gli2* and *Gli3* reduces tumor growth through the recruitment of NK cells. **A**) Cartoon depicting experimental strategy. Tumor cells were injected subcutaneously either alone or in combination with pancreatic fibroblasts into nude mice. (**B-C**) Volume (mm^3) of implanted tumors over time. Tumor cells were injected alone (gray), or co-injected with WT (black), *Gli2/3* KO (red), *Gli1* KO (blue), or *Gli1/Gli2/Gli3* KO (purple) pancreatic fibroblasts. Displayed p-values compare *Gli* KO fibroblasts to their corresponding parental line control. (**D-F**) Flow cytometry analysis of total immune cells (**D**), MDSCs (**E**), or NK cells (**F**) in subcutaneous tumors. (**G**) Cartoon depicting experimental strategy for NK cell depletion experiment. Animals were either treated with an IgG control or an anti-NK cell depleting antibody (anti-asialo GM1). (**H**) Volume (mm^3) of implanted tumors following NK Cell depletion. P-values determined by ordinary one-way ANOVA with Tukey's multiple comparison test. The displayed p-values compare Tumor + *Gli2/Gli3* KO + anti-NK conditions to Tumor + WT + IgG conditions. For all analyses, $n \geq 5$ tumors for each experimental condition. Mouse drawing acquired from the open source repository SciDraw.io (doi.org/10.5281/zenodo.3925901).

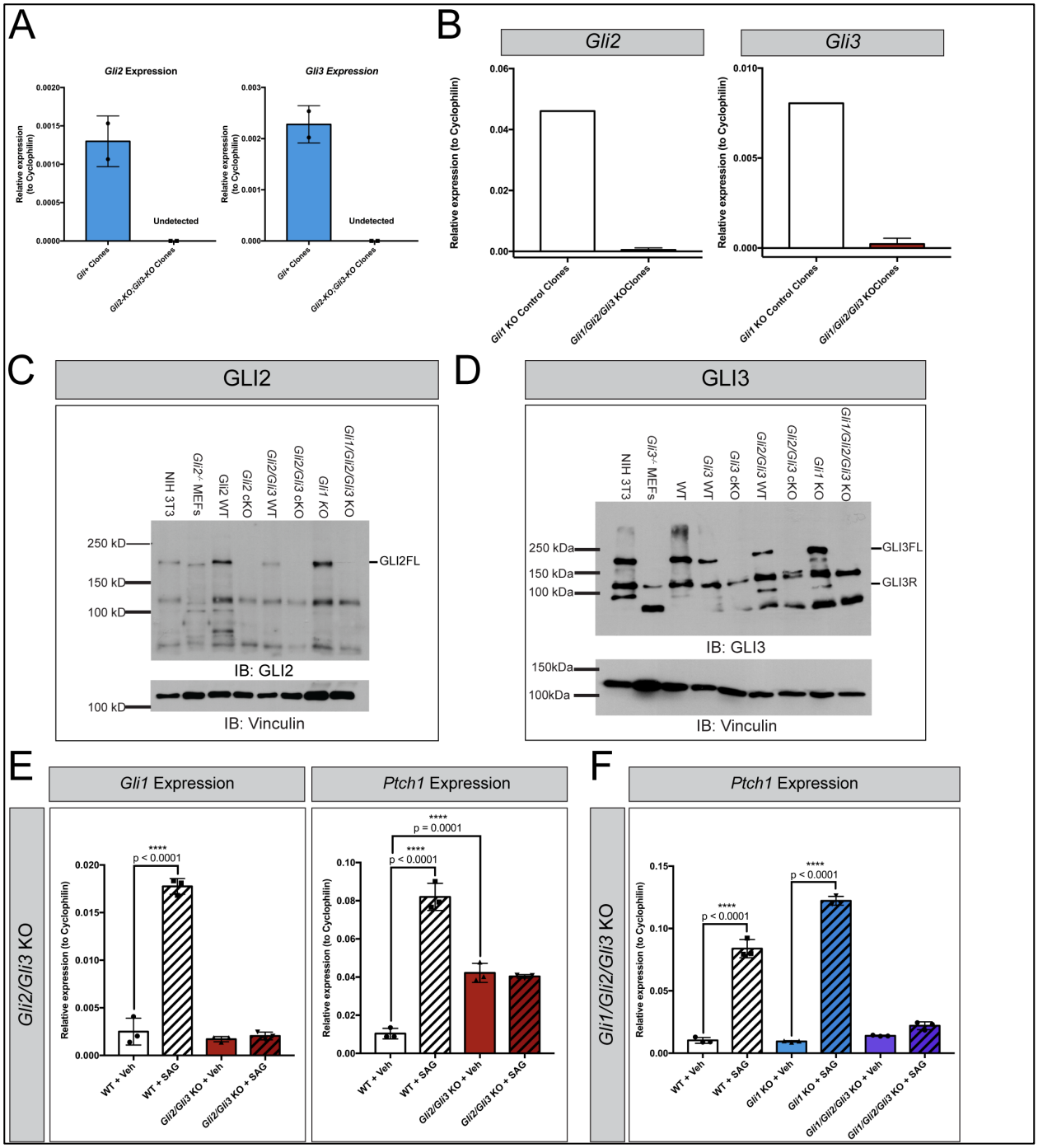
A
Gli2 Expression
Relative expression (to Cyclophilin)
Undetected
Gli+ Clones
Gli2-KO;Gli3-KO Clones
Gli3 Expression
Undetected
Gli+ Clones
Gli2-KO;Gli3-KO Clones
B
Gli2
Gli3
Relative expression (to Cyclophilin)
Gli1 KO Control Clones
Gli1/Gli2/Gli3 KOClones
Gli1 KO Control Clones
Gli1/Gli2/Gli3 KOClones
C
GLI2
NIH 3T3
Gli2-/- MEFs
Gli2 WT
Gli2 cKO
Gli2/Gli3 WT
Gli2/Gli3 cKO
Gli1 KO
Gli1/Gli2/Gli3 KO
250 kD
150 kD
100 kD
GLI2FL
IB: GLI2
100 kD
IB: Vinculin
D
GLI3
NIH 3T3
Gli3-/- MEFs
WT
Gli3 WT
Gli3 cKO
Gli2/Gli3 WT
Gli2/Gli3 cKO
Gli1 KO
Gli1/Gli2/Gli3 KO
250 kDa
150 kDa
100 kDa
GLI3FL
GLI3R
IB: GLI3
150kDa
100kDa
IB: Vinculin
E
Gli1 Expression
Ptch1 Expression
Gli2/Gli3 KO
Relative expression (to Cyclophilin)
****
p < 0.0001
****
p = 0.0001
****
p < 0.0001
WT + Veh
WT + SAG
Gli2/Gli3 KO + Veh
Gli2/Gli3 KO + SAG
F
Ptch1 Expression
Gli1/Gli2/Gli3 KO
Relative expression (to Cyclophilin)
****
p < 0.0001
****
p < 0.0001
WT + Veh
WT + SAG
Gli1 KO + Veh
Gli1 KO + SAG
Gli1/Gli2/Gli3 KO + Veh
Gli1/Gli2/Gli3 KO + SAG

Figure 2.9 Validation and HH-responsiveness of *Gli* KO pancreatic fibroblast lines
A-B) qPCR analysis of *Gli2* and *Gli3* expression in WT (**A**, blue bars) *Gli2/Gli3* KO (**A**, red bars), *Gli1* KO (**B**, white bars) and *Gli1/Gli2/Gli3* KO (**B**, red bars) pancreatic fibroblast lines. **C-D**) Western Blot analysis for GLI2 (**C**) and GLI3 (**D**) in *Gli* WT and *Gli* KO pancreatic fibroblast lines. Vinculin was used as a loading control. **E-F**) qPCR analysis for HH target genes *Gli1* and *Ptch1* in *Gli2/Gli3* KO (**E**) and *Gli1/Gli2/Gli3* KO (**F**) pancreatic fibroblasts following treatment with vehicle or SAG (600nM). P-values determined by ordinary one-way ANOVA with Tukey's multiple comparison test.

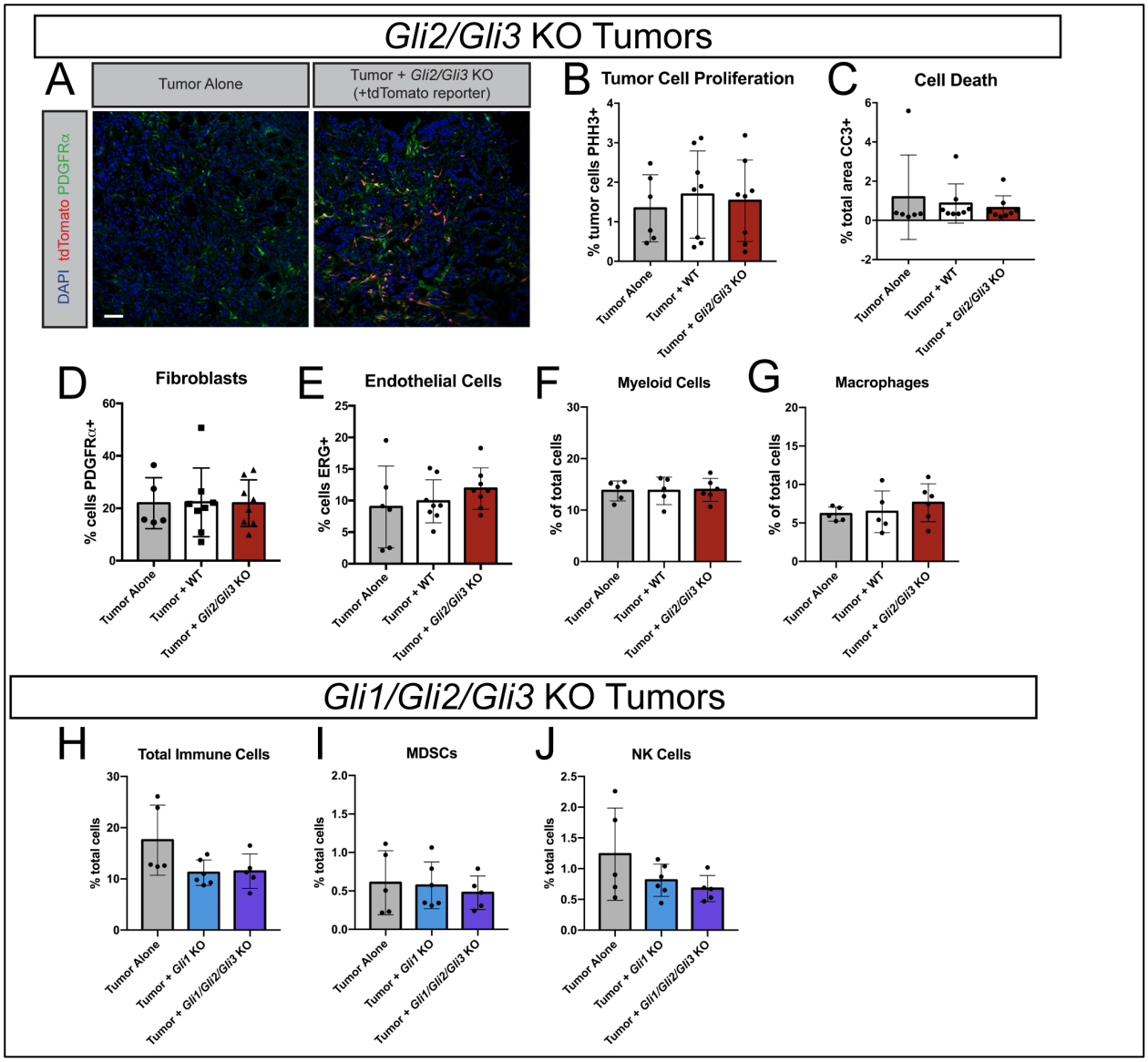

Figure 2.10 Additional analysis of *Gli2/Gli3* KO and *Gli1/Gli2/Gli3* KO subcutaneous tumor growth experiments.
(**A**) Immunofluorescent antibody detection of a reporter allele (tdTomato, Red) expressed by *Gli2/Gli3* KO pancreatic fibroblasts. Additional antibodies detect fibroblasts (PDGFRα, Green). DAPI staining in blue. Scale bar = 50 μm. (**B-E**) Quantitation of tumor cell proliferation (**B**), cell death (**C**), fibroblast number (**D**), and endothelial cell number (**E**) across experimental conditions. (**F-G**) Flow cytometry analysis of myeloid cells (**F**) and macrophages (**G**) from *Gli2/Gli3* KO subcutaneous tumors. (**H-J**) Flow cytometry analysis of total immune cells (**H**), MDSCs (**I**), and NK cells (**J**) from *Gli1/Gli2/Gli3* KO subcutaneous tumors. For all analyses, n ≥ 5 tumors for each experimental condition. Significance was determined by ordinary one-way ANOVA with Tukey's multiple comparisons test.

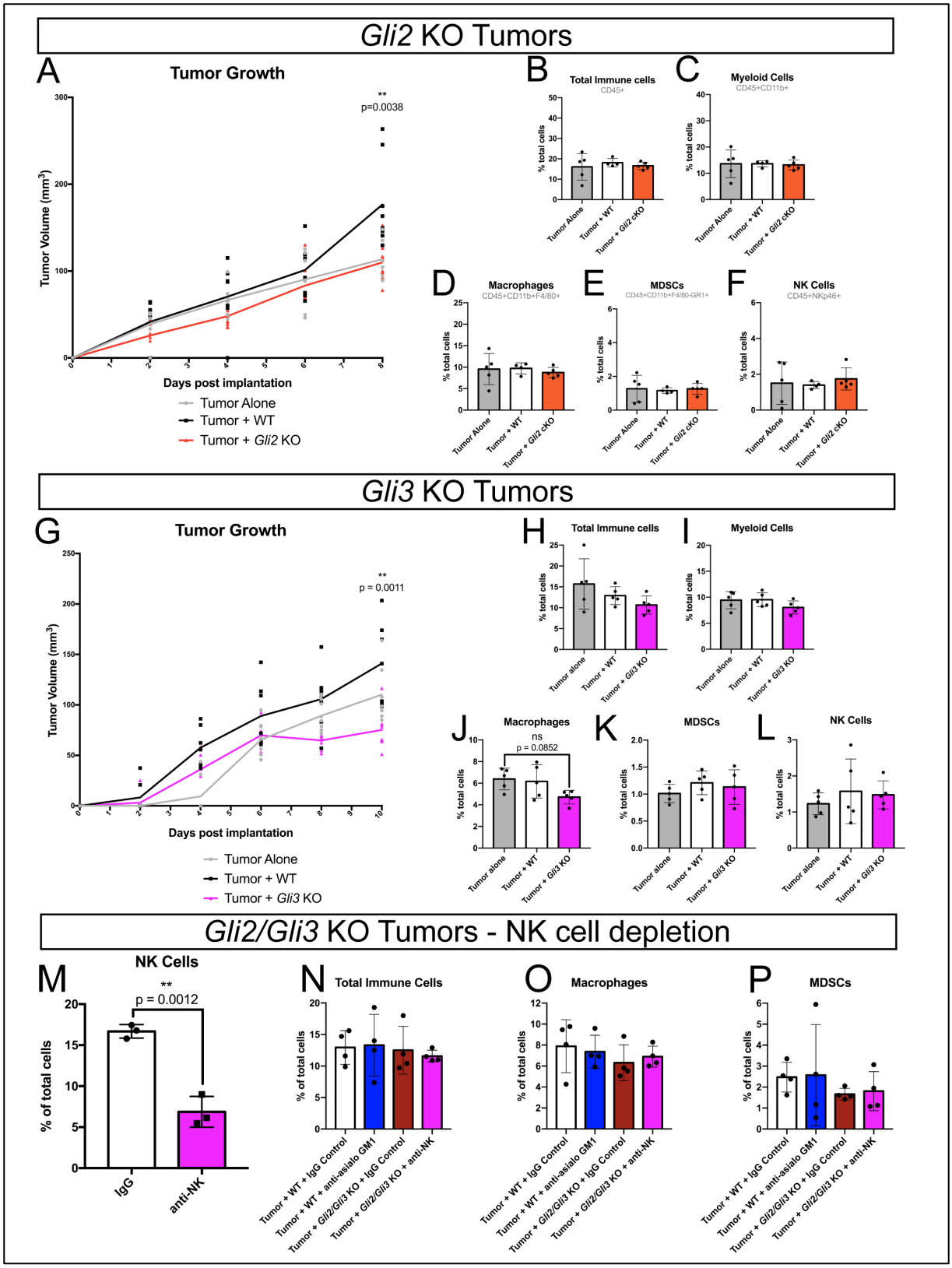
Gli2 KO Tumors
A
Tumor Growth
**
p=0.0038
Tumor Volume (mm3)
Days post implantation
Tumor Alone
Tumor + WT
Tumor + Gli2 KO
B
Total Immune cells
CD45+
% total cells
C
Myeloid Cells
CD45+CD11b+
D
Macrophages
CD45+CD11b+F4/80+
E
MDSCs
CD45+CD11b+F4/80-GR1+
F
NK Cells
CD45+NKp46+
Tumor + Gli2 cKO
Gli3 KO Tumors
G
Tumor Growth
**
p = 0.0011
Tumor + Gli3 KO
H
Total Immune cells
I
Myeloid Cells
J
Macrophages
ns
p = 0.0852
K
MDSCs
L
NK Cells
Gli2/Gli3 KO Tumors - NK cell depletion
M
NK Cells
**
p = 0.0012
% of total cells
IgG
anti-NK
N
Total Immune Cells
Tumor + WT + IgG Control
Tumor + WT + anti-asialo GM1
Tumor + Gli2/Gli3 KO + IgG Control
Tumor + Gli2/Gli3 KO + anti-NK
O
Macrophages
P
MDSCs

Figure 2.11 Analysis of tumor growth and immune infiltration in *Gli2* KO, *Gli3* KO, and NK cell depletion subcutaneous tumor growth experiments.
(**A-L**) Analysis of tumor implantation experiments incorporating *Gli2* KO (**A-F**), *Gli3* KO (**G-L**) pancreatic fibroblasts. (**A, G**) Tumor volume (mm^3) over time for *Gli2* KO (**A**) and *Gli3* KO (**G**) tumors. The displayed p-value compares *Gli* KO fibroblasts to their corresponding parental line control. (**B-F, H-L**) Flow cytometry analysis of total immune cells (**B, H**), myeloid cells (**C, I**), macrophages (**D, J**), MDSCs (**E, K**), and NK cells (**F, L**) from subcutaneous tumors. (**M-P**) Further analysis of NK-cell depletion experiments. **M**) Validation of NK cell depletion in anti-NK (anti-asialo GM1)-treated mice compared to IgG control mice. P-value determined by unpaired t-test. **N-P**) Flow cytometry analysis of total immune cells (**N**), macrophages (**O**), and MDSCs (**P**). For all flow cytometry data, values displayed as a percentage of total cells. For all analyses, $n \geq 3$ samples for each experimental condition. For all analyses (except **M**), p-values were determined by ordinary one-way ANOVA with Tukey's multiple comparison test.

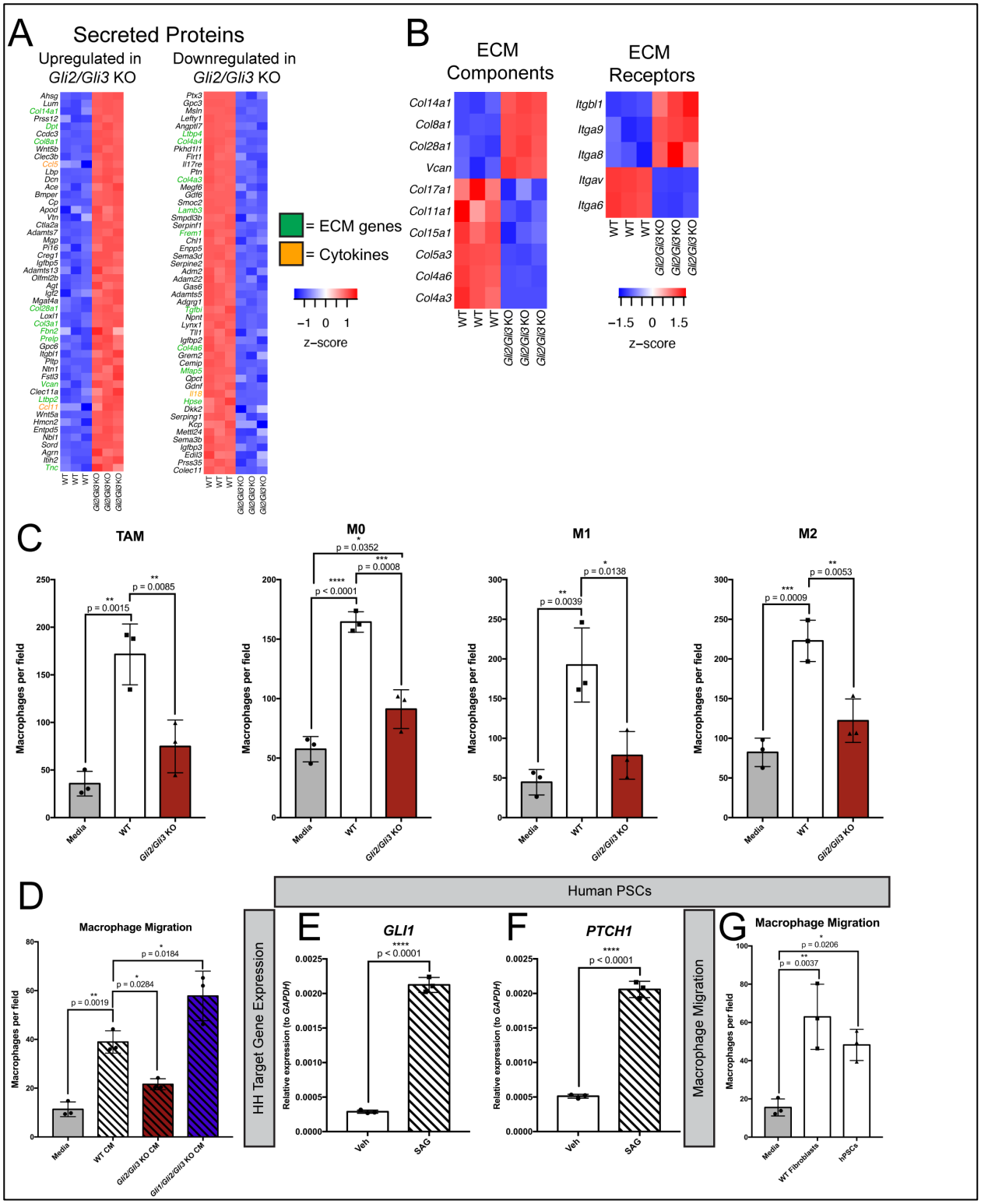
A
Secreted Proteins
Upregulated in Gli2/Gli3 KO
Downregulated in Gli2/Gli3 KO
= ECM genes
= Cytokines
−1 0 1
z−score
B
ECM Components
ECM Receptors
−1.5 0 1.5
z−score
C
TAM
M0
M1
M2
Macrophages per field
Media
WT
Gli2/Gli3 KO
D
Macrophage Migration
WT CM
Gli2/Gli3 KO CM
Gli1/Gli2/Gli3 KO CM
Human PSCs
HH Target Gene Expression
E
GLI1
F
PTCH1
Relative expression (to GAPDH)
Veh
SAG
Macrophage Migration
G
Macrophage Migration
WT Fibroblasts
hPSCs

Figure 2.12 Loss of *Gli* alters the transcriptional profile of pancreatic fibroblasts and impacts fibroblast-immune cross-talk.
A-B) RNA sequencing analysis of *Gli2/Gli3* KO pancreatic fibroblasts and *Gli2/Gli3* WT pancreatic fibroblasts. **A**) Top upregulated (left) and downregulated (right) genes of membrane-bound and secreted proteins. Green gene names indicate ECM genes, and orange gene names indicate cytokines. **B**) Curated gene expression lists of ECM components (left) and ECM receptors (right). **C**) Migration of different macrophage phenotypes (TAM, M0, M1, M2) when co-cultured with WT or *Gli2/Gli3* KO pancreatic fibroblasts. **D**) Macrophage migration following co-culture with pancreatic fibroblast-conditioned media. **E-F**) RT-qPCR analysis of HH target genes (*GLI1, PTCH1)* in human pancreatic stellate cells (hPSCs) following stimulation with SAG. Gene expression levels are relative to *GAPDH*. **G**) Macrophage migration following co-culture with media alone, WT mouse fibroblasts, or hPSCs. P-values for (**E-F**) calculated by un-paired t test. All other P-values were calculated by ordinary one-way ANOVA with Tukey's multiple comparison test.

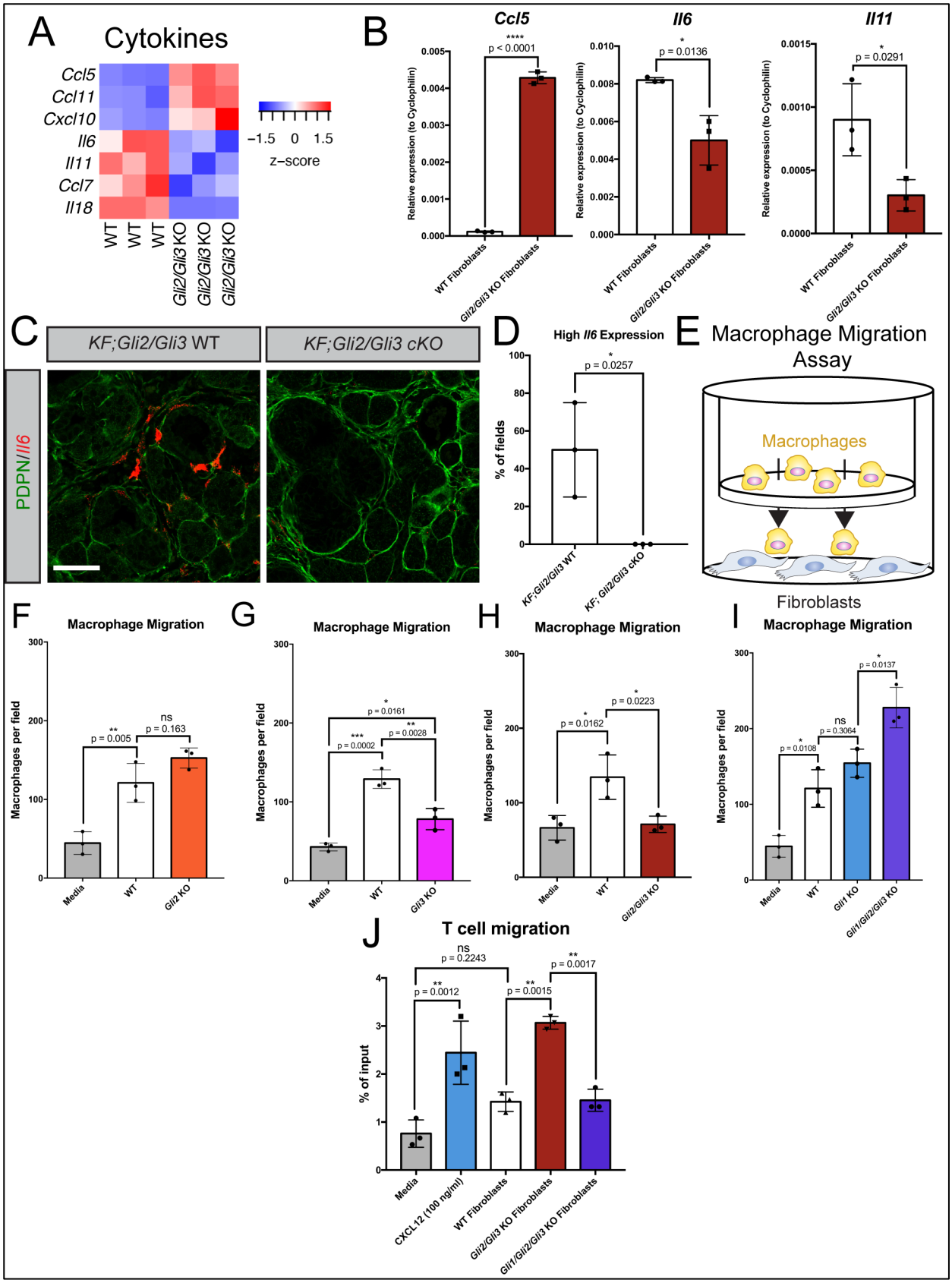
A
Cytokines
Ccl5
Ccl11
Cxcl10
Il6
Il11
Ccl7
Il18
WT
WT
WT
Gli2/Gli3 KO
Gli2/Gli3 KO
Gli2/Gli3 KO
−1.5 0 1.5
z-score
B
Ccl5
Il6
Il11
Relative expression (to Cyclophilin)
p < 0.0001
p = 0.0136
p = 0.0291
WT Fibroblasts
Gli2/Gli3 KO Fibroblasts
C
KF;Gli2/Gli3 WT
KF;Gli2/Gli3 cKO
PDPN/Il6
D
High Il6 Expression
% of fields
p = 0.0257
KF;Gli2/Gli3 WT
KF; Gli2/Gli3 cKO
E
Macrophage Migration Assay
Macrophages
Fibroblasts
F
Macrophage Migration
Macrophages per field
p = 0.005
p = 0.163
Media
WT
Gli2 KO
G
Macrophage Migration
p = 0.0161
p = 0.0002
p = 0.0028
Gli3 KO
H
Macrophage Migration
p = 0.0162
p = 0.0223
Gli2/Gli3 KO
I
Macrophage Migration
p = 0.0108
p = 0.3064
p = 0.0137
Gli1 KO
Gli1/Gli2/Gli3 KO
J
T cell migration
% of input
p = 0.2243
p = 0.0012
p = 0.0015
p = 0.0017
Media
CXCL12 (100 ng/ml)
WT Fibroblasts
Gli2/Gli3 KO Fibroblasts
Gli1/Gli2/Gli3 KO Fibroblasts

Figure 2.13 *Gli1*-3 in fibroblasts directly control macrophage and T cell migration.
A) Differential expression of cytokines in *Gli2/Gli3* WT and *Gli2/Gli3* KO fibroblasts, as determined by RNA sequencing. **B**) qPCR analysis of *Ccl5* (left) and *Il6* (center) and *Il11* (right) in *Gli2/Gli3* WT and *Gli2/Gli3* KO fibroblasts. **C**) *Il6* expression (red) by fibroblasts (PDPN, green) in *KF;Gli2/Gli3* WT and *KF;Gli2/Gli3* cKO mice, as determined by RNAscope. Scale bar = 50 μm **D**) Quantification of high *Il6*-expressing fields of view in in *KF;Gli2/Gli3* WT and *KF;Gli2/Gli3* cKO mice (n = 3 for each genotype). High *Il6* expression defined as an integrated density value (for the *Il6* probe channel) >2300000. P-values for (**B**) and (**D**) determined by un-paired T test. **E**) Cartoon depicting macrophage migration assay experimental strategy. Macrophages and *Gli* KO fibroblasts are separated by an 8μm pore transwell membrane, and macrophages are allowed to migrate through the membrane for 12h. (**F-I**) Quantitation of macrophage migration following co-culture with WT fibroblasts (**F-I**), *Gli2* KO fibroblasts (**F**), *Gli3* KO fibroblasts (**G**), *Gli2/Gli3* KO fibroblasts (**H**), *Gli1 KO* fibroblasts (**I**), and *Gli1/Gli2/Gli3* KO fibroblasts (**I**). **J**) Quantitation of T cell migration following co-culture with WT, *Gli2/Gli3* KO, and *Gli1/Gli2/Gli3* KO fibroblasts. Recombinant CXCL12 (100 ng/ml) added to media was used as a positive control. P-values for (**F-J**) were determined by ordinary one-way ANOVA with Tukey's multiple comparison test.

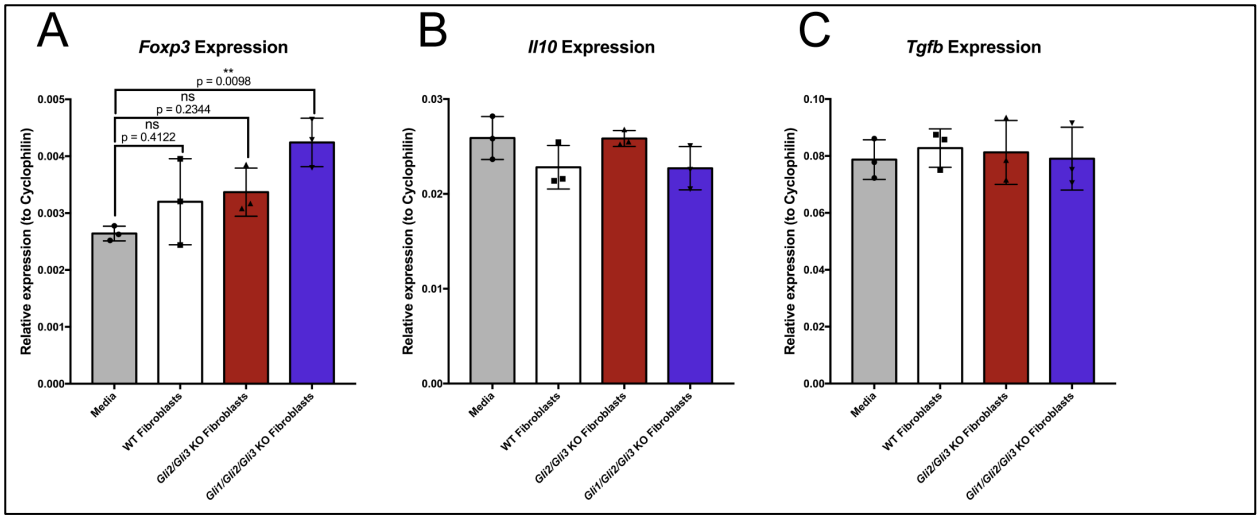

Figure 2.14 *Gli* expression in pancreatic fibroblasts regulates Treg differentiation.
A-C) RT-qPCR analysis of T cells following transwell co-culture with pancreatic fibroblasts. Target genes include markers for Treg identity (*Foxp3*, **A**) as well as markers associated with an immunosuppressive Treg phenotype (*Il10* and *Tgfb*, **B** and **C**, respectively). Gene expression levels are relative to *Cyclophilin*. P-values were determined by ordinary one-way ANOVA with Dunnett's multiple comparison test.

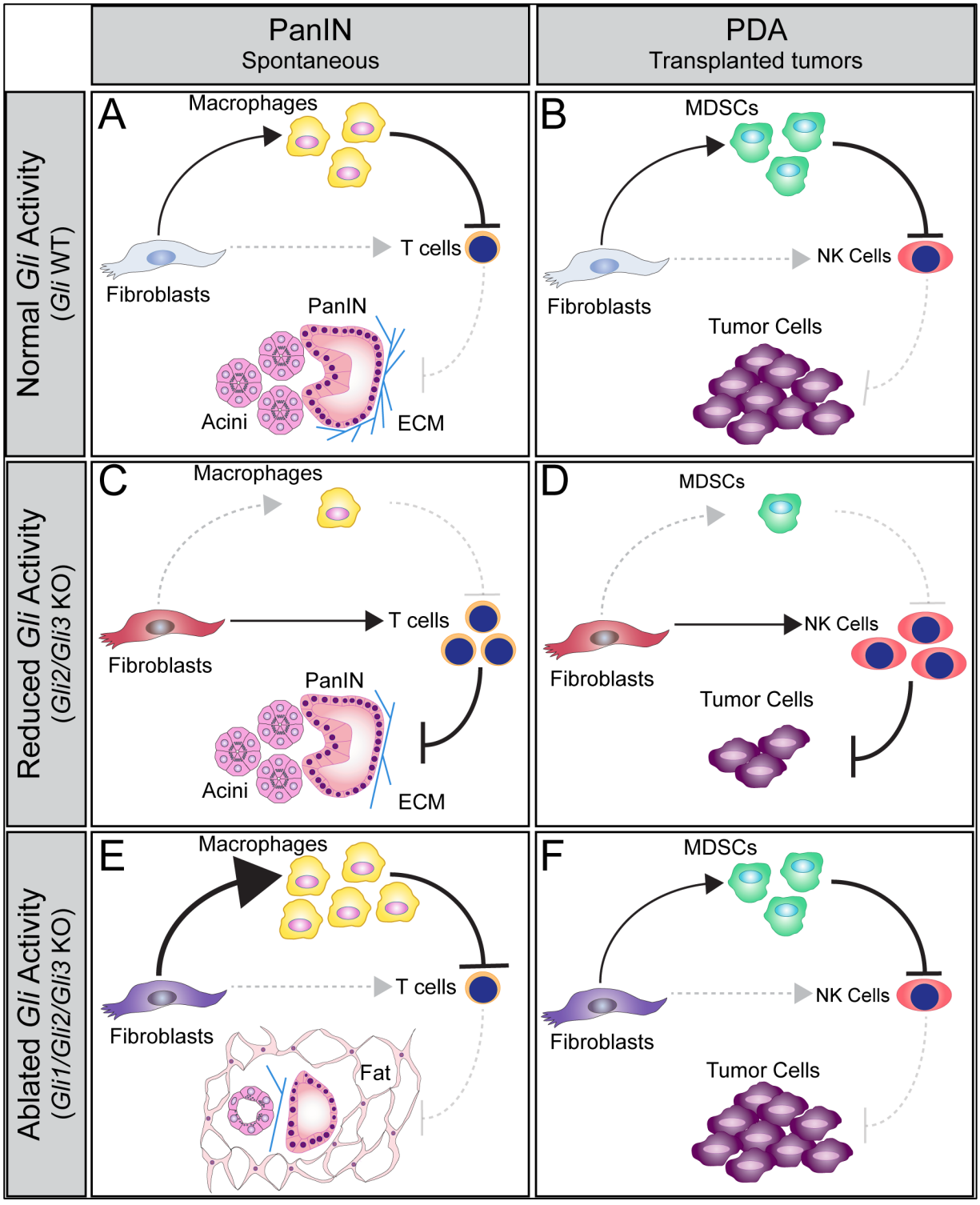
PanIN
Spontaneous
PDA
Transplanted tumors
Normal Gli Activity
(Gli WT)
Reduced Gli Activity
(Gli2/Gli3 KO)
Ablated Gli Activity
(Gli1/Gli2/Gli3 KO)
A
Macrophages
T cells
Fibroblasts
PanIN
Acini
ECM
B
MDSCs
NK Cells
Fibroblasts
Tumor Cells
C
Macrophages
T cells
Fibroblasts
PanIN
Acini
ECM
D
MDSCs
NK Cells
Fibroblasts
Tumor Cells
E
Macrophages
T cells
Fibroblasts
Fat
F
MDSCs
NK Cells
Fibroblasts
Tumor Cells

Figure 2.15 Model of GLI function during PDA progression.
(**A-B**) *Gli*-expressing fibroblasts directly promote the recruitment of macrophages and MDSCs (**A,B**, top) at PanIN and PDA stages, respectively. These myeloid cells suppress T cells and NK cells (**A,B**, right), facilitating disease progression. (**C-D**) *Gli2* and *Gli3* deletion in fibroblasts directly reduces the recruitment of myeloid cells, and directly promotes T cell and NK cell infiltration (**C,D**, right). Loss of *Gli2* and *Gli3* also decreases collagen deposition and slows tumor growth (**C,D**, bottom). However, when all three *Glis* are deleted (**E**, **F**), fibroblasts have an enhanced ability to recruit macrophages (**E**, top) and a sustained ability to recruit MDSCs (**F**, top), leading to T cell and NK cell exclusion (**E,F**, right). Thus, *Gli1/Gli2/Gli3* KO fibroblasts support tumor growth (**F**, bottom). Interestingly, loss of *Gli1/Gli2/Gli3* also leads to the loss of pancreas tissue and an accumulation of fat at PanIN stages (**E**, bottom), indicating that a baseline level of GLI activity is necessary to maintain pancreas integrity.

2.10 References

Adams CR, Htwe HH, Marsh T, Wang AL, Montoya ML, Subbaraj L, Tward AD, Bardeesy N, Perera RM. 2019. Transcriptional control of subtype switching ensures adaptation and growth of pancreatic cancer. *Elife* **8**.

Ahn S, Joyner AL. 2004. Dynamic changes in the response of cells to positive hedgehog signaling during mouse limb patterning. *Cell* **118**: 505-516.

Apte MV, Haber PS, Darby SJ, Rodgers SC, McCaughan GW, Korsten MA, Pirola RC, Wilson JS. 1999. Pancreatic stellate cells are activated by proinflammatory cytokines: implications for pancreatic fibrogenesis. *Gut* **44**: 534-541.

Apte MV, Phillips PA, Fahmy RG, Darby SJ, Rodgers SC, McCaughan GW, Korsten MA, Pirola RC, Naidoo D, Wilson JS. 2000. Does alcohol directly stimulate pancreatic fibrogenesis? Studies with rat pancreatic stellate cells. *Gastroenterology* **118**: 780-794.

Bai CB, Auerbach W, Lee JS, Stephen D, Joyner AL. 2002. Gli2, but not Gli1, is required for initial Shh signaling and ectopic activation of the Shh pathway. *Development* **129**: 4753-4761.

Bai CB, Joyner AL. 2001. Gli1 can rescue the in vivo function of Gli2. *Development* **128**: 5161-5172.

Bai CB, Stephen D, Joyner AL. 2004. All Mouse Ventral Spinal Cord Patterning by Hedgehog Is Gli Dependent and Involves an Activator Function of Gli3. *Developmental Cell* **6**: 103-115.

Bailey JM, Swanson BJ, Hamada T, Eggers JP, Singh PK, Caffery T, Ouellette MM, Hollingsworth MA. 2008. Sonic hedgehog promotes desmoplasia in pancreatic cancer. *Clin Cancer Res* **14**: 5995-6004.

Berman DM, Karhadkar SS, Maitra A, Montes De Oca R, Gerstenblith MR, Briggs K, Parker AR, Shimada Y, Eshleman JR, Watkins DN et al. 2003. Widespread requirement for Hedgehog ligand stimulation in growth of digestive tract tumours. *Nature* **425**: 846-851.

Biffi G, Oni TE, Spielman B, Hao Y, Elyada E, Park Y, Preall J, Tuveson DA. 2019. IL1-Induced JAK/STAT Signaling Is Antagonized by TGFbeta to Shape CAF Heterogeneity in Pancreatic Ductal Adenocarcinoma. *Cancer Discov* **9**: 282-301.

Blaess S, Stephen D, Joyner AL. 2008. Gli3 coordinates three-dimensional patterning and growth of the tectum and cerebellum by integrating Shh and Fgf8 signaling. *Development* **135**: 2093-2103.

Briscoe J, Therond PP. 2013. The mechanisms of Hedgehog signalling and its roles in development and disease. *Nat Rev Mol Cell Biol* **14**: 416-429.

Cano DA, Sekine S, Hebrok M. 2006. Primary cilia deletion in pancreatic epithelial cells results in cyst formation and pancreatitis. *Gastroenterology* **131**: 1856-1869.

Carriere C, Young AL, Gunn JR, Longnecker DS, Korc M. 2009. Acute pancreatitis markedly accelerates pancreatic cancer progression in mice expressing oncogenic Kras. *Biochem Biophys Res Commun* **382**: 561-565.

Catenacci DV, Junttila MR, Karrison T, Bahary N, Horiba MN, Nattam SR, Marsh R, Wallace J, Kozloff M, Rajdev L et al. 2015. Randomized Phase Ib/II Study of Gemcitabine Plus Placebo or Vismodegib, a Hedgehog Pathway Inhibitor, in Patients With Metastatic Pancreatic Cancer. *J Clin Oncol* **33**: 4284-4292.

Chung MI, Bujnis M, Barkauskas CE, Kobayashi Y, Hogan BLM. 2018. Niche-mediated BMP/SMAD signaling regulates lung alveolar stem cell proliferation and differentiation. *Development* **145**.

Cornish TC, Hruban RH. 2011. Pancreatic Intraepithelial Neoplasia. *Surg Pathol Clin* **4**: 523-535.

Corrales JD, Blaess S, Mahoney EM, Joyner AL. 2006. The level of sonic hedgehog signaling regulates the complexity of cerebellar foliation. *Development* **133**: 1811-1821.

Criscimanna A, Speicher JA, Houshmand G, Shiota C, Prasadan K, Ji B, Logsdon CD, Gittes GK, Esni F. 2011. Duct cells contribute to regeneration of endocrine and acinar cells following pancreatic damage in adult mice. *Gastroenterology* **141**: 1451-1462, 1462 e1451-1456.

Elliott KH, Chen X, Salomone J, Chaturvedi P, Schultz PA, Balchand SK, Servetas JD, Zuniga A, Zeller R, Gebelein B et al. 2020. Gli3 utilizes Hand2 to synergistically regulate tissue-specific transcriptional networks. *Elife* **9**.

Elyada E, Bolisetty M, Laise P, Flynn WF, Courtois ET, Burkhart RA, Teinor JA, Belleau P, Biffi G, Lucito MS et al. 2019. Cross-Species Single-Cell Analysis of Pancreatic Ductal Adenocarcinoma Reveals Antigen-Presenting Cancer-Associated Fibroblasts. *Cancer Discov* **9**: 1102-1123.

Feig C, Jones JO, Kraman M, Wells RJ, Deonarine A, Chan DS, Connell CM, Roberts EW, Zhao Q, Caballero OL et al. 2013. Targeting CXCL12 from FAP-expressing carcinoma-associated fibroblasts synergizes with anti-PD-L1 immunotherapy in pancreatic cancer. *Proc Natl Acad Sci U S A* **110**: 20212-20217.

Fernando MR, Reyes JL, Iannuzzi J, Leung G, McKay DM. 2014. The pro-inflammatory cytokine, interleukin-6, enhances the polarization of alternatively activated macrophages. *PLoS One* **9**: e94188.

Francescone R, Barbosa Vendramini-Costa D, Franco-Barraza J, Wagner J, Muir A, Lau AN, Gabitova L, Pazina T, Gupta S, Luong T et al. 2021. Netrin G1 Promotes Pancreatic

Tumorigenesis through Cancer-Associated Fibroblast-Driven Nutritional Support and Immunosuppression. *Cancer Discov* **11**: 446-479.

Garcia AD, Petrova R, Eng L, Joyner AL. 2010. Sonic hedgehog regulates discrete populations of astrocytes in the adult mouse forebrain. *J Neurosci* **30**: 13597-13608.

Garcia PE, Adoumie M, Kim EC, Zhang Y, Scales MK, El-Tawil YS, Shaikh AZ, Wen HJ, Bednar F, Allen BL et al. 2020a. Differential Contribution of Pancreatic Fibroblast Subsets to the Pancreatic Cancer Stroma. *Cell Mol Gastroenterol Hepatol* **10**: 581-599.

Garcia PE, Scales MK, Allen BL, Pasca di Magliano M. 2020b. Pancreatic Fibroblast Heterogeneity: From Development to Cancer. *Cells* **9**.

Halbrook CJ, Lyssiotis CA. 2017. Employing Metabolism to Improve the Diagnosis and Treatment of Pancreatic Cancer. *Cancer Cell* **31**: 5-19.

Hao Y, Hao S, Andersen-Nissen E, Mauck WM, 3rd, Zheng S, Butler A, Lee MJ, Wilk AJ, Darby C, Zager M et al. 2021. Integrated analysis of multimodal single-cell data. *Cell* **184**: 3573-3587 e3529.

Helms E, Onate MK, Sherman MH. 2020. Fibroblast Heterogeneity in the Pancreatic Tumor Microenvironment. *Cancer Discov* **10**: 648-656.

Hessmann E, Patzak MS, Klein L, Chen N, Kari V, Ramu I, Bapiro TE, Frese KK, Gopinathan A, Richards FM et al. 2018. Fibroblast drug scavenging increases intratumoural gemcitabine accumulation in murine pancreas cancer. *Gut* **67**: 497-507.

Hingorani SR, Petricoin EF, Maitra A, Rajapakse V, King C, Jacobetz MA, Ross S, Conrads TP, Veenstra TD, Hitt BA et al. 2003. Preinvasive and invasive ductal pancreatic cancer and its early detection in the mouse. *Cancer Cell* **4**: 437-450.

Hingorani SR, Wang L, Multani AS, Combs C, Deramaudt TB, Hruban RH, Rustgi AK, Chang S, Tuveson DA. 2005. Trp53R172H and KrasG12D cooperate to promote chromosomal instability and widely metastatic pancreatic ductal adenocarcinoma in mice. *Cancer Cell* **7**: 469-483.

Holloway EM, Czerwinski M, Tsai YH, Wu JH, Wu A, Childs CJ, Walton KD, Sweet CW, Yu Q, Glass I et al. 2021. Mapping Development of the Human Intestinal Niche at Single-Cell Resolution. *Cell Stem Cell* **28**: 568-580 e564.

Hosein AN, Huang H, Wang Z, Parmar K, Du W, Huang J, Maitra A, Olson E, Verma U, Brekken RA. 2019. Cellular heterogeneity during mouse pancreatic ductal adenocarcinoma progression at single-cell resolution. *JCI Insight* **5**.

Hui CC, Angers S. 2011. Gli proteins in development and disease. *Annu Rev Cell Dev Biol* **27**: 513-537.

Hui CC, Joyner AL. 1993. A mouse model of greig cephalopolysyndactyly syndrome: the extra-toesJ mutation contains an intragenic deletion of the Gli3 gene. *Nat Genet* **3**: 241-246.

Hwang RF, Moore T, Arumugam T, Ramachandran V, Amos KD, Rivera A, Ji B, Evans DB, Logsdon CD. 2008. Cancer-associated stromal fibroblasts promote pancreatic tumor progression. *Cancer Res* **68**: 918-926.

Ireland L, Santos A, Ahmed MS, Rainer C, Nielsen SR, Quaranta V, Weyer-Czernilofsky U, Engle DD, Perez-Mancera PA, Coupland SE et al. 2016. Chemoresistance in Pancreatic Cancer Is Driven by Stroma-Derived Insulin-Like Growth Factors. *Cancer Res* **76**: 6851-6863.

Jacobetz MA, Chan DS, Neesse A, Bapiro TE, Cook N, Frese KK, Feig C, Nakagawa T, Caldwell ME, Zecchini HI et al. 2013. Hyaluronan impairs vascular function and drug delivery in a mouse model of pancreatic cancer. *Gut* **62**: 112-120.

Jones S, Zhang X, Parsons DW, Lin JC, Leary RJ, Angenendt P, Mankoo P, Carter H, Kamiyama H, Jimeno A et al. 2008. Core signaling pathways in human pancreatic cancers revealed by global genomic analyses. *Science* **321**: 1801-1806.

Karin N, Razon H. 2018. Chemokines beyond chemo-attraction: CXCL10 and its significant role in cancer and autoimmunity. *Cytokine* **109**: 24-28.

Kawaguchi Y, Cooper B, Gannon M, Ray M, MacDonald RJ, Wright CV. 2002. The role of the transcriptional regulator Ptf1a in converting intestinal to pancreatic progenitors. *Nat Genet* **32**: 128-134.

Kim EJ, Sahai V, Abel EV, Griffith KA, Greenson JK, Takebe N, Khan GN, Blau JL, Craig R, Balis UG et al. 2014. Pilot clinical trial of hedgehog pathway inhibitor GDC-0449 (vismodegib) in combination with gemcitabine in patients with metastatic pancreatic adenocarcinoma. *Clin Cancer Res* **20**: 5937-5945.

Ko AH, LoConte N, Tempero MA, Walker EJ, Kate Kelley R, Lewis S, Chang WC, Kantoff E, Vannier MW, Catenacci DV et al. 2016. A Phase I Study of FOLFIRINOX Plus IPI-926, a Hedgehog Pathway Inhibitor, for Advanced Pancreatic Adenocarcinoma. *Pancreas* **45**: 370-375.

Kraman M, Bambrough PJ, Arnold JN, Roberts EW, Magiera L, Jones JO, Gopinathan A, Tuveson DA, Fearon DT. 2010. Suppression of antitumor immunity by stromal cells expressing fibroblast activation protein-alpha. *Science* **330**: 827-830.

Lee JJ, Perera RM, Wang H, Wu DC, Liu XS, Han S, Fitamant J, Jones PD, Ghanta KS, Kawano S et al. 2014. Stromal response to Hedgehog signaling restrains pancreatic cancer progression. *Proc Natl Acad Sci U S A* **111**: E3091-3100.

Liu X, Pitarresi JR, Cuitino MC, Kladney RD, Woelke SA, Sizemore GM, Nayak SG, Egriboz O, Schweickert PG, Yu L et al. 2016. Genetic ablation of Smoothened in pancreatic fibroblasts increases acinar-ductal metaplasia. *Genes Dev* **30**: 1943-1955.

Long KB, Gladney WL, Tooker GM, Graham K, Fraietta JA, Beatty GL. 2016. IFNgamma and CCL2 Cooperate to Redirect Tumor-Infiltrating Monocytes to Degrade Fibrosis and Enhance Chemotherapy Efficacy in Pancreatic Carcinoma. *Cancer Discov* **6**: 400-413.

Madisen L, Zwingman TA, Sunkin SM, Oh SW, Zariwala HA, Gu H, Ng LL, Palmiter RD, Hawrylycz MJ, Jones AR et al. 2010. A robust and high-throughput Cre reporting and characterization system for the whole mouse brain. *Nat Neurosci* **13**: 133-140.

Maghazachi AA, Al-Aoukaty A, Schall TJ. 1996. CC chemokines induce the generation of killer cells from CD56+ cells. *Eur J Immunol* **26**: 315-319.

Mathew E, Collins MA, Fernandez-Barrena MG, Holtz AM, Yan W, Hogan JO, Tata Z, Allen BL, Fernandez-Zapico ME, di Magliano MP. 2014a. The transcription factor GLI1 modulates the inflammatory response during pancreatic tissue remodeling. *J Biol Chem* **289**: 27727-27743.

Mathew E, Zhang Y, Holtz AM, Kane KT, Song JY, Allen BL, Pasca di Magliano M. 2014b. Dosage-dependent regulation of pancreatic cancer growth and angiogenesis by hedgehog signaling. *Cell Rep* **9**: 484-494.

Maurer C, Holmstrom SR, He J, Laise P, Su T, Ahmed A, Hibshoosh H, Chabot JA, Oberstein PE, Sepulveda AR et al. 2019. Experimental microdissection enables functional harmonisation of pancreatic cancer subtypes. *Gut* **68**: 1034-1043.

Mews P, Phillips P, Fahmy R, Korsten M, Pirola R, Wilson J, Apte M. 2002. Pancreatic stellate cells respond to inflammatory cytokines: potential role in chronic pancreatitis. *Gut* **50**: 535-541.

Mills LD, Zhang L, Marler R, Svingen P, Fernandez-Barrena MG, Dave M, Bamlet W, McWilliams RR, Petersen GM, Faubion W et al. 2014. Inactivation of the transcription factor GLI1 accelerates pancreatic cancer progression. *J Biol Chem* **289**: 16516-16525.

Mills LD, Zhang Y, Marler RJ, Herreros-Villanueva M, Zhang L, Almada LL, Couch F, Wetmore C, Pasca di Magliano M, Fernandez-Zapico ME. 2013. Loss of the transcription factor GLI1 identifies a signaling network in the tumor microenvironment mediating KRAS oncogene-induced transformation. *J Biol Chem* **288**: 11786-11794.

Mo R, Freer AM, Zinyk DL, Crackower MA, Michaud J, Heng HH, Chik KW, Shi XM, Tsui LC, Cheng SH et al. 1997. Specific and redundant functions of Gli2 and Gli3 zinc finger genes in skeletal patterning and development. *Development* **124**: 113-123.

Morris JPt, Cano DA, Sekine S, Wang SC, Hebrok M. 2010. Beta-catenin blocks Kras-dependent reprogramming of acini into pancreatic cancer precursor lesions in mice. *J Clin Invest* **120**: 508-520.

Muranen T, Iwanicki MP, Curry NL, Hwang J, DuBois CD, Coloff JL, Hitchcock DS, Clish CB, Brugge JS, Kalaany NY. 2017. Starved epithelial cells uptake extracellular matrix for survival. *Nat Commun* **8**: 13989.

Nolan-Stevaux O, Lau J, Truitt ML, Chu GC, Hebrok M, Fernandez-Zapico ME, Hanahan D. 2009. GLI1 is regulated through Smoothened-independent mechanisms in neoplastic pancreatic ducts and mediates PDAC cell survival and transformation. *Genes Dev* **23**: 24-36.

Ohlund D, Handly-Santana A, Biffi G, Elyada E, Almeida AS, Ponz-Sarvise M, Corbo V, Oni TE, Hearn SA, Lee EJ et al. 2017. Distinct populations of inflammatory fibroblasts and myofibroblasts in pancreatic cancer. *J Exp Med* **214**: 579-596.

Olive KP, Jacobetz MA, Davidson CJ, Gopinathan A, McIntyre D, Honess D, Madhu B, Goldgraben MA, Caldwell ME, Allard D et al. 2009. Inhibition of Hedgehog signaling enhances delivery of chemotherapy in a mouse model of pancreatic cancer. *Science* **324**: 1457-1461.

Ozdemir BC, Pentcheva-Hoang T, Carstens JL, Zheng X, Wu CC, Simpson TR, Laklai H, Sugimoto H, Kahlert C, Novitskiy SV et al. 2014. Depletion of carcinoma-associated fibroblasts and fibrosis induces immunosuppression and accelerates pancreas cancer with reduced survival. *Cancer Cell* **25**: 719-734.

Pasca di Magliano M, Sekine S, Ermilov A, Ferris J, Dlugosz AA, Hebrok M. 2006. Hedgehog/Ras interactions regulate early stages of pancreatic cancer. *Genes Dev* **20**: 3161-3173.

Persson M, Stamataki D, te Welscher P, Andersson E, Bose J, Ruther U, Ericson J, Briscoe J. 2002. Dorsal-ventral patterning of the spinal cord requires Gli3 transcriptional repressor activity. *Genes Dev* **16**: 2865-2878.

Pitarresi JR, Liu X, Avendano A, Thies KA, Sizemore GM, Hammer AM, Hildreth BE, 3rd, Wang DJ, Steck SA, Donohue S et al. 2018. Disruption of stromal hedgehog signaling initiates RNF5-mediated proteasomal degradation of PTEN and accelerates pancreatic tumor growth. *Life Sci Alliance* **1**: e201800190.

Provenzano PP, Cuevas C, Chang AE, Goel VK, Von Hoff DD, Hingorani SR. 2012. Enzymatic targeting of the stroma ablates physical barriers to treatment of pancreatic ductal adenocarcinoma. *Cancer Cell* **21**: 418-429.

Putoczki T, Ernst M. 2010. More than a sidekick: the IL-6 family cytokine IL-11 links inflammation to cancer. *J Leukoc Biol* **88**: 1109-1117.

Rajurkar M, De Jesus-Monge WE, Driscoll DR, Appleman VA, Huang H, Cotton JL, Klimstra DS, Zhu LJ, Simin K, Xu L et al. 2012. The activity of Gli transcription factors is essential for Kras-induced pancreatic tumorigenesis. *Proc Natl Acad Sci U S A* **109**: E1038-1047.

Rhim AD, Oberstein PE, Thomas DH, Mirek ET, Palermo CF, Sastra SA, Dekleva EN, Saunders T, Becerra CP, Tattersall IW et al. 2014. Stromal elements act to restrain, rather than support, pancreatic ductal adenocarcinoma. *Cancer Cell* **25**: 735-747.

Sakamoto H, Koma YI, Higashino N, Kodama T, Tanigawa K, Shimizu M, Fujikawa M, Nishio M, Shigeoka M, Kakeji Y et al. 2021. PAI-1 derived from cancer-associated fibroblasts in esophageal squamous cell carcinoma promotes the invasion of cancer cells and the migration of macrophages. *Lab Invest* **101**: 353-368.

Schonhuber N, Seidler B, Schuck K, Veltkamp C, Schachtler C, Zukowska M, Eser S, Feyerabend TB, Paul MC, Eser P et al. 2014. A next-generation dual-recombinase system for time- and host-specific targeting of pancreatic cancer. *Nat Med* **20**: 1340-1347.

Shek FW-T, Benyon RC, Walker FM, McCrudden PR, Pender SLF, Williams EJ, Johnson PA, Johnson CD, Bateman AC, Fine DR et al. 2002. Expression of Transforming Growth Factor-β1 by Pancreatic Stellate Cells and Its Implications for Matrix Secretion and Turnover in Chronic Pancreatitis. *The American Journal of Pathology* **160**: 1787-1798.

Siegel RL, Miller KD, Fuchs HE, Jemal A. 2022. Cancer statistics, 2022. *CA Cancer J Clin* **72**: 7-33.

Steele NG, Biffi G, Kemp SB, Zhang Y, Drouillard D, Syu L, Hao Y, Oni TE, Brosnan E, Elyada E et al. 2021. Inhibition of Hedgehog Signaling Alters Fibroblast Composition in Pancreatic Cancer. *Clin Cancer Res* **27**: 2023-2037.

Steele NG, Carpenter ES, Kemp SB, Sirihorachai V, The S, Delrosario L, Lazarus J, Amir ED, Gunchick V, Espinoza C et al. 2020. Multimodal Mapping of the Tumor and Peripheral Blood Immune Landscape in Human Pancreatic Cancer. *Nat Cancer* **1**: 1097-1112.

Tan MC, Goedegebuure PS, Belt BA, Flaherty B, Sankpal N, Gillanders WE, Eberlein TJ, Hsieh CS, Linehan DC. 2009. Disruption of CCR5-dependent homing of regulatory T cells inhibits tumor growth in a murine model of pancreatic cancer. *J Immunol* **182**: 1746-1755.

Thayer SP, di Magliano MP, Heiser PW, Nielsen CM, Roberts DJ, Lauwers GY, Qi YP, Gysin S, Fernandez-del Castillo C, Yajnik V et al. 2003. Hedgehog is an early and late mediator of pancreatic cancer tumorigenesis. *Nature* **425**: 851-856.

Tian H, Callahan CA, DuPree KJ, Darbonne WC, Ahn CP, Scales SJ, de Sauvage FJ. 2009. Hedgehog signaling is restricted to the stromal compartment during pancreatic carcinogenesis. *Proc Natl Acad Sci U S A* **106**: 4254-4259.

Todaro GJ, Green H. 1963. Quantitative studies of the growth of mouse embryo cells in culture and their development into established lines. *J Cell Biol* **17**: 299-313.

Wen HJ, Gao S, Wang Y, Ray M, Magnuson MA, Wright CVE, Di Magliano MP, Frankel TL, Crawford HC. 2019. Myeloid Cell-Derived HB-EGF Drives Tissue Recovery After Pancreatitis. *Cell Mol Gastroenterol Hepatol* **8**: 173-192.

Xu Z, Vonlaufen A, Phillips PA, Fiala-Beer E, Zhang X, Yang L, Biankin AV, Goldstein D, Pirola RC, Wilson JS et al. 2010. Role of pancreatic stellate cells in pancreatic cancer metastasis. *Am J Pathol* **177**: 2585-2596.

Yauch RL, Gould SE, Scales SJ, Tang T, Tian H, Ahn CP, Marshall D, Fu L, Januario T, Kallop D et al. 2008. A paracrine requirement for hedgehog signalling in cancer. *Nature* **455**: 406-410.

Zhang X, Goncalves R, Mosser DM. 2008. The isolation and characterization of murine macrophages. *Curr Protoc Immunol* **Chapter 14**: Unit 14 11.

Zhang Y, Crawford HC, Pasca di Magliano M. 2019. Epithelial-Stromal Interactions in Pancreatic Cancer. *Annu Rev Physiol* **81**: 211-233.

Zhang Y, Lazarus J, Steele NG, Yan W, Lee HJ, Nwosu ZC, Halbrook CJ, Menjivar RE, Kemp SB, Sirihorachai VR et al. 2020. Regulatory T-cell Depletion Alters the Tumor Microenvironment and Accelerates Pancreatic Carcinogenesis. *Cancer Discov* **10**: 422-439.

Zhang Y, Yan W, Mathew E, Bednar F, Wan S, Collins MA, Evans RA, Welling TH, Vonderheide RH, di Magliano MP. 2014. CD4+ T lymphocyte ablation prevents pancreatic carcinogenesis in mice. *Cancer Immunol Res* **2**: 423-435.

Chapter 3 Mesenchymal *Gli3* regulates endocrine development and tissue morphogenesis in the developing pancreas

3.1 Abstract

Pancreas development relies on crosstalk between the developing pancreatic epithelium and the surrounding mesenchyme. This process requires the activation of certain signaling pathways paired with the suppression of others, and interfering with this regulation can impair pancreas organogenesis. In particular, negative regulation of Hedgehog (HH) signaling is essential during pancreas development, as aberrant activation of HH signaling disrupts multiple cellular compartments within the developing pancreas. Although this repression of HH signaling is known to be necessary, the mechanisms restricting HH signaling on a transcriptional level remain unknown. In other developing tissues, the GLI family of HH transcription factors (GLI1, GLI2, GLI3) are responsible for both activating and repressing HH target genes. However, the roles of GLI1-3 in the developing pancreas remain unknown. In this study, we determined that conditional deletion of mesenchymal *Gli3* leads to enhanced epithelial proliferation and drives abnormal pancreas growth. In addition, our preliminary data indicate that loss of *Gli3* restricts the development of β-cells. Interestingly, our data also suggest that the contribution of GLI3 to pancreas development depends on timing, as *Gli3* deletion during the primary transition impacts tissue morphogenesis and endocrine development, while deleting *Gli3* during the secondary transition only impacts endocrine cells. Together, our data indicate that mesenchymal GLI3 plays multiple roles throughout pancreas development, and that these roles affect multiple cellular compartments within the pancreatic microenvironment.

3.2 Introduction

The pancreas is a crucial organ that regulates organism health through both exocrine and endocrine functions. Diseases of the pancreas remain a significant clinical burden, as type 2 diabetes alone affects more than 382 million adults globally, and rates continue to rise (DeFronzo et al. 2015). In order to properly generate the diverse cell types of the pancreas, pancreatic progenitor cells undergo a tightly regulated process of development (Shih et al. 2013). Maintaining these different cell populations is essential to organ function, as targeted loss of specific pancreatic cell types can lead to pancreatic disease, including type 1 diabetes (DiMeglio et al. 2018). Therefore, understanding the mechanisms that regulate pancreas development is essential to our understanding of proper organ function and health.

Pancreas embryonic development occurs in two main phases: primary transition and secondary transition. In mouse models, primary transition begins around E9.0, with emergence of the dorsal and ventral pancreatic buds (Shih et al. 2013). Following the fusion of the pancreatic buds at E12.5, the pancreas enters secondary transition, in which the multipotent progenitors differentiate into distinct endocrine and exocrine lineages (Shih et al. 2013). Throughout pancreatic development, epithelial cells rely on cross-talk from the surrounding mesenchyme in order to properly grow and differentiate into mature cell types (Sakhneny et al. 2019). In the absence of mesenchyme, pancreas cultures fail to grow and form lobes (Golosow and Grobstein 1962), and targeted depletion of the mesenchyme *in vivo* leads to impaired organ formation (Landsman et al. 2011). Although the mesenchyme is known to be essential throughout pancreas development, the mechanisms regulating mesenchymal-epithelial crosstalk are still not fully understood.

In multiple organ systems, activation of the Hedgehog (HH) signaling pathway is necessary for tissue patterning and growth (Briscoe and Therond 2013). In contrast, the initiation of pancreas development requires the absence of HH signaling. *Shh* expression is excluded from pancreatic endoderm, and ectopically expressing *Shh* in the pancreatic epithelium drives the expansion of mesenchyme at the expense of epithelial pancreas tissue (Apelqvist et al. 1997; Hebrok et al. 1998; Kawahira et al. 2005). In addition, loss of inhibitory HH receptors *Hhip* or *Ptch1* aberrant activates HH signaling, leading to reduced pancreas growth and impaired formation of endocrine cells (Kawahira et al. 2003; Hibsher et al. 2016). Together, these data indicate that the negative regulation of HH signaling is crucial for proper pancreas development.

While controlled HH repression is necessary for pancreas development, the mechanisms regulating this process on a transcriptional level remain poorly understood. In particular, the role of GLI transcription factors (GLI1, GLI2, GLI3), the transcriptional regulators of the HH pathway, during pancreas development remain unknown. While GLI1 functions exclusively as an activator, GLI2 and GLI3 have dual roles as both transcriptional activators and repressors (Hui and Angers 2011). Further, the balance of GLI activator (GLI-A) and GLI repressor (GLI-R) in developing tissues is important for regulating HH responses, as different levels of GLI activity can drive distinct cell fates (Persson et al. 2002; Stamataki et al. 2005).

In this study, we investigated the role of GLI transcription factors during pancreas development. Our data reveal that *Gli2* and *Gli3* are expressed throughout the mesenchyme of the developing pancreas, but *Gli1* is not expressed. While deleting *Gli2* did not consistently impact pancreas development, conditionally deleting *Gli3* in the mesenchyme during the primary transition disrupts pancreas morphogenesis. Specifically, mesenchymal *Gli3* deletion leads to a thickening of the pancreatic head and abnormal growth of the pancreatic tail. In contrast, loss of

Gli3 during the secondary transition had no gross effect on pancreas morphology. However, preliminary data indicate that deleting *Gli3* in the mesenchyme at both stages of pancreas development impairs the formation of β-cells. Together, our data suggest that mesenchymal GLI3 regulates tissue morphogenesis and endocrine development in the developing pancreas.

3.3 Results

3.3.1 Gli2 and Gli3 are expressed in the mesenchyme of the developing pancreas

To determine whether *Gli1*, *Gli2*, and *Gli3* were expressed in the developing pancreas, $Gli1^{lacZ/+}$, $Gli2^{lacZ/+}$, and $Gli3^{lacZ/+}$ embryos were analyzed for β-galactosidase expression at E13.5 (Figure 3.1A-H). This stage falls within the secondary transition, when cross-talk between the mesenchyme and epithelium is essential for the expansion of both exocrine and endocrine lineages (Landsman et al. 2011). X-gal staining of $Gli1^{lacZ/+}$mice revealed that *Gli1* is not expressed in the developing pancreas (Figure 3.1B). In contrast, both *Gli2* and *Gli3* display broad expression at E13.5 (Figure 3.1C-D). Immunofluorescent analysis (IF) revealed that *Gli2* and *Gli3* are excluded from the epithelium and expressed throughout the mesenchyme at E13.5 (Figure 3.1G-H). To evaluate *Gli2* and *Gli3* expression at later stages of pancreas development, we analyzed β-galactosidase expression in E18.5 $Gli2^{lacZ/+}$ and $Gli3^{lacZ/+}$ embryos. At this stage, acinar cells have formed into lobular clusters connected to ducts, and endocrine cells have de-laminated and formed aggregates throughout the tissue (Shih et al. 2013). X-gal staining and IF analysis revealed that *Gli2* and *Gli3* remain broadly expressed by mesenchymal cells at E18.5 (Figure 3.1I-N). These data indicate that both *Gli2* and *Gli3* are expressed by mesenchymal cells during pancreas development

3.3.2 Mesenchymal Gli3 deletion leads to disrupted pancreas morphogenesis

To investigate the functional role of mesenchymal GLI in pancreas development, we utilized the *Pdgfrα*$^{CreER/+}$ allele (Chung et al. 2018) to target *Gli* expression in the pancreatic mesenchyme. Our data from the adult organ indicates that this allele effectively drives fibroblast-specific recombination in the mature pancreatic fibroblasts (see Chapter 2, Figure 2.4A). To determine if this allele effectively targets the developing pancreatic mesenchyme, we crossed *Pdgfrα*$^{CreER/+}$ mice to a CRE-dependent tdTomato reporter line. Pregnant females were given a single dose of tamoxifen at E9.5 (Figure 3.2A), to drive recombination in the mesenchyme at the beginning of pancreas development. IF analysis of E18.5 embryos revealed that the *Pdgfrα*$^{CreER/+}$ allele specifically labeled mesenchymal cells in the developing pancreas (Figure 3.2B-C), and approximately 85% of mesenchymal cells were labeled with tdTomato (Figure 3.2D).

To determine the role *Gli2* during pancreas development, we administered tamoxifen to *Pdgfrα*$^{CreER/+}$*;Gli2*$^{fl/fl}$ embryos at E9.5 (Figure 3.3A). The pancreata of *Pdgfrα*$^{CreER/+}$*;Gli2*$^{fl/fl}$ embryos appear largely normal by gross morphology (Figure 3.3.B-E, Table 3.1). One in three *Pdgfrα*$^{CreER/+}$*;Gli2*$^{fl/fl}$ embryos display a thickening of the pancreatic head (Figure 3.3C, white arrowhead), but the majority of the embryos show no defects. Further, the tails of all *Pdgfrα*$^{CreER/+}$*;Gli2*$^{fl/fl}$ pancreata appear normal (Figure 3.3B-E, green arrowheads), and show no significant differences in shape or size compared to *Gli2*$^{fl/fl}$ pancreata. These data indicate that GLI2 is largely dispensable to pancreas morphogenesis.

To evaluate whether GLI3 regulates pancreas development, we conditionally deleted *Gli3* in *Pdgfrα*$^{CreER/+}$*;Gli3*$^{fl/fl}$ embryos at E9.5 (Figure 3.4A). At E18.5, *Pdgfrα*$^{CreER/+}$*;Gli3*$^{fl/fl}$ embryos display polydactyly (Figure 3.4B-E), consistent with a loss of *Gli3* function in the embryonic mesenchyme. In the pancreas, conditional deletion of mesenchymal *Gli3* leads to disrupted

pancreas morphology (Figure 3.4F-I). Specifically, all *Pdgfrα*$^{CreER/+}$;*Gli3*$^{fl/fl}$ embryos display a thickening of tissue in the head of the pancreas (Figure 3.4F-I, white arrowheads). Deleting *Gli3* in the mesenchyme also leads to a spectrum of phenotypes in the tail of the pancreas (Figure 3.4F-I, green arrowheads). All *Pdgfrα*$^{CreER/+}$;*Gli3*$^{fl/fl}$ embryos lack the characteristic "anvil" shape to the tail of the pancreas, and a majority of *Pdgfrα*$^{CreER/+}$;*Gli3*$^{fl/fl}$ embryos display tissue expansion in the pancreas tail (Table 3.2), albeit to varying degrees. These data indicate that GLI3 regulates pancreas tissue morphogenesis.

We next wanted to determine if GLI3 plays distinct roles at different stages of pancreas development. Since many lineages of the pancreas differentiate during the secondary transition (Shih et al. 2013), we tested whether the phenotypes we observed were due to disruptions during this critical window of development. *Pdgfrα*$^{CreER/+}$;*Gli3*$^{fl/fl}$ embryos were given tamoxifen at E13.5 and collected at E18.5 (Figure 3.4J). In contrast to deleting *Gli3* at E9.5, conditional deletion *Gli3* at E13.5 has no obvious effect on pancreas morphology (Figure 3.4K-M, Table 3.3). The pancreatic heads of *Pdgfrα*$^{CreER/+}$;*Gli3*$^{fl/fl}$ embryos are comparable to *Gli3*$^{fl/fl}$ embryos (Figure 3.4K-M, white arrowheads). While one *Pdgfrα*$^{CreER/+}$;*Gli3*$^{fl/fl}$ embryo showed a mild expansion of the pancreatic tail (Figure 3.4L, green arrowhead), all *Pdgfrα*$^{CreER/+}$;*Gli3*$^{fl/fl}$ embryos maintain the typical anvil morphology of the pancreatic tail (Figure 3.4K-M, green arrowheads). These data suggest that the contribution of mesenchymal GLI3 to tissue morphogenesis is restricted to the primary transition.

Prior studies have indicated that disrupted HH signaling can impair the generation of epithelial tissue in the developing pancreas (Kawahira et al. 2003; Kawahira et al. 2005; Hibsher et al. 2016). To determine if the phenotypes we observe following loss of *Gli3* are due to abnormal epithelial development, we analyzed the cellular composition of pancreata from

Pdgfrα$^{CreER/+}$;*Gli3*$^{fl/fl}$ embryos by IF (Figure 3.5A-C). In contrast to conditional deletion of *Ptch1* (Hibsher et al. 2016), conditional deletion of *Gli3* at E9.5 does not affect the prevalence of epithelial cells in the developing pancreas (Figure 3.5C). However, epithelial cell proliferation is elevated in *Pdgfrα*$^{CreER/+}$;*Gli3*$^{fl/fl}$ embryos (Figure 3.5D). Deleting *Gli3* at E13.5 does not increase epithelial proliferation, consistent with a lack of morphology defects in these embryos (Figure 3.5E-H). These data suggest that deleting mesenchymal *Gli3* during the primary transition increases epithelial proliferation, leading to abnormal organ growth. However, additional replicates are required to determine if these changes in epithelial proliferation are statistically significant.

Prior work has also indicated that dysregulated HH signaling can also impair the generation of endocrine cells (Kawahira et al. 2003; Kawahira et al. 2005; Cervantes et al. 2010; Hibsher et al. 2016). To test if mesenchymal GLI3 regulates endocrine development, we stained *Pdgfrα*$^{CreER/+}$;*Gli3*$^{fl/fl}$ embryos with markers for β-cells (Insulin) and α-cells (Glucagon) (Figure 3.6A-H). Interestingly, our preliminary data suggest that deleting *Gli3* at both E9.5 and E13.5 leads to a decrease in insulin-expressing β-cells (Figure 3.6A-C, E-G), while glucagon-expressing α-cells are unaffected (Figure 3.6D, H). Together, these data indicate that mesenchymal GLI3 may regulate epithelial growth and the formation of endocrine cells during pancreas development. However, further analysis is required to determine the reproducibility of these results, and to identify the molecular mechanisms at play.

3.4 Discussion

In this study, we investigated to role of GLI transcription factors in pancreas development. We have determined that *Gli2* and *Gli3* are expressed broadly throughout the pancreatic mesenchyme during pancreas development, while *Gli1* is absent.

Our data indicate that deleting *Gli2* has no consistent effect on pancreas development, while conditionally deleting mesenchymal *Gli3* at the onset of pancreas development leads to an increase in epithelial proliferation and abnormal tissue growth. Deleting *Gli3* at this stage may also lead to a decrease in β-cells, although further analysis is needed to confirm this result. Interestingly, deleting *Gli3* during the secondary transition does not significantly impact pancreas morphogenesis, but has a similar effect on β-cells. Together these data suggest that GLI3 regulates both pancreas growth and endocrine development, but its role changes at different stages of pancreas development.

3.4.1 The role of GLIs and HH signaling in pancreas development

Prior data has demonstrated that the specification of the pancreas from the endoderm requires the absence of HH signaling (Apelqvist et al. 1997; Hebrok et al. 1998), and that HH signaling must be restricted for proper organ growth and endocrine development (Hebrok et al. 2000; Kawahira et al. 2003; Cervantes et al. 2010; Hibsher et al. 2016). The absence of *Gli1* expression indicates a lack of HH signaling in the developing pancreas. Thus, the broad expression of *Gli2* and *Gli3* in the pancreatic mesenchyme suggests that GLI2 and GLI3 may function primarily as transcriptional repressors of HH signaling, ensuring proper pancreas development by suppressing levels of HH response. Consistent with this idea, loss of *Gli3* leads to a decrease in β-cells, a phenotype that has also been seen following aberrant activation of HH signaling (Kawahira et al. 2003; Kawahira et al. 2005; Cervantes et al. 2010; Hibsher et al. 2016). However, our data also indicate that loss of *Gli3* leads to an increase in epithelial proliferation and organ growth. This conflicts with previous work, which has indicated that aberrant activation of HH signaling reduces epithelial growth (Kawahira et al. 2003; Kawahira et

al. 2005; Hibsher et al. 2016). These conflicting results raise the question: why does loss of *Gli3* drive divergent phenotypes during pancreas development?

One possible explanation could be that GLI3 performs HH-dependent as well as HH-independent roles during pancreas development. In this scenario, GLI3-mediated repression of HH target genes permits proper endocrine development. As a result, loss of GLI3-R phenocopies aberrant activation of HH signaling (via ectopic ligand expression or loss of *Ptch1/Hhip*) (Kawahira et al. 2003; Kawahira et al. 2005; Hibsher et al. 2016), leading to the impaired formation of β-cells. In addition to these canonical HH target genes, GLI3 could also be regulating the expression HH-independent, GLI3-dependent target genes. Evidence from craniofacial development indicates that GLI3 can partner with co-factors to bind to low affinity "divergent" GLI binding motifs at tissue-specific loci that lack high affinity "canonical" GLI binding motifs (Elliott et al. 2020). These data suggest that GLI3 can regulate the expression of unique target genes outside of canonical HH targets in a tissue-specific manner. Thus, the combination of decreased β-cells and increased epithelial growth following the loss of *Gli3* may represent canonical and non-canonical functions for GLI3, respectively. Future work will utilize ChIP-capable *Gli3* alleles (e.g. *3xFlag-Gli3*, the Jackson laboratory #026135) to map GLI3 binding sites in the developing pancreatic mesenchyme. Further, RNA sequencing analysis of WT and *Gli3* KO pancreatic mesenchymal cells will reveal how loss of *Gli3* regulates the expression of identified target genes. In particular, identifying changes in secreted factors will provide insight into the mechanisms through which GLI3 in mesenchymal cells regulates multiple cell types within the developing pancreatic microenvironment.

Our data indicate that GLI activity plays multiple roles in the developing pancreas. However, it remains unknown whether the coordinated activity of multiple GLIs contribute to

these processes. While loss of *Gli2* alone did not significantly affect pancreas development, it is possible that compensation by GLI3 could be masking GLI2's role. It is also possible that the absence of a phenotype in our *Pdgfrα*$^{CreER/+}$;*Gli2*$^{fl/fl}$ embryos could be due to incomplete deletion of *Gli2*. Although our tdTomato reporter expression indicates that the *Pdgfrα*^{CreER} allele broadly targets the pancreatic mesenchyme (Figure 3.2), it is still possible that recombination of the *Gli2* locus is not as effective as the *ROSA26 tdTomato* locus. *Gli2* expression analysis of *Pdgfrα*$^{CreER/+}$;*Gli2*$^{fl/fl}$ embryos by RNAscope could be used to quantitatively determine the efficiency of *Gli2* recombination in *Pdgfrα*$^{CreER/+}$;*Gli2*$^{fl/fl}$ embryos.

Evidence from the adult organ indicates that a baseline level of *Gli* expression is necessary to maintain organ integrity during carcinogenesis (see Chapter 2, Figure 2.6B). To investigate the combined function of GLI in pancreas development, future work will utilize *Pdgfrα*$^{CreER/+}$;*Gli2*$^{fl/fl}$;*Gli3*$^{fl/fl}$ mice to determine whether combined loss of *Gli2* and *Gli3* exacerbates the phenotypes we observe following the loss of *Gli3*. In addition, evaluating pancreas development in *Gli1*$^{lacZ/lacZ}$;*Pdgfrα*$^{CreER/+}$;*Gli2*$^{fl/fl}$;*Gli3*$^{fl/fl}$ embryos will determine if a baseline level of *Gli* activity is necessary for pancreas organogenesis.

3.4.2 Role of Gli in mesenchymal epithelial cross-talk

Although aberrant activation of HH signaling has been shown to drive mesenchymal hyperplasia during pancreas development (Kawahira et al. 2005; Hibsher et al. 2016), deleting *Gli3* had no gross effect on the mesenchyme (data not shown). Instead, deleting mesenchymal *Gli3* primarily had cell extrinsic effects, driving increased epithelial proliferation and a decrease in β-cells. This mesenchymal-epithelial cross-talk is an essential process during pancreas development, as disruptions in this intercellular communication severely hinders organ formation

(Sakhneny et al. 2019). Although our data indicate that *Gli3* plays a role in this process the molecular mechanisms remain unknown.

HH signaling has previously been linked to FGF signaling during pancreas development. Aberrant activation of HH signaling via loss of *Hhip* leads to a delay in *Fgf10* expression (Kawahira et al. 2003). Loss of mesenchyme-derived *Fgf10* has been shown to reduce epithelial progenitor proliferation and severely impair the generation of endocrine cells (Bhushan et al. 2001), which could explain the reduction in endocrine area seen in *Hhip* mutants (Kawahira et al. 2003). Conditional deletion of mesenchymal *Gli3* also appears to decrease β-cells, raising the possibility that GLI3 could regulate *Fgf10* expression during pancreas development. The data generated from the RNA sequencing experiments described above could be interrogated to evaluate *Fgf10* expression in WT vs. *Gli3* KO mesenchymal cells, to determine if coordinated HH-FGF signaling is regulated by GLI3.

The phenotypes described in this study bear a striking resemblance to the phenotypes observed in *Hox6* paralogous mutants (*Hox6 aabbcc*) (Larsen et al. 2015). All three *Hox6* paralogs are expressed in the developing pancreatic mesenchyme, and *Hox6 aabbcc* mutant embryos feature a thicker, more compact pancreas head and reduction in endocrine cells (including β-cells) (Larsen et al. 2015). These phenotypes are remarkably similar to embryos described in this study, in which *Gli3* has been deleted at E9.5. The similarity in phenotypes raises the question of whether HOX and GLI3 could be coordinating in mesenchymal cells to regulate pancreas epithelial development. Coordinated activity between *Hox* genes and *Gli3* have been shown to regulate tissue patterning and the formation of digits in the developing limb (Litingtung et al. 2002; te Welscher et al. 2002; Sheth et al. 2007; Zakany et al. 2007; Xu and Wellik 2011; Bastida et al. 2020). Further, GLI3 and HOXD12 have been shown to physically

interact in the developing limb, and the presence of HOXD12 promotes GLI3-A activity (Chen et al. 2004). Our data raise the possibility that mesenchymal HOX6 and GLI3 could be directly interacting to direct epithelial development in the pancreas. The development of ChIP-capable *Gli* alleles (e.g. *3xFlag-Gli3*, the Jackson laboratory #026135) and *Hox* constructs (Huang et al. 2012) have demonstrated that the binding sites of these historically elusive transcription factors can be identified. Thus, the generation of mice co-expressing ChIP-capable *Gli3* and *Hox6* alleles (e.g. *3xFlag-Gli3;HA-Hoxb6*) would provide an opportunity to determine whether GLI and HOX work in concert to regulate mesenchyme function during pancreas development.

Together our data indicate that mesenchymal GLI3 regulates pancreas morphogenesis and endocrine development. Future investigation will determine whether the GLI3 coordinates with other transcription factors (e.g. GLI2, HOX) to influence pancreas development, and what molecular mechanisms regulate the cross-talk between the pancreatic mesenchyme and epithelium.

3.5 Materials and methods

Animal models

All mice were housed in specific pathogen-free facilities at the University of Michigan. This study was approved by the University of Michigan Institutional Animal Care and Use Committee (IACUC). *Gli1*^{lacZ} (Bai et al. 2002), *Gli2*^{lacZ} (Bai and Joyner 2001), *Gli3*^{lacZ} (Garcia et al. 2010), *Pdgfrα*^{CreERt2} (Chung et al. 2018), *Gli2*$^{fl/fl}$ (Corrales et al. 2006), *Gli3*$^{fl/fl}$ (Blaess et al. 2008), *LSL-tdTomato* (Madisen et al. 2010) mice have all been described previously. To induce CRE-ER recombination, tamoxifen (Sigma T5648) was administered at the specified stages to pregnant females in a single dose of 25 mg/kg by intraperitoneal injection. Whole pancreata were imaged using a Nikon SMZ1500.

X-gal Staining

Embryos were dissected in chilled 1x PBS (pH 7.4). Pancreata were isolated and fixed in 4% PFA on ice for 1h. Pancreata were then washed 3x5min in PBS and transferred to a PBS+30% sucrose solution overnight at 4°C. The next day, tissue was washed 3x5min in OCT. Tissues were frozen in OCT and sectioned on a Leica CM1950 cryostat (12μm sections). β-Galactosidase activity was detected with X-gal staining solution [5 mM K3Fe(CN)6, 5 mM K4Fe(CN)6, 2 mM MgCl2, 0.01% Na deoxycholate, 0.02% NP-40, 1 mg/ml X-gal] and stained for 2 – 36h at 37°C. After staining, the sections were washed 3x5min in PBS and counterstained with Nuclear Fast Red for 5min. Sections were dehydrated 70% ethanol, 95% ethanol, 100% ethanol and 100% xylene) and mounted with coverslips using Permount Mounting Medium (Thermo Fisher Scientific).

Immunofluorescence

Pancreata were collected as described above and fixed in either 4% PFA for 1 hour on ice or 10% neutral-buffered formalin for 1.5 hours at room temperature. Tissue was then washed 3x5min in PBS and embedded in OCT as described above. Frozen sections were warmed to room temperature (RT), then baked at 60°C for 10min. Sections were washed 3x5min in PBS and blocked in blocking buffer [3% bovine serum albumin, 1% heat-inactivated sheep serum, 0.1% Triton X-100 in PBS] for 1h at RT. Sections were incubated with primary antibodies overnight at 4°C in a humidified chamber. Primary antibodies are listed in Table 3.4. Secondary antibodies were diluted in blocking buffer and incubated for 1h at RT, followed by 3x5min washes in PBS. All secondary antibodies were used at a 1:500 dilution. Nuclei were labeled with

DAPI for 10min at RT. Slides were mounted with coverslips using Immu-mount aqueous mounting medium. Sections were visualized on a Leica SP5X upright confocal. For quantitation, 3 – 5 fields of view were imaged per section, and multiple sections were analyzed for each embryo. In quantitation figures, each dot represents an independent embryo. Images were analyzed using FIJI (version 2.0.0-rc-69/1.52p).

Statistical Analysis

All statistical analysis was performed using Graphpad Prism software. For quantitative analysis, each data point represents an independent biological replicate. Information such as sample size, P value, and the statistical test used is either displayed in the figure or stated in the figure legend.

3.6 Acknowledgements

We thank members of the Allen and Pasca di Magliano Labs, for providing input on this project. We acknowledge members of the Department of Cell and Developmental Biology who provided access to equipment, including the O'Shea, Engel, and Spence labs. We thank Corentin Cras-Meneur for providing reagents and valuable protocols for analysis of the developing pancreas. We thank Ethan Tyler and Dr. L. Kravitz for providing the mouse drawing used in our schematics (doi.org/10.5281/zenodo.3925901) through Scidraw.io. Finally, we thank the University of Michigan Biomedical Research Core Facilities for providing access to research equipment and services.

3.7 Author Contributions

Conceptualization: MKS, MPM, BLA

Methodology: MKS, MPM, BLA

Software: MKS

Validation: MKS, MPM, BLA

Formal Analysis: MKS

Investigation: MKS, MPM, BLA

Resources: MPM, BLA

Writing – Original Draft: MKS

Writing - Review & Editing: MKS, MPM, BLA

Visualization: MKS, MPM, BLA

Supervision: MPM, BLA

Project Administration: MPM, BLA

Funding Acquisition: MKS, MPM, BLA

3.8 Tables

Table 3.1 Phenotypes following conditional *Gli2* deletion at E9.5

Genotype	Phenotype			
	Polydactyly	**Thickening of pancreatic head**	**Loss of anvil shape in pancreatic tail**	**Expansion pancreatic tail**
Gli2$^{fl/fl}$	0/3 (0%)	0/3 (0%)	0/3 (0%)	0/3 (0%)
Pdgfrα$^{CreER/+}$;Gli2$^{fl/fl}$	0/3 (0%)	1/3 (33%)	0/3 (0%)	0/3 (0%)

Table 3.2 Phenotypes following conditional *Gli3* deletion at E9.5

Genotype	Phenotype			
	Polydactyly	**Thickening of pancreatic head**	**Loss of anvil shape in pancreatic tail**	**Expansion pancreatic tail**
Gli3$^{fl/fl}$	0/18 (0%)	0/18 (0%)	0/18 (0%)	0/18 (0%)
Pdgfrα$^{CreER/+}$;Gli3$^{fl/fl}$	4/4 (100%)	4/4 (100%)	4/4 (100%)	3/4 (75%)

Table 3.3 Phenotypes following conditional *Gli3* deletion at E13.5

Genotype	Phenotype			
	Polydactyly	**Thickening of pancreatic head**	**Loss of anvil shape in pancreatic tail**	**Expansion pancreatic tail**
Gli3$^{fl/fl}$	0/9 (0%)	0/9 (0%)	0/9 (0%)	0/9 (0%)
Pdgfrα$^{CreER/+}$;Gli3$^{fl/fl}$	0/2 (0%)	0/2 (0%)	0/2 (0%)	1/2 (50%)

Table 3.4 Antibodies used for immunofluorescence

Antibody	Host species	Catalog Number	Dilution
β-Gal	Chicken	ICL Cgal-45A-Z	1:2000
Vimentin	Rabbit	Cell Signaling cs5741	1:500
Ecad	Mouse	BD Biosciences 610181	1:100
Pdgfrβ	Rabbit	Abcam ab32570	1:200
pHH3	Mouse	Cell Signaling 9706S	1:100
Insulin	Guinea Pig	Invitrogen PA126938	1:800
Glucagon	Rabbit	Immunostar 20076	1:800

3.9 Figures

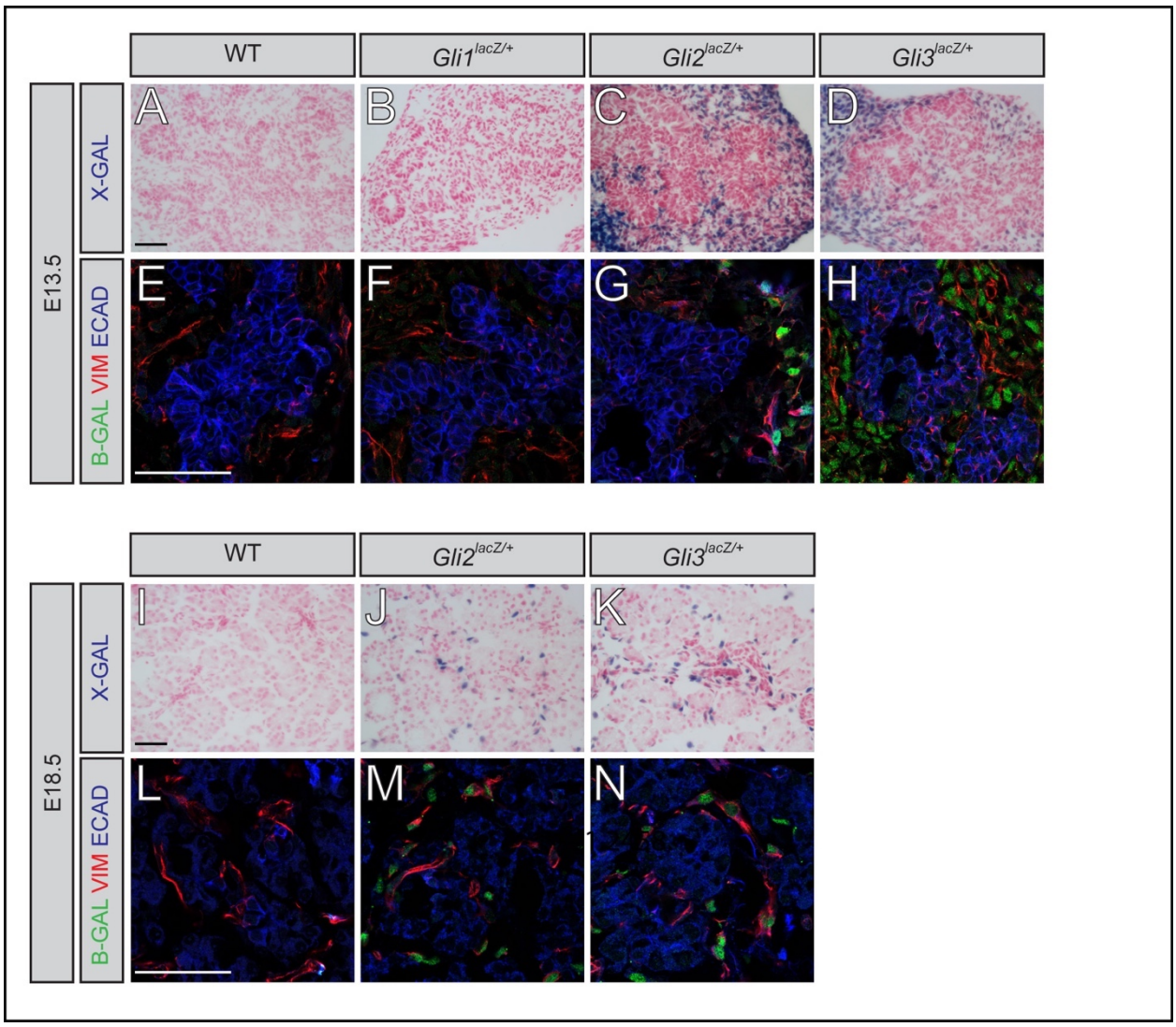

Figure 3.1 *Gli2* and *Gli3* are expressed broadly in the developing pancreatic mesenchyme
A-N) β-galactosidase reporter gene expression in E13.5 (**A-H**) and E18.5 (**I-N**) pancreata from WT, *Gli1*$^{lacZ/+}$, *Gli2*$^{lacZ/+}$, and *Gli3*$^{lacZ/+}$ mice. Expression of β-galactosidase detected by X-gal staining (**A-D**, **I-K**, blue) or immunofluorescent antibodies (**E-H**, **L-N**, green). Additional immunofluorescent antibodies detect mesenchymal cells (VIM, red) and epithelial cells (ECAD, blue). Scale bar = 50 μm.

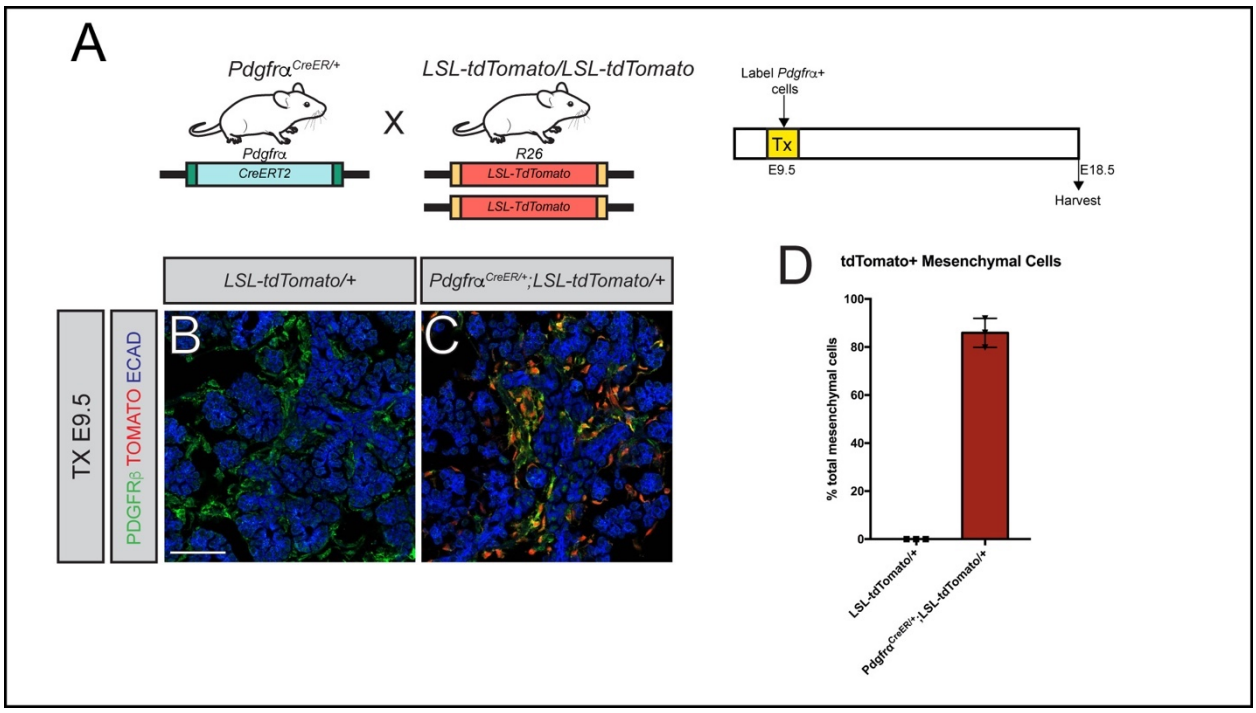

Figure 3.2 *Pdgfrα*$^{CreER/+}$ allele effectively drives recombination in the developing pancreatic mesenchyme.

A) Cartoon depicting experimental strategy. *Pdgfrα*$^{CreER/+}$ mice were crossed to *LSL-tdTomato/LSL-tdTomato* reporter mice, and pregnant females received a single dose of tamoxifen (25 mg/kg) at E9.5 by I.P. injection. Embryos were then collected at E18.5, and analyzed for *tdTomato* reporter allele expression by immunofluorescent analysis. **B-C**) Immunofluorescent antibody detection of tdTomato reporter (red). Additional antibodies detect mesenchymal cells (PDGFRβ, green) and epithelial cells (ECAD, blue). Scale bar = 50 μm. **D**) Quantification of tdTomato reporter expression in mesenchymal cells.

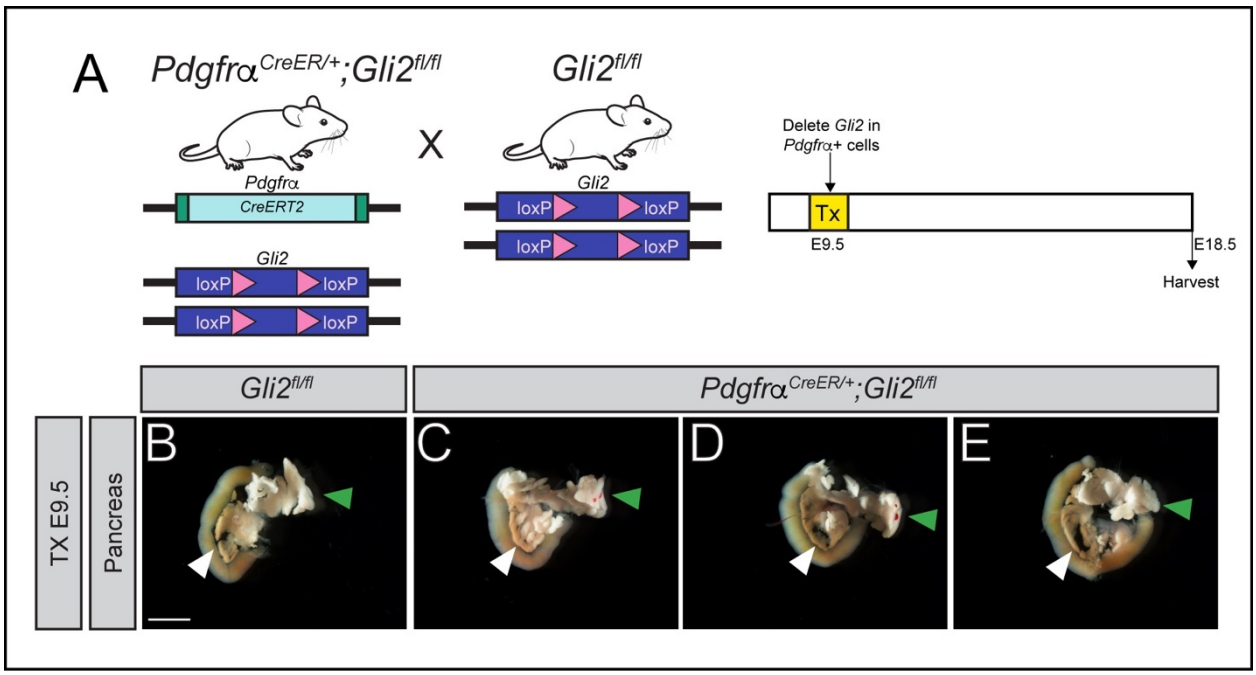

Figure 3.3 Conditional deletion of mesenchymal *Gli2* does not grossly affect pancreas development.

A) Cartoon depicting experiment strategy. *Pdgfrα*$^{CreER/+}$;*Gli2*$^{fl/fl}$ mice were crossed to *Gli2*$^{fl/fl}$ mice, and pregnant females received a single dose of tamoxifen (25 mg/kg) at E9.5 by I.P. injection. Embryos were then collected at E18.5, and analyzed for gross morphological defects. **B-E**) Brightfield images of whole pancreata isolated from *Gli2*$^{fl/fl}$ (**B**) and *Pdgfrα*$^{CreER/+}$;*Gli2*$^{fl/fl}$ (**C-E**) embryos. White arrowheads indicate the head of the pancreas. Green arrowheads indicate the tail of the pancreas. Scale bar = 5000 μm.

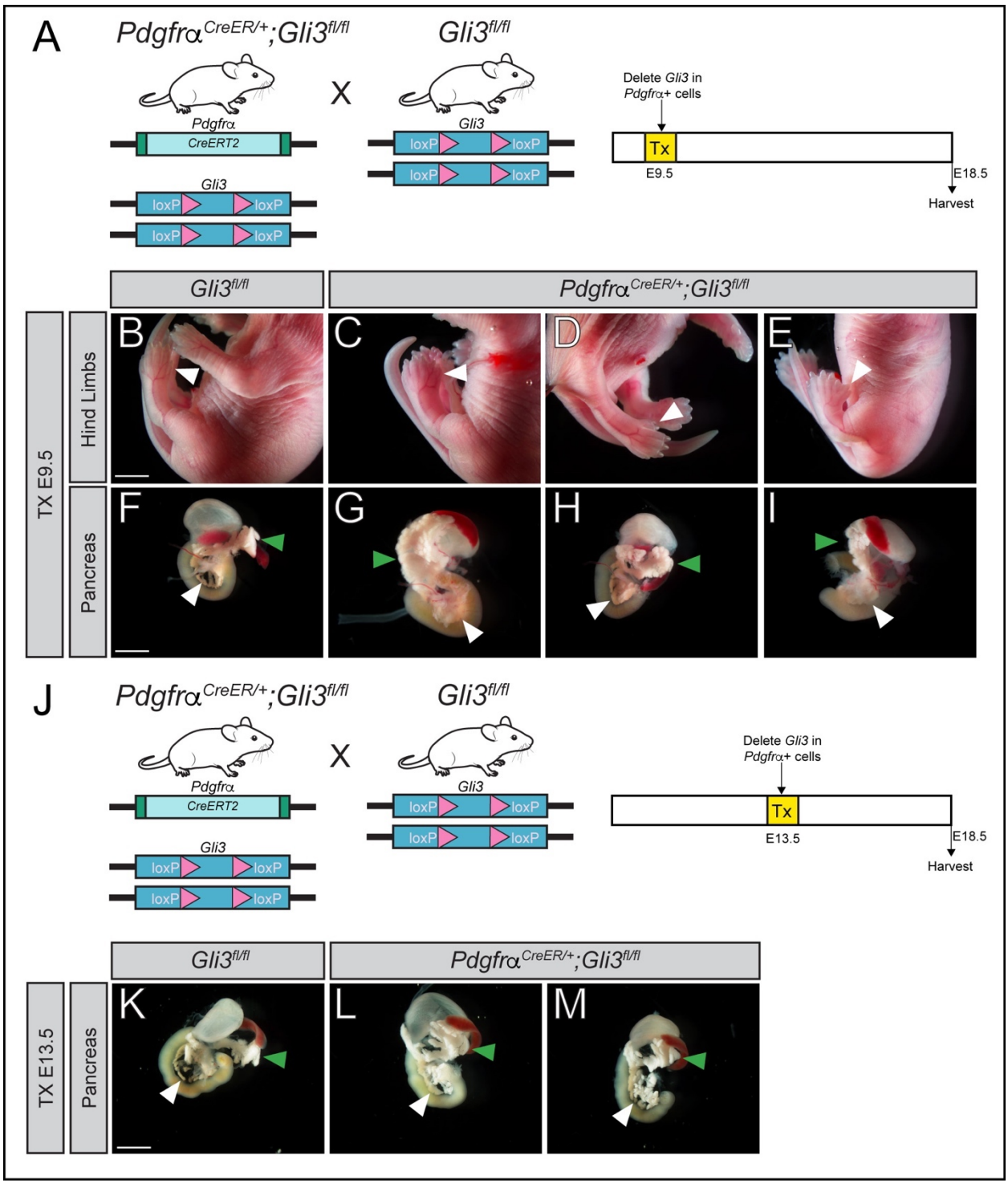
A
Pdgfrα CreER/+;Gli3 fl/fl
Gli3 fl/fl
X
Pdgfrα
CreERT2
Gli3
loxP
loxP
loxP
loxP
Delete Gli3 in
Pdgfrα+ cells
Tx
E9.5
E18.5
Harvest
Gli3 fl/fl
Pdgfrα CreER/+;Gli3 fl/fl
TX E9.5
Hind Limbs
Pancreas
B
C
D
E
F
G
H
I
J
Pdgfrα CreER/+;Gli3 fl/fl
Gli3 fl/fl
X
Pdgfrα
CreERT2
Gli3
loxP
loxP
loxP
loxP
Delete Gli3 in
Pdgfrα+ cells
Tx
E13.5
E18.5
Harvest
Gli3 fl/fl
Pdgfrα CreER/+;Gli3 fl/fl
TX E13.5
Pancreas
K
L
M

Figure 3.4 Conditional deletion of mesenchymal *Gli3* at E9.5 disrupts pancreas morphogenesis.
A) Cartoon depicting experiment strategy. *Pdgfrα*$^{CreER/+}$;*Gli3*$^{fl/fl}$ mice were crossed to *Gli3*$^{fl/fl}$ mice, and pregnant females received a single dose of tamoxifen (25 mg/kg) at E9.5 by I.P. injection. Embryos were then collected at E18.5, and analyzed for gross morphological defects. **B-E**) Brightfield images of hindlimbs, demonstrating a *Gli3* loss of function phenotype (polydactyly) in the developing limbs of *Pdgfrα*$^{CreER/+}$;*Gli3*$^{fl/fl}$ embryos. White arrowheads indicate digit 1, which is duplicated in *Pdgfrα*$^{CreER/+}$;*Gli3*$^{fl/fl}$ embryos. **F-I**) Brightfield images of *Gli3*$^{fl/fl}$ (**F**) and *Pdgfrα*$^{CreER/+}$;*Gli3*$^{fl/fl}$ (**G-I**) pancreata. **J**) Cartoon depicting experimental strategy. Mice were crossed and analyzed as described in (**A**), but pregnant females received tamoxifen at E13.5. **K-M**) Brightfield images of *Gli3*$^{fl/fl}$ (**K**) and *Pdgfrα*$^{CreER/+}$;*Gli3*$^{fl/fl}$ (**L-M**) pancreata following tamoxifen administration at E13.5. For all brightfield images of pancreata, white arrowheads indicate the head of the pancreas. Green arrowheads indicate the tail of the pancreas. Scale bar = 5000 μm.

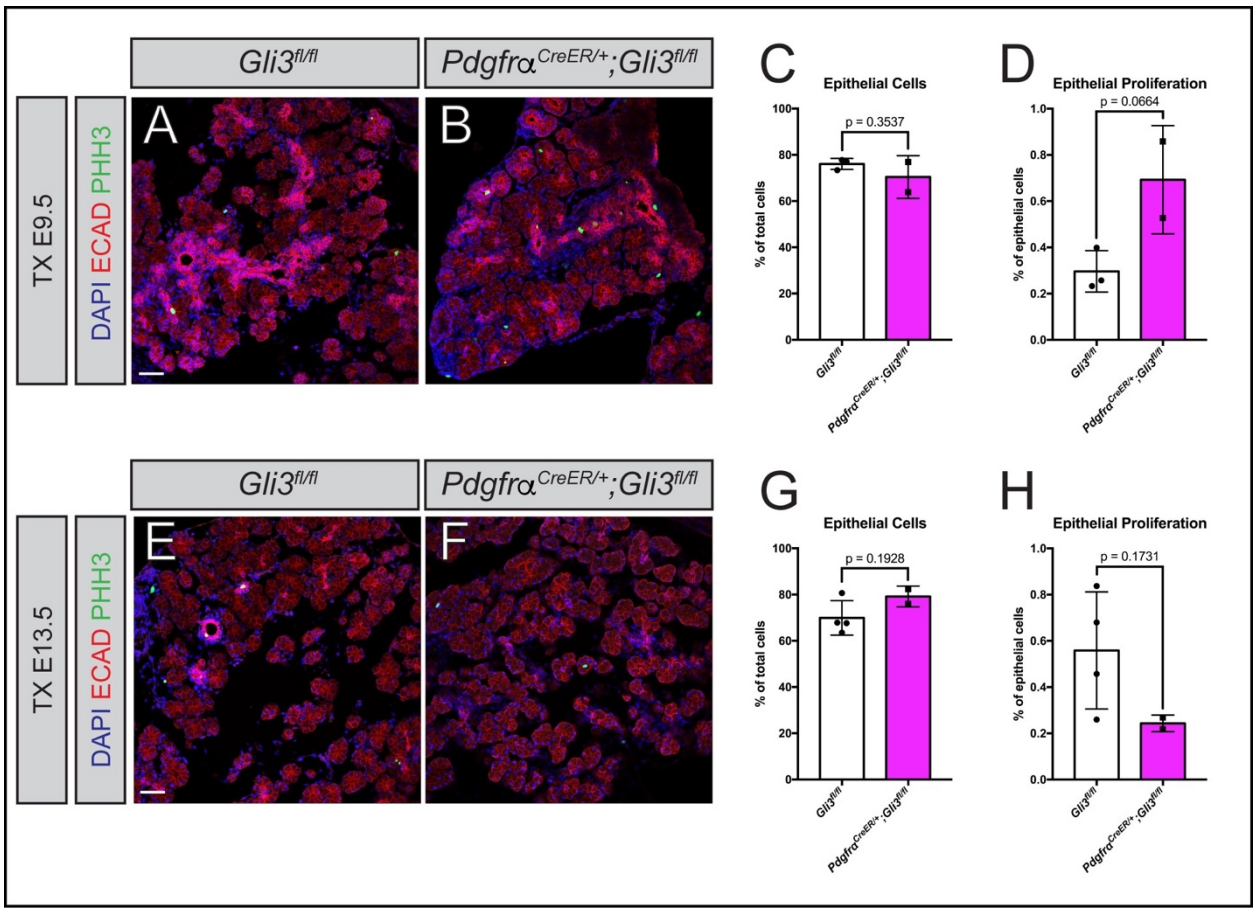

Figure 3.5 Elevated epithelial proliferation following deletion of mesenchymal *Gli3* at E9.5
A-H) Analysis of pancreatic epithelium following conditional *Gli3* deletion at E9.5 (**A-D**) and E13.5 (**E-H**). **A-B**, **E-F**) Immunofluorescent antibody detection of epithelial cells (ECAD, red) and proliferating cells (PHH3, green) in $Gli3^{fl/fl}$ and $Pdgfr\alpha^{CreER/+};Gli3^{fl/fl}$ pancreata. DAPI staining in blue. Scale bar = 50 μm. **C**, **G**) Relative abundance of epithelial cells in the developing pancreas, expressed as a percentage of total cells. **D**, **H**) Quantification of proliferating of epithelial cells, expressed as a percentage of total epithelial cells. P-values determined by un-paired t-test.

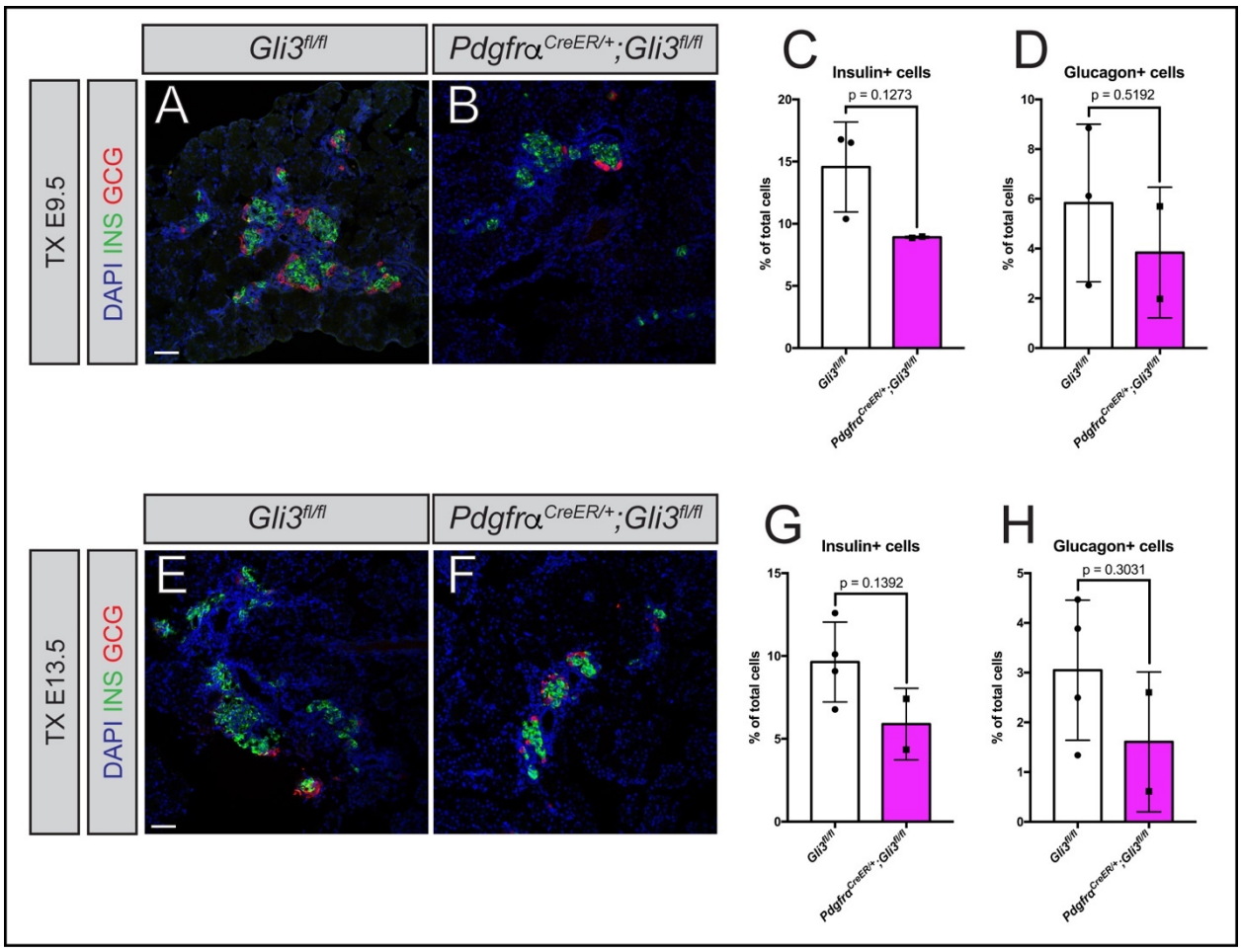

Figure 3.6 Disrupted β-cell development following loss of *Gli3* in the pancreatic mesenchyme.

A-H) Analysis of β-cells and α-cells following conditional deletion of *Gli3* at E9.5 (**A-D**) and E13.5 (**E-H**). **A-B**, **E-F**) Immunofluorescent antibody detection of β-cells (INS, green) and α-cells (GCG, red) in *Gli3*$^{fl/fl}$ and *Pdgfrα*$^{CreER/+}$*;Gli3*$^{fl/fl}$ pancreata. DAPI staining in blue. Scale bar = 50 μm. (**C-D**, **G-H**) Quantification of β-cell (**C**, **G**) and α-cell (**D**, **H**) abundance, expressed as a percentage of total cells. P-values determined by un-paired t-test.

3.10 References

Apelqvist Å, Ahlgren U, Edlund H. 1997. Sonic hedgehog directs specialised mesoderm differentiation in the intestine and pancreas. *Current Biology* **7**: 801-804.

Bai CB, Auerbach W, Lee JS, Stephen D, Joyner AL. 2002. Gli2, but not Gli1, is required for initial Shh signaling and ectopic activation of the Shh pathway. *Development* **129**: 4753-4761.

Bai CB, Joyner AL. 2001. Gli1 can rescue the in vivo function of Gli2. *Development* **128**: 5161-5172.

Bastida MF, Perez-Gomez R, Trofka A, Zhu J, Rada-Iglesias A, Sheth R, Stadler HS, Mackem S, Ros MA. 2020. The formation of the thumb requires direct modulation of Gli3 transcription by Hoxa13. *Proc Natl Acad Sci U S A* **117**: 1090-1096.

Bhushan A, Itoh N, Kato S, Thiery JP, Czernichow P, Bellusci S, Scharfmann R. 2001. Fgf10 is essential for maintaining the proliferative capacity of epithelial progenitor cells during early pancreatic organogenesis. *Development* **128**: 5109-5117.

Blaess S, Stephen D, Joyner AL. 2008. Gli3 coordinates three-dimensional patterning and growth of the tectum and cerebellum by integrating Shh and Fgf8 signaling. *Development* **135**: 2093-2103.

Briscoe J, Therond PP. 2013. The mechanisms of Hedgehog signalling and its roles in development and disease. *Nat Rev Mol Cell Biol* **14**: 416-429.

Cervantes S, Lau J, Cano DA, Borromeo-Austin C, Hebrok M. 2010. Primary cilia regulate Gli/Hedgehog activation in pancreas. *Proc Natl Acad Sci U S A* **107**: 10109-10114.

Chen Y, Knezevic V, Ervin V, Hutson R, Ward Y, Mackem S. 2004. Direct interaction with Hoxd proteins reverses Gli3-repressor function to promote digit formation downstream of Shh. *Development* **131**: 2339-2347.

Chung MI, Bujnis M, Barkauskas CE, Kobayashi Y, Hogan BLM. 2018. Niche-mediated BMP/SMAD signaling regulates lung alveolar stem cell proliferation and differentiation. *Development* **145**.

Corrales JD, Blaess S, Mahoney EM, Joyner AL. 2006. The level of sonic hedgehog signaling regulates the complexity of cerebellar foliation. *Development* **133**: 1811-1821.

DeFronzo RA, Ferrannini E, Groop L, Henry RR, Herman WH, Holst JJ, Hu FB, Kahn CR, Raz I, Shulman GI et al. 2015. Type 2 diabetes mellitus. *Nat Rev Dis Primers* **1**: 15019.

DiMeglio LA, Evans-Molina C, Oram RA. 2018. Type 1 diabetes. *The Lancet* **391**: 2449-2462.

Elliott KH, Chen X, Salomone J, Chaturvedi P, Schultz PA, Balchand SK, Servetas JD, Zuniga A, Zeller R, Gebelein B et al. 2020. Gli3 utilizes Hand2 to synergistically regulate tissue-specific transcriptional networks. *Elife* **9**.

Garcia AD, Petrova R, Eng L, Joyner AL. 2010. Sonic hedgehog regulates discrete populations of astrocytes in the adult mouse forebrain. *J Neurosci* **30**: 13597-13608.

Golosow N, Grobstein C. 1962. Epitheliomesenchymal interaction in pancreatic morphogenesis. *Developmental Biology* **4**: 242-255.

Hebrok M, Kim SK, Melton DA. 1998. Notochord repression of endodermal Sonic hedgehog permits pancreas development. *Genes Dev* **12**: 1705-1713.

Hebrok M, Kim SK, St Jacques B, McMahon AP, Melton DA. 2000. Regulation of pancreas development by hedgehog signaling. *Development* **127**: 4905-4913.

Hibsher D, Epshtein A, Oren N, Landsman L. 2016. Pancreatic Mesenchyme Regulates Islet Cellular Composition in a Patched/Hedgehog-Dependent Manner. *Sci Rep* **6**: 38008.

Huang Y, Sitwala K, Bronstein J, Sanders D, Dandekar M, Collins C, Robertson G, MacDonald J, Cezard T, Bilenky M et al. 2012. Identification and characterization of Hoxa9 binding sites in hematopoietic cells. *Blood* **119**: 388-398.

Hui CC, Angers S. 2011. Gli proteins in development and disease. *Annu Rev Cell Dev Biol* **27**: 513-537.

Kawahira H, Ma NH, Tzanakakis ES, McMahon AP, Chuang PT, Hebrok M. 2003. Combined activities of hedgehog signaling inhibitors regulate pancreas development. *Development* **130**: 4871-4879.

Kawahira H, Scheel DW, Smith SB, German MS, Hebrok M. 2005. Hedgehog signaling regulates expansion of pancreatic epithelial cells. *Dev Biol* **280**: 111-121.

Landsman L, Nijagal A, Whitchurch TJ, Vanderlaan RL, Zimmer WE, Mackenzie TC, Hebrok M. 2011. Pancreatic mesenchyme regulates epithelial organogenesis throughout development. *PLoS Biol* **9**: e1001143.

Larsen BM, Hrycaj SM, Newman M, Li Y, Wellik DM. 2015. Mesenchymal Hox6 function is required for mouse pancreatic endocrine cell differentiation. *Development* **142**: 3859-3868.

Litingtung Y, Dahn RD, Li Y, Fallon JF, Chiang C. 2002. Shh and Gli3 are dispensable for limb skeleton formation but regulate digit number and identity. *Nature* **418**: 979-983.

Madisen L, Zwingman TA, Sunkin SM, Oh SW, Zariwala HA, Gu H, Ng LL, Palmiter RD, Hawrylycz MJ, Jones AR et al. 2010. A robust and high-throughput Cre reporting and characterization system for the whole mouse brain. *Nat Neurosci* **13**: 133-140.

Persson M, Stamataki D, te Welscher P, Andersson E, Bose J, Ruther U, Ericson J, Briscoe J. 2002. Dorsal-ventral patterning of the spinal cord requires Gli3 transcriptional repressor activity. *Genes Dev* **16**: 2865-2878.

Sakhneny L, Khalifa-Malka L, Landsman L. 2019. Pancreas organogenesis: Approaches to elucidate the role of epithelial-mesenchymal interactions. *Semin Cell Dev Biol* **92**: 89-96.

Sheth R, Bastida MF, Ros M. 2007. Hoxd and Gli3 interactions modulate digit number in the amniote limb. *Dev Biol* **310**: 430-441.

Shih HP, Wang A, Sander M. 2013. Pancreas organogenesis: from lineage determination to morphogenesis. *Annu Rev Cell Dev Biol* **29**: 81-105.

Stamataki D, Ulloa F, Tsoni SV, Mynett A, Briscoe J. 2005. A gradient of Gli activity mediates graded Sonic Hedgehog signaling in the neural tube. *Genes Dev* **19**: 626-641.

te Welscher P, Zuniga A, Kuijper S, Drenth T, Goedemans HJ, Meijlink F, Zeller R. 2002. Progression of vertebrate limb development through SHH-mediated counteraction of GLI3. *Science* **298**: 827-830.

Xu B, Wellik DM. 2011. Axial Hox9 activity establishes the posterior field in the developing forelimb. *Proc Natl Acad Sci U S A* **108**: 4888-4891.

Zakany J, Zacchetti G, Duboule D. 2007. Interactions between HOXD and Gli3 genes control the limb apical ectodermal ridge via Fgf10. *Dev Biol* **306**: 883-893.

Chapter 4 Discussion and Future Directions

4.1 Summary

The body of work presented in this thesis investigates the role of GLI1, GLI2, and GLI3 in pancreas development and disease. Through a combination of mouse genetics, *ex vivo* assays, and bioinformatic analysis, I have determined that GLIs in fibroblasts regulate tissue growth and disease progression in the pancreas by regulating the microenvironment.

In the context of PDA, the combined activity of all three GLI proteins controls immune infiltration and tumor growth. In the healthy pancreas, *Gli1, Gli2,* and *Gli3* are all expressed by pancreatic fibroblasts, and the expression of all three *Gli* genes expands in the context of PDA. Conditionally deleting *Gli2* and *Gli3* in pancreatic fibroblasts reduces the migration of immunosuppressive macrophages and promotes the migration of T cells during PDA initiation. In contrast, combined deletion of *Gli1/Gli2/Gli3* enhances the infiltration of macrophages, excludes T cells from the TME, and compromises the integrity of the neoplastic organ. Further, *Gli*-driven changes in immune infiltration regulate tumor growth, as *Gli2/Gli3* KO fibroblasts restrain tumor growth through the recruitment of NK cells. RNA sequencing analysis revealed that loss of *Gli2/Gli3* alters the fibroblast transcriptional program, leading to a decrease in myeloid-recruiting cytokines and an increase in T cell recruiting cytokines. Finally, my data indicate that loss of *Gli* in fibroblasts controls the migration of both macrophages and T cells through direct intercellular regulation.

The work presented in this thesis also reveals a role for GLI in pancreas development. My data demonstrate that *Gli2* and *Gli3* are expressed broadly throughout the mesenchyme of the developing pancreas. While loss of *Gli2* does not significantly impact pancreas development, conditionally deleting mesenchymal *Gli3* during the primary transition drives an increase in epithelial proliferation and abnormal growth of the organ. Interestingly, deleting *Gli3* during the secondary transition does not impact pancreas morphogenesis, but our preliminary data indicate that *Gli3* deletion at either stage of development leads to a decrease in β-cells. These data indicate that GLI3 plays multiple roles during pancreas development, and that these roles occur in distinct phases of organogenesis.

Together, this work enhances our understanding of HH signaling in the pancreas and reveals a new level of complexity to the regulation of HH in pancreas development and PDA. Subtle differences in *Gli* expression drive dramatically different phenotypes throughout the pancreatic microenvironment, revealing that fibroblast function is highly sensitive to differences in GLI activity.

4.2 Future directions

The data presented in this thesis raise a number of unanswered questions regarding the role of GLI1-3 and fibroblasts within the pancreatic microenvironment. In this section, I highlight a selection of research areas that have yet to be explored and propose a series experiments to investigate these subjects.

4.2.1 Role of GLI1-3 at different stages of pancreas disease and recovery

Evidence from embryonic development indicates that the role of HH signaling is highly dependent on two key factors: levels and timing. While the levels of HH signaling have been

shown to directly affect tumor growth in PDA (Mathew et al. 2014b), the role of timing remains largely unexplored. Our data indicate that conditionally deleting *Gli* prior to the formation of PanIN lesions directly regulates immune infiltration. However, the role of *Gli* at different stages of pancreatic disease progression remains poorly understood. Specifically, the combined roles of *Gli1-3* in spontaneous tumors and during recovery from neoplasia are unknown. Fortunately, the inducible nature of the $Pdgfr\alpha^{CreER/+}$ allele opens up the possibility of modifying the timing of *Gli* deletion to determine what role *Gli1-3* play at different stages of pancreas disease and repair.

Our data from subcutaneous tumor assays indicate that loss of *Gli2/Gli3* reduces tumor growth by recruiting NK cells (see Chapter 2, Figure 2.8H). However, a caveat to this result is that these experiments took place outside of the native organ in mice lacking functional T cells. To determine the role of *Gli1-3* in spontaneous pancreatic tumors, I propose to cross a FlpO-driven loss-of-function $p53^{Frt/+}$ allele (Garcia et al. 2020a) into our $KF;Pdgfr\alpha^{CreER/+};Gli2^{fl/fl};Gli3^{fl/fl}$ mice. These $KPF;Pdgfr\alpha^{CreER/+};Gli2^{fl/fl};Gli3^{fl/fl}$ mice can be monitored for tumor formation by ultrasound, and *Gli2/Gli3* can be inducibly deleted once tumors have been detected. Tumor growth and survival can be measured over time, and immune infiltration can be analyzed in tumors at endpoint.

Based on my data, I predict *Gli2/Gli3* deletion in spontaneous tumors will reduce immunosuppression in the TME, reducing the infiltration of immunosuppressive myeloid cells and increasing the infiltration of T cells. While this decrease in immunosuppressive immune cells might be sufficient to reduce tumor growth (as seen in my subcutaneous tumor experiments), my prediction is that this will not be the case in an immune-competent system. The failure of conditional *Gli2/Gli3* deletion to delay PanIN formation *in vivo* (see Chapter 2 Figure 2.5F) suggests that in an immune-competent system, compensatory immunosuppressive

mechanisms may prevent an effective anti-tumor immune response. However, prior research indicates that antagonizing the immunosuppressive function of myeloid cells in combination with T cell activation (via checkpoint inhibitors) effectively reduces tumor growth (Zhu et al. 2014). Therefore, I predict that the combination of *Gli2/Gli3* deletion in fibroblasts and administration of checkpoint inhibitors (e.g. αPD-1, αCTLA4) will reduce the infiltration of myeloid cells, promote the infiltration of T cells, and drive an effective anti-tumor immune response, leading to a significant reduction in tumor growth. These experiments would expand our understanding of GLI function in PDA by defining the role of GLIs in established, spontaneous tumors. More broadly, these proposed experiments could reveal new avenues for potential therapies, in which multiple compartments of the immunosuppressive TME (fibroblasts, myeloid cells, T cells) are targeted at once.

Thus far, we have primarily explored the role of GLI1-3 in different stages of progressing disease. However, the *Gli*-dependent relationship between fibroblasts and immune cells raises the question of whether combined GLI1-3 function plays a role in the recovery of the pancreas from PanIN lesions. *Gli1* is known to play a role in this process, as loss of a single copy of *Gli1* impairs tissue remodeling following inactivation of oncogenic *Kras* (Mathew et al. 2014a). However, the roles of *Gli2* and *Gli3*, individually or in combination with other *Glis*, remains unknown. Our evidence indicates that the infiltration of myeloid cells is highly sensitive to *Gli* expression in fibroblasts, as combined loss of *Gli2/Gli3* reduces macrophage migration, while total elimination of *Gli1/Gli2/Gli3* promotes migration (see Chapter 2, Figure 2.13). Since myeloid cells are crucial to tissue remodeling (Zhang et al. 2017), these *Gli*-driven changes in myeloid cells could dramatically impact the ability of the pancreas to recover from oncogenic *Kras*-driven PanIN lesions.

Addressing the combined role of *Gli* in tissue recovery could be achieved by generating an inducible, FlpO recombinase-driven model of oncogenic *Kras* expression (iKF mice, Figure 4.1A). Fortunately, existing alleles could be incorporated into this model to minimize the time and resources needed to generate these mice. The one novel allele that would need to be generated is a *ROSA26 Frt-STOP-Frt rtTA*. By combining this allele with $Ptf1a^{FlpO/+}$ (Wen et al. 2019) and a $TRE\text{-}Kras^{G12D}$ allele (the Jackson Laboratory, #004375), this iKF mouse would mimic the $Ptf1a^{Cre}$-driven iKras* mouse model (Collins et al. 2012). $Ptf1a^{FlpO/+}$ would recombine the *Frt-STOP-Frt* site, driving rtTA expression in the pancreatic epithelium. Administration of doxycycline would facilitate rtTA binding to the Tet response element (TRE), driving the expression of the $Kras^{G12D}$ transgene. By using a FlpO recombinase to drive expression of rtTA, iKF mice can be crossed to Cre and CreER-based models to target different elements in the stroma, including the $Pdgfr\alpha^{CreER/+};Gli2^{fl/fl};Gli3^{fl/fl}$ and $Gli1^{CreER/CreER};Gli2^{fl/fl};Gli3^{fl/fl}$ mouse lines described in Chapter 2.

To test for a role for combined GLI function during tissue recovery, $iKF;Pdgfr\alpha^{CreER/+};Gli2^{fl/fl};Gli3^{fl/fl}$ mice (Figure 4.1B) could be given doxycycline for 3 weeks to drive oncogenic *Kras* expression, and treated with caerulein to initiate PanIN lesion formation. After 3 weeks, doxycycline would be removed, leading to the inactivation of oncogenic *Kras*. At this stage, administration of tamoxifen would drive the conditional deletion of *Gli2/Gli3* in pancreatic fibroblasts. Mice could then be collected at multiple time points over the following 5 weeks, to analyze the histology and immune infiltration of recovering pancreata in the presence or absence of *Gli2* and *Gli3*. If *Gli2/Gli3* deletion reduces macrophage infiltration during tissue recovery (as observed *in vitro* and during PanIN progression), I predict that tissue repair would be delayed following loss of *Gli2/Gli3.* Alternatively, if *Gli2/Gli3* deletion has no effect on

immune infiltration or tissue repair, this would suggest that the transcriptional program of these fibroblasts has changed in the context of tissue recovery. To clarify the role of *Gli* in this context, WT and *Gli2/Gli3* KO fibroblasts could be isolated from recovering and neoplastic pancreata, and transcriptionally profiled by RNA sequencing. Specifically, analyzing the expression of secreted factors would inform how *Gli*-driven interactions with immune cells (and/or recovering epithelial cells) changes between neoplastic and recovering tissue. This analysis would reveal how the combined function of *Gli2/Gli3* regulates these distinct processes.

In addition to investigating the combined role of *Gli2/Gli3* in tissue remodeling, I would also evaluate tissue recovery in *iKF;Gli1*$^{CreER/CreER}$*;Gli2*$^{fl/fl}$*;Gli3*$^{fl/fl}$ mice (Figure 4.1C). Our data from *in vitro* migration assays and KF mice indicate that combined loss of *Gli1/Gli2/Gli3* promotes macrophage migration. Since myeloid cells facilitate tissue recovery following oncogenic *Kras* inactivation (Zhang et al. 2017), I predict that complete *Gli* deletion will enhance tissue recovery in iKF mice. However, it is possible that combined *Gli1/Gli2/Gli3* deletion does not promote tissue recovery, and in fact might delay tissue recovery. This would be consistent with the idea that canonical HH signaling is required for tissue recovery, as eliminating canonical HH signaling (via LDE225) impairs tissue remodeling in iKras* mice (Mathew et al. 2014a). In either scenario, transcriptome profiling by RNA sequencing (as described above) would reveal how the transcriptional profile of *Gli1/Gli2/Gli3* KO fibroblasts changes during tissue recovery.

One potential concern for this experiment is whether pancreas integrity would be maintained in *iKF;Gli1*$^{CreER/CreER}$*;Gli2*$^{fl/fl}$*;Gli3*$^{fl/fl}$ mice following inactivation of oncogenic *Kras.* Our data indicate that complete loss of *Gli* does not impact tissue integrity in WT *Kras* mice (See Chapter 2, Figure 2.6D-E). Thus, since *Gli2* and *Gli3* would not be conditionally deleted until

after *Kras* inactivation, I predict that the pancreata of these mice will remain intact. However, it is possible that the presence of residual lesions following *Kras* inactivation would still sensitize the tissue to widespread cell death following *Gli1/Gli2/Gli3* deletion. This would indicate that the loss of tissue integrity in *KF;Gli1*$^{CreER/CreER}$*;Gli2*$^{fl/fl}$*;Gli3*$^{fl/fl}$ mice is not due to the combination of *Gli* deletion and oncogenic *Kras* per se, but rather due to a requirement for a baseline level of *Gli* expression in injured tissues. In this scenario, *Gli1*$^{CreER/CreER}$*;Gli2*$^{fl/fl}$*;Gli3*$^{fl/fl}$ mice could be challenged with non-*Kras*-driven injuries (such as chronic pancreatitis), to determine whether a baseline level of *Gli* expression is necessary for organ maintenance in the context of injury.

While the work presented in this thesis reveals novel, *Gli*-dependent interactions between fibroblasts and the TME, the role of GLI1-3 may vary at different stages of disease. The experiments described above will investigate how removing *Gli* expression from established tumors impacts immune infiltration and tumor growth, and whether *Gli*-mediated changes in immune infiltration can be leveraged to enhance tissue recovery. These experiments will be particularly interesting from a clinical perspective, as they will investigate the potential utility of *Gli*-based interventions in established disease. These experiments would also help resolve some of the enduring controversy in the field of PDA, as efforts to make conclusions about HH signaling have been confounded by interventions made at different stages of disease. In combination with the data presented in this thesis, these experiments will provide a thorough investigation of GLI function in pancreatic disease.

4.2.2 Utilizing in vitro assays with in vivo models to explore fibroblast-immune crosstalk

Our data indicate that the role of GLI in PDA is intimately linked with immune cells. Further, this cross-talk impacts implanted tumor growth; *Gli2/Gli3* KO fibroblasts restrain tumor growth by recruiting NK cells, while *Gli1/Gli2/Gli3* KO fibroblasts sustain tumor growth. From

a technical perspective, our data also show that *in vitro* fibroblast-immune cell assays are a relevant system for asking mechanistic questions about PDA, as changes in both macrophages and T cells *in vitro* fully recapitulated the phenotypes we observe *in vivo*. This powerful combination of *in vitro* assays with an inducible, fibroblast-specific PDA model *in vivo* opens up many opportunities for future investigation (Figure 4.2).

In our *in vitro* assays, we see that loss of *Gli2/Gli3* in fibroblasts promotes total T cell migration. However, in these assays both CD4+ and CD8+ T cells are present in the total T cell input. While our *in vivo* data indicates that both CD4+ T cells and CD8+ T cells increase following loss of *Gli2* and *Gli3,* it remains unknown whether both of these populations are affected directly. To determine how *Gli2/Gli3* KO fibroblasts impact different T cell populations, I would analyze T cell populations from both the top (non-migrated), and bottom (migrated) chamber by flow cytometry. Analyzing the relative abundance of T cells populations in each chamber will determine if specific T cell populations are preferentially recruited by *Gli2/Gli3* KO fibroblasts. Further, we can transcriptionally profile sorted T cells to see how loss of *Gli* in fibroblasts differentially affects the phenotype of different T cell populations. Our RNA sequencing data indicates that *Gli2/Gli3* KO fibroblasts upregulate *Ccl5* and *Cxcl10.* While *Ccl5* has been primarily associated with the recruitment of CD4+ Tregs (Tan et al. 2009), CCL5-CCR5 signaling has been shown to enhance the cooperation between CD4+ and CD8+ T cells to restrict tumor growth (Gonzalez-Martin et al. 2011), demonstrating that CCL5 can affect the function of both T lineages. Similarly, CXCL10 regulates the function of both CD4+ and CD8+ T cells, and has been linked to Th1 polarization of CD4+ T cells as well as granzyme B expression by CD8+ T cells (Karin and Razon 2018). Therefore, I predict that *Gli2/Gli3* KO fibroblasts will recruit both CD4+ T cells and CD8+ T cells but promote effector T cell function.

However, it is possible that the loss of *Gli2/Gli3* alone may not be sufficient to promote effector T cell function. This result would strengthen the rationale for utilizing checkpoint inhibitors to activate T cells in combination with *Gli2/Gli3* deletion *in vivo* (as described above), to determine if this combined strategy enables an effective T cell response.

In addition to profiling recruited T cell populations, these *in vitro* assays also provide an opportunity to determine whether the increased expression of *Ccl5* and *Cxcl10* by *Gli2/Gli3* KO fibroblasts is responsible for enhanced T cell recruitment. By incorporating α–CXCL10 (Invitrogen MA5-23774) and α–CCL5 (R&D AF478) neutralizing antibodies into our existing *in vitro* system, we can determine whether the increased expression of these factors is responsible for promoting T cell migration in our *Gli2/Gli3* KO fibroblasts. These same neutralizing antibodies could be administered to *KF;Pdgfrα*$^{CreER/+}$*;Gli2*$^{fl/fl}$*;Gli3*$^{fl/fl}$ mice, in order to determine if the enhanced T cell infiltration we observe *in vivo* is due to increased *Ccl5* and *Cxcl10* expression by *Gli2/Gli3* KO fibroblasts. Together, these experiments would provide mechanistic insight into the molecular mechanisms linking *Gli* expression and T cell recruitment during PDA progression.

This experimental system can be leveraged further to explore *Gli*-dependent relationships between fibroblasts and other immune cells. Evidence from our subcutaneous tumor assays has shown that loss of *Gli* can impact the infiltration of MDSCs and NK cells. Further, prior research has demonstrated that both NK cells and MDSCs can be isolated from blood or living tissue and used acutely in functional migration assays (Sinha et al. 2008; Edsparr et al. 2010; Ding et al. 2015; Olofsson et al. 2019; Xu et al. 2019). Thus, future experiments could test whether *Gli* expression in fibroblasts regulates the migration of NK cells and MDSCs directly. Based on the changes in cytokine expression we observed in our RNA sequencing analysis, I predict that

Gli2/Gli3 KO fibroblasts will fail to promote MDSC migration but will enhance the recruitment of NK cells. If these populations are responding to the same cytokines as macrophages and T cells, respectively, I would also predict that neutralizing antibodies for CCL5 and CXCL10 would similarly reduce NK cell migration in *Gli2/Gli3* KO co-cultures. However, it is also possible that these immune populations will show no change in migration due to loss of *Gli*. This result would suggest the changes in MDSC/NK cell infiltration that we see in our subcutaneous tumors is due to an indirect effect between *Gli2/Gli3* KO fibroblasts and other cell types within the TME. In this scenario, multi-cell co-culture assays would provide an opportunity to identify which intermediate cell types drive this effect in tumors.

In addition to these direct fibroblast-immune cell functional assays, this experimental system can be expanded to incorporate multiple cell types at once. For example, our data indicate that fibroblasts directly regulate macrophage and T cell migration in a *Gli*-dependent manner. However, it remains unclear whether *Gli*-driven changes on macrophages impacts the function of T cells. Conversely, *Gli*-driven changes on T cells may also impact the function of macrophages. To explore these possibilities, future experiments could combine both macrophages and T cells to the top chamber of transwells, with different *Gli* KO fibroblast lines in the bottom chamber. Since macrophages adhere to transwell membranes while T cells remain suspended in media, the migration of T cells and macrophages can be evaluated independently. The results of these triple-culture experiments could then be compared to our original migration assays to determine how the presence of macrophages impacts fibroblast-T cell interactions.

While including all three cell types in a single functional assay would maximize intercellular cross-talk, this may prove technically challenging. For example, finding culture conditions (media composition, experiment duration, etc.) that are permissive to the function of

all three cell types may be difficult to achieve *in vitro*. As an alternative approach, serial conditioned media experiments may prove to be a more tractable experimental system. Prior research has utilized conditioned media systems to explore reciprocal signaling between tumor cells and fibroblasts (Tape et al. 2016). In addition, conditioned media from fibroblasts is sufficient to drive *Gli*-dependent changes in macrophage migration (See Chapter 2, Figure 2.12D). We could therefore perform T cell migration assays using either conditioned media from fibroblasts alone or fibroblasts/macrophage co-cultures to determine how the presence of macrophages impacts fibroblast-T cell interactions. By incorporating our different *Gli* KO fibroblast lines, we can gain mechanistic insight into how *Gli* activity regulates the interactions between different immune populations.

Beyond the role of GLI/HH in fibroblast-immune cell cross-talk, this co-culture system also provides the opportunity to ask more fundamental questions about how different fibroblast populations interact with immune cells. In recent years, there has been a growing interest in fibroblast heterogeneity in PDA (Garcia et al. 2020b; Helms et al. 2020). Although numerous subpopulations of fibroblasts exist in the TME, three populations that have received substantial focus are myCAFs, iCAFs, and apCAFs (Ohlund et al. 2017; Elyada et al. 2019). iCAFs have been proposed to be more immune-modulatory than myCAFs due to an increase in cytokine expression (such as *Il6*), while apCAFs express MHC class II genes associated with antigen presentation (Ohlund et al. 2017; Biffi et al. 2019; Elyada et al. 2019). While apCAFs have been shown to present antigens to T cells *in vitro* (Elyada et al. 2019), iCAFs have never been shown to functionally impact immune cells. Further, the relative ability of these different fibroblast populations to directly affect immune cell infiltration has not been compared *in vitro* nor *in vivo*.

The combined *in vitro/in vivo* system utilized in this thesis provides the opportunity to answer some of these questions directly. Fibroblasts can adopt an iCAF or myCAF phenotype *in vitro* by adjusting culture conditions (Ohlund et al. 2017; Biffi et al. 2019). Future experiments could generate these different cell types in culture and determine whether iCAFs and myCAFs differentially affect macrophage and T cell migration. Further, one could plumb deeper into the mechanisms that determine myCAF/iCAF function by evaluating the role of iCAF or myCAF signature genes in regulating fibroblast-immune cross-talk. For example, iCAFs are defined in part by their expression of *Il6* (Ohlund et al. 2017), and have been ascribed an immunomodulatory role as a result. However, this role has never been shown directly. Future work could assess the ability of iCAFs to recruit immune cells in the presence/absence of an αIL6 neutralizing antibody (BioXcell BE0046). This experiment would determine 1) if iCAFs are capable of recruiting immune cells, and 2) whether *Il6* expression is necessary for this effect. This process could then be applied to other iCAF-defining cytokines, to determine if expression of these signature genes have functional significance. Since our *Pdgfrα*$^{CreER/+}$ allele broadly targets fibroblasts in the neoplastic stroma, future work could extend these *in vitro* findings to determine if conditional deletion of iCAF/myCAF/apCAF signature genes significantly impacts PDA progression *in vivo*. Together, these experiments would address a significant gap in the field by determining whether transcriptionally distinct populations of fibroblasts perform unique functions in PDA.

4.2.3 Identifying GLI1-3 target genes at different stages of PDA progression

The work presented in this thesis reveals coordinated roles of multiple GLIs *in vivo* within the context of PDA progression. Our RNA sequencing analysis reveals that the coordinated activity of GLI2 and GLI3 drive a transcriptional program that shapes the

extracellular and immune landscape of PDA. However, the individual functions of GLI are not identical. While both *Gli2* KO and *Gli3* KO fibroblast lines reduce tumor growth, loss of *Gli2* alone has no effect on immune cells. In contrast, loss of *Gli3* alone is sufficient to reduce the migration of macrophages. One explanation could be that GLI1, GLI2, and GLI3 are binding to unique target genes throughout the genome, and differentially regulating shared target genes. Although GLI1-3 share an optimal binding sequence (Hallikas et al. 2006), GLIs are able to bind to sites of varying affinity throughout the genome (Peterson et al. 2012). The presence of these high and low-affinity GLI binding sites allows for finely tuned spatiotemporal control of HH target genes (Peterson et al. 2012). Further, it was recently demonstrated that individual GLIs can partner with other transcription factors to utilize low-affinity sites and drive unique transcriptional programs (Elliott et al. 2020). Thus, individual GLIs are likely binding to a diverse array of target sequences in PDA, and the patterns of GLI-dependent gene expression could be changing throughout disease progression.

In order to test this, future work could utilize ChIP-capable tagged alleles of GLI1, GLI2, and GLI3 to investigate GLI1-3 binding. Specifically, $Gli1^{Flag/Flag};Gli2^{HA/HA};Gli3^{V5/V5}$ mice have been generated and are viable (unpublished data), enabling binding site analysis of multiple GLIs. To evaluate GLI1-3 binding at multiple stages of PDA progression, $Gli1^{Flag/Flag};Gli2^{HA/HA};Gli3^{V5/V5}$ mice could be crossed into the KC and KPC mouse models. $Gli1^{Flag/Flag};Gli2^{HA/HA};Gli3^{V5/V5};$KC mice would be given caerulein to initiate PanIN lesion formation, and collected 3 weeks later once PanIN lesions are abundant throughout the pancreas. $Gli1^{Flag/Flag};Gli2^{HA/HA};Gli3^{V5/V5};$KPC mice would be collected once tumor-bearing mice reach humane endpoint. Fibroblasts would be isolated from each of these mice (along with healthy $Gli1^{Flag/Flag};Gli2^{HA/HA};Gli3^{V5/V5}$ mice), and processed for ChIP or CUT&RUN sequencing.

Sequencing analysis would reveal the binding sites for GLI1, GLI2, and GLI3 at healthy, PanIN, and PDA stages of disease. This dataset would determine whether GLI1, GLI2, and GLI3 binding sites change at different stages of PDA progression. In addition, this dataset would also reveal the degree of overlap between GLI1, GLI2, and GLI3 target genes during PDA progression, providing insight into the mechanisms of HH target gene regulation during PDA progression.

Beyond the identity of GLI1-3 target genes and the degree of overlap between different GLIs, this dataset would provide insight into the dynamics of GLI binding to target genes during PDA progression. In canonical HH stimulation, HH target genes can become activated as a result of de-repression (i.e. GLI-R releases from the target gene) or activation (i.e. GLI-A binds to the target gene) (Falkenstein and Vokes 2014). From this ChIP-seq dataset, we can gain insight into how different HH target genes are regulated during PDA progression. For example, prior work as well as our RNAseq data indicate that GLI activity regulates the expression of cytokines by pancreatic fibroblasts (Mills et al. 2013; Mathew et al. 2014a). To determine how cytokines are regulated by GLIs during PDA progression, we can assess GLI1, GLI2, GLI3 binding to regulatory regions of cytokines at each stage of disease. By evaluating changes in site occupancy at different stages of disease, this analysis would provide insight into the molecular mechanisms (de-repression vs. activation) that regulate HH-dependent cytokines expression in PDA. Further, understanding the mechanisms that induce immunosuppressive cytokine expression could open new opportunities for therapies.

4.3 Figures

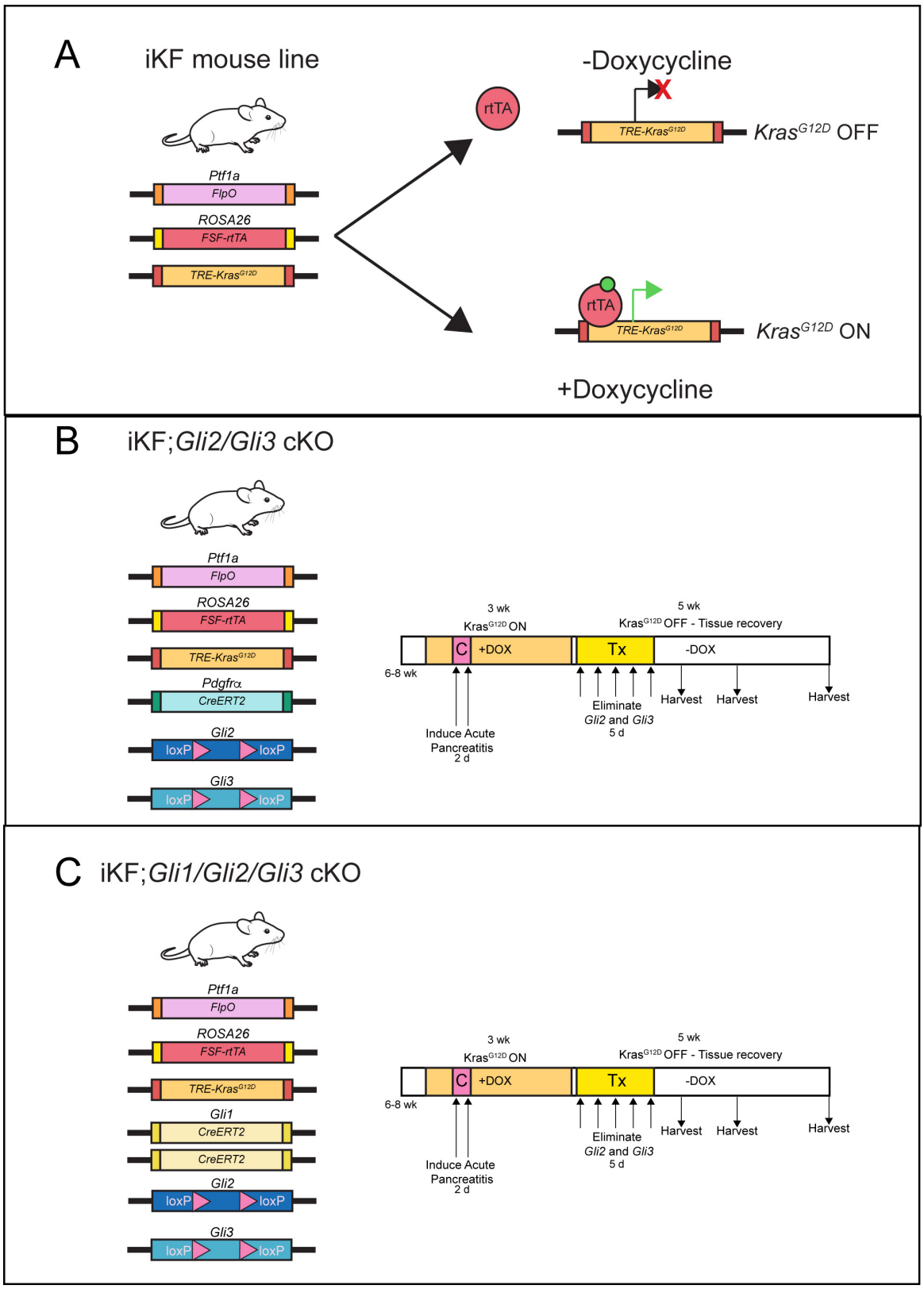
A
iKF mouse line
Ptf1a
FlpO
ROSA26
FSF-rtTA
TRE-Kras^G12D
rtTA
-Doxycycline
TRE-Kras^G12D
Kras^G12D OFF
rtTA
TRE-Kras^G12D
Kras^G12D ON
+Doxycycline
B
iKF;Gli2/Gli3 cKO
Ptf1a
FlpO
ROSA26
FSF-rtTA
TRE-Kras^G12D
Pdgfrα
CreERT2
Gli2
loxP
loxP
Gli3
loxP
loxP
3 wk
Kras^G12D ON
5 wk
Kras^G12D OFF - Tissue recovery
C
+DOX
Tx
-DOX
6-8 wk
Induce Acute Pancreatitis 2 d
Eliminate Gli2 and Gli3 5 d
Harvest
Harvest
Harvest
C
iKF;Gli1/Gli2/Gli3 cKO
Ptf1a
FlpO
ROSA26
FSF-rtTA
TRE-Kras^G12D
Gli1
CreERT2
CreERT2
Gli2
loxP
loxP
Gli3
loxP
loxP
3 wk
Kras^G12D ON
5 wk
Kras^G12D OFF - Tissue recovery
+DOX
Tx
-DOX
6-8 wk
Induce Acute Pancreatitis 2 d
Eliminate Gli2 and Gli3 5 d
Harvest
Harvest
Harvest

Figure 4.1 iKF mouse model for investigating GLI function in tissue recovery
A) Cartoon depicting iKF model in the presence and absence of doxycycline. B-C) Cartoon depicting experimental strategy for investigating the role of *Gli2/Gli3* (B) and *Gli1/Gli2/Gli3* (C) during tissue recovery.

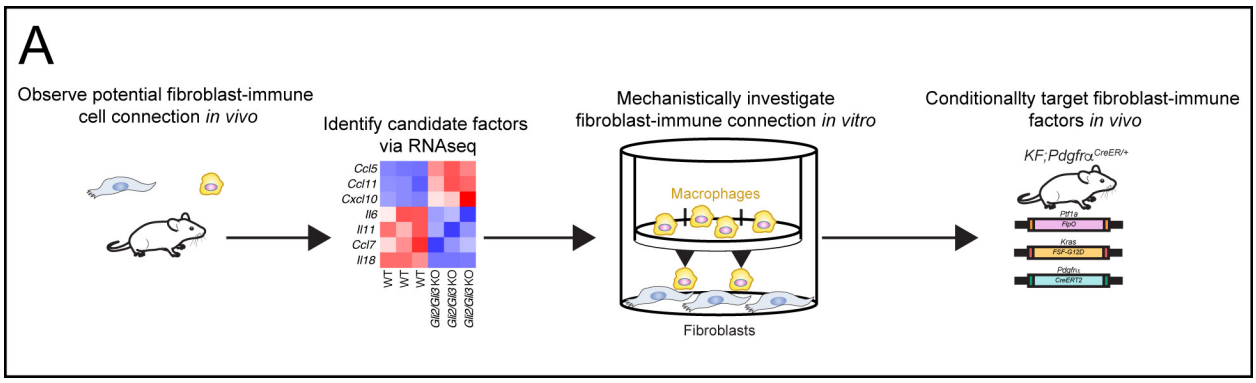

Figure 4.2 Pipeline for investigating fibroblast-immune cell interactions *in vitro* and *in vivo*
A) Cartoon depicting experimental process for investigating fibroblast-immune cell interactions.

4.4 References

Biffi G, Oni TE, Spielman B, Hao Y, Elyada E, Park Y, Preall J, Tuveson DA. 2019. IL1-Induced JAK/STAT Signaling Is Antagonized by TGFbeta to Shape CAF Heterogeneity in Pancreatic Ductal Adenocarcinoma. *Cancer Discov* **9**: 282-301.

Collins MA, Bednar F, Zhang Y, Brisset JC, Galban S, Galban CJ, Rakshit S, Flannagan KS, Adsay NV, Pasca di Magliano M. 2012. Oncogenic Kras is required for both the initiation and maintenance of pancreatic cancer in mice. *J Clin Invest* **122**: 639-653.

Ding Y, Shen J, Zhang G, Chen X, Wu J, Chen W. 2015. CD40 controls CXCR5-induced recruitment of myeloid-derived suppressor cells to gastric cancer. *Oncotarget* **6**: 38901-38911.

Edsparr K, Speetjens FM, Mulder-Stapel A, Goldfarb RH, Basse PH, Lennernas B, Kuppen PJ, Albertsson P. 2010. Effects of IL-2 on MMP expression in freshly isolated human NK cells and the IL-2-independent NK cell line YT. *J Immunother* **33**: 475-481.

Elliott KH, Chen X, Salomone J, Chaturvedi P, Schultz PA, Balchand SK, Servetas JD, Zuniga A, Zeller R, Gebelein B et al. 2020. Gli3 utilizes Hand2 to synergistically regulate tissue-specific transcriptional networks. *Elife* **9**.

Elyada E, Bolisetty M, Laise P, Flynn WF, Courtois ET, Burkhart RA, Teinor JA, Belleau P, Biffi G, Lucito MS et al. 2019. Cross-Species Single-Cell Analysis of Pancreatic Ductal Adenocarcinoma Reveals Antigen-Presenting Cancer-Associated Fibroblasts. *Cancer Discov* **9**: 1102-1123.

Falkenstein KN, Vokes SA. 2014. Transcriptional regulation of graded Hedgehog signaling. *Semin Cell Dev Biol* **33**: 73-80.

Garcia PE, Adoumie M, Kim EC, Zhang Y, Scales MK, El-Tawil YS, Shaikh AZ, Wen HJ, Bednar F, Allen BL et al. 2020a. Differential Contribution of Pancreatic Fibroblast Subsets to the Pancreatic Cancer Stroma. *Cell Mol Gastroenterol Hepatol* **10**: 581-599.

Garcia PE, Scales MK, Allen BL, Pasca di Magliano M. 2020b. Pancreatic Fibroblast Heterogeneity: From Development to Cancer. *Cells* **9**.

Gonzalez-Martin A, Gomez L, Lustgarten J, Mira E, Manes S. 2011. Maximal T cell-mediated antitumor responses rely upon CCR5 expression in both CD4(+) and CD8(+) T cells. *Cancer Res* **71**: 5455-5466.

Hallikas O, Palin K, Sinjushina N, Rautiainen R, Partanen J, Ukkonen E, Taipale J. 2006. Genome-wide prediction of mammalian enhancers based on analysis of transcription-factor binding affinity. *Cell* **124**: 47-59.

Helms E, Onate MK, Sherman MH. 2020. Fibroblast Heterogeneity in the Pancreatic Tumor Microenvironment. *Cancer Discov* **10**: 648-656.

Karin N, Razon H. 2018. Chemokines beyond chemo-attraction: CXCL10 and its significant role in cancer and autoimmunity. *Cytokine* **109**: 24-28.

Mathew E, Collins MA, Fernandez-Barrena MG, Holtz AM, Yan W, Hogan JO, Tata Z, Allen BL, Fernandez-Zapico ME, di Magliano MP. 2014a. The transcription factor GLI1 modulates the inflammatory response during pancreatic tissue remodeling. *J Biol Chem* **289**: 27727-27743.

Mathew E, Zhang Y, Holtz AM, Kane KT, Song JY, Allen BL, Pasca di Magliano M. 2014b. Dosage-dependent regulation of pancreatic cancer growth and angiogenesis by hedgehog signaling. *Cell Rep* **9**: 484-494.

Mills LD, Zhang Y, Marler RJ, Herreros-Villanueva M, Zhang L, Almada LL, Couch F, Wetmore C, Pasca di Magliano M, Fernandez-Zapico ME. 2013. Loss of the transcription factor GLI1 identifies a signaling network in the tumor microenvironment mediating KRAS oncogene-induced transformation. *J Biol Chem* **288**: 11786-11794.

Ohlund D, Handly-Santana A, Biffi G, Elyada E, Almeida AS, Ponz-Sarvise M, Corbo V, Oni TE, Hearn SA, Lee EJ et al. 2017. Distinct populations of inflammatory fibroblasts and myofibroblasts in pancreatic cancer. *J Exp Med* **214**: 579-596.

Olofsson PE, Brandt L, Magnusson KEG, Frisk T, Jalden J, Onfelt B. 2019. A collagen-based microwell migration assay to study NK-target cell interactions. *Sci Rep* **9**: 10672.

Peterson KA, Nishi Y, Ma W, Vedenko A, Shokri L, Zhang X, McFarlane M, Baizabal JM, Junker JP, van Oudenaarden A et al. 2012. Neural-specific Sox2 input and differential Gli-binding affinity provide context and positional information in Shh-directed neural patterning. *Genes Dev* **26**: 2802-2816.

Sinha P, Okoro C, Foell D, Freeze HH, Ostrand-Rosenberg S, Srikrishna G. 2008. Proinflammatory S100 proteins regulate the accumulation of myeloid-derived suppressor cells. *J Immunol* **181**: 4666-4675.

Tan MC, Goedegebuure PS, Belt BA, Flaherty B, Sankpal N, Gillanders WE, Eberlein TJ, Hsieh CS, Linehan DC. 2009. Disruption of CCR5-dependent homing of regulatory T cells inhibits tumor growth in a murine model of pancreatic cancer. *J Immunol* **182**: 1746-1755.

Tape CJ, Ling S, Dimitriadi M, McMahon KM, Worboys JD, Leong HS, Norrie IC, Miller CJ, Poulogiannis G, Lauffenburger DA et al. 2016. Oncogenic KRAS Regulates Tumor Cell Signaling via Stromal Reciprocation. *Cell* **165**: 910-920.

Wen HJ, Gao S, Wang Y, Ray M, Magnuson MA, Wright CVE, Di Magliano MP, Frankel TL, Crawford HC. 2019. Myeloid Cell-Derived HB-EGF Drives Tissue Recovery After Pancreatitis. *Cell Mol Gastroenterol Hepatol* **8**: 173-192.

Xu Y, Fang F, Jiao H, Zheng X, Huang L, Yi X, Zhao W. 2019. Activated hepatic stellate cells regulate MDSC migration through the SDF-1/CXCR4 axis in an orthotopic mouse model of hepatocellular carcinoma. *Cancer Immunol Immunother* **68**: 1959-1969.

Zhang Y, Yan W, Mathew E, Kane KT, Brannon A, 3rd, Adoumie M, Vinta A, Crawford HC, Pasca di Magliano M. 2017. Epithelial-Myeloid cell crosstalk regulates acinar cell plasticity and pancreatic remodeling in mice. *Elife* **6**.

Zhu Y, Knolhoff BL, Meyer MA, Nywening TM, West BL, Luo J, Wang-Gillam A, Goedegebuure SP, Linehan DC, DeNardo DG. 2014. CSF1/CSF1R blockade reprograms tumor-infiltrating macrophages and improves response to T-cell checkpoint immunotherapy in pancreatic cancer models. *Cancer Res* **74**: 5057-5069.